" STUDY OF THE VISCOELASTIC PROPERTIES OF LIQUIDS "

" AT MICROWAVE FREQUENCIES "

A thesis submitted for the degree of Doctor of Philosophy,

by

Herb Joseph John Seguin

Electrical Engineering Department,
Imperial College of Science and Technology
University of London
November, 1963.

ABSTRACT

The development of an " S " band system for use in viscoelastic relaxation investigations in liquids at high frequencies is discussed.

The experimental microwave ultrasonic system ,operating at a frequency of 3000 meagacycles per second , employed piezoelectric single quartz crystals,operating in a nonresonant, surface excitation mode, as the electromechanical transducers.

The real and imaginary components of the shear mechanical impedance,of various test liquids , were obtained from measurements of the relative amplitude and phase change of an acoustic decay pattern,initiated within the quartz crystal by pulse excitation, upon application of the test liquid to the crystal surfaces.

Theoretical and practical measurement accuracies of the apparatus are investigated, along with the limitations of the system as a tool in the studies of the fundamentals of the liquid state. Possible avenues of improvement are suggested as are possible extensions of the basic system design to the higher microwave frequency spectrum.

ACKNOWLEDGEMENTS

The author wishes to express deepest thanks and appreciation to Professor J. Lamb and Dr. J. Barlow for the original presentation of the project and for continued guidance, assistance and encouragement, throughout this work.

The author is also indebted to Mr. J. Collins for continued interest and assistance in the design and development of the experimental system .

Sincere appreciation is expressed to Mr. J. Ritcher for help in the theoretical acoustic aspects of the project.

A vote of thanks is given to Mr. R. Hutchins for help and encouragement in the construction of the experimental system.

The generosity and kind assistance of the engineering staff of Ferranti Ltd. of Edinburgh, Mircowave Division, is also acknowledged.

Special thanks is also given to Mr. R. Watters for assistance in the preparation of this thesis.

Appreciation is also expressed to the Athlone Fellowship Managing Committee and the National Research Council of Canada for providing financial support during the execution of this research project.

CONTENTS

UNITS AND SYMBOLS

The centimeter-gram-second system of units has been adopted in chapter 2 , which deals with the viscoelastic aspect of this work, in order to be consistant with the system of units normally found in the literature. In this respect also,the symbols used in chapter 2 are , as far as possible, those commonly accepted in this field.

Elsewhere in this work the meter-kilogram-second system has been used.

Several duplications of symbols have arisen however since these duplications occur in completely different contexts, no ambiguity should be presented.

The main symobls used in the various parts of this work are as follows:

Chapter 2

Symbol	Name	Dimension
ρ	density	gram/cm.^{3}
η_0	viscosity (poise)	dyne.sec./cm.^{2}
μ	rigidity modulus	dyne/cm^2
G^*	complex shear rigidity modulus	dyne/cm^2
$G_\infty = \mu$	limiting value of shear rigidity modulus	dyne/cm^2
Z_L	liquid shear impedance	dyne.sec./cm^3
Z_o	characteristic impedance	dyne.sec./cm^3
R_L	real component of liquid shear impedance.	dyne.sec./cm.^{3}
X_L	imaginary part of liquid shear impedance.	dyne.sec./cm.^{3}
T_{xy}	stress	dyne/cm^2
S_{xy}	strain	dimensionless.
τ	relaxation time	seconds.
t	time	seconds.
C	velocity of shear wave propagation	cm./sec.
α	viscosity ratio	dimensionless.

Symbol	Name	Dimension
$\underline{\rho}$	complex reflection coefficient	dimensionless.
Z_c	impedance of quartz crystal	dyne.sec./cm.^{3}
u,v,w,	particle displacements	cms.
$\omega = 2\pi f$	angular frequency	radians/sec.
f	frequency	cycles/sec.
$\Gamma = \alpha + j\beta$	propagation constant	
α	attenuation constant	nepers/cm.
β	phase constant	radians/cm.
δ	skin depth	cm.
T	temperature	degrees centigrade.

Appendix A

i,j,k,	unit vectors in cartesian coordinates	dimensionless
∇	Del , vector operator	

Appendix B

E	electric intensity	volts/meter.
B	magnetic induction	webers/meter.^{2}
D	electric displacement	coulombs/meter^2
H	magnetic intensity	ampereturns/m.^{2}
J	current density	amperes/m^2.
σ	electric conductivity	mhos/meter.
ε	dielectric permittivity	farads/meter.
μ	magnetic permeability	henry/meter.
ρ_v	volume charge density	coulombs/meter^3.
C	velocity of propagation	meters/sec.
μ_r	relative permeability	dimensionless.
ε_r	relative permittivity	dimensionless.
C_o	free space electromagnetic propagation velocity	meters/sec.
ε_o	free space permittivity	farads/meter.
μ_o	free space permeability	henry/meter.

Symbol	Name	Dimension
$\Gamma = \alpha + j\beta$	propagation constant	
α	attenuation constant	nepers/meter
$\beta = 2\pi/\lambda_g$	phase constant	radians/meter
$\beta_o = 2\pi/\lambda_o$	free space phase constant	radian/meter
C_p	phase velocity	meters/sec.
λ	wavelength in unbounded media	meters
λ_g	waveguide wavelength	meters
λ_c	cut off wavelength	meters
λ_o	free space wavelength	meters
$k_c = 2\pi/\lambda_c$	cut off wave number	radians/meter
k_x	wave number for x coordinate axis	radians/meter
k_y	wave number for y coordinate axis	radians/ meter
ω	angular frequency	radians/sec.
ω_c	cut off angular frequency	radians/sec.
f	frequency	cycles/sec.
Z_w	wave impedance	ohms
$k = \omega^2\mu\varepsilon$	unbounded wave number	radians/meter
$J_\chi()$	Bessel function of the first kind and order χ.	
$N_\chi()$	Bessel function of the second kind and order χ.	
Z_i	intrinsic impedance	ohms
Z_o	characteristic impedance	ohms
	reflection coefficient	dimensionless
"r"	V.S.W.R.(voltage standing wave ratio)	dimensionless.
Appendix D		
ρ	density	kilograms/m^3
u,v,w,	elastic particle displacement in x, y,and z directions	meters.
T_{ij}	stress tensor	newtons/m^2
S_{ij}	strain tensor	dimensionless.

Symbol	Name	Dimension
F	force	newtons
h_{xx}	Christoffel Constant	newtons/m^2
λ , μ	Lame's constants	newtons/m^2
P_i	acoustic power flow	kilowatts
α, β, γ	elastic particle displacement direction cosines.	dimensionless.
l ,m ,n	wave normal direction cosines	dimensionless.
C_{ijkl}	elastic constant tensor	newtons/m^2
ψ_i	deviation angle of mode displacements from wave normal	degrees.
$W_{s(i)}$	sonic energy density	newton-meter.
W_e	stored electrical energy density	newton-meters.
K	electromechanical coupling coefficient	dimensionless.
η_o	electromechanical conversion efficiency	% or db.

Appendix E

Ps	angular momentum	kilogram-m^2/sec.
ms	spin quantum number	dimensionless.
us	magnetic moment	
τ	torque	kilogram-m^2/$sec.^2$
Γ_e	gyromagnetic ratio	rad/sec./ampturn/m
M	electron magnetic moment per unit volume	
α	electron precession damping coefficient	dimensionless.
ω_o	Larmor precessional frequency	radians/sec.
H_j	total internal D.C. magnetic field	oersted.
χ, κ	susceptibility tensor elements	
S	susceptibility tensor	meters/henry
μ	permeability tensor	henry/meter.
N_x, N_y, N_z	demagnetising factors	dimensionless.

Appendix F

Q_{un}	unloaded cavity quality factor	dimensionless.

Symbol	Name	Dimension
$W_{s(m)}$	magnetic energy storage in cavity	joules
$W_{s(e)}$	electrical energy storage in cavity	joules
σ	electrical conductivity	mhos/meter
δ	skin depth	meters
V/S	volume to surface ratio of cavity	
β	coupling parameter	dimensionless
C	lumped capacity	farads
L	lumped inductance	henry
G= 1/R	lumped shunt cavity conductance	mhos
P_{in}	power input to cavity	watts.
Y_{gap}	cavity gap admittance	mhos
W_{diss}	energy dissipated in cavity	Joules

Appendix G

f_c	varactor diode cut off frequency	cycles/sec.
C_o	varactor diode static capacitance	micromicro farads
R_s	varactor series resistance	ohms
Γ_n	normalised diode capacitance excursion	dimensionless.
Q_d	diode quality factor	dimensionless.
ω_1	signal frequency	radians/sec.
ω_2	idler frequency	radians/sec.
ω_3	pump frequency	radians/sec.
X_1	reactance of signal circuit	ohms
R_{T_1}	total resistance of signal circuit	ohms
R_{neg}	effective diode negative resistance	- ohms
G	gain	dimensionless.
F	noise figure	dimensionless.
T_e	effective input noise temperature	degrees Kelvin
T_{op}	effective operating noise temperature of receiver	degrees Kelvin.

PART I

" FIELD OF STUDY "

Part I of this work consisting of chapters number one and two, is concerned with the general background of the field of study along with the pertinent mathematical theory.

CHAPTER 1

INTRODUCTION

1;1 (HISTORICAL)

Historically most substances were considered to be completely characterised by classical viscous and elastic theory in the sense that liquids were assumed to respond to conditions of stress only by viscous flow, while solid substances were considered to exhibit only pure elasticity according to Hooke's Law.

The then small group of materials which were experimentally observed to exhibit mechanical behaviour departing from classical concepts were termed " anelastic " , and since in most instances these anelastic effects represented only small correction factors, the classical concepts were taken as being basically valid.

However with the development of long chain polymer type liquids and other synthetic substances, so currently predominant in the chemical industry, the situation completely changed since these materials were found to exhibit anelastic effects to such a degree as to mask any classical behaviour. It was thus apparent that the mechanical properties of these materials could not be adequately defined unless simultaneous consideration was made of both viscous and elastic effects.

Maxwell's work of 1867, (89), introducing the concept of a relaxation time and its subsequent extension to include a distributed relaxation function, was probably the first attempt at specifying the time and magnitude relationship between stress and strain for a " viscoelastic " substance.

Basically, it was found that the exact behaviour of a liquid is completely specified by its relaxation spectrum, which may be determined from shear mechanical impedance measurements, provided experimental data is available over the whole relaxation range of the material.

Subsequent research into this field rapidly widened the scope of knowledge , the ever increasing amount of investigation being spurred on by the fact that the precise knowledge of the mechanical behaviour of these viscoelastic materials had become of immense practical value as well as of fundamental scientific interest. A wealth of experimental data has consequently been amassed and analysed thereby shedding considerable light into the fundamentals of the liquid state.

The physical properties of liquids differ from those of an amorphous solid mainly because the the liquid structure can change both with pressure and temperature. Moreover, changes brought about in the liquid structure by mechanical or electrical excitation do not follow instantaneously , but reach a new equilibrium state exponentially in time. It follows therefore that the time of measurement is an additional variable in studies of this nature. If the excitation alternates simple harmonically in time, the time scale of the measurement is inversely related to the frequency of the sinusoidal excitation.

Since relaxation times may range from years to micro-microseconds for different liquids, it is desirable to have apparatus capable of obtaining shear impedance measurements over the whole of this frequency spectrum. Many devices have been developed for accomplishing these investigations,where purely mechanical systems are favoured for materials having relaxation times in excess of one hundred seconds, while electromagnetic devices have proved practical throughout the audio range and upwards to about one hundred kilocycles. Above one hundred kilocycles and up into the kilomegacycle region, piezoelectric transducer systems have found general acceptance.

In many instances it has been found that it is possible to construct reduced functions,of temperature and frequency, with the experimental data obtained from shear impedance investigations such that all the experimental curves may be reduced to form a single curve which is characteristic of the particular liquid. When this reduction principle holds it is often possible to obtain the complete relaxation spectrum

from single frequency measurements, merely by altering the test temperature. However for cases in which this reduction principle is not valid, a wide operating frequency range is necessary to cover the whole of the relaxation region at a particular temperature.

Investigations into the liquid state have a direct application in problems of lubrication, praticularly those relating to the lubrication of high speed bearings and gears subjected to high stresses. This may be appreciated by considering that the hydrostatic pressure in the thin lubrication film of bearings and gears subjected to high stresses, may readily exceed many thousand atmospheres. Thus in its passage between load bearing surfaces, this thin film of lubricant is subjected to a pressure impulse, which in high speed gears for example, may be produced in a time as small as a microsecond while the complete transit of the oil through the load bearing surfaces may be a millisecond or less. Clearly any molecular configuration rearrangements in the liquid which require time periods for their completion exceeding a microsecond, are important in attempting to understand the basic process of lubrication. Moreover owing to the relatively high pressures in the lubricating film these configurational rearrangements in the liquid require much longer times for their completion, than at atmospheric pressure. It follows therefore that in many lubrication problems the transit of the oil through the load bearing surfaces may be of the same order as the molecular relaxation time which determines its viscosity, and hence the oil no longer behaves as a simple viscous liquid. It is evident therefore that time, temperature, pressure and shear rate must all be considered in lubrication problems and so part of the purpose of this research is to obtain information on liquid behaviour under these conditions.

1;2 (PRESENT WORK)

As mentioned in section (1;1) , in cases when the reduction principle is valid it is found that the shear mechanical properties of a liquid may be expressed in the form of universal curves, in which the shear mechanical impedance or dynamic viscosity is plotted on a reduced frequency scale against ($\log(\alpha f)$) , where α is the ratio of the static viscosity,at the test temperature and pressure, to the static viscosity of the liquid,at the reference temperature and pressure, generally taken to be 30 degrees centigrade and one atmosphere. Here the term static viscosity is meant to signify the limiting value of the liquid viscosity as the shear rate approaches zero.

In order to make full use of these impedance measurements it is essential to have availiable experimental data at the highest values of (αf) since these are needed to derive the spectrum of relaxation times, which in turn leads to a correlation of mechanical behaviour with chemical composition.

Large values of (αf) may be obtained in two ways, firstly by cooling the liquid to a low temperature and performing the experiment at a relatively low frequency of approximately 10 megacycles per second. There is however a definite limit to the utilisation of this technique such that the lowest temperature at which a measurement may be obtained on a particular liquid is in practice governed by the condition that the liquid becomes a glass . Thus in order to obtain relaxation data over the whole of the relaxation spectrum it is necessary to restrict measurements to the higher viscosity liquids, which are correspondingly very complex chemically and hence the correlation between mechanical behaviour and chemical composition becomes increasingly difficult.

The second means of obtaining large values of (αf) is to perform the measurement at very high frequencies , this technique having the advantage that much simpler liquids may be investigated

thereby making the interpretation of results easier.

Ideally experimental systems operating at " M " band (50 to 75 KMc/s) would be desirable for measurements on water and similar 0.01 poise liquids which should exhibit viscoelastic relaxation phenomenon at room temperatures.

Unfortunately measurement systems operating at these frequency levels have not as yet been devised due mainly to the absence of a satisfactory transducer, capable of converting this high frequency electromagnetic energy, into mechanical energy reasonably efficiently.

The work described in this thesis is concerned with the development of an experimental system capable of obtaining relaxation data on liquids at microwave frequencies. This investigation was limited to the " S " band frequency of 3 KMc/s. , since it was felt that this was the highest frequency at which there was any real possibility of success , utilising crystal quartz as the electro-mechanical transducer.

1;3 (PRESENTATION)

This thesis is presented in three parts, part I, constitued by chapter 2 contains the general viscoelastic theory pertinent to the field of investigation. Part II comprised of chapters 3 to 11 describes in detail the experimental system developed for the study of viscoelastic relaxation phenomenon in liquids at a frequency of 3 kilomegacycles per second. Part III consisting of appendices A to H , summarises all the theory pertaining to the design, construction and operation of the experimental system.

CHAPTER 2

VISCOELASTIC THEORY

2;1 (GENERAL)

It is well known that there is a strong structural resemblance between solids and liquids in the neighbourhood of crystallisation, and Frenkel,(88), further suggests that liquids much closer resemble solids to the extent that experimental distinction between both states is merely a function of the time scale of the experiment.Frenkel proposes that liquids have a definite " short range " molecular order such as solids exhibit. The equilibrium positions of the atoms in the liquid body are not however permanent but rather after remaining in a certain equilibrium position for a time (τ) , each atom can jump to a new equilibrium site. If now a force is applied to the liquid in a time t such that $t \gg (\tau)$, the liquid body will yield in the sense described by ordinary viscous flow , as a consequence of a superimposed preferred direction of atomic jumps from equilibrium position to equilibirum position.

If on the other hand a force is applied in a time $t \ll (\tau)$ only elastic deformation of the liquid body will result, similar to a purely elastic body. Thus Frenkel states that the characteristic fluidity of liquids can be displayed only under conditions where the applied forces have a time dependence , with respect to magnitude and direction, very much greater than the mean life time of an atom in a particular equilibrium site. The shear elasticity of liquids under such conditions may be considered to be masked by their fluidity.

The same argument may be applied to solid substances and it is found experimentally that provided a stress is maintained sufficiently long on a solid body , flow results. Under normal conditions the mean life time or relaxation time (τ) for a solid is extremely long due to the regularity and stability of atoms in the crystal lattice.

2;2 (VISCOELASTIC MODELS)

In an attempt to develop theory capable of explaining the phenomenological behaviour of viscoelastic materials several mechanical models were devised. These models were subsequently used as a basis for developing the equations of motion and other pertinent parameters of the substances they were intended to represent.

Two mechanical models find general acceptance in the literature, these being the Maxwell ,(89) and Voigt,(90), representations for a viscoelastic liquid and solid respectively. Since the main concern in this work is for liquids, the Voigt viscoelastic model will not be considered here.

2;3 (MAXWELL LIQUID)

Probably the first developement of a model to represent the general viscoelastic nature of a material was due to Maxwell,(89). Originally devised to represent relaxation effects observed in gases, this model has subsequently found wide application to the liquid state.

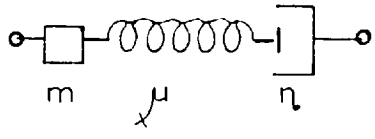

μ = rigidity modulus
η = viscosity
m = mass

FIG. (2;3;1)

Mechanical Maxwell model

Electrical equivalent of mechanical Maxwell model

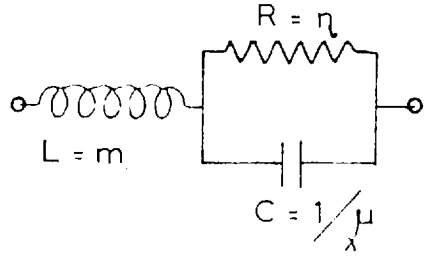

FIG. (2;3;2)

A Maxwell element is given in FIG.(2;3;1) and in mechanical form is seen to constitute of a spring and dashpot in series, the spring depicting the elastic character of the substance while the dashpot represents the viscous nature. Inertial or body parameters are shown as a lumped mass.

It is possible to construct an electrical analogue of every mechanical system, both being specified by the same type of equations of motion, and so the electrical equivalent to the Maxwell mechanical model is as shown in FIG.(2;3;2). In the equivalent circuit resistance represents viscosity while capacitance represents the reciprocal of regidity and inductance replaces mass. Consideration of the differential equations governing the two equivalent systems reveals that the following are also analogous:

stress	.....	emf.
velocity	.....	current
strain	.....	charge.

From Maxwell's mechanical model it is evident that for a given shear stress T_{xy}, the total strain is given by the sum of an elastic part characteristic of a rigid body and a viscous part characteristic of a Newtonian or purely viscous liquid.

Considering first the Newtonian substance depicted in FIG.(2;3;3), where an element, of an isotropic liquid, having unit dimensions in the Z direction and height dy, is undergoing viscous flow in the x direction under the influence of a shearing force P. The velocity of liquid flow at the plane $y = y_1$ is specified as $v_{x(1)}$ and therefore the flow velocity at $y = y_{11}$ is $v_{x(11)}$ where:

$$y_{11} = y_1 + dy$$

and

$$v_{x(11)} = v_{x(1)} + \frac{\partial}{\partial y} v_{x(1)}\, dy \qquad (2;3;1)$$

Thus there is a velocity gradient across dy such that the relative velocity of the film at the point $y=y_{11}$ with respect to y_1 is:

$$v_{x(11)} - v_{x(1)} = \frac{\partial}{\partial y}\left(v_{x(1)}\right) dy \qquad (2;3;2)$$

This velocity gradient is a consequence of the applied shear stress T_{xy} acting at y_{11}. The proportionality between the shearing stress and the relative velocity of the fluid layers may be expressed as:

$$T_{xy} = \eta \frac{\partial}{\partial y}\left(v_{x(1)}\right) \quad \text{for a unit volume} \qquad (2;3;3)$$

where the proportionality constant η is termed the coefficient of viscosity.

In the above treatment the period of the stress T_{xy} was considered

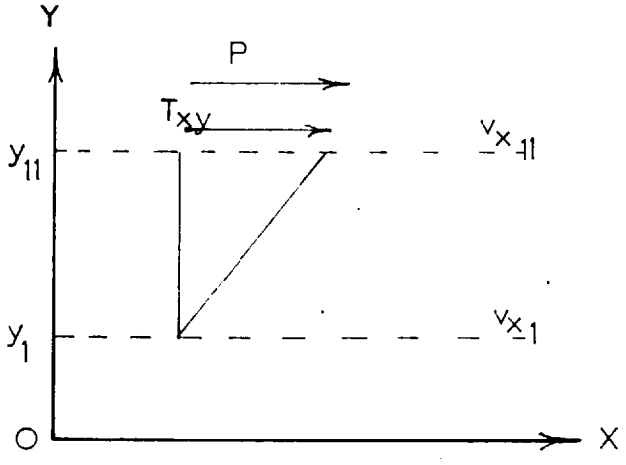

FIG. (2;3;3)

Schematic representation of a Newtonian fluid subjected to a shearing stress T_{xy}.

to be very large with respect to the mean life time (τ_s) of molecules in particular equilibrium positions, and thus only purely viscous flow results.

If now the same situation as shown in FIG.(2;3;3) is considered except that the applied stress T_{xy} is specified as alternating with a period less than (γ_s) , the fluid is found to no longer exhibit viscous flow but rather develops a shear rigidity which is given by:

$$\frac{\partial u_x}{\partial y} = \frac{1}{\mu} T_{xy} \qquad (2;3;4)$$

where u_x is the particle displacement and μ is the rigidity modulus for a purely isotropic solid as given in appendix (D; 7) . Equation (2;3;4) is occassionally written as:

$$\frac{\partial u_x}{\partial y} = \frac{1}{G_\infty} T_{xy} \qquad (2;3;5)$$

where G_∞ is the limiting value of the rigidity modulus of a substance under conditions where T_{xy} alternates at infinite frequency.

Taking the time derivative of equation (2;3;5) gives:

$$\frac{\partial}{\partial y}\left(\frac{d}{dt} u_x\right) = \frac{1}{G_\infty}\left(\frac{d}{dt} T_{xy}\right) \qquad (2;3;6)$$

but

$$d/dt(u_x) = v'_x \qquad (2;3;7)$$

and so

$$\frac{\partial}{\partial y}(v'_x) = (1/G_\infty)\ \frac{d}{dt}(T_{xy}) \qquad (2;3;8)$$

where v'_x is the velocity of propagation of the elastic displacement.

Combining the two effects, such that the total velocity of flow ($v_{x(T)}$) of a viscoelastic body is equal to the sum of the individual viscous and elastic velocities gives:

$$v_{x(T)} = v'_x + v_{x(1)} \qquad (2;3;9)$$

also

$$\frac{\partial}{\partial y} v_{x(T)} = \frac{\partial}{\partial y} v'_x + \frac{\partial}{\partial y} v_{x(1)}$$

which upon substitution yields:

$$\frac{\partial}{\partial y} v_{x(T)} = \frac{T_{xy}}{\eta_0} + \frac{d}{dt} \frac{T_{xy}}{G_\infty} \qquad (2;3;10)$$

now

$$\frac{\partial}{\partial y} v_{x(T)} = \frac{\partial}{\partial y} \frac{d}{dt} u_x = \frac{d}{dt} (S_{xy}) \qquad (2;3;11)$$

therefore

$$\frac{d}{dt} (S_{xy}) = T_{xy}/\eta_0 + \frac{1}{G_\infty} \frac{d}{dt} T_{xy} \qquad (2;3;12)$$

where S_{xy} is the shear strain.

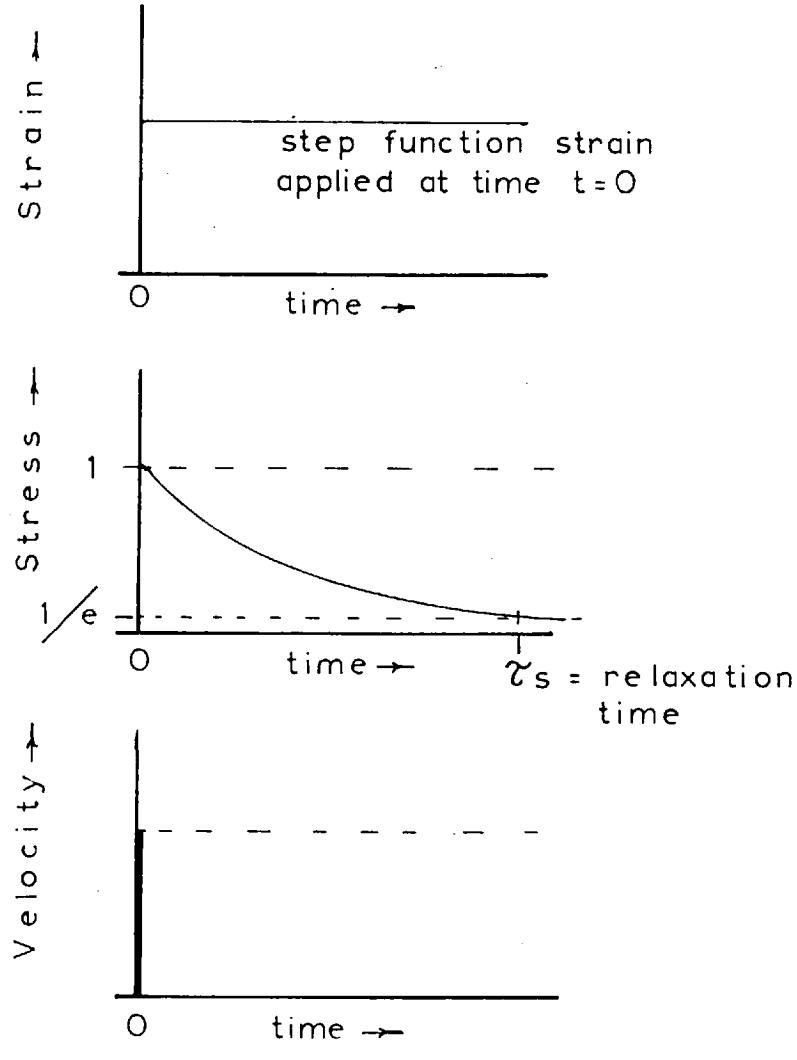

FIG. (2;3;4)

Stress-strain response of a single Maxwell element.

If the elemental liquid volume of FIG.(2;3;3) is suddenly subjected to a strain S_{xy} and constrained in this deformed position, viscous flow results which gradually relaxes the initially generated stress . This particular situation is depicted in FIG.(2;3;4). In FIG.(2;3;4) the liquid is found to exhibit an instantaneous shear modulus of rigidity G_{∞} since the time scale of the strain application is very much less than the relaxation time (τ_s) , consequently the generated stress is instantaneously very large and then is gradually exponentially relaxed to zero, being relaxed to 1/e of its maximum value in a time $t = (\tau_s)$.

The foregoing may be seen by considering equation (2;3;12) and setting $\frac{d}{dt}(S_{xy}) = 0$. Thus:

$$\frac{T_{xy}}{\eta} + \frac{d}{dt}(T_{xy})\,\frac{1}{G_{\infty}} = 0$$

and so: $$T_{xy} = T_{xy}(o)\; e^{-G_{\infty}\, t/\eta} \qquad (2;3;13)$$

When $t = \eta/G_{\infty} = \tau_s$ the stress T_{xy} has fallen to $T_{xy(o)}/e$, and so τ_s is the relaxation time of the liquid. (2;3;14)

If the stress time dependence is assumed to be of the form $e^{j\omega t}$, equation (2;3;13) becomes:

$$j\omega S_{xy} = T_{xy}(1/\eta + j\omega / G_{\infty}) \qquad (2;3;15)$$

or $$T_{xy} = S_{xy} (j\omega\eta / (1+j\omega/\omega_s)) \qquad (2;3;16)$$

where $$\omega_s = 2\pi f_s \qquad (2;3;17$$

and $$f_s = 1/ 2\pi \tau_s = G_{\infty}/ 2\pi\eta \qquad (2;3;18)$$

here f_s is the relaxation frequency.

2;4 (SHEAR WAVE PROPAGATION IN MAXWELL VISCOELASTIC MEDIA)

To investigate wave propagation in a Maxwell medium a simple infinite transmission line may be constructed from elementry Maxwell elements , as shown in FIG.(2;4;1).

From equation (D;2;7) of appendix(D) , the one dimensional equation of motion for adiabatic conditions may be obtained as:

$$\rho \frac{\partial^2 u_x}{\partial^2 t} = \frac{\partial}{\partial y} T_{xy} \qquad \text{for a unit volume.} \qquad (2;4;1)$$

For the case of interest here,(plane shear wave propagation), the particle displacement is taken in the x direction and the phase velocity propagation is in the y direction.

Sustitution of equation (2;3;16) into (2;4;1) gives:

$$\frac{\partial^2 u_x}{\partial^2 y} - \frac{\rho(1 + j\omega/\omega_s)}{j\omega \eta_\infty} \frac{\partial^2 u_x}{\partial^2 t} = 0 \qquad (2;4;2)$$

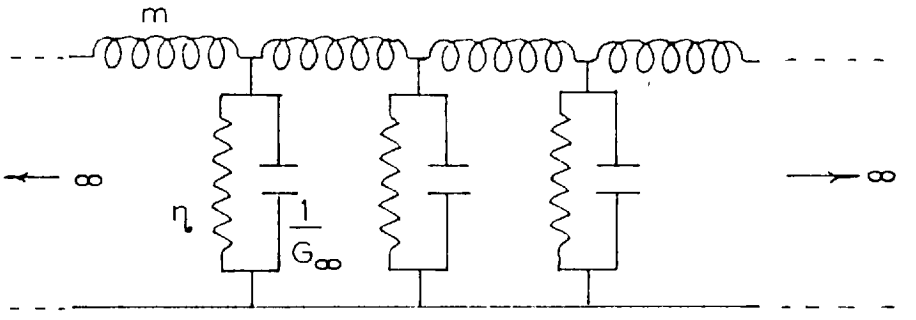

FIG. (2;4;1)

Electrical equivalent network of Maxwell transmission line, representing an infinite volume of fluid having a single relaxation mechanism.

Equation (2;4;2) is clearly of the form:

$$\nabla^2 \phi - \frac{1}{C^2} \frac{\partial^2 \phi}{\partial^2 t} = 0 \qquad (2;4;3)$$

which is obviously the general wave equation and where C is the velocity of propagation, and ∇ is the vector operator of appendix A

It follows therefore that the velocity of propagation of equation (2;4;2) may be written by inspection as:

$$C = \left(\frac{j\omega \eta_0}{\rho(1+ j\omega/\omega_s)} \right)^{\frac{1}{2}} = \left(\frac{j\omega \eta_0}{\rho(1+ j\omega \eta/G_\infty)} \right)^{\frac{1}{2}} \qquad (2;4;4)$$

From equation (2;4;4) it is evident that for a frequency of propagation far below the relaxation frequency such that $\omega \ll \omega_s$, the velocity of propagation becomes:

$$C = (j\omega \eta/\rho) \qquad \text{for } \omega \ll \omega_s \qquad (2;4;5)$$

Under these conditions the mechanical impedance of the medium as given by equation (D;7;23) on page (279), is found to be:

$$Z_{o(L)} = R_L + j X_L = \rho C = (j\omega \eta\rho)^{\frac{1}{2}}$$

$$= (\omega \eta\rho/2)^{\frac{1}{2}}(1+ j) \qquad \text{for } \omega \ll \omega_s \qquad (2;4;6)$$

If however $\omega \not\ll \omega_s$ the shear mechanical impedance expression is:

$$Z_{o(L)} = (j\omega \eta\rho/ (1+ j\omega /\omega_s))^{\frac{1}{2}} \qquad (2;4;7)$$

If a time dependence of the form $e^{j\omega t}$ is assumed, equation(2;4;2) is found to reduce to:

$$\frac{\partial^2 u_x}{\partial^2 y} + \frac{\omega \rho u_x}{\eta} (1/j + \omega /\omega_s) = 0 \qquad (2;4;8)$$

which has a solution of the form:

$$u_x = A\, e^{j(\omega t - \Gamma y)} \qquad (2;3;9)$$

where Γ is the propagation constant as given in appendix B and is equal to:

$$\Gamma = \alpha + j\beta \qquad (2;3;10)$$

here α is the attenuation constant and β is the phase constant .

For the low frequency case , ie: $\omega << \omega_s$

$$\Gamma = (j\omega\rho/\eta)^{\frac{1}{2}} = (\pi f\rho/\eta)^{\frac{1}{2}}(1+j) \qquad (2;4;11)$$

and so $\alpha = \beta = (\pi f\rho/\eta)^{\frac{1}{2}} = (\omega\rho/2\eta)^{\frac{1}{2}}$ nepers/ cms. (2;4;12)

The attenuation of shear waves in liquids is extremely high and this can be easily be verified from a simple calculation using equation (2;4;12).

Taking as an example alow viscosity liquid such as water, having a density of unity, and a viscosity of 0.01 poise, at a frequency equal to the system operating frequency of 3000 Mc/s., the attenuation constant is found to be:

$$\alpha = \left(\frac{\text{x } 3\text{x } 10^9 \text{ x } 1}{0.01}\right)^{\frac{1}{2}} = 1 \times 10^6 \text{ nepers/cm.}$$

$$\text{" } = 8.686 \times 10^6 \text{ db./ cm.} \qquad (2;4;13)$$

If now an effective skin depth is defined such that after this distance of propagation within the medium, the amplitude of the particle displacement has fallen to 1/e of its original value, it follows that:

$$\text{skin depth } \delta = 1/\alpha = 1 \times 10^{-7} \text{ cms.} \qquad (2;4;14)$$

From the magnitude of δ it is evident that it is similar to the skin depth associated with the propagation of electromagnetic energy within waveguides discussed in appendix (B). Clearly therefore only a very slight amount of fluid is necessary to give complete attenuation of the shear wave and so under such conditions the medium may be regarded as infinite. Special use has been made of this particular feature in the design of the microwave ultrasonic apparatus used in the measurement of the shear mechanical liquid impedance such that only a minute quantity of the test liquid was employed.

Alternatively the shear mechanical impedance of a substance is defined as the ratio of the shear stress to the particle displacement velocity and so:

$$Z_{o(L)} = R_L + jX_L = \frac{T_{xy}}{\frac{\partial u_x}{\partial t}} = \frac{\partial u_x}{\partial y}\left\{\frac{j\omega\eta_e}{1+j\omega/\omega_s}\right\} \Big/ \frac{\partial u_x}{\partial t} \qquad (2;4;15)$$

but since $\partial/\partial t = j\omega$ and $\partial/\partial y = -\gamma$

$$Z_{o(L)} = \frac{-\gamma}{j\omega}\left\{\frac{j\omega\eta_e}{1+j\omega/\omega_s}\right\} \qquad (2;4;16)$$

which for $\omega \ll \omega_s$ reduces to:

$$Z_{o(L)} = (\omega\rho\eta/2)^{\frac{1}{2}}(1+j) \qquad (2;4;17)$$

which is the same as obtained previously in equation (2;4;6).

For the general case where $\omega \nless \omega_s$ Mason has shown that: (110).

$$\gamma = \alpha + j\beta = \left(\frac{-A+(B+C)^{\frac{1}{2}}}{2}\right)^{\frac{1}{2}} + j\left(\frac{A+(B+C)^{\frac{1}{2}}}{2}\right)^{\frac{1}{2}} \qquad (2;4;18)$$

and

$$Z_{o(L)} = \left(\frac{\frac{A}{\eta_e^2} + \left(\frac{B}{\eta_e^4} + \frac{C}{\eta_e^2}\right)^{\frac{1}{2}}}{D}\right)^{\frac{1}{2}} j \left(\frac{\frac{-A}{\eta_e^2} + \left(\frac{B}{\eta_e^4} + \frac{C}{\eta_e^2}\right)^{\frac{1}{2}}}{D}\right)^{\frac{1}{2}} \qquad (2;4;19)$$

where: $A = \left(\frac{\omega}{\omega_s}\right)^2 \rho\, G_\infty / \eta_\infty^2$, $B = \left(\frac{\omega}{\omega_s}\right)^2 \rho^2 G_\infty^2 / \eta_\infty^4$

and $C = \left(\frac{\omega}{\omega_s}\right)^2 (\rho G_\infty / \eta_\infty)^2$, $D = 2(1+(\omega/\omega_s)^2)$ (2;4;20)

The variation of the real and imaginary parts of the shear mechanical liquid impedance with frequency for a single relaxation mechanism is given in FIG.(2;4;2).

For conditions of very high frequency, ie: $\omega >> \omega_s$, the attenuation constant of equation (2;4;18) approaches the limiting value of :

$$\alpha = (\rho\, G_\infty)^{\frac{1}{2}} / 2\,\eta_\infty \quad \text{nepers/cm.} \qquad (2;4;21)$$

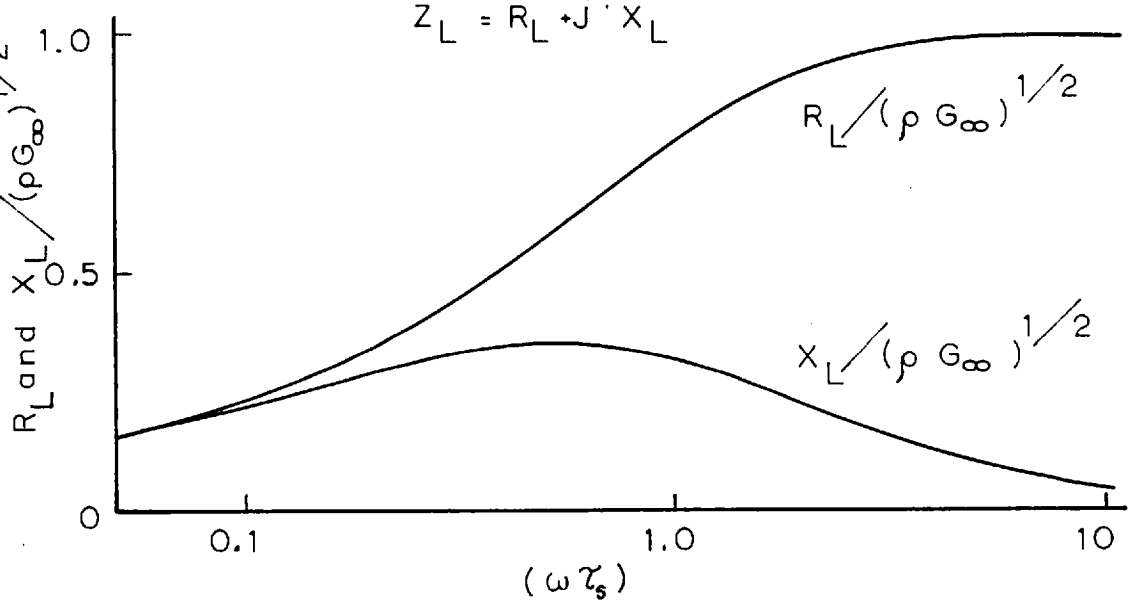

FIG.(2;4;2)

Theoretical variation of the normalised liquid shear impedance with frequency, for a single relaxation process.

while the phase constant approaches the value of:

$$\beta = \omega / (G_\infty / \rho)^{\frac{1}{2}} \qquad (2;4;22)$$

It is of interest to calculate the acoustic attenuation and skin depth of a liquid at very high frequencies: Thus for water having $\rho = 1$, $n = 0.01$ poise and $G_\infty \cong 10^{10}$ dynes/cm.^{2} equation (2;4;21) gives:

$$\alpha = (1 \times 10^{10})^{\frac{1}{2}} / 2 \times 0.01 = 5 \times 10^{6} \text{ nepers/cms}$$
$$\times 10^{7}$$
$$= 4.343 \text{ db./ cms.}$$

and so $\delta = 2 \times 10^{-7}$ cms.

For completely relaxed liquids having a viscosity of 100 poise the attenuation and skin depth are:

$$\alpha = 500 \text{ nepers/cms.} = 4.343 \times 10^{3} \text{ db./cms.}$$

$$\delta = 2 \times 10^{-3} \text{ cms.}$$

From the above sample calculations it may be concluded that even for completely relaxed liquids of relatively high viscosity, still only a very thin film of liquid is sufficient to act as an infinite medium.

The velocity of acoustic shear wave propagation through a completely relaxed medium may be obtained by inspection of equation (2;4;4) , and therefore:

$$C = (\omega_s \eta / \rho)^{\frac{1}{2}} = (G_\infty / \rho)^{\frac{1}{2}} \qquad (2;4;23)$$

and thus it can be seen that at very high frequencies the sound propagation velocity in a liquid is the same as through a purely solid substance.

2;5 (COMPLEX RIGIDITY MODULUS G^*)

Equation (2;3;16) may be written in the form:

$$\frac{T_{xy}}{S_{xy}} = \frac{j\omega \tau_s G_\infty}{(1+ j\omega \tau_s)} = G^* \qquad (2;5;1)$$

since $\eta / G_\infty = \tau_s = 1/\omega_s$ (2;3;15)

and where $G^* = G' + j\, G''$ (2;5;2)

and G^* is defined as the complex rigidity modulus.

Clearly $G' = G_\infty \omega^2 \tau_s^2 \; /(1+\omega^2\tau_s^2)$ (2;5;3)

and $G'' = G_\infty \omega \tau_s \; / (1+\omega^2\tau_s^2)$ (2;5;4)

For the low frequency case, ie: $\omega << \omega_s$ or $\omega \tau_s << 1$, equation (2;5;1) reduces to:

$$\frac{T_{xy}}{S_{xy}} = j\omega \tau_s G_\infty = j\omega \eta = G^* \qquad (2;5;5)$$

and thus η may be considered to be the static viscosity of the liquid.

The wave equation may now be expressed in terms of G^* and so from equation (2;4;2) :

$$\frac{\partial^2 u_x}{\partial^2 y} - \frac{\rho}{G^*} \frac{\partial^2 u_x}{\partial^2 t} = 0 \qquad (2;5;6$$

where now the velocity of propagation is given by:

$$C = (G^* / \rho)^{\frac{1}{2}} \qquad (2;5;7)$$

and therefore C must be complex.

The shear mechanical impedance as defined in equation(2;4;15) - now becomes:

$$Z_{o(L)} = \rho C = (\rho G)^{\frac{1}{2}} = (\rho(G' + j G''))^{\frac{1}{2}} \qquad (2;5;8)$$

thus:

$$R_L = \left(\frac{\rho G'}{2} \left((1+(G''/G')^2)^{\frac{1}{2}} + 1 \right) \right)^{\frac{1}{2}} \qquad (2;5;9)$$

$$X_L = \left(\frac{\rho G'}{2} \left((1+(G''/G')^2)^{\frac{1}{2}} - 1 \right) \right)^{\frac{1}{2}} \qquad (2;5;10)$$

Upon inserting the expressions for G' and G'' the above equations become :

$$R_L = \left(\frac{\rho G_\infty \omega^2 \tau_s^2}{2(1+\omega^2\tau_s^2)} \left((1+1/\omega^2\tau_s^2)^{\frac{1}{2}} + 1 \right) \right)^{\frac{1}{2}} \qquad (2;5;11)$$

$$X_L = \left(\frac{\rho G_\infty \omega^2 \tau_s^2}{2(1+\omega^2\tau_s^2)} \left((1+1/\omega^2\tau_s^2)^{\frac{1}{2}} - 1 \right) \right)^{\frac{1}{2}} \qquad (2;5;12)$$

Considering once again the low frequency case , ie: $\omega \tau_s << 1$, it is evident that:

$$R_L = (\omega \eta \rho / 2)^{\frac{1}{2}} \qquad (2;5;13)$$

and

$$X_L = (\omega \eta \rho / 2)^{\frac{1}{2}} \qquad (2;5;14)$$

while for high frequencies , ie: $\omega \tau_s >> 1$:

$$R_L = (\rho G_\infty)^{\frac{1}{2}} \quad \text{and} \quad X_L = 0 \qquad (2;5;15)$$

From equation (2;5;15) it may be seen that the limiting value of the rigidity modulus G_∞ can be obtained from a direct measurement of the shear mechanical impedance of a liquid, at very high frequencies. This particular aspect is one of the reasons why it is desirable to devise apparatus capable of obtaining these shear impedance measurements in the higher microwave frequency spectrum.

The dynamic liquid viscosity is usually defined as:

$$\eta_d = \frac{G''}{\omega} = \frac{G_\infty \tau_s}{(1+\omega^2\tau_s^2)} \qquad (2;5;16)$$

which approaches zero a high frequencies and the static viscosity η at low frequencies.

FIG.(2;5;1) depicts the variation of η_d with frequency.

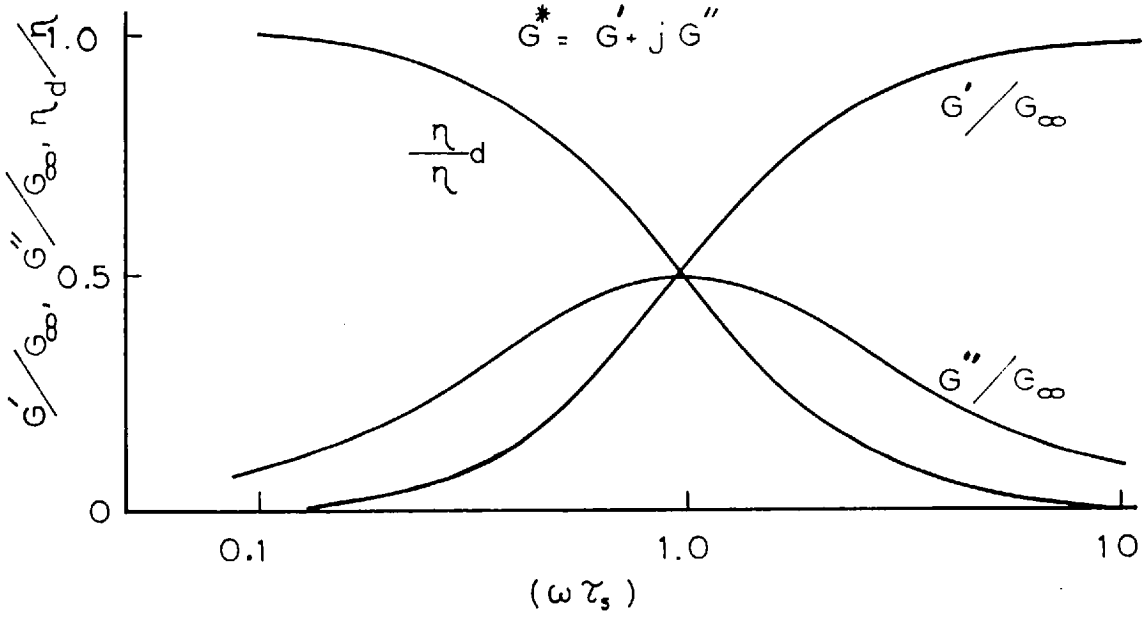

FIG. (2;5;1)

Theoretical variation of the normalised complex shear modulus and dynamic viscosity , with frequency , for a liquid having a single relaxation mechanism.

2;6 (REDUCTION PRINCIPLE)

Barlow ,(91), has extended the analysis of polymer relaxation devised by Tobolsky and Andrews ,(92), to show that in general relaxation theory it is possible to construct reduced functions with the salient experimentally measured properties of liquids, such as $R^2_{L/\rho}$ and $X^2_{L/\rho}$. The advantage of such reduced function formation is that all the experimental data obtained, for a given liquid, at different frequencies, temperatures and pressures, may be plotted on a single or " universal " curve.

It can be shown,(93), that provided the liquid parameters may be expressed as a function of temperature and pressure through the product of frequency and relaxation time , the reduction principle is valid. More precisely, a reduced function of the liquid parameters may be formed provided all the processes, which govern the mechanical properties of the particular liquid, have the same temperature and pressure dependence.

Thus for example if $$R' = R^2_L/\rho G_\infty = \frac{\omega^2\tau_s^2}{2(1+\omega^2\tau_s^2)}\left((1+1/\omega^2\tau_s^2)^{\frac{1}{2}} + 1\right)$$

is plotted against $(\omega\tau_s)$ a single curve results.

That the above is in fact the case is possibly more fully appreciated by examining the treatment given by Barlow,(91) , which is given here.

The temperature dependence of the limiting value of the rigidity modulus and relaxation time, at a particular temperature (T) , are expressed in terms of the temperature coefficient β and α as indicated below:

$$(G_\infty)_T = \beta\,(G_\infty)_{T_o} = \beta\, G_\infty(o) \qquad (2;6;1)$$

$$(\tau_s)_T = \alpha\,(\tau_s)_{T_o} = \alpha\,\tau_{s(o)} \qquad (2;6;2)$$

where T_o is the reference temperature.

Thus: $$(G')_T = \beta G_\infty(o) \frac{(\alpha\omega\tau_{s(o)})^2}{(1+(\alpha\omega\tau_{s(o)})^2)} = \beta(G')_{T_o} \quad (2;6;3)$$

similarly $$(G'')_T = \beta G_\infty(o) \frac{(\alpha\omega\tau_{s(o)})}{(1+(\alpha\omega\tau_{s(o)})^2)} = \beta(G'')_{T_o} \quad (2;6;4)$$

now $$(\eta)_T = \alpha\beta G_\infty(o)\tau_{s(o)} = \alpha\beta(\eta)_{T_o} \quad (2;6;5)$$

and so $$\alpha\beta = \frac{(\eta)_T}{(\eta)_{T_o}} \quad (2;6;6)$$

Equation (2;6;6) is quite general with respect to α and β and so these coefficients may be any function without invalidating the treatment. Barlow has indicated that as a first approximation it is permissible to let $\beta = 1$, since it represents the temperature dependence of the elastic modulus and hence should be negligible in comparison with α, the temperature coefficient of the molecular relaxation times.

It follows therefore that:

$$\alpha \cong (\eta)_T / (\eta)_{T_o} = (\tau_s)_T / (\tau_s)_{T_o} \quad (2;6;7)$$

In practice the values of $R_L/(p)^{\frac{1}{2}}$ and $X_L/(p)^{\frac{1}{2}}$ are plotted against $\log(\alpha f)$, where f is the operating frequency. FIG.(2;6;1) shows a typical plot of the reduced impedance functions. These impedance curves are then used to determine the real and imaginary parts of the complex rigidity modulus G^*, since from equation (2;5;8)

$$G^* = Z_L^2 / p = (R_L + j X_L)^2 / p \quad (2;5;8)$$

and so: $$G' = (R_L^2 - X_L^2)/p \quad (2;6;8)$$

while: $$G'' = 2 R_L X_L / p \quad (2;6;9)$$

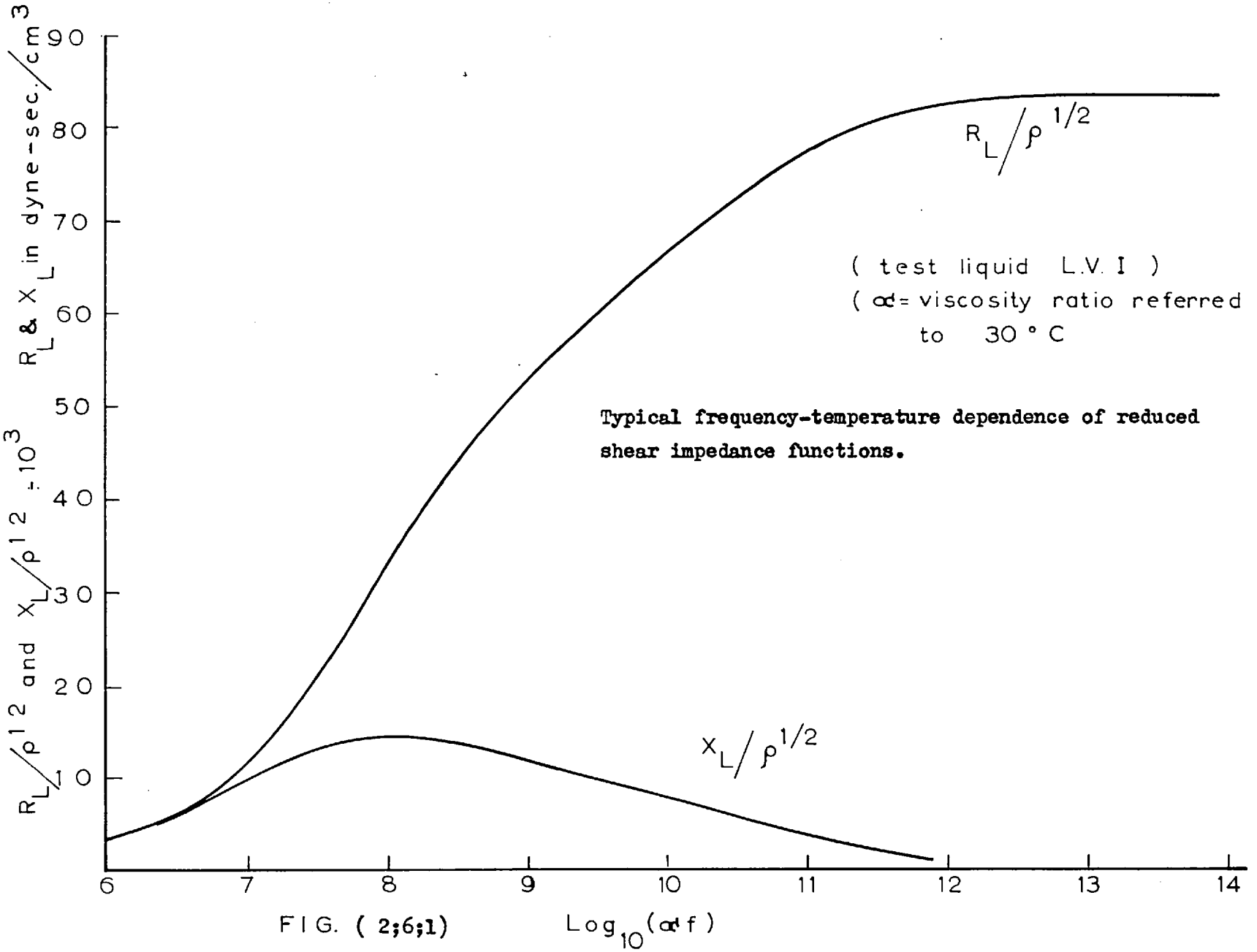

Typical frequency-temperature dependence of reduced shear impedance functions.

FIG. (2;6;1)

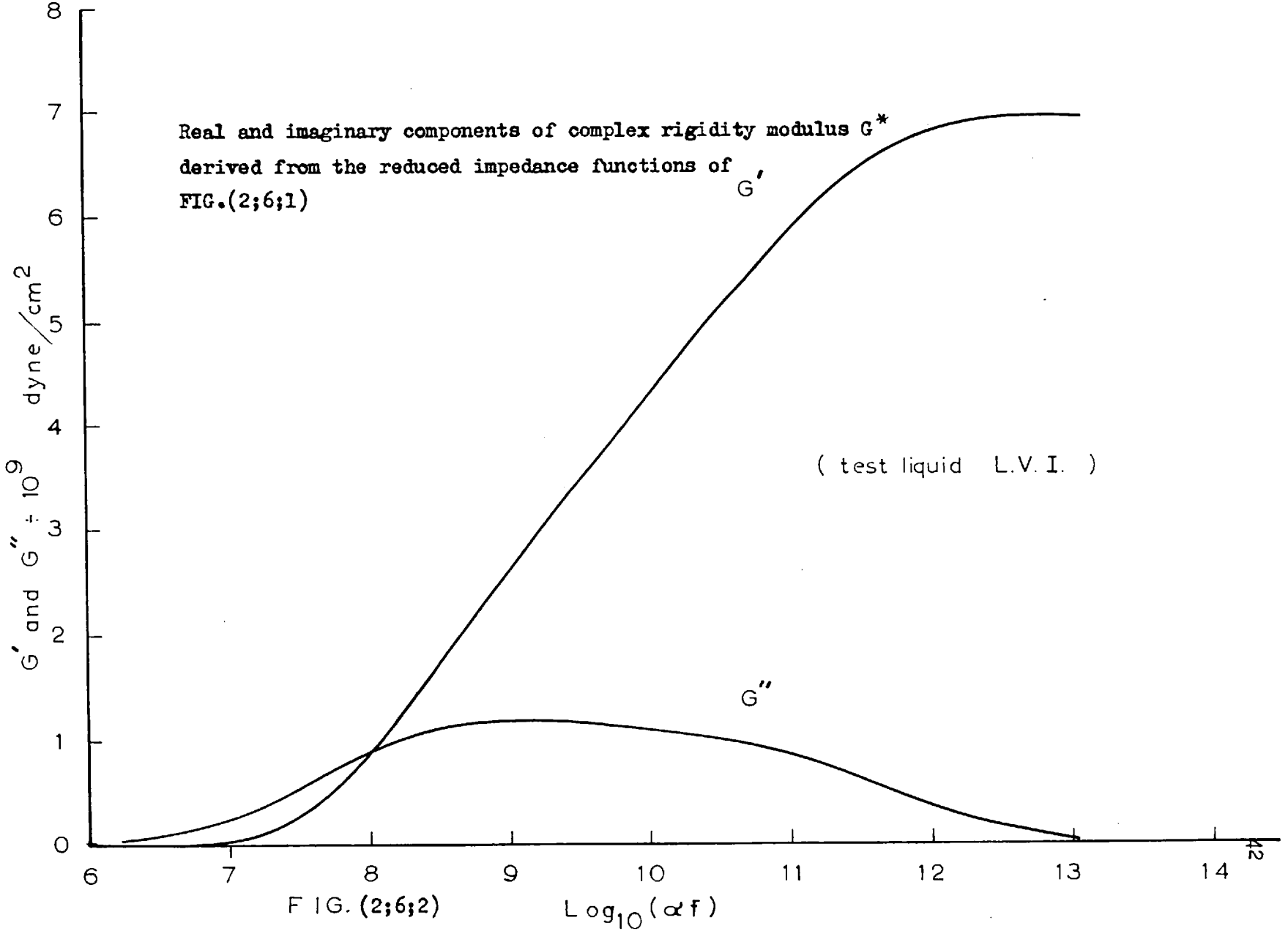
Real and imaginary components of complex rigidity modulus G*
derived from the reduced impedance functions of
FIG.(2;6;1)
G'
(test liquid L.V.I.)
G''
G' and G'' ÷ 10^9 dyne/cm^2
Log10(αf)
0
1
2
3
4
5
6
7
8
6
7
8
9
10
11
12
13
14

FIG. (2;6;2)

FIG.(2;6;2) shows typical real and imaginary components of the liquid rigidity modulus G^* derived from the reduced impedance functions of FIG.(2;6;1).

2;7 (DISTRIBUTION OF RELAXATION TIMES)

It is found that plotting of the reduced functions, for a particular liquid , does not generally give the same curve as expected from calculations based on equation (2 ; 4; 19) , which assumes a single relaxation mechanism .

Gross,(94), and others have shown that it is possible to obtain good agreement between experiment and theory if a " distribution of relaxation times " is postulated, such that there are n discrete processes which collectively contribute to the total shear rigidity modulus G^*. This situation is illustrated graphically in FIG.(2;7;1), as a general Maxwell model consisting of numerous single elements connected in parallel, each elements being characterised by a different static viscosity and limiting rigidity modulus. The transmission line model for an infinite volume of liquid having n discrete relaxation times is given in FIG.(2;7;2).

The **existence** of a distribution of relaxation times may be visualised by considering the process of molecular flow described earlier asa **preferred** direction of molecular jumps from equilibrium position to equilibrium position. For such molecular jumps to occur it is necessary for the molecules to accumulate sufficient thermal energy to overcome the potential barriers constraining them. Thus in general , the finite time period required for a particular molecule to attain its threshold energy level may be considered as constituting the molecular relaxation time τ_s . This life time τ_s is dependent on the potential barrier ΔF and is given by the expression :(95).

$$\tau_s = \underline{\tau}_o \; e^{\Delta F / R_t T} \qquad (2;7;1)$$

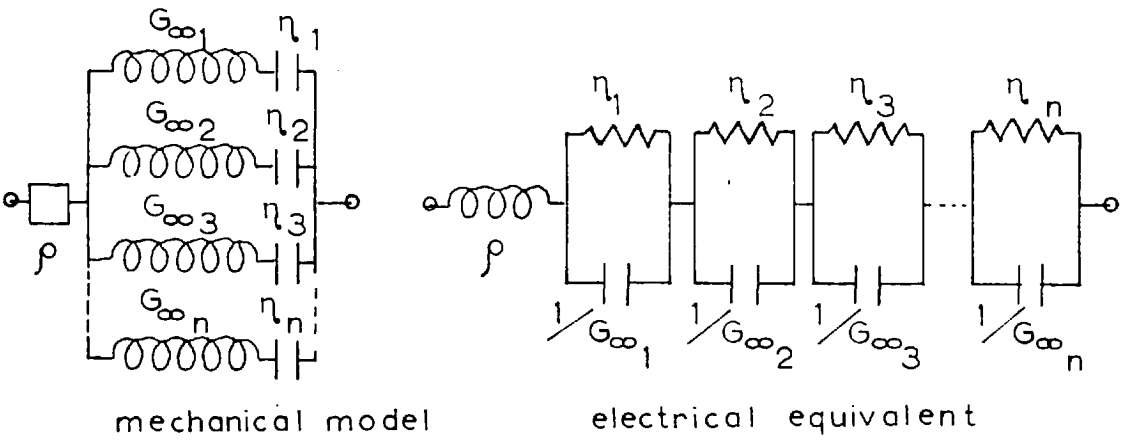

FIG. (2; 7;1)

Model of general Maxwell element having n relaxation times.

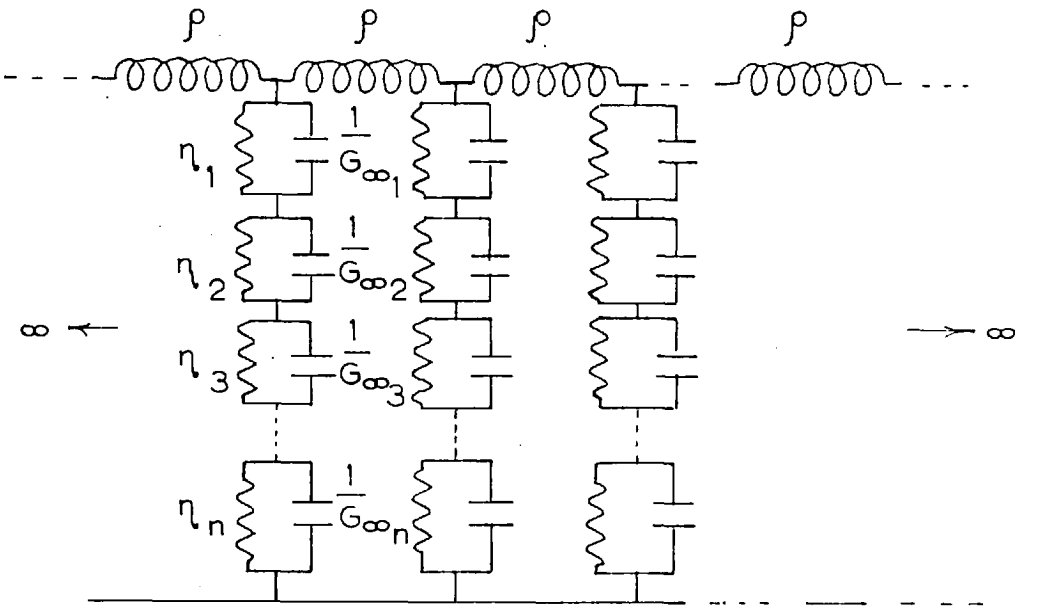

FIG. (2;7;2)

Electrical transmission line model for an infinite volume of fluid having n discrete relaxation times.

where τ_o is the molecular oscillation period in a particular equilibrium, T is the absolute temperature and R_l is the equivalent of the gas constant for a liquid.

Obviously the life time of individual molecules in a given liquid will be different since ΔF, the molecular potential well, changes from one molecular site to another being dependent on the number of nearest neighbours and their respective orientations. Liquid structure theory developed by Green,(96) and experimentally substantiated by X ray investigations , strongly supports the assumption of inconsistent molecular environment, and hence in general the existence of a distribution function of relaxation times characterising a liquid is to be expected.

It follows from the foregoing discussion that in general equation (2;5;1) should be written as:

$$G^* = \sum_{n=o}^{\infty} \frac{j\omega\tau_n \; G_\infty(n)}{(1+ j\omega\tau_n)} \qquad (2;7;2)$$

where the summation indicates a continuous distribution of relaxation mechanisms each being characterised by a shear rigidity modulus $G_\infty(n)$ and a relaxation time τ_n

Equation (2;7;2) may be written in slightly modified form by normalising $G_\infty(n)$ and τ_n with respect to G_∞ and τ_s respectively. (98).

Thus: $$G_\infty(n) = g(n)\, G_\infty \qquad (2;7;3)$$

and $$\tau_n = q\, \tau_s \qquad (2;7;4)$$

where now τ_s may be considered to be the average relaxation time. Thus equation (2;7;2) may be written as:

$$G^* = \int_o^{\infty} \frac{G_\infty\, j\omega\tau_s\, q}{(1+ j\omega\tau_s\, q)} \left\{ g_{(q)} \right\} dq \qquad (2;7;5)$$

where ($g_{(q)}$) may be considered to be the distribution function of relaxation times normalised with respect to τ_s .

Barlow has indicated that it is more convenient to express equation(2;7;5) as : (111) .

$$G^* = \int_{-\infty}^{\infty} \frac{G_\infty \, j\omega \tau_s \, q}{(1 + j\omega \tau_s \, q)} \left\{ g_{(\log(q))} \right\} \, d\,(\log(q)) \qquad (2;\ 7;6)$$

which when separated into real and imaginary parts yields:

$$G' = \int_{-\infty}^{\infty} \frac{G_\infty \omega^2 \tau_s^2 \, q^2}{(1 + \omega^2 \tau_s^2 \, q^2)} \left\{ g_{(\log(q)} \right\} \, d\,(\log(q)) \qquad (2;\ 7;7)$$

and

$$G'' = \int_{-\infty}^{\infty} \frac{G_\infty \omega \, \tau_s \, q}{(1 + \omega^2 \tau_s^2 \, q^2)} \left\{ g_{(\log(q)} \right\} \, d\,(\log(q)) \qquad (2;\ 7;8)$$

where now ($g_{(\log(q)}$) is considered to be the distribution function.

Equations (2;7;7 and 8) may also be expressed in terms of the relaxation frequence f_s through the use of equation (2;3;18). Consequently :

$$G' = \int_{-\infty}^{\infty} \frac{G_\infty \, f^2 \, q^2}{(f_s^2 + f^2 q^2)} \left\{ g_{(\log(q)} \right\} \, d\,(\log(q)) \qquad (2;\ 7;9)$$

and

$$G'' = \int_{-\infty}^{\infty} \frac{G_\infty \, f \, f_s \, q}{(f_s^2 + f^2 q^2)} \left\{ g_{(\log(q)} \right\} \, d\,(\log(q)) \qquad (2;\ 7;10)$$

2;8 (DERIVATION OF DISTRIBUTION FUNCTION OR RELAXATION SPECTRUM)

It is desirable to determine the distribution function since it completely specifies the behaviour of a particular fluid, Several methods, both analytical and numerical , have been developed by which this distribution function or relaxation spectrum may be obtained from experimental data . (99). Restriction is however here made to a basically numerical method developed by Alfrey,(100) , and further extended by Barlow,(99). Barlow's derivation is given below:

Equation (2;7;9) may be written as:

$$G' = \int_{-\infty}^{\infty} G_{\infty} \left\{ g_{(\log(q))} \right\} \frac{f^2}{f_n^2 + f^2} \quad d(\log(q)) \qquad (2;8;1)$$

through substitution of the expression for q from equation(2;7;4) since:

$$q = \tau_n / \tau_s = f_s / f_n$$

where f_n is the relaxation frequency of the n th relaxation process.

Now for conditions such that $f \gg f_n$, the term $\frac{f^2}{f_n^2 + f^2}$ approaches 1 . While for $f \ll f_n$, $\frac{f^2}{f_n^2 + f^2} = 0$.

Consequently as a first approximation:

$$G' = \int_{-\infty}^{q} G_{\infty} \left\{ g_{(\log(q))} \right\} \quad d(\log(q)) \qquad (2;8;2)$$

where the term $f^2/(f_n^2 + f^2)$ has been replaced by a unit step function at frequency f.

It follows that equation (2;8;2) may be differentiated with respect to q and so :

$$\frac{d(G')}{d(\log(q))} = G_{\infty} \left\{ g_{(\log(q))} \right\}$$

Thus it can be seen that a first approximation to the distribution function is obtained from the slope of the G' curve when plotted against $\log(f)$. Having obtained this first approximation a new curve of G' is then calculated using equation (2;7;9). This calculated G' curve is then compared with the experimental G' curve and their difference used to construct yet another curve. The slope of this difference curve is treated as a correction term to be added to the original spectrum approximation. The same process is then repeated until the desired similarity exsists between the recalculated and experimental G' curves.

A typical relaxation spectrum is shown in FIG.(2;8;1)

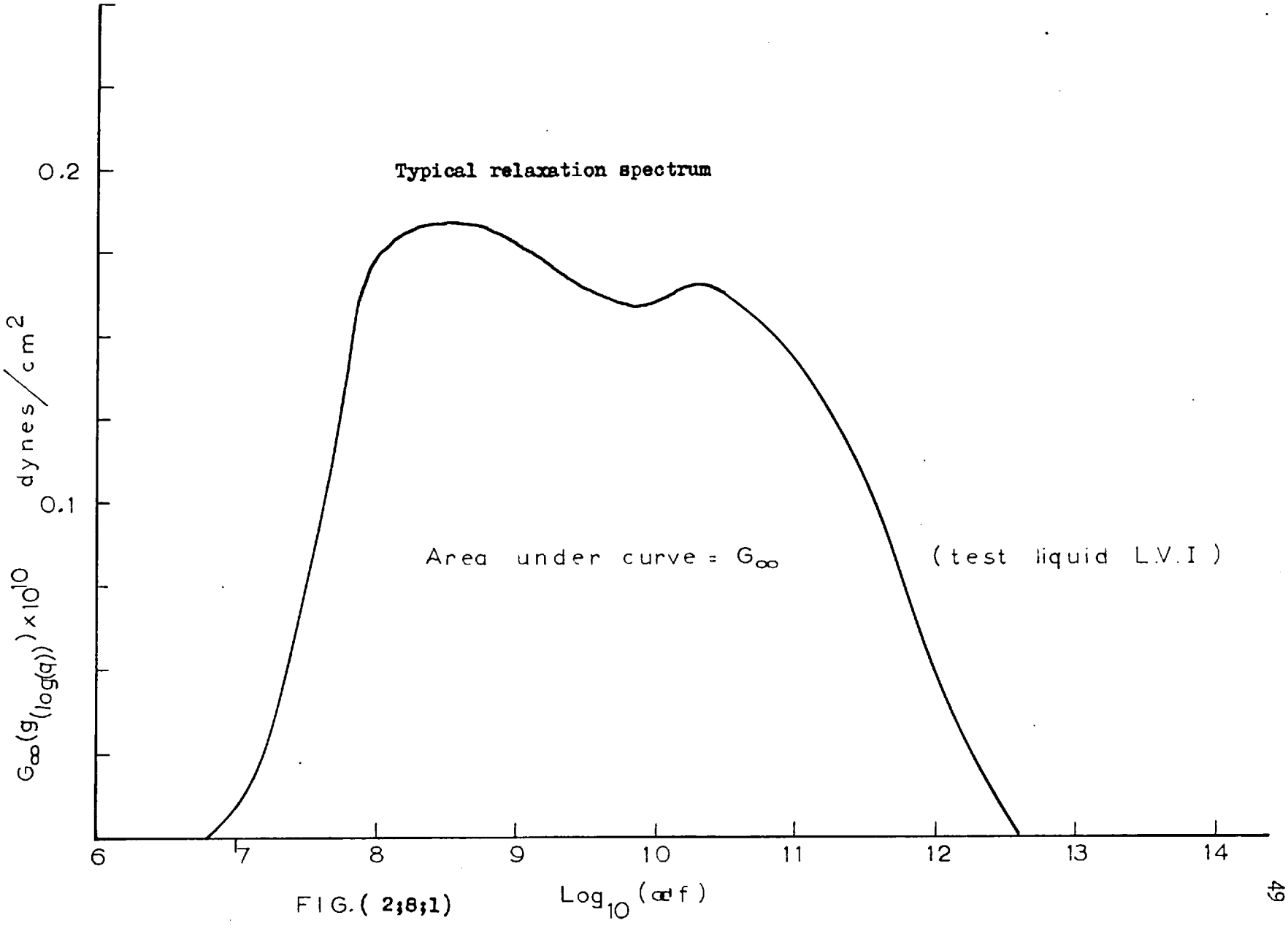
Typical relaxation spectrum
0.2
0.1
$G_\infty(g_{(\log(q))}) \times 10^{10}$ dynes/cm^2
Area under curve = G_∞
(test liquid L.V.I)
6
7
8
9
10
11
12
13
14
$\log_{10}(\omega f)$

FIG.(2;8;1)

PART II

" EXPERIMENTAL SYSTEM "

Part II of this work , comprised of chapters, 3 to 11 , is concerned with the development of a system for the study of viscoelastic relaxation phenomenon in liquids at 3000 megacycles.

CHAPTER 3

DESCRIPTION OF APPARATUS

3;1 (INTRODUCTION)

The experimental system developed in this work was composed of such a large number of individual items, whose functions were in most cases so closely interdependent, that it is difficult to discuss them separately. Collective description however would only lead to confusion , and so an attempt will be made to partition the system into four basic units and to discuss the overall system operation with respect to these four units. After considering the purpose and function of the basic units , the design , construction and performance of their constituents will be investigated.

3;2 (GENERAL DESCRIPTION OF APPARATUS)

The four basic units comprising the experimental system are shown in FIG.(3;1;1) . The microwave transmitter was used to generate high powered, high frequency , narrow pulses of electromagnetic energy which were coupled through the microwave bridge to both test and reference microwave ultrasonic transducers. The function of the ultrasonic transducers was to transform this electromagnetic radiation into mechanical energy. Shear mechanical vibrations propagating in single crystal piezoelectric quartz media, were the form of mechanical energy of particular interest in this work, as these propagating waves were utilised in the measurement of the shear mechanical impedance of liquids. The reference ultrasonic transducer was used, as the name implies, to provide a standard against which the effects introduced,by the application of the test liquid to the test ultrasonic transducer , could be compared. It follows therefore that the purpose of the microwave bridge was to balance the response of the test transducer against that of the reference transducer, and this was accomplished through appropriate insertion of attenuation and

phase shift into the bridge arms. The microwave receiver was used only to determine bridge balance.

Unfortunately due to the very poor efficiency of the microwave ultrasonic transducers, it has been found necessary to develop a very elaborate system in order that the required accuracy of measurement be achieved.

The deficiency of the quartz transducer was twofold, namely very poor electromechanical conversion efficiency,(-85 db), and very high acoustic attenuation within the transducer material, (20 db/cm.). These two factors therefore stipulated that a high powered transmitter and,or, a highly sensitive receiver be utilised. Unfortunately the peak power handling capacity of the precision rotory attenuator used in the microwave bridge precluded the use of pulsed powers above 25

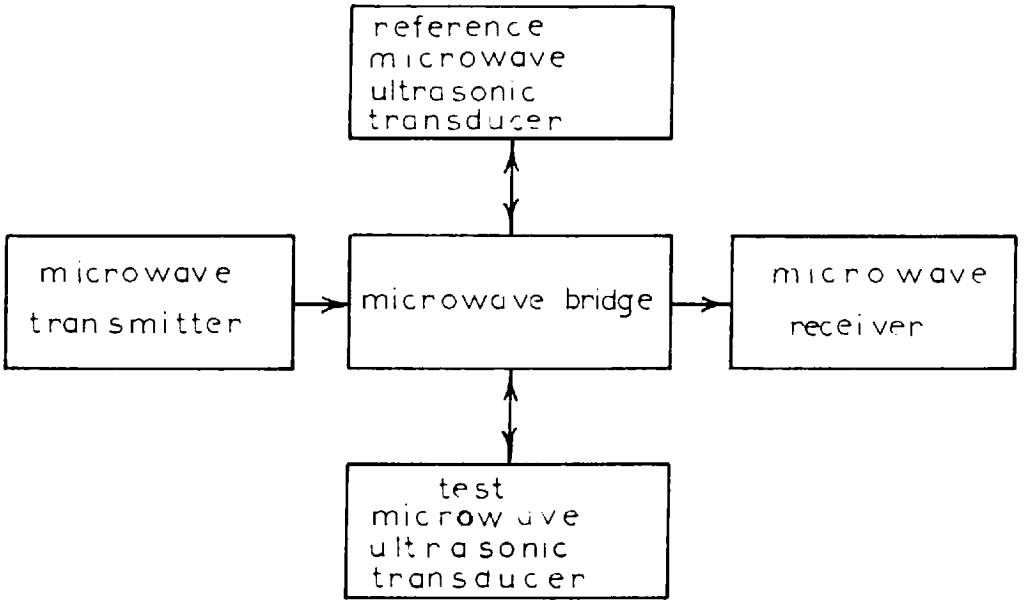

FIG. (3;1;1)

Block diagram of four basic system units.

kilowatts. In addition the ionisation level of the transducer environment also imposed an upper limit on the peak pulsed electromagnetic power. Initially the ionisation level restricted the usable power to a relatively low value, however introduction of a controlled environment technique raised the limit to a level approaching that of the rotory attenuator. Being thus restricted to a comparatively low peak pulsed power level it was imperative that a highly sensitive receiver be constructed. In point of fact it was finally necessary to resort to the complexity of parametric amplification to achieve the required receiver sensitivity.

It should be noted here that the system was almost entirely fabricated from " S " band No.10 waveguide, the reason being that the high precision components required in the system could only be realised in waveguide.

FIG.(3;2;1) represents the complete schematic diagram of the microwave ultrasonic system and as such contains all the individual items used. Following the four unit classification adopted in section (3;1;1) , the articles of apparatus are itemised as given below:

1. MICROWAVE TRANSMITTER

(1). Second time base of Tektronix 585 oscilloscope.
(2). Low level millimicrosecond pulse generator.
(3). High level , line type pulse generator.
(4). Modulator.
(5). High voltage modulator power supply.
(6). Magnetron and associated equipment.
(7). Launching section.
(8). Waveguide twist section.
(9). Precision attenuator and R.F. power monitor.
(10). Waveguide bend.

SCHEMATIC DIAGRAM OF MICROWAVE ULTRASONIC SYSTEM

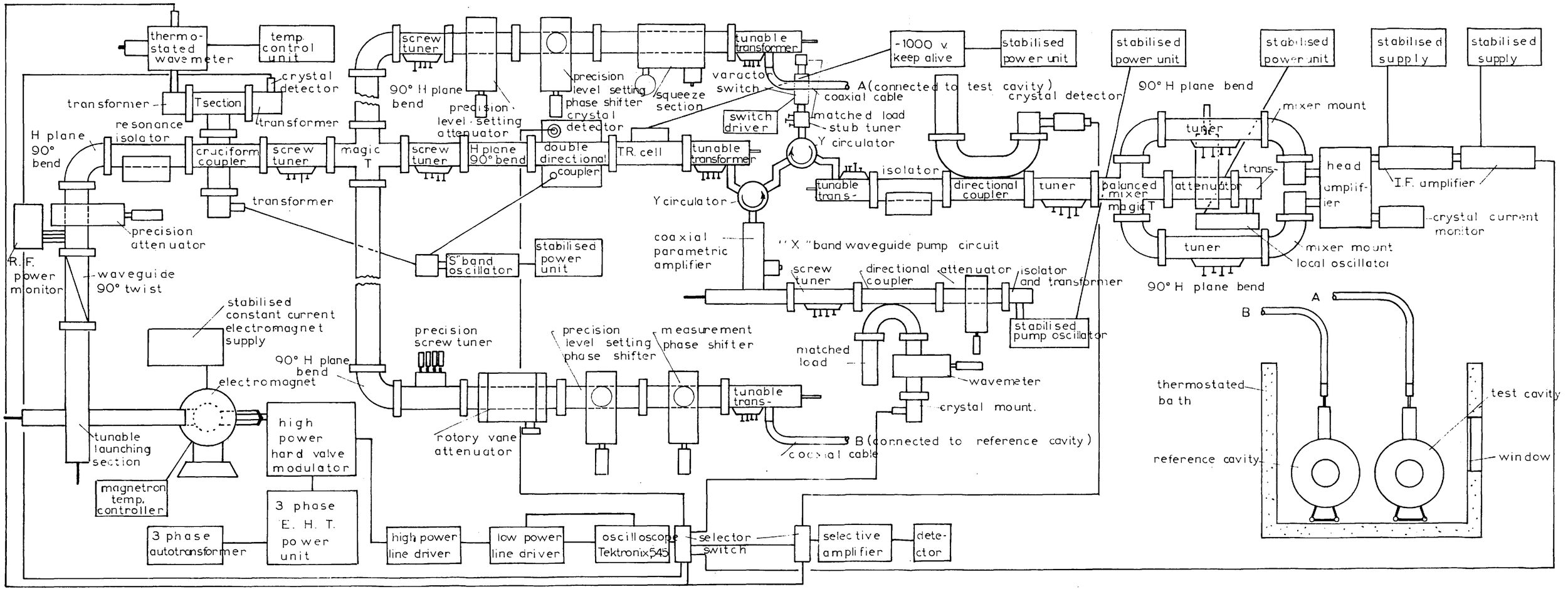

FIG.(3;2;1)

(11). Ferrite resonance isolator.
(12). Magnetron frequency and pulse shape monitor system.
(13). Ultrasonic cavity alignment and test system.

2. MICROWAVE BRIDGE.

(1). 4 screw tuner.
(2). Magic T.
(3). Bridge test and reference channels.

BRIDGE REFERENCE CHANNEL

(1). H plane bend.
(2). Precision tuner
(3). Precision rotory attenuator.
(4). Precision phase shifter.
(5). Precision phase shifter.
(6). Tunable waveguide to coaxial transformer.

BRIDGE TEST CHANNEL

(1). H plane bend.
(2). 4 screw tuner
(3). Precision attenuator.
(4). Precision phase shifter.
(5). Precision phase shifter.
(6). Tunable waveguide to coaxial transformer.

3. TEST AND REFERENCE MICROWAVE ULTRASONIC TRANSDUCERS.

(1). Loop coupled resonant radial cavity.
(2). Piezoelectric single crystal quartz disk.

4. MICROWAVE RECEIVER.

(1). 4 screw tuner.
(2). Double directional coupler.
(3). T.R. cell.
(4). Tunable waveguide to coaxial line transformer.
(5). Strip line Y circulator.
(6). Parametric amplifier and associated equipment.
(7). Strip line Y circulator.
(8). Coaxial varactor switch and associated equipment.
(9). Tunable coaxial line to waveguide transformer.
(10). Ferrite resonance isolator.

(11). Parametric amplifier test and alignment monitor.
(12). 4 screw tuner.
(13). Magic T. of balanced mixer.
(14). Local oscillator channel
  (1). Variable attenuator.
  (2). Waveguide to coaxial line transformer.
  (3). Klystron local oscillator.
  (4). Stabilised local oscillator power unit.
(15). Balanced mixer channels.
  (1). H plane bends.
  (2). 4 screw tuner.
  (3). H plane bends.
  (4). Mixer mounts.
(16). Crystal current monitor.
(17). Head amplifier.
(18). First intermediate amplifier.
(19). Second intermediate amplifier.
(20). Tektronix 585 oscilloscope.

3;3 (GENERAL DESCRIPTION OF SYSTEM COMPONENTS AND OPERATION)

The second time base of a 585 Tektronix oscilloscope was utilised as the main trigger generator to initiate the sequence of events which comprised one cycle of system operation. This time base was synchronised to the supply frequency but still could give variable pulse repetition frequency above or below mains frequency. The output from this time base was used to trigger a low level "line type", millimicrosecond pulse generator, which in turn was used to fire the hydrogen thyratron of the following " high level" line type pulse generator.

The high voltage pulse obtained from the " high level" line driver, was used as the main grid drive for the "hard valve" modulator

switch tubes, which in turn produced a very high voltage negative pulse to drive the M type magnetron, which was directly coupled to it.

Electromagnetic energy was coupled from the coaxial output of the magnetron to the main "S" band waveguide channel by means of a specially designed launching section. Output from the magnetron was in the form of pulses of 0.35 microseconds length and 250 kilowatts maximum peak power.

A precision attenuator was inserted at this point in the system to enable the optimum power level in the waveguide channel to be established and still maintain magnetron operation near full power and highest stability condition. It was found necessary to incorporate an electromagnetic magnetron biasing system in order to achieve adequate stability under the short pulse operation. It was also necessary to provide a thermostating system for the magnetron body so as to minimise frequency drift due to variations in ambient room temperature. An R.F. mean power level monitor was incorporated into the same body as the attenuator, to provide a means of determining satisfactory magnetron performance.

The next item in the system was a 90 degree H plane waveguide bend, which was inserted merely to properly orient the layout of the apparatus.

The following item was a ferrite resonance isolator, whose purpose it was to present, at all instances, a proper impedance match to the magnetron , so as to produce optimum performance. In addition the isolator was required to function as an extremely well matched load for the waveguide bridge , which was coupled into the system further on.

At this point it was found desirable to include a monitoring system for both magnetron frequency and pulse shape. This was accomplished through the insertion of a highly directional , twin port,

crossed coupler into the main waveguide channel, one auxiliary arm of which was connected to both a broad band waveguide crystal mount and a high Q "S" band wavemeter, by means of a T junction. The outputs of both wavemeter and crystal mount were viewed on an oscilloscope. The second auxiliary arm of the crossed directional coupler was connected to a low power " S " band oscillator. In this way it was possible to inject a low level test signal into the system at the same frequency as the magnetron and hence facilitate alignment. This facility was of special importance in tuning the ultrasonic transducer cavities to resonance.

The main output from the directional coupler was applied to a " magic T ", which has been rendered truly magic at the system operating frequency through the action of two, four screw tuners, one on the input H plane arm and the other on the E plane arm. This magic T served as the main bridge element of the system, having one of its symmetrical H plane arms connected to the test channel and the other connected to the reference channel. The E plane arm of the magic T was coupled to the microwave receiver, which served as the detector for the bridge .

The reference bridge channel had incorporated into it, a four screw tuner, a precision vane attenuator, a precision phase shifter, a squeeze section and a tunable waveguide to coaxial line transformer. The purpose of the tuner was to match out any small standing wave which might be present in the reference channel, while the attenuator and phase shifters were used to set the level of attenuation and phase in the same channel. The object of the tunable transformer was to terminate the waveguide run and to transform the pulsed electromagnetic energy from the waveguide through a three foot length of precision coaxial cable to the reference microwave ultrasonic transducer.

This microwave ultrasonic transducer was in fact a re-entrant hybrid,radial, resonant microwave cavity containing a single crystal disk of piezoelectric quartz, in which travelling mechanical shear waves at 3020 megacycles were generated through a piezoelectric surface effect.(See appendix (D;8) for detailed analysis.)

Similarly the test channel of the microwave bridge contained a precision four screw tuner, a precision rotory attenuator, two precision phase shifters and a tunable waveguide to coaxial line transformer. Here the function of the precision tuner was to tune out the mismatch introduced by the rotory attenuator. The rotory attenuator on the other hand was used as the main attenuation measurement device, having high reset and measurement accuracy. Of the two phase shifters present in the test channel only one was accurately calibrated and used in the measurement of small phase shifts , the other being used as a level setting device. As in the case of the reference channel, the test arm of the microwave bridge terminated in another resonant microwave cavity , identical to that in the reference channel.

The purpose of both test and reference cavities was to apply an R.F. voltage pulse of 3020 Mcs. across the face of a specially cut BC. single crystal of piezoelectric quartz. This pulsed electric field induced polarisation charges at the crystal surface which resulted in a displacement of the center of gravity of the crystal molecules. The molecular displacement then generated a shear mechanical wave which propagated through the remainder of the disk. Upon arrival of this elastic wave at the other crystal face, the reverse process occured , and so the cavity was re-excited with a pulse of R.F. after a period of time corresponding to the one way travel time of the mechanical wave through the quartz disk. When ever this travelling acoustic wave was incident upon one of the crystal surfaces, not only was the cavity re-excited electrically but the acoustic wave itself was reflected back along its original path towards the surface of

generation, the magnitude and phase of the reflected wave being determined by the shear mechanical impedance of the medium in contact with the crystal surface. It follows that since the acoustic wave was reflected back within the crystal when ever it was incident upon either of the surfaces, and also since the cavity was re-excited electrically at each reflection, an exponential decay pattern of pulses or " echoes " was obtained from the cavity as the acoustic wave bounced back and forth between the crystal surfaces, and was gradually attenuated. The exponential decrease in the amplitude of successive echoes was due to the intrinsic acoustic attenuation of the quartz medium, which was found to be approximately 14.6 db. per centimeter of acoustic path length, corresponding to a decrease in amplitude of about 4.4 db. between consecutive echoes for the crystal disk used. FIG.(3;3;1) indicates the type of response obtained from one of the microwave ultrasonic transducer cavities .

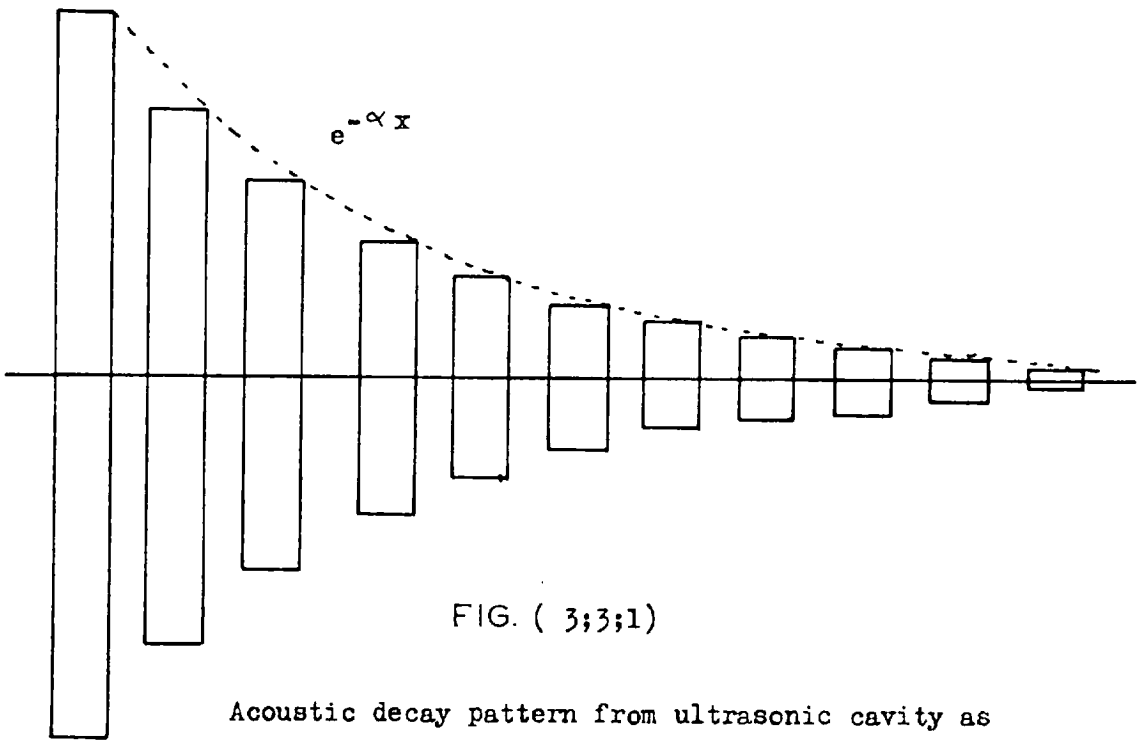

FIG. (3;3;1)

Acoustic decay pattern from ultrasonic cavity as seen on oscilloscope.

It should be noted at this point that since both the microwave resonant cavity and the quartz crystal were symmetrical, an acoustic wave was generated at each surface and these waves propagated within the crystal in phase.

Since the amplitude and phase of each of the reflected pulses, or echoes, was a function of the crystal terminating impedance, it was possible to measure the shear mechanical impedance of various liquids merely by " loading" or applying these liquids to the surface of the crystal in the test cavity and noting the change in the acoustic decay pattern, with respect to the decay pattern of the " unloaded " reference cavity. (See appendix (D;7) for mathematical justification of measurement technique.)

As a result of the high acoustic attenuation in the quartz medium and the corresponding rapid deterioration of signal to noise ratio with increasing echo number, it was found necessary to construct a very low noise receiver system in order to obtain a sufficient number of echoes , of amplitude far enough above noise level so that the desired accuracy of measurement could be achieved. This receiver system was directly coupled to the E plane arm of the bridge magic T, immediately following a four screw tuner, included at this point to render the bridge T truly magic at the operating frequency.

A double directional coupler followed the tuner in the receiver channel, this item being incorporated for the purpose of testing the receiver and monitoring power coupled to the receiver arm during the main transmitter pulse. In addition this directional coupler was used to observe the power reflected from the " T.R " cell, which was next in series.

The " T.R. cell " , a special fast recovery ionisation cell, was used to protect the sensitive receiver units from damage during the

high powered main transmitter pulse, by effectively short circuiting the receiver waveguide input.

Next in line came a tunable waveguide to coaxial line transformer, which was directly coupled to a strip line Y circulator. The Y circulator functioned to isolate the input and output of a low noise,coaxial, parametric amplifier, which was built into the receiver system when it became obvious that a conventional low noise balanced mixer superhetrodyne reciver was inadequate.

This parametric amplifier , which was pumped by a suitably isolated, highly stable " X " band oscillator, had a single side band noise figure of some 3 db, under conditions of 20 db gain and 20 megacycles bandwidth. Excellent long term stability was a particularly useful feature possessed by the above amplifier, such that re-alignment was seldom required , only slight monthly adjustments of pump frequency and power level being necessary. A self contained parametric amplifier alignment and monitoring system however was built into the receiver unit to enable observation of amplifier performance to be speedily achieved and realignment quickly performed, should such be required.

A coaxial,R.F.,receiver isolation switch unit was inserted immediately following the parametric amplifier to provide additional isolation for the main receiver assembly during the high powered transmitter pulse. This R.F. switch unit consisted of a second Y circulator, a coaxial varactor switch,operating in the circulator mode, a coaxial multi screw tuner and a coaxial matched termination. A transistorised pulser having very low output impedance was used to activate the R.F. switch.

Another tunable coaxial line to waveguide transformer was incorporated at this point to convert the receiver channel back to " S " band waveguide since the remainder of the receiver had been

built in waveguide.

A ferrite resonance isolator was next coupled into the system to isolate the parametric amplifier from any local oscillator power which might be present.

The following item in the layout was the parametric amplifier alignment and monitoring system refered to previously. This unit also provided a means of testing the balanced mixer receiver unit independently of the parametric amplifier.

The main part of the balanced mixer unit was next in line, being basically another matched magic T and two waveguide mixer crystal mounts. These mixer mounts were coupled to each of the symmetrical H plane arms of the hybrid junction. The mounts were well matched and suitably oriented through the use of two stub tuners and four 90 degree H plane bends , such that their I.F. output terminals were in close proximity. The mixers were mounted in this manner so as to arrive at a condition where there was the absolute minimum length of line between the mixer outputs and the head amplifier input. It was found necessary to employ stub tuners in the mixer arms since the individual mixers were not sufficiently well matched or identical to arrive at a condition of R.F. and I.F. impedance balance. In addition the mixer crystals used were sufficiently dissimilar to introduce appreciable unbalance.

Local oscillator power, derived from a suitably stabilised " S " band klystron, was injected into the balanced mixer through a variable attenuator inserted in the other H plane arm of the four terminal T.

The signal was coupled into the balanced mixer assembly through the E plane arm of the junction.

The mixer I.F. output terminals were coupled into a highly screened inclosure containing the crystal current monitoring apparatus and a low noise head amplifier.

Both second and third intermediate frequency amplifiers were inserted at this point. The undemodulated output of the third amplifier was then viewed directly on the C.R.T. of a 585 Tektronix oscilloscope, the same oscilloscope incidently whose second time base originally triggered the millimicrosecond pulse generator.

In condensed form the system operating sequence was as follows:

The oscilloscope triggered the microwave transmitter, which then pulse excited both test and reference ultrasonic transducer cavities by way of the microwave bridge. This high powered, pulsed, cavity excitation set up travelling acoustic waves within the quartz crystals, and these acoustic waves in turn periodically re-excited the cavities electrically such that an exponential decay pattern of echoes was obtained from each cavity. These two separate decay patterns were then compared and balanced in the microwave bridge, the receiver and oscilloscope being used to indicate a balanced condition. Application of a test liquid to the surfaces of the test quartz transducer then unbalanced the bridge. Balance was then restored through insertion of attenuation and phase shift in the test arm of the bridge. The values of differential attenuation and phase shift required to restore bridge balance were then used to calculate the complex shear impedance of the liquid under test.

CHAPTER 4

DETAILED ANALYSIS OF INDIVIDUAL COMPONENTS IN TRANSMITTER UNIT

4;1 (GENERAL)

A detailed analysis of the individual components constituting the basic microwave transmitter unit will now be given. These items will be considered, where appropriate, with respect to:

(a). Reason for inclusion in the system
(b), Design and construction
(c). Performance.

4;2 (Oscilloscope)

A Tektronix 585 oscilloscope, having a bandwidth of D.C. to 30 megacycles was used both to initiate the transmitter pulse and to display the train of received echoes. Several other types of oscilloscopes were tried but were found to be unsatisfactory for one or more of the following reasons.

(1). Saturation and or, blocking of the main time base sweep generator, due to intense radiation emitted from the modulator and associated driving equipment.

(2). In ability of sweep to start sufficiently quickly to enable the fast rising portion of the trigger and driver as well as main transmitter pulses to be observed.

(3). Insufficient rise time and bandwidth to allow accurate observation of leading and trailing edges of various pulses.

The 585 Tektronix oscilloscope however to meet all requirements and this was the reason for its inclusion in the system.

Another feasure of this oscilloscope which was exploited was the second time base. This second time base can be utilised as an

auxilary trigger generator whose pulse repetition frequency is continuously variable from one to several hundred pulses per second. In this respect the time base was used as the trigger generator which initiated the system sequence by triggering off the low level pulse generator. The reason for requiring a variable P.R.F. was associated with the maximum permissible mean R.F. power level which could be tolerated in the ultrasonic cavities. This particular aspect is discussed in section (10;5).

4;3 (LOW LEVEL PULSE GENERATOR)

The main purpose of this pulse generator was to act as trigger source for the modulator " line driver ". The requirements imposed on this trigger were as follows.

(1). Fast rise, required so as to obtain maximum rate of rise from the hydrogen thyratron, which it fired.

(2). Low output impedance, this being also dictated by the thyratron.

(3). Generator had to be capable of withstanding the sudden, high voltage spike associated with the grid drive conditions on the thyratron.

Operation of Device

Refering to the circuit diagram of the low level pulse generator given in FIG.(4;3;1), when the selector switch was in the external trig position, the triggering pulse of approximately three volts, derived from the oscilloscope, was coupled to the grid of valve (V_{1a}) which acted as a trigger amplifier, having 10 db. gain. This amplified trigger was then inverted by (V_{1b}) and then applied to the grid of (V_{2a}), which was part of a monostable multivibrator. The flip flop action obtained from the multivibrator produced a positive pulse of

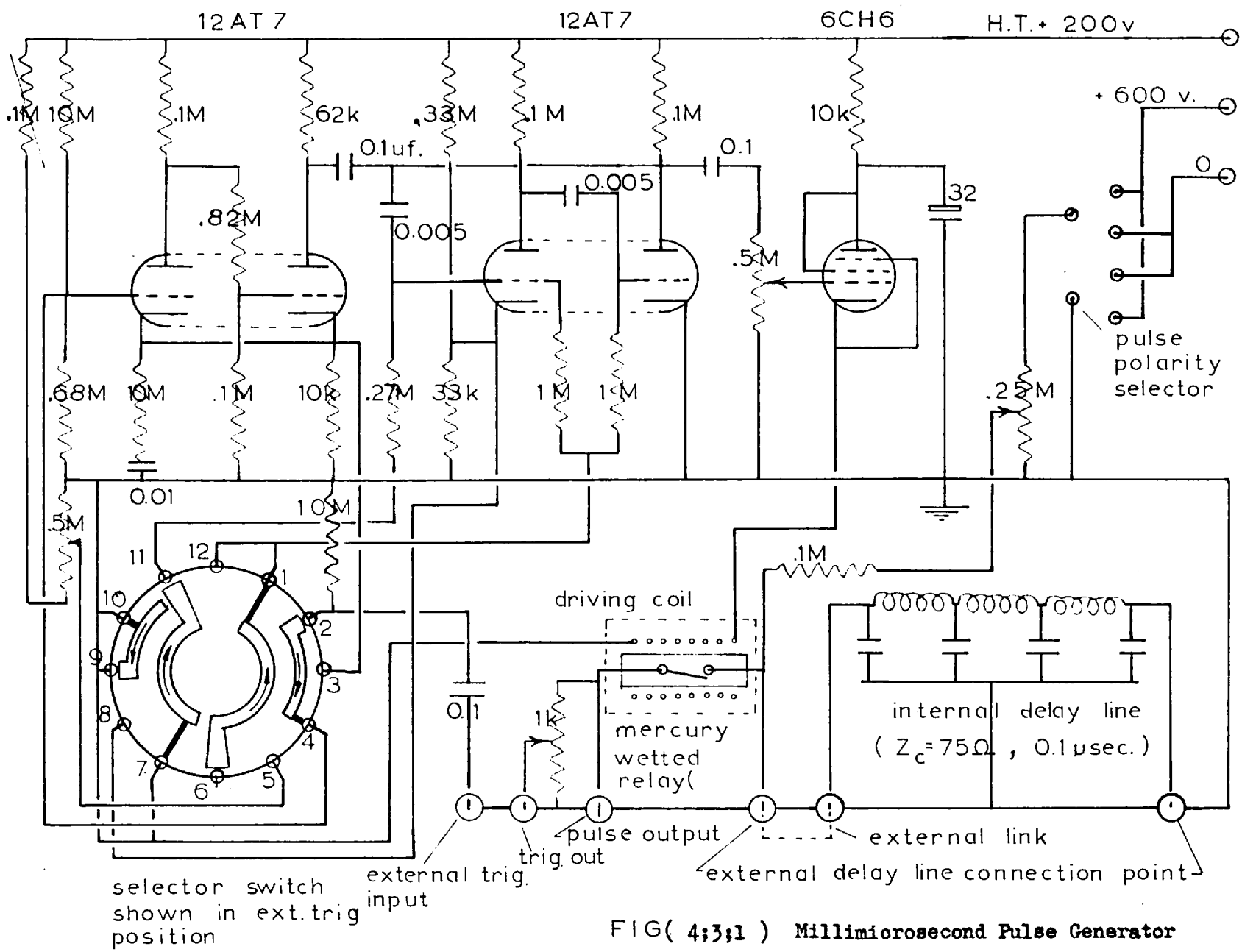

FIG(4;3;1) **Millimicrosecond Pulse Generator**

fixed length and 200 volts amplitude, which in turn was used to drive (V_3). Here (V_3) was a simple cathode follower whose cathode load was the driving solenoid for the " mercury wetted relay " , utilised as the switch for this line type pulse generator.

The main part of the generator was the line, ordinary 75 ohm coaxial cable, which was charged , either positively or negatively to some 600 volts, by a D.C. power supply. This transmission line was then instantaneously terminated in its characteristic impedance by the nanosecond action of the mercury switch. Initiation of this process resulted in half the line voltage being applied across the terminating load resistance. In addition a voltage wave of the same amplitude propagated down the transmission line, however the effective polarity of the travelling wave was negative since the line voltage fell from 600 volts to 300 volts.

At the open circuited end of the transmission line the travelling wave was reflected without change of polarity and thus propagated back towards the load resistance. In so doing the line was completely discharged and therefore the outout pulse was terminated. It follows therefore that the pulse length obtained from the generator was determined by the double transit time of the voltage wave in the transmission line.

Equation (C;1;7) of appendix C gives the velocity of propagation of electromagnetic waves in coaxial transmission lines as:

$$C_p = C_o / (\mu_r \cdot \mathcal{E}_r)^{\frac{1}{2}} \qquad (C;1;7)$$

where C_o is the velocity of free space propagation and is equal to 3×10^8 meters per second.

For the particular cable used in this pulser $\mu_r = 1$ and $\mathcal{E}_r = 2.25$ and so:

$$C_p = 2 \times 10^8 \text{ meters per second.}$$

which means that the pulse length (τ) obtained from the generator was given by the relation:

$$\tau = L\,(100)\ \text{microseconds.}$$

where L corresponds to the length of the transmission cable in meters.

For convenience a 0.1 microsecond line was permanently built into the generator unit which could be externally connected or disconnected from the mercury relay at will. In this manner shorter pulses could be obtained by direct external connection of short cables to the mercury relay switch and longer pulses by connection of additional lengths of 75 ohm coaxial cable in series with the 0,1 microsecond line.

The sharpness or rise time of the output pulse was due almost entirely to the extremely fast switching action of the mercury relay. This switch derived its useful characteristics from the fact that the contacts were permanently wetted with mercury,thus insuring low contact resistance as well as fast switching action. In addition the cell was highly pressurised with hydgogen , which still further enhanced its performance.

Activationof the mercury relay was accomplished by means of a small solenoid which surrounded it, since the main contact arm of the switch was fabricated of magnetic material and hence vibrated in synchronism with the solenoid magnetisation. The pulse repetition frequency of the pulse generator was therefore determined by the solenoid magnetisation and was made to be continuously variable from zero to 200 pps. Above 200 pulses per second the inertia of the spring loaded contact arm in the switch became prohibitive.

Pulse generator performance.

The amplitude of the output pulse obtained from the constructed pulse generator was continuously variable from 0 to 300 volts, either

polarity. The output impedance of the pulser was normally 75 ohms however since there was provision for externally connecting any cable to the mercury swtich , any impedance could be obtained in accordance with the impedance of the particular cable used. It was necessary at all times to operate the pulser into its characteristic impedance if optimum pulse shape was to be realised. Rise times of less than 3 nanoseconds should be possible with this type of pulse generator, however the best available oscilloscope rise time was some 6 nanoseconds and therefore accurate pulser rise time could not be established. The fall times were found to be equally as good and this was to be expected since it is essentially derived from the leading edge. The limiting factor here is the frequency response of the delay line used. The quality of the top or flat portion of the pulse is determined mainly by the low frequency response of the delay line and consequently was found to be very good.

4;4 (HIGH LEVEL PULSE GENERATOR)

The high voltage generator as supplied with the modulator , obtained to drive the magnetron, was found to be unsuitable with respect to pulse shape produced. It was essential for reasons of accurate determination of microwave bridge balance , that the magnetron R.F. output pulse be as rectangular as possible. This in turn required that the modulator output pulse be also very good. Now since the modulator used was of the "hard valve" type ,its output pulse could be no better than its driving waveform. The requirements of the driver were therefore as follows:

(1). Very rectangular positive pulse of 3.5 to 4 kv. amplitude.
(2). Very fast rise and fall times, ie; 0.01 microsecond.
(3). Driver must be capable of working into a variable impedance.

The variable impedance load into which the driver had to operate

arose from the fact that the modulator was essentially a reservoir capacitor which was momentarily connected across the magneton through the action of three large U.H.F. triodes connected in parallel. The driver was therefore required to drive the grids of these " keyer" valves. Initially at the begining of the pulse the grid input impedance of these valves was near opencircuit , but this value suddenly fell to about 100 ohms as the grids were driven some 2000 volts positive and drew 8 to 10 amperes of grid current over the flat portion of the pulse. At the trailing edge of the pulse the grid input impedance again returned to its initial value. The driving pulse amplitude required for proper modulator "keyer" valve operation was + 3.5 to 4 kilovolts.

The circuit diagrams of the drivers constructed in an attempt to meet the requirements specified above , are shown in FIG.(4;4;1to3).

Analysis of operation

All of the driver units constructed were basically the same type as the low level pulse generator previously described except that in this case a hydrogen thyratron was utilised as the switch element. As in the previous case the pulse cable was initially charged to a D.C. potential V_o and then suddenly discharged into its characteristic impedance. The value of V_o in this line driver was + 8 kv. and the switch used was a 4C35 hydrogen thyratron,which was fired by the output pulse of the low level pulse generator. Because of the nature of thyratrons it is essential that the line be charged only positively and thus to realise a positive output pulse the circuit of FIG.(4;4;1) was initially tried.

The configuration shown in FIG.(4;4;1) required the use of an isolation heater transformer and despite the incorporation of an ultra low capacitance unit, it was not possible to obtain the required

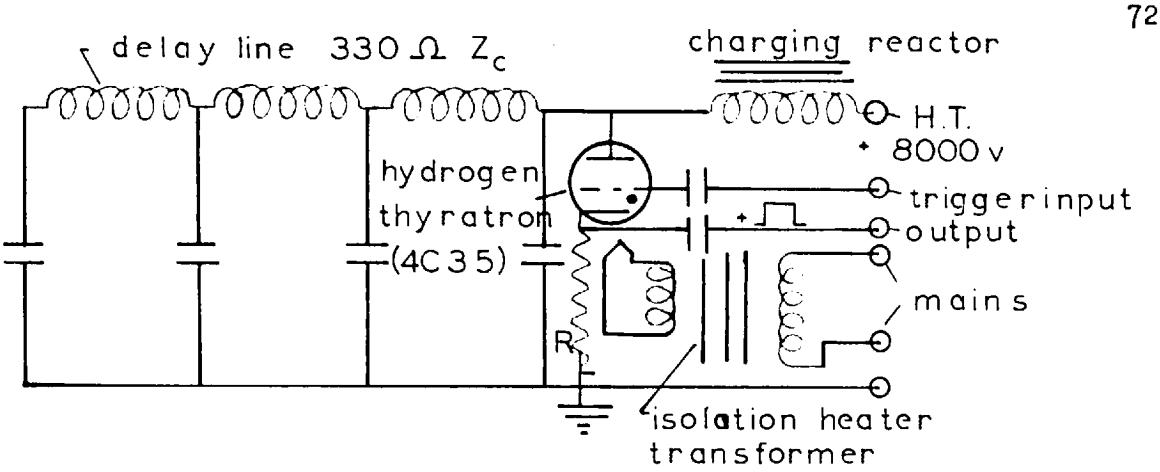

FIG.(4;4;1)

High voltage modulator driver for positive output pulse using isolation heater transformer.

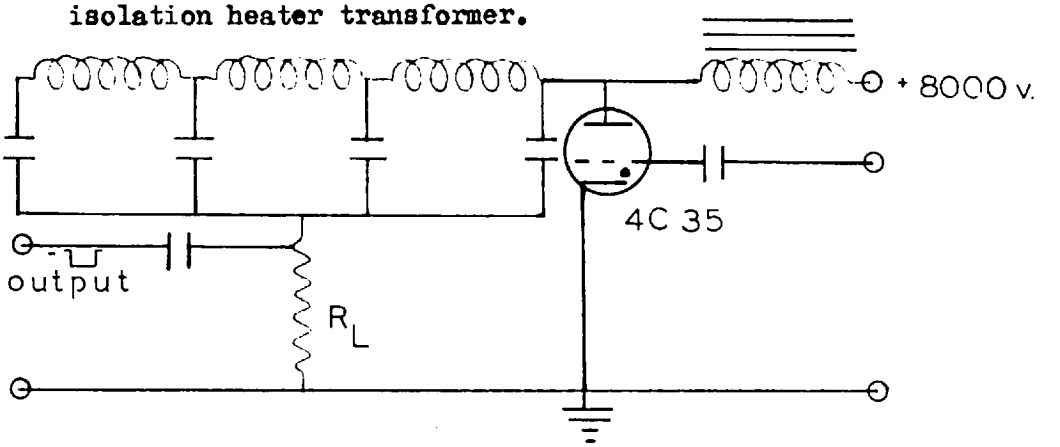

FIG.(4;4;2)

High voltage driver unit with negative output pulse.

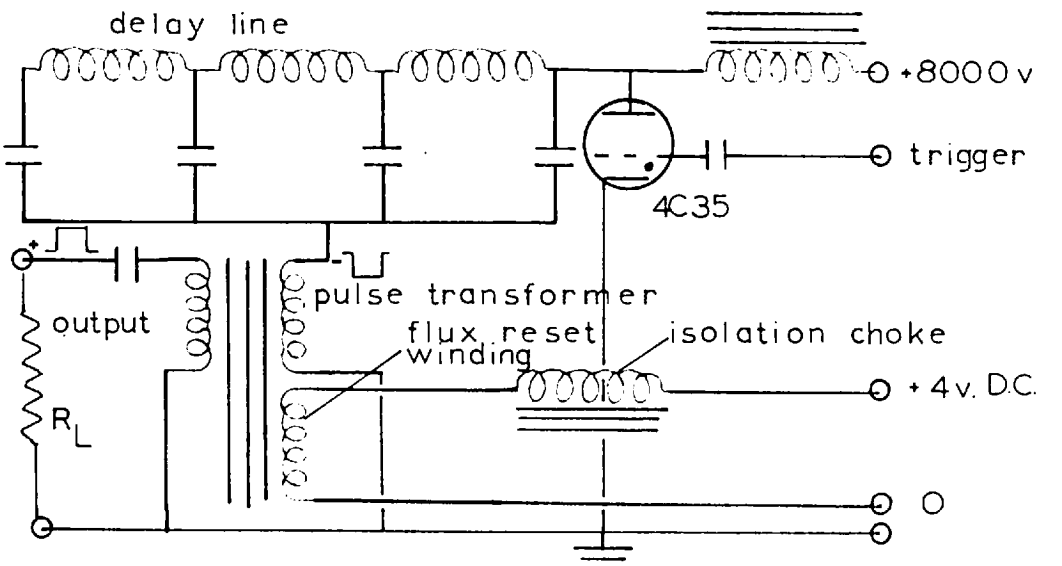

FIG. (4;4;3)

pulse rectangularity due to the shunt capacitance loading effect of the filament transformer.

The circuit shown in FIG.(4;4;2) was found to give very good results, however the output pulse polarity was of the wrong sense and so a pulse inverting transformer had to be employed as shown in FIG.(4;4;3).

Construction details

As was previously described, it was necessary to eliminate the shunt capacitance across the thyratron in order to achieve the rate of rise of anode current required and this entailed connecting the cathode directly to the common negative line. This however meant that a phase inverting pulse transformer had to be used. Care was taken to keep all leads as short as possible and to this effect the pulse transformer and pulse cable were mounted directly at the thyratron top cap. The pulse cable used was the standard "Telcon" high voltage delay cable having a helically wound center conductor and characteristic impedance of 330 ohms. A delay of 0.017 microseconds per foot of cable length was obtained and consequently for the 0.35 microsecond pulse length required, the cable length needed was 10.3 feet.

Provision was made so that any length of pulse cable could be connected to the driver unit without any alteration being required.

A self contained voltage doubling power supply , employing solid state pencil rectifiers , was built into the driver cabinet to supply the D.C. potential of 8000 volts for charging the pulse cable. This D.C. power supply was made to be continuously variable from 0 to 10 kv. at five milliamperes. Continuous voltage monitoring was accomplished by means of a high impedance potential divider and an electrostatic voltmeter. The potential divider also served as

a discharge path for the voltage doubling circuit whenever the device was switched off, thus rendering it nonlethal . A 50 henry choke was used to isolate the high voltage D.C. power supply during the line discharge process.

The driver was constructed to be a completely self contained unit built into a well screened cabinet so that it could be used externally and independently to the main modulator if required. Heavy screening was required due to the rather intense radiation emitted by the hydrogen thyratron.

A schematic diagram of the completed driver unit is given in FIG.(4;4;4).

Pulse transformer

Considerable difficulty was incountered in obtaining a suitable pulse transformer which would invert a 0.1 to 0.5 microsecond pulse of 4000 volts amplitude and maintain its rectangularity , while working into a dynamic load impedance variation of approximately∞ to 100 ohms.

It was not possible to obtain such a transformer commercially and thus experimental units were constructed employing different core materials and winding techniques, in an effort to find a suitable design. Ferroxcube toroidal cores wound with bifilar windings were found to perform well into constant resistive loads but serious waveform deterioration was observed under dynamic load impedance variations. Strip wound "Supermumetal" toroids with bifilar windings gave considerable improvement but still not completely satisfactory.

Adequate results were however obtained using "Permalloy F" spiral tape wound toroidal cores using layer windings and a flux resetting technique. (38).

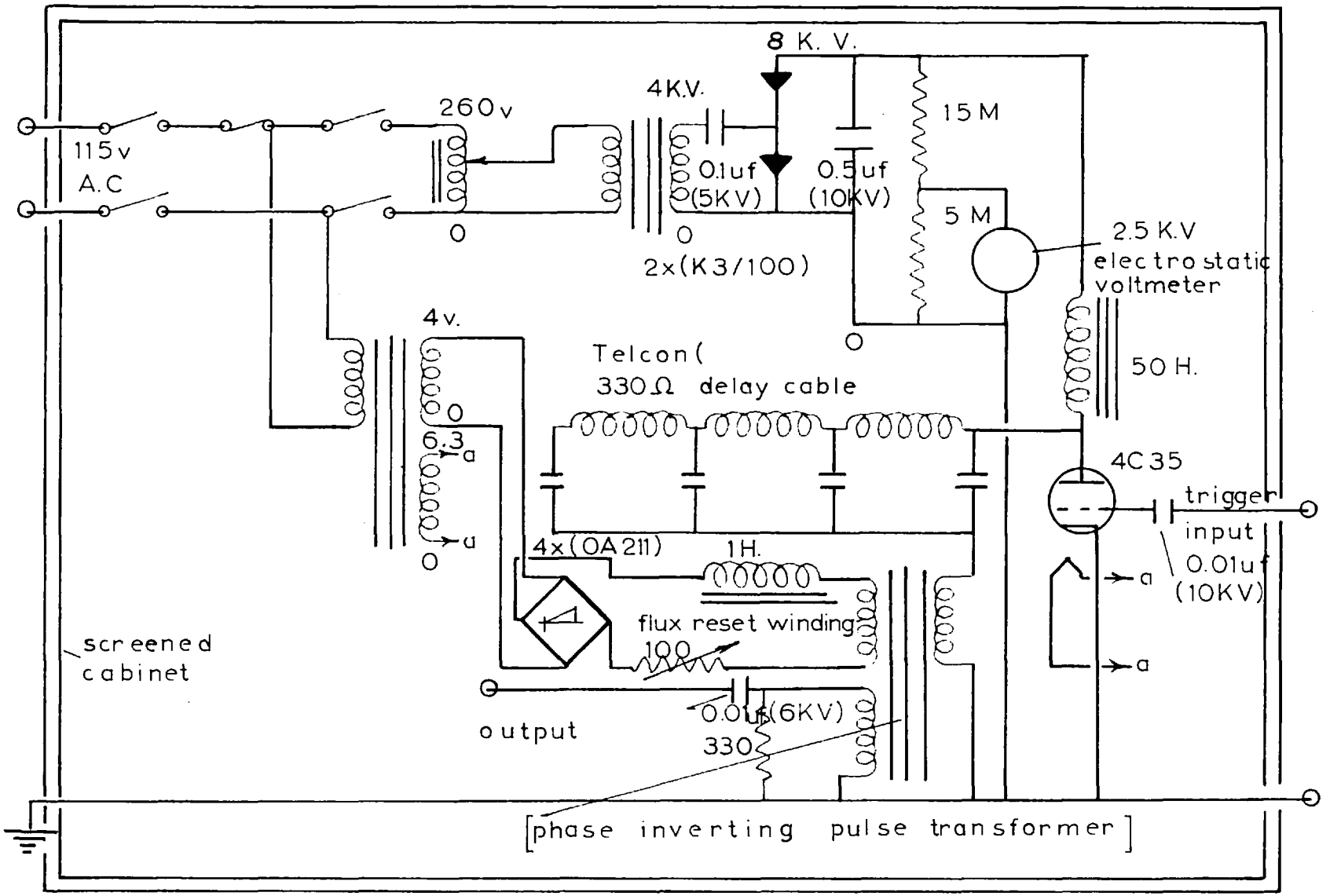

FIG.(4;4;4;)

Schematic diagram of completed driver unit.

This flux resetting concept can best be illustrated by considering a typical D.C. B-H curve for a given material, forming the core of a pulse transformer, shown in FIG.(4;4;5). If the core is initially unmagnetised and single polarity, constant amplitude, rectangular voltage pulses are applied, the resultant incremental B H loops,of constant flux swing ΔB_s, will, after an initial period of transition, bring the core material to the condition where the flux excursion , from the remanent flux density B_r to the B H curve, is equal to ΔB. The location of the particular remanent point B_r depends on the value of ΔB_s, but if ΔB is large this value of B_r will be found to be very nearly equal to $B_{r\ max.}$ which is the remanent flux density when the core material is driven into saturation. (39).

It is desirable from considerations of core size and the number of turns on the winding , to have a large flux excursion ΔB, but for most core materials the saturation remanent flux density $B_{r\ max.}$ is typically about 90 percent of the saturation flux density $B_{sat.}$ and hence the maximum value of ΔB over which the core may be operated during the pulse, without saturation is very small indeed. The foregoing statement is well illustrated in FIG.(4;4;5) , where the operating flux excursion region is shown to be small in comparison to the initial transient magnetisation region.

If however a third winding is put on the transformer core and biased with a constant D.C. current such that a reverse magnetic field H'_r is produced , it can be seen from FIG.(4;4;6), that the resultant remanent value of B is at B'_r and hence a much greater flux excursion $\Delta B'$ can be achieved. In actual fact the core used was biased to $-B_{sat.}$ where $-B_{sat.}$ was the saturation flux density for negative H. It follows therefore that the permissible flux excursion $\Delta B''$ was equal to twice the saturation flux density $B_{sat.}$ Clearly this is a great improvment over the nonresetting flux condition.

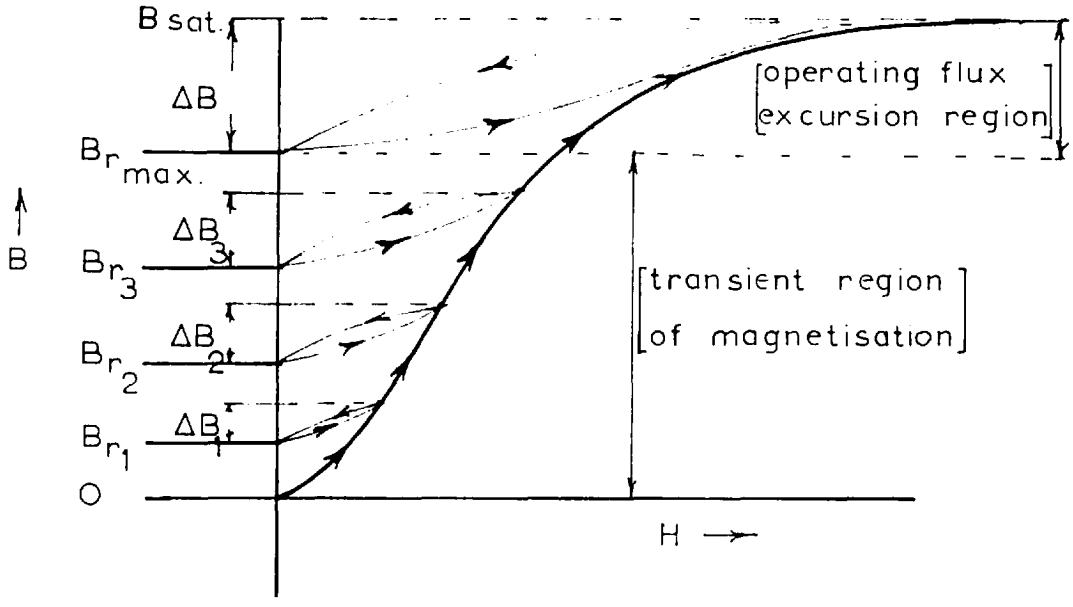

FIG. (4;4;5)

D.C. B H curve for a typical pulse transformer core.

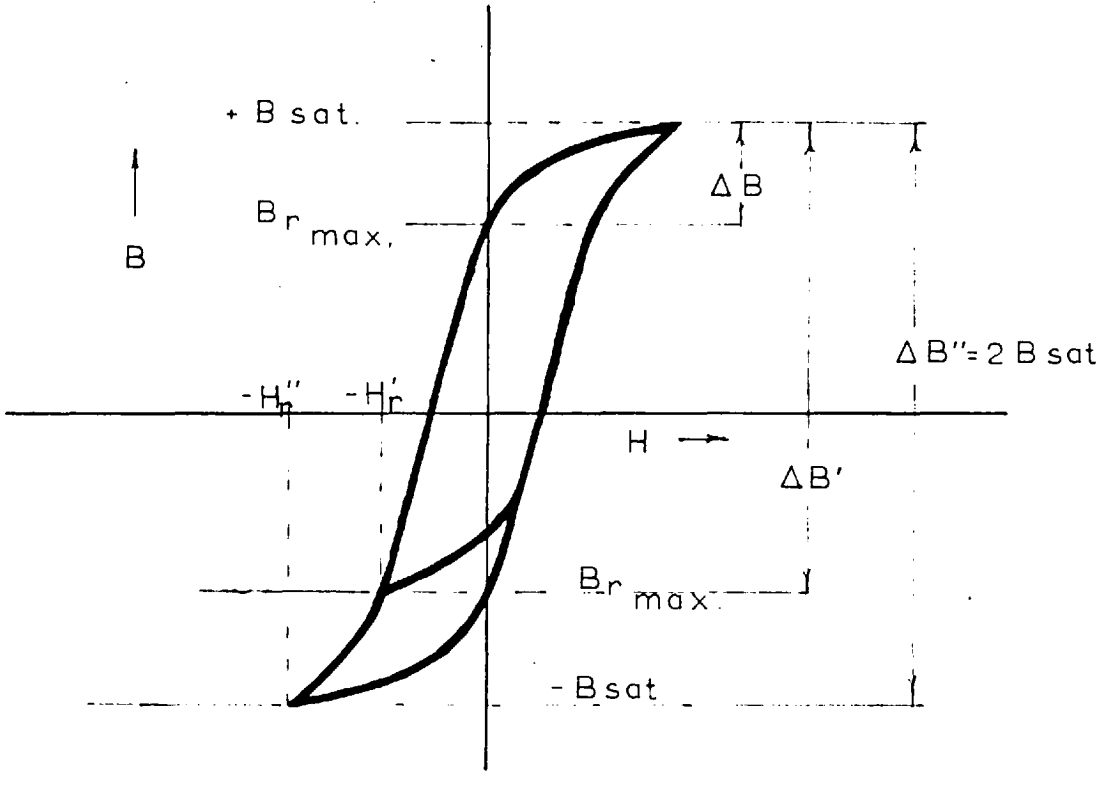

FIG (4;4;6)

D.C. magnetisation loop for a typical pulse transformer core having flux resetting winding.

The core material which was found to give the best performance was Permalloy F , wound in the form of a toroid from 0.002 inch tape. This core, obtained from "S.T.C." was a domain oriented , nickeliron alloy exhibiting a very rectangular hysteresis loop and having a high saturation flux density and permeability as shown in FIG.(4;4;7) .

The exsistance of this rectangular B H curve was the reason why this pulse transformer was able to work into a dynamically varying load impedance without suffering serious pulse shape deterioration. The number of turns on the winding was arranged such that the pulse leading edge magnetisation drove the core material well into saturation. Any subsequent decrease in load impedance, resulting in large pulse current and increased magnetisation merely drove the material into a higher state of saturation without effecting the flux density and consequently the voltage pulse shape was unaffected .

An inductive reactance was inserted in series with the D.C. flux resetting winding so as to effectively isolate it from the pulse.

Since the pulse transformer insulation was adequate for only approximately 6 kv. , a dummy resistive load was placed across the secondary as protection against damage from high voltage build up should the load become accidentally disconnected during operation. This dummy load was chosen to be 330 ohms so that it could act as a proper termination for the pulse transformer during test sequences.

Winding data for the pulse transformer was as follows;

Primary turns	= 30
Secondary turns	= 30
Wire size (S.W.G.)	= 20
D.C. winding turns	= 10
D.C. resetting current	= 0.25 amperes.
Core cross section	= 0.375 x 0.5 inches
Core diameter	= 2.25 O.D. x 1.5 I.D.

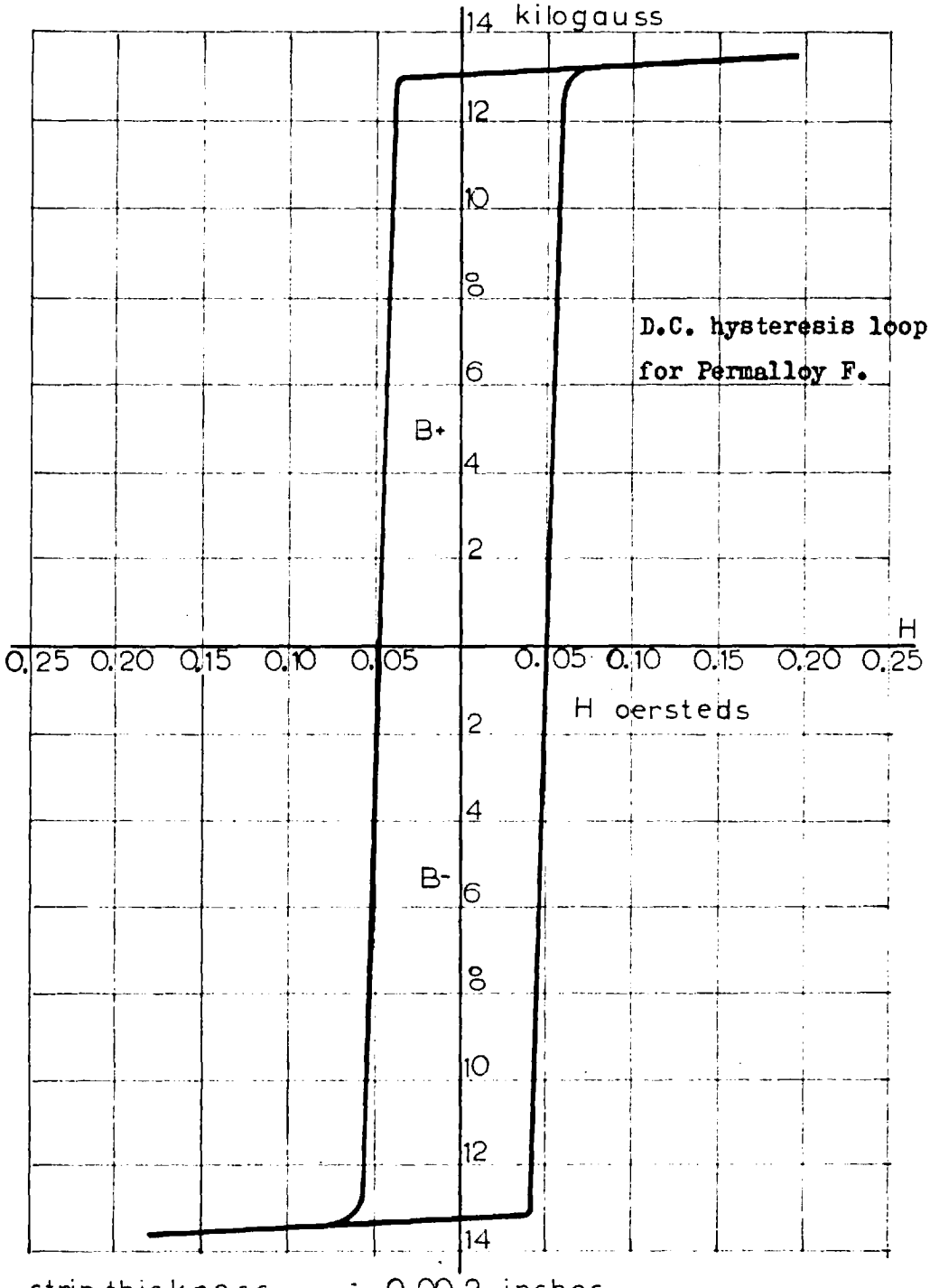

strip thickness = 0.002 inches
specific gravity = 8.4
electrical resistivity = 26 microhms/cm^3
initial permeability = 400 to 1000
maximum permeability (μ max.) = 200000 to 400000
magnetising force for μ max. = 0.03 to 0.10 oersteds
maxium flux density (B max = 14000 gauss
coercive force for B max. = 0.05 oersteds
remanence for B max. = 13300 gauss
hysteresis loss for B max. = 220 ergs/c.c./cycle.

FIG. (4;4;7)

The hydrogen thyratron switch used initially was the B.T. 83 which had a current rise rate of 1500 amperes per microsecond. This valve however didnot give a sufficiently good leading edge to the pulse and so a 4035 thyraton having a current rise rate of 2500 amperes per microsecond was substituted. Completely satisfactory performance was obtained with this valve.

The triggering voltage rate of rise is of considerable importance if the maximum thyratron current rise rate is to be achieved.(40). A trigger rate of rise of approximately 40,000 volts per microsecond was obtained from the low level pulse generator and this was found to be adequate. The minimum trigger amplitude required for stable thyratron operation was approximately + 1.50 volts.

Performance.

The performance obtained from the high voltage driver was completely satisfactory in all respects. Output pulse amplitude was continuously variable from 500 volts to 4.5 kv. with a nominal output impedance of 330 ohms. The design of the pulse transformer however enabled the load impedance to be varied over a wide range without any appreciable deterioriation of pulse shape. Driver rise time was limited mainly by the pulse transformer high frequency response, being approximately 20 nanoseconds. The pulse fall time was of the same magnitude.

Very good pulse shape was obtained , having only a small oscillation superimposed on the flat top. This oscillation was probably due to imperfections in the delay cable, since it could be altered by manipulation of the cable.

The maximum pulse repetition frequency attainable with this driver was approximately 1000 pps. , but this value was never used since the system pulse repetition frequency was restricted to a much lower figure from other considerations.

As in the case of the low level pulse generator , the pulse length obtained from the high voltage pulser was determined by the length of the delay cable used, and as such any pulse length within about 0.1 to 2 microseconds could be achieved. Satisfactory pulse shapes outside of this range were not obtained due to the limitations of the pulse transformer.

Since the maximum power output of the D.C. high voltage ,delay line charging supply was 50 watts , the highest pulse repetition frequency obtainable from this driver was determined by the condition that the duty ratio was not greater than 0.002. Duty ratio is here defined as the product of pulse length and pulse repetition frequency.

4:5 (HIGH POWER MODULATOR)

The modulator was included in the system to drive the " S " band magnetron,used as transmitter, and as was mentioned in the discussion of the high voltage driver, it was essential that the modulator output be of high quality with respect to shape. The demands imposed on the modulator output pulse were as follows:

(1). Negative pulse of 10 to 20 kv. amplitude at 25 amps , continuously variable.

(2). Fast rise and fall times. ie: 10 nanoseconds.

(3). Flat top .

(4). Pulse shape to be maintained despitedynamic variation in load impedance, as magnetron fires.

(5). Only one pulse required and no post pulse radiation tolerable.

(6). Variable pulse width.

Previous experiences with a high powered line type modulator indicated that such a device was unsuitable for this application since unless the line is always properly terminated during the pulse, reflections travel back and forth on the delay line resulting in post pulse radiation. Such radiation was found to have a serious jamming effect on the highly sensitive receiver system, which was built in close proximity . An additional objection to the line type modulator for this application was the inability to alter pulse length.

A " hard valve " modulator, the circuit of which is given in FIG.(4;5;1) , was found to satisfy all requirements. This unit was a one megawatt exservice model originally developed by M.I.T. Although this device was quite old it was possible to obtain completely satisfactory performance when it was driven by the newly constructed high voltage driver unit described in section (4;4;).

This modulator was constructed in two separate units, one unit being the high voltage D.C. power supply and the other the actual pulser. Both units were contained in well screened cabinets to minimise radiation.

High voltage D.C. power supply.

A 3 phase high voltage transformer employing thermionic diodes in a voltage doubling circuit constituted the main portion of the D.C. power unit. A D.C. output ,continuously variable from 10 to 30 kv. at 100 milliamperes was available through means of a motor driven induction regulator, which supplied the primary of the high voltage 3 phase transformer. Several,relay operated, protective devices were incorporated into the cabinet to safeguard the operator. A schematic circuit diagram of this D.C. power unit is given in FIG.(4;5;2).

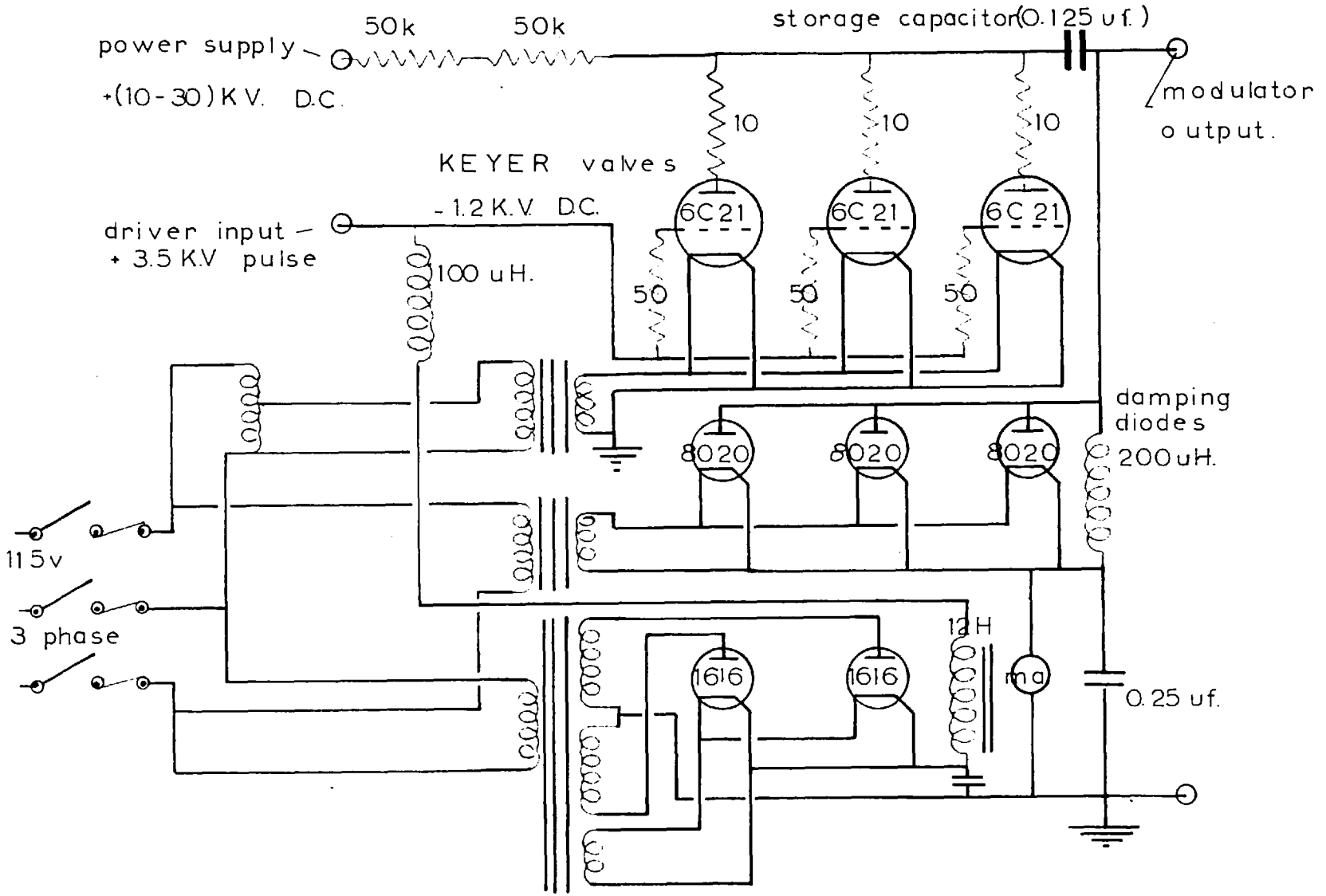

FIG. (4;5;1) **Modulator schematic diagram**

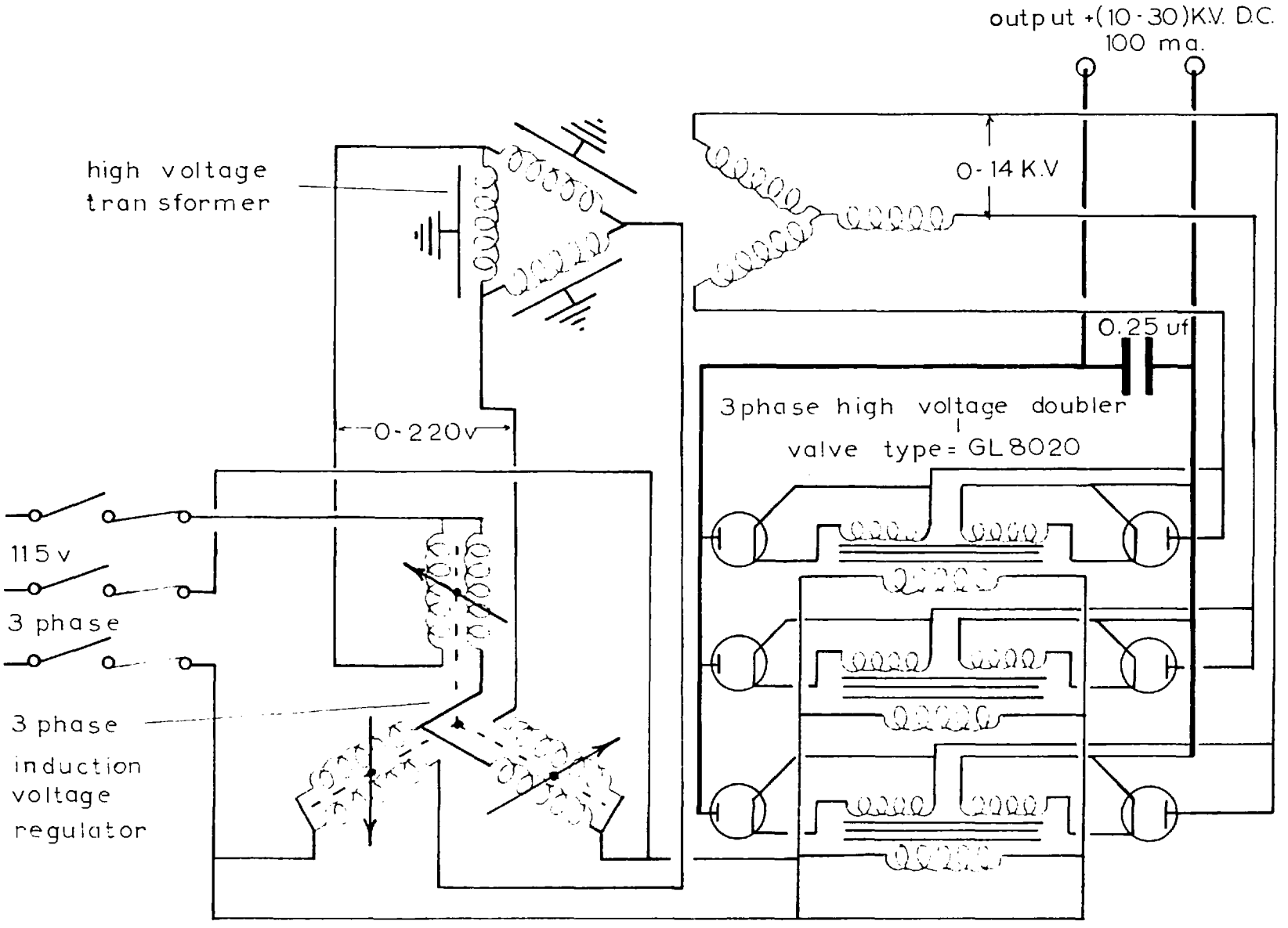

FIG. (4;5;2) Schematic diagram of High voltage D.C. power unit.

Main pulser

The basic components in this " hard valve " type of modulator was a charged reservoir capacitor which was momentarily connected across the magnetron by the action of three U.H.F. switching triodes, connected in parallel. The grids of these triodes were held at a negative potential of 1500 volts to insure no conduction between pulses. Driver pulses were coupled to the valve grids through a suitable high voltage capacitor. This insured that no D.C. current would flow in the secondary winding of the pulse transformer, as any such flow would seriously disturb the flux resetting system.

A 0.125 microfarad , high voltage capacitor, resistively isolated from the D.C. high voltage power unit, acted as the reservoir. It can easily be shown that the voltage drop in the output pulse due to the discharge of this reservoir capacitor was only 0.38 % when the pulse length was .0.38 microseconds, and this value was completely negligible.

One particularly desirable feature of the pulser was its relatively low output impedance, which rendered it insensitive to large load impedance changes. This aspect was of particular importance in this case where the modulator load was a magnetron, which acts as a reverse biased diode , and as such possessed a dynamic impedance variation.

Performance

Quite acceptable performance was obtained from this " hard valve" pulser, in that pulse rise and fall times of 30 and 40 nanoseconds respectively were achieved. These figures were some what worse than the 20 nanoseconds rise and fall times given by the modulator driver, however this was to be expected due to the stray capacitance loading effect of the output circuit as well as the shunt capacitance of the magnetron and its associated isolation heater transformer.

4;6;1 (MAGNETRON AND ASSOCIATED EQUIPMENT)

It was necessary to use a magnetron as the transmitter due to the relatively high pulsed powers required. . This particular magnetron , a CV1495 , was of the "M " type catagory , having an operational frequency of 3020 megacycles and maximum pulsed output of 300 kilowatts. Pulse lengths of 0.1 to 0.4 were used but best performance was obtained at 0.35 microseconds . Since this valve was not originally designed for such short pulses it was necessary to use an electromagnet biasing system, in place of the normal permanent type, in order to achieve the required rectangularity of R.F. pulse shape.

In addition to the electromagnet biasing system, a special R L pulse shaping network was inserted in series with the magnetron input. With this network it was possible to so shape the magnetron current pulse such that the R.F. output pulse was perfectly flat with rise and fall times of 6 to 10 nanoseconds. The ability to obtain a flat topped R.F. pulse from the magnetron was an important aspect in the development of the system as it enabled the balanced condition in the microwave bridge system to be accurately determined.

The magnetron specifications are as follows:

Magnetic field	= 2o5o gauss
Anode voltage	= 24 kv. peak
Anode current	= 25 A. peak
Input power	= 6oo kw. peak
Input power	= 5oo w. mean
Duty cycle	= o.ool max.
pulse length	= o.5 min.
Pulling figure	= 7 Mcs.
Pushing figure	= o.5 Mcs/ ampere.
Output	= 3oo kw. max.
frequency	= 3o2o Mcs.

4;6;2 (CONSTANT CURRENT ELECTROMAGNET POWER SUPPLY)

It was found that very slight variations in the magnetron biasing field produced large variations in the magnetron operating frequency. It was also observed that any slight variation in the magnetron operating frequency , during or between either part of the two separate pulse cancellation sequences comprising a particular test, greatly reduced the accuracy of the measurement. Now since these two separate cancellation sequences were usually performed two hours apart, it was essential that the magnetron frequency be absolutely stable for this period. Clearly therefore it was required to construct a constant current source for the magnetron biasing electromagnet, so as to eliminate variations in the magnetic field as a possible source of error.

The electromagnet used , a No.3 NewPort , required a 125 volt o.5 ampere supply to produce the required magnetic field of 2o5o gauss. For reasons of simplicity a transistorised constant current supply was developed, the circuit diagram of which is given in FIG.(4;6;2;1).

The power supply constructed consisted mainly of a series regulator controlled by a differential amplifier. The differential amplifier, formed by the two (GT 114) transistors , was basically a long tailed pair, the reference voltage for which was obtained from the zenner diode (SX 56). A high resistance potentiometer shunting the high stability,16 ohm sampling resistor, was used to provide the comparing voltage. In this manner it was possible to have continuous adjustment of the power supply output current merely by varying the potentiometer . Two stages of common collector current amplification followed the differential amplifier , terminating as the base drive for the series regulating transistor,(OC 28). For reasons of stability it was found desirable to have a separate supply for the differential amplifier section.

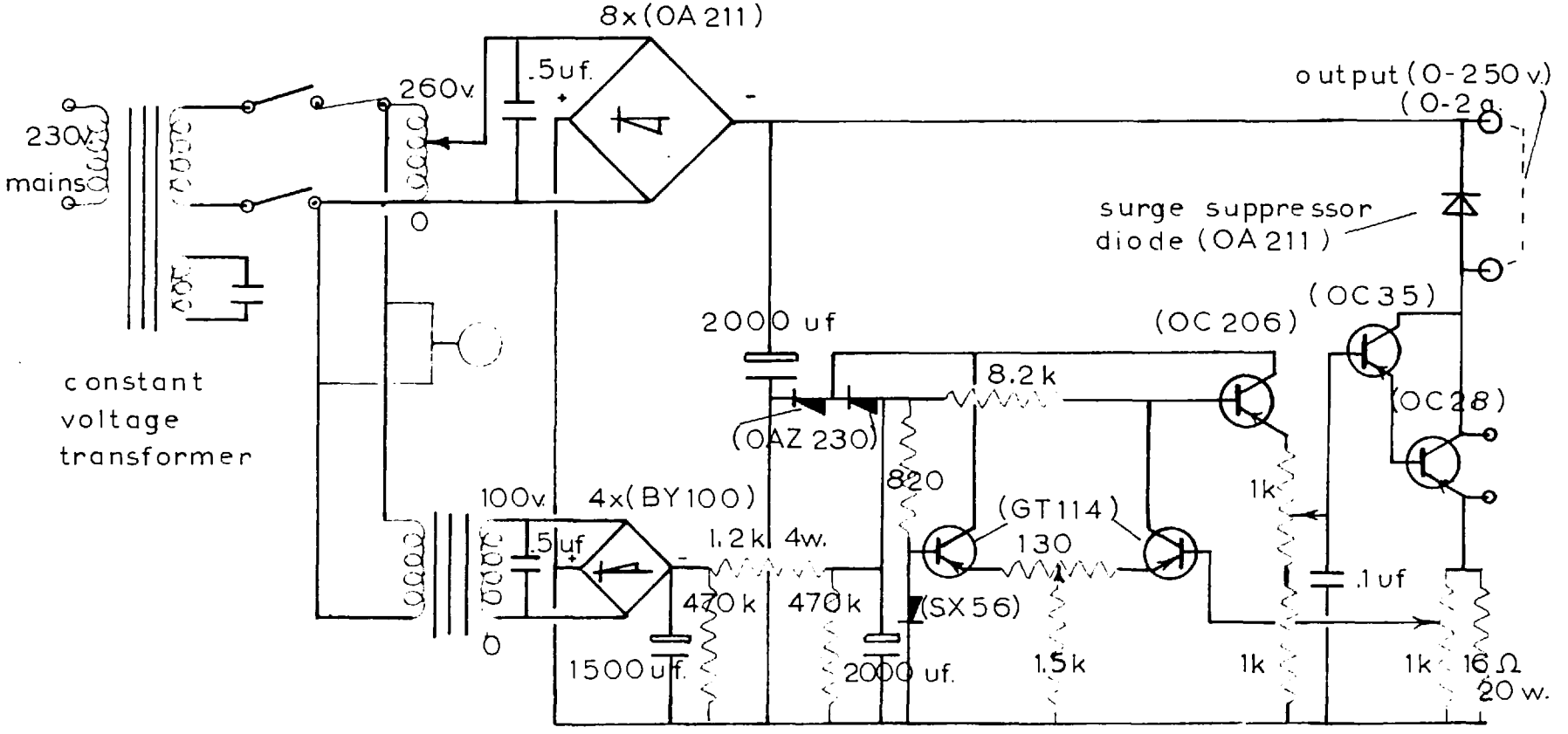

F I G. (4;6;2;1)

Circuit diagram of constant current electromagnet power supply.

Since the output voltage obtained from the current regulator was well in excess of the maximum voltage ratings of the series regulating transistor, it was necessary that the load be first connected and that the circuit voltage be gradually increased by means of the autotransformer. Any sudden break in the output circuit would immediately destroy the regulating transistor due to discharge of the electromagnet back into the power unit. For the above reasons the electromagnet load was permanently connected to the power unit and the autotransformer decreased to zero before the mains supply switch was turned off. A monitor point across the series regulator was incorporated so that neither maximum emitter to collector voltage or the permissible transistor dissipation would be exceeded.

A current stability of approximately one part in ten thousand was achieved over the limited range of interest with this power unit. The frequency drift of the magnetron due to changes in the biasing magnetic field strength was therefore rendered negligible. As an added measure of stability, a constant voltage transformer was used as mains supply for the power unit.

A series relay was incorporated in the electromagnet supply . This relay was then inserted in series with the main modulator control such that any failure of the electromagnet supply automatically shut down the high powered modulator. In this manner it was possible to insure adequate protection for the magnetron. This protective device was installed after a mains failure resulted in damage to a magnetron due to operation without biasing magnetic field. If a magnetron is driven by a modulator under zero biasing field conditions the cathode is rapidly deterioriated since there is nothing to limit the magnetron pulse current.

4;6;3 (MAGNETRON TEMPERATURE CONTROLLER)

The magnetron used in the system was found to have a frequency temperature coefficient of 0.07 megacycles per degree centigrade, and since the ambient room temperature was continuously varying over several degrees , the possible error introduced by the variation of magnetron operating frequency with temperature was considerable.

In an effort at reducing or eliminating this possible source of error an attempt was made to control the temperature of the magnetron anode block. This was done by mounting a thermostatically operated blower directly above the magnetron body. An Electro Methods mercury contact thermometer was used as the temperature sensing element which controlled the blower through the action of an electronic relay. This relay has identical to that used on the thermostated cavity temperature control system described in section (8;1), and as such its circuit diagram is given in FIG.(8;1;2).

With this blower system it was possible to control the magnetron anode block temperature to + or - 0.2 of a degree centigrade, over a period of approximately two hours. Stabilisation of the magnetron temperature in this manner was found to produce a definite improvement in system accuracy , this aspect is considered in greater detail in section (10;6) of this work.

4;7 (LAUNCHING SECTION)

Since the CV 1495 magnetron had a 36 ohm air dielectric coaxial output , it was necessary to design and construct a launching section which would transform the R.F. energy into " S " band number 10 waveguide, out of which the main portion of the apparatus was constructed . The system was built in waveguide due to the relatively high pulsed power involved and also because of the extremely high precision required of the measurement components, such components only being

attainable in waveguide.

The requirements imposed on the launching section were as follows:

(1). Device must be capable of handling the highest pulsed powers involved without sparking or arcing.

(2). The launching must be tunable so as to present the best possible match to the magnetron and thus obtain high performance.

(3). Section must be capable of correctly coupling to the magnetron such as to bring its loaded Q down to approximately 200. This requirement arose as a consequence of the relatively short pulses used since fast rise and fall times of the R.F. pulse could only be achieved by lowering the magnetron cavity Q .

Discription of launching section.

The construction adopted in the launching section is given in FIG.(4;7;1). As can be seen from the drawing, the inner conductor of the magnetron output section was capacitively coupled to the central conductor of the launcher. This 36 ohm coaxial line then passed through the broad wall of a standard number 10 waveguide and acted as an antenna. Movable short circuits were built into both waveguide and coaxial line sections of the launcher , to allow tuning for optimum performance. Both short circuits were of the capacitively coupled folded $\frac{1}{2}$ wavelength choke type, in which the actual short circuit was reflected back $\frac{1}{2}$ wavelength to a position where it could be machined out of solid brass. This enabled the sliding joint to be made at a point where the wall currents were zero. In this manner it was possible to obtain a movable short circuiting plunger giving very good and consistant electrical properties and still be free from sparking under high pulsed power conditions.

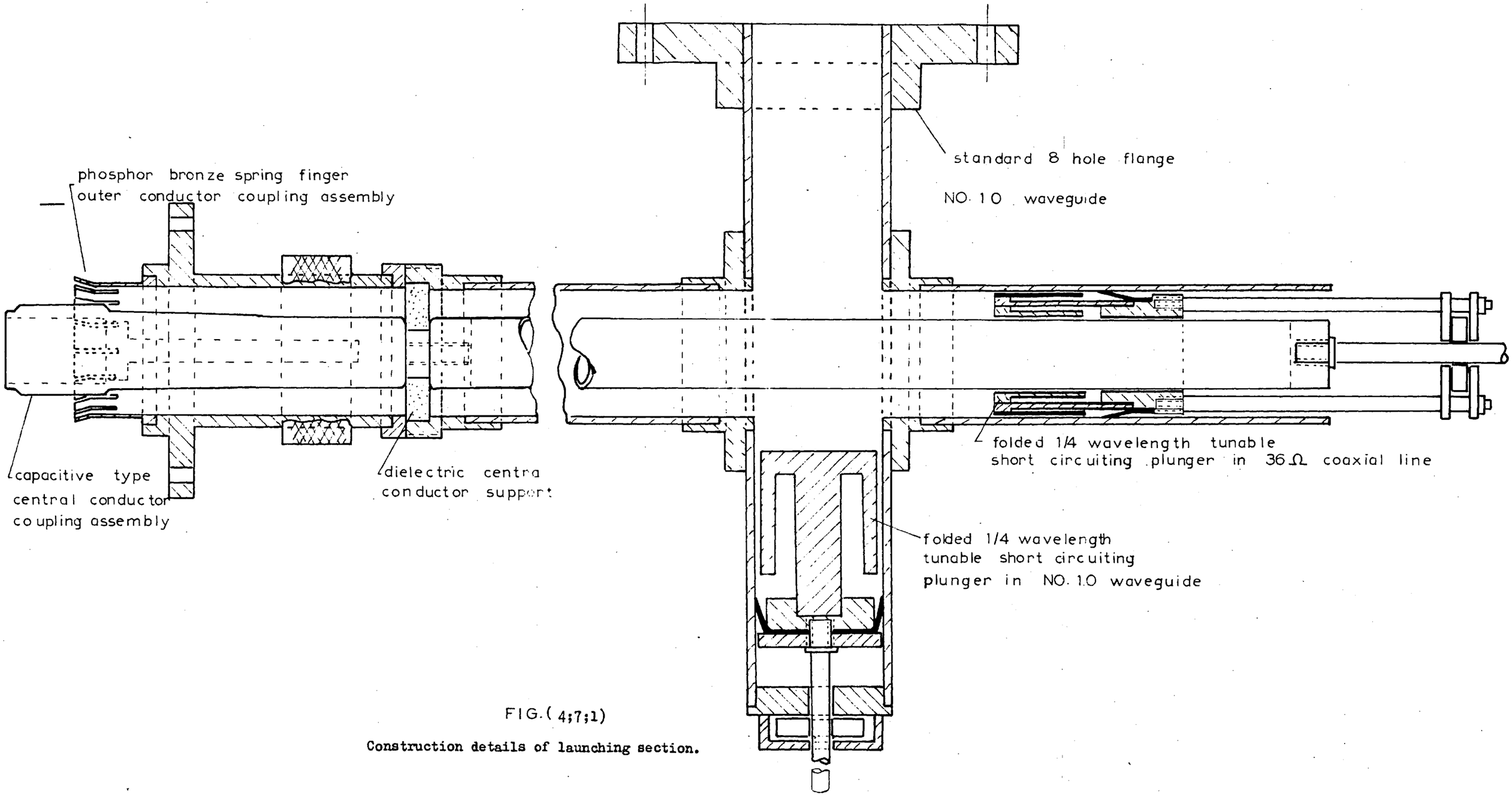

FIG.(4;7;1)

Construction details of launching section.

4;8 (WAVEGUIDE TWIST SECTION)

A waveguide twist section was incorporated into the system to rotate the plane of the waveguide through 90^{o}. It was necessary to do this since the modulator output terminal was situated in such a position that the launching section could not be satisfactorily oriented.

Because of space limitation factors it was required to restrict the twist section to the minimum length conducive to acceptable V.S.W.R. (voltage standing wave ratio). An electroformed twist section obtained from " Decca Radar Ltd." gave satisfactory performance, having a V.S.W.R. of 0.99 over the band of interest , ie(3000 to3040) Mcs. and an overall length of eight inches.

4;9 (PRECISION POWER LEVEL SETTING ATTENUATOR)

A precision attenuator was inserted in the magnetron output channel so as to enable the correct power level to be established in the microwave bridge system. It was found advantageous to use an attenuator rather than change the magnetron drive , when ever power level adjustments were required since it was impossible to obtain frequency stability under these conditions. In addition the R.F. output pulse shape was also effected by the drive conditions, and so the magnetron was continually operated at a fixed drive level. The optimum power level for the bridge system was dictated by the maximum pulsed power that could be coupled into the microwave resonant cavities without sparking occurring. Attenuator details are given in section. (5;3;2).

4;10 (MAGNETRON MEAN POWER MONITOR)

A mean power monitor was built so that a continuous check could be made on the power output of the magnetron if required , to determine

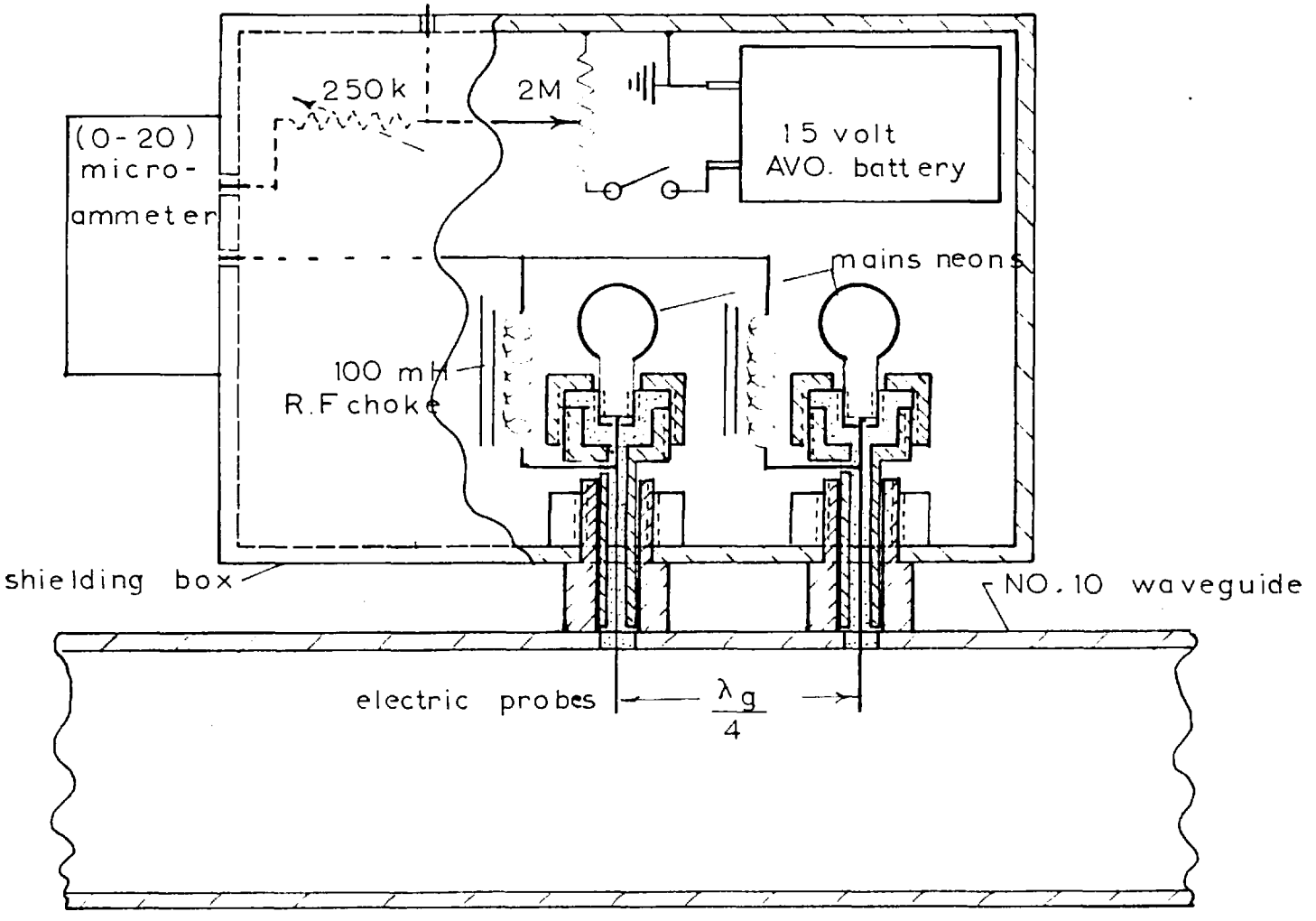

FIG. (4;10;1)

Magnetron R.F. mean power monitor.

its performance. This device had the advantage of being compact and self contained. The construction and circuit diagram of this power monitor is given in FIG.(4;10;1).

Discription of operation

From FIG.(4;10;1) it is evident that the device was merely two mains neon bulbs (S.L. 90/ SB) connected in parallel and coupled through the broad wall of a number 10 waveguide. A small portion of the R.F. energy in the waveguide was coupled to the neon lamps causing them to ionise slightly and thereby changing their D.C. resistance. This ionisation was proportional to the mean R.F. power level in the waveguide and hence the D.C. of the circuit was also proportional to this level. The D.C. current flowing in the circuit, as indicated by a microammeter, due to the impressed voltage from the Avo. battery, was therefore a measure of the mean power output of the magnetron. It was necessary initially to calibrate the monitor against a waterload , but once this was done the instrument could then be used directly. The device was found to be remarkably consistant provided the battery voltage did not change, and to this effect apotentiometer and a battery voltage set point were included in the unit.

Clearly it is evident that if there were no standing waves in the waveguide, the monitor indication would be proportional to the mean R.F. power level , however it can also be shown that even when a standing wave was present the monitor indication was still reasonably accurate due to the quarter wavelength spacing of the neons.

The expressions for the minimum and maximum error of the monitor indication are as follows;

$$\text{Maximum error} = (r-1)^2 / 2r$$

$$\text{Minimum error} = (r-1)^2 / 4r$$

where r is the standing wave ratio in the waveguide.

For a V.S.W.R of 1.2, which is very large compared to the actual value of approximately 1.01 , which was present in the channel, the maximum and minimum errors introduced are 2.5 and 1.25 % respectively, and so the actual error lies between these two values. . The above percentages indicate that the power monitor device constructed was a reasonably accurate instrument despite the presence of large standing wave ratios in the waveguide.

The power monitor was built into a completely enclosed metal box which was bolted to the waveguide body of the power level setting attenuator. In this manner is was possible to eliminate any R.F. leakage problems. Electric coupling to the neon lamps was made adjustable so that the monitor could be used over a wide range of mean power levels.

4;11 (H PLANE BEND)

An H plane 90^{o} was incorporated in the system at this point merely to change the direction of the waveguide run. This bend was an electroformed unit and as such had excellent electrical properties while still maintaining small physical size.

4;12 (FERRITE RESONANCE ISOLATOR)

An isolator was inserted into the main transmitter channel for the following reasons:

(1). To present a good match to the magnetron at all times and so obtain best performance.

(2). To protect the magnetron against possible damage to glass seals as a result of reflected power due to sparking in either of the

microwave cavities.

(3). During the transient period of the magnetron output pulse, the microwave resonant cavities act as a pure reactance and therefore reflect most of the power incident upon them. If allowed to return to the magnetron, this reflected power can result in frequency pulling of the transmitter during the remaining portion of the R.F. pulse.

(4). In order to achieve high accuracy of pulse cancellation in the measurement sequence it was necessary that the input arm of the bridge be perfectly matched. However the input (V.S.W.R.)of the magnetron was greater than 1.5 and so an isolator was essential.

The theory of operation of the ferrite resonance isolator is given in (appendix E) Part III , of this work.

Construction details

The ferrite and dielectric configuration adopted in the construction of this resonance isolator is shown in FIG.(4;12;1). The final cross sectional dimensions of the ferrite slabs were determined mainly by the shape of the ferrite pieces available at the time and consequently were not optimum.

All ferrite surfaces were ground on a surface grinder to achieve uniformity of cross section. In addition , very long tapers were ground at either end of both ferrite and dielectric slabs, to minimise relections.

The ferrite used was supplied by the Ferrite Division of Ferranti's in Edinbourg , and had the following specifications:

Type number	= F28X
Saturation Magnetisation($4\pi M_o$)	= 560 gauss
Gyromagnetic ratio ($\Gamma_e/2\pi$)	= 2.12 Mcs/ oersted .
Line width	= 330 oersteds.
Dielectric loss tangent	= 0.003

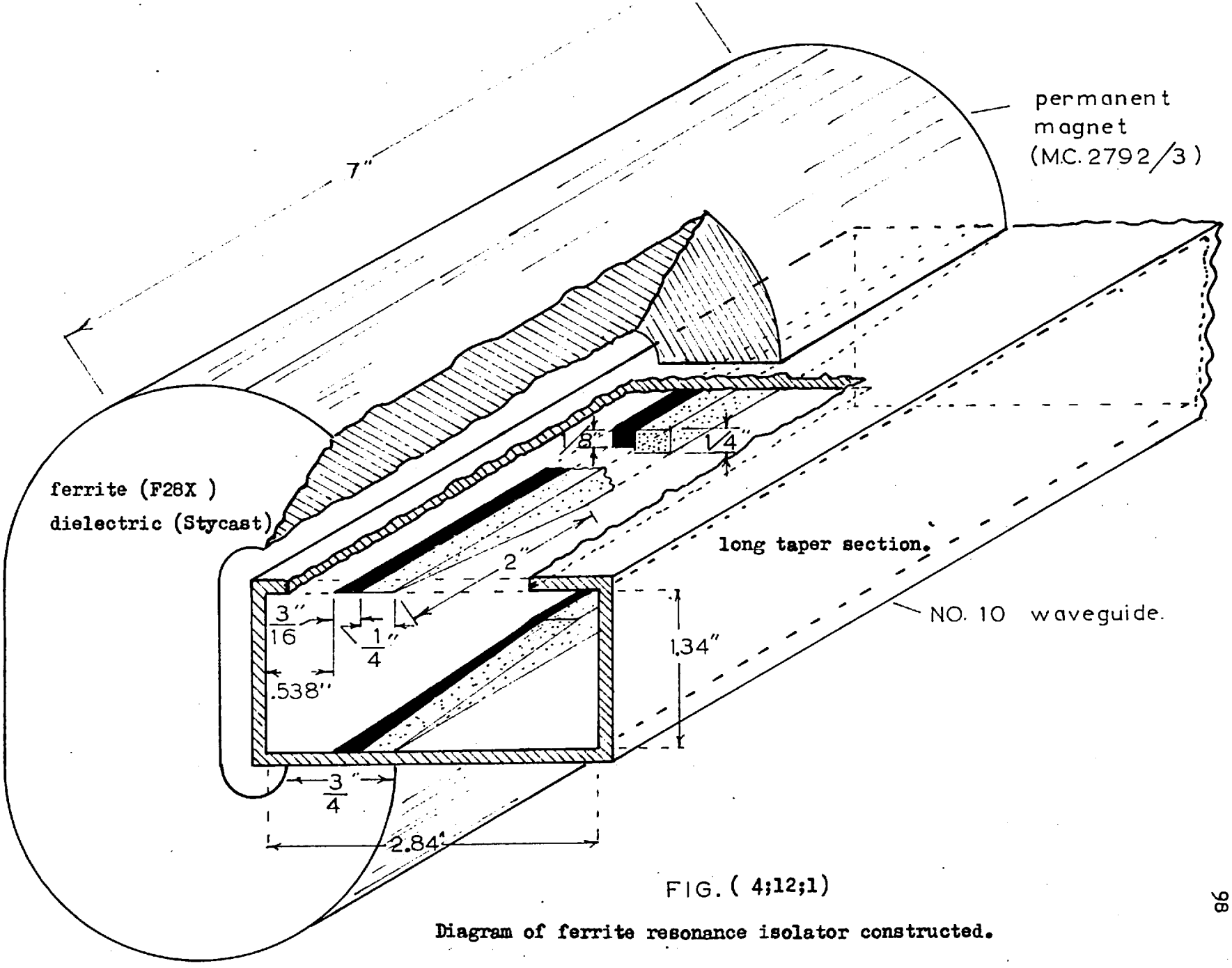

FIG. (4;12;1)

Diagram of ferrite resonance isolator constructed.

The dielectric used was Stycast, having a dielectric constant of approximately 13.

The internal field required for resonance (H_{eff}) , at the system operating center frequency of 3020 Mcs., was found from equation (E;5;11) as:

$$H_{eff} = \omega / \gamma_e = \frac{2\pi (3020)}{2\pi (2.12)} = 1425 \text{ oersteds}$$

Now the actual internal field required was determined from equation (E;5;10) by applying the appropriate demagnetisation factors. For the ferrite slab configuration used it may be shown that:(50).

$$N_x = N_y = 0$$

and $N_z = 4\pi$ in the MKS system of units.

or $N_x = N_y = 0$

and $N_z = 1$ in the cgs. system of units.

Equation (E;5;10) is therefore:

$$H_{eff} = ((H_{z(e)} + (0- 4\pi)(M_o)^2)^{\frac{1}{2}} = H_{z(e)} - 4\pi M_o$$

in MKS.

and so, $H_{z(e)} = 79.5(1425+560)$ ampere turns/ meter.

" = 1985 oersteds.

This biasing field was obtained from a C type magnet, which produced a field of slightly over 2000 oersteds and hence it was necessary to insert small magnetic shunts to arrive at the optimum condition.

Both ferrite and dielectric slabs were cemented directly to the

waveguide walls thus giving the isolator both high mean and pulsed power capacity.

Performance.

Quite acceptable performance was obtained from this isolator, the forward to reverse ratio being approximately 14 db. and the insertion loss 0.2 db.

The tedious task of machining the long tapers on the ferrite and dielectric sections was amply rewarded from the view point of impedance match obtained from the isolator. The V.S.W.R. looking in the forward direction was found to be 0.99 and in the reverse direction 0.995 , which was well within the requirements imposed by both magnetron and microwave bridge considerations.

4;13 (MAGNETRON FREQUENCY AND PULSE SHAPE MONITOR AND ALIGNMENT SIGNAL INJECTION SYSTEM.)

4;13;1 (GENERAL DESCRITPION)

Since the technique of measurement involved cancellation of one R.F. pulse against another , it was necessary that both pulses have the same shape if perfect cancellation, and hence high measurement accuracy,was to be achieved. As these R.F. pulses are derived initially from acoustic waves set up in two independent piezoelectric crystals, they do not have the same shape due to the slightly different transient response of the two cyrstals.

It is possible however to obtain sufficient accuracy of cancellation provided that the R.F. pulses have flat tops. This therefore necessitates that the exciting magnetron have a very flat topped R.F. output pulse. As explained in section (4;6;1) this condition was in fact achievable through proper design and adjustment of the

transmitter and its associated equipment. It was thus essential that there be some facility to continuously monitor the magnetron R.F. pulse shape to determine when the desired pulse shape had been achieved.

Such a monitor system was developed by means of inserting a loosely coupled, highly directive, directional coupler into the main transmitter channel. One end of the auxiliary branch of this coupler was connected to a waveguide T section, the output arms of which were in turn attached to a broadband crystal holder and a high Q, transmission type, " S " band wavemeter. The outputs from the wavemeter and crystal holder could be alternatively switched to the main oscilloscope display. In this manner it was possible to monitor, at will, both magnetron frequency and pulse shape. The other end of the auxiliary arm of the directional coupler was connected, through a waveguide to coaxial line transformer, to a low level " S " band signal generator, such that a low level signal could be injected into the transmitter arm of the microwave bridge. It was in this way that all alignment of the system was accomplished. In addition this injected test signal was used to indicate when both ultrasonic cavities were tuned to resonance and critically coupled to the bridge test and reference arms. Thus magnetron pulsed power was never applied until the system was completely matched. Since the high Q wavemeter frequency monitoring system was common to both the magnetron and signal generator channels it was possible to insure that the alignment signal frequency was identical to the magnetron operating frequency.

This test signal injection system was also used to determine when the ultrasonic cavities had reached equilibrium , with respect to temperature and were thus ready for a measurement sequence, the condition of equilibrium being indicated by cessation of the frequency drift of both cavities. In fact this signal injection system was used to determine the presence of any drift or instability in any part of the microwave bridge , the ultrasonic transducer, and the receiver system since it was functional even when the magnetron

was operating under high pulsed power conditions.

The individual components comprising the monitor system will now considered.

4;13;2 (CROSSED DIRECTIONAL COUPLER)

The directional coupler constructed for the magnetron monitor was of the cruciform type having two coupling slots arranged in the broad face of the wave guide , as shown in FIG.(4;13;2;1).

The dimensions of the coupling slots were obtained from the following equation:

$$\text{Coupling in db.} = 10 \log\left\{ \frac{4\pi^4}{9 a^4 b^2} \left\{ \frac{L^5}{\left(\ln\left(\frac{4L}{w} - 1 \right) \right)^2} \right\} \cos^2\left(\frac{\pi d}{2a}\right) \right\}$$

where , L, is the coupling slot length w, the width and d/2, the displacement of the slot center line from the waveguide center line. The letters a, and b, refer to the waveguide broad and narrow dimensions respectively.

The desired coupling was -40 db. and the pertinent parameters were as follows:

λ_o = 10 cms

g = 13.94 cms.

a = 7.2 cms

b = 3.4 cms.

d = 3.49 cms.

Specifying that L = 5 w and inserting the above values into the coupling equation gave the following:

L = 0.89 cms and w = 0.177 cms.

The coupling equation given above holds for a single waveguide wall thickness and so the top face of the auxiliary coupler arm was machined off prior to assembly.

The actual coupling obtained was - 45 db under a V.S.W.R. of 0.99. The directivity was found to be better than 40 db.

4;13;3 (BROADBAND CRYSTAL MOUNT)

The waveguide crystal holder designed for the pulse shape monitoring system was of the bar and post type, the crystal diode forming part of the post. This holder was fitted with a tunable short circuiting plunger similar to that described in the section on the launching section. The unit was so constructed that either cartridge or coaxial type crystals could be accomodated. A folded $\frac{1}{2}$ wavelength coaxial choke was used to isolate the R.F. from the video output connection.

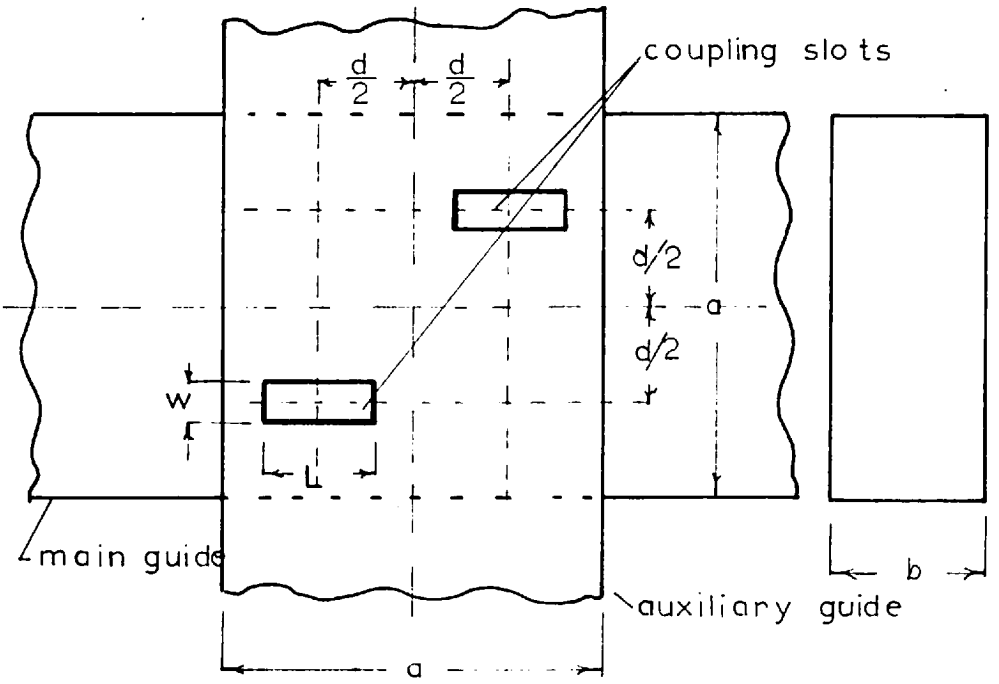

FIG. (4;13;2;1)

Details of crossed directional coupler.

Due to the very low capacitance of the unit, excellent pulse reproduction was achieved.

4;13;4 (TEMPERATURE STABILISED WAVEMETER)

For the sake of high measurement accuracy it was necessary that the pulse train cancellation sequences , before and after application of the test liquid to the test transducer, be conducted at the same operating frequency. Since however there was normally a two hour time lapse between the consecutive parts of the test,this long period being required for temperature equilibrium to be reestablished after crystal loading, it was important that some extremely stable frequency reference be available , against which the system operating frequency could be checked.

An " S " band wavemeter having a loaded Q of 9000 was found to give reasonable frequency definition, but was not sufficiently stable due to large ambient room temperature variations. In an attempt at improving the frequency stability of the wavemeter a special temperature stabilising system was developed. For convenience the unit was transistorised and made portable so that the wavemeter could still function as a standard laboratory instrument if required.

The circuit employed in the stabiliser is shown in FIG.(4;13;4;1) along with a sketch of the arrangement.

Basically the temperature controller consisted of a heating coil wound around the wavemeter, the heating power of which was made to vary so as to compensate for any temperature change in the wavemeter body. This variation in coil heating power was accomplished by means of a series regulat ing (OC35) transistor which was driven by a D.C. amplifier. whose output level was proportional to the temperature of the wavemeter body. A Stantel (G.25) thermistor was utilised as the temperature sensing element which supplied the input for the D.C. -

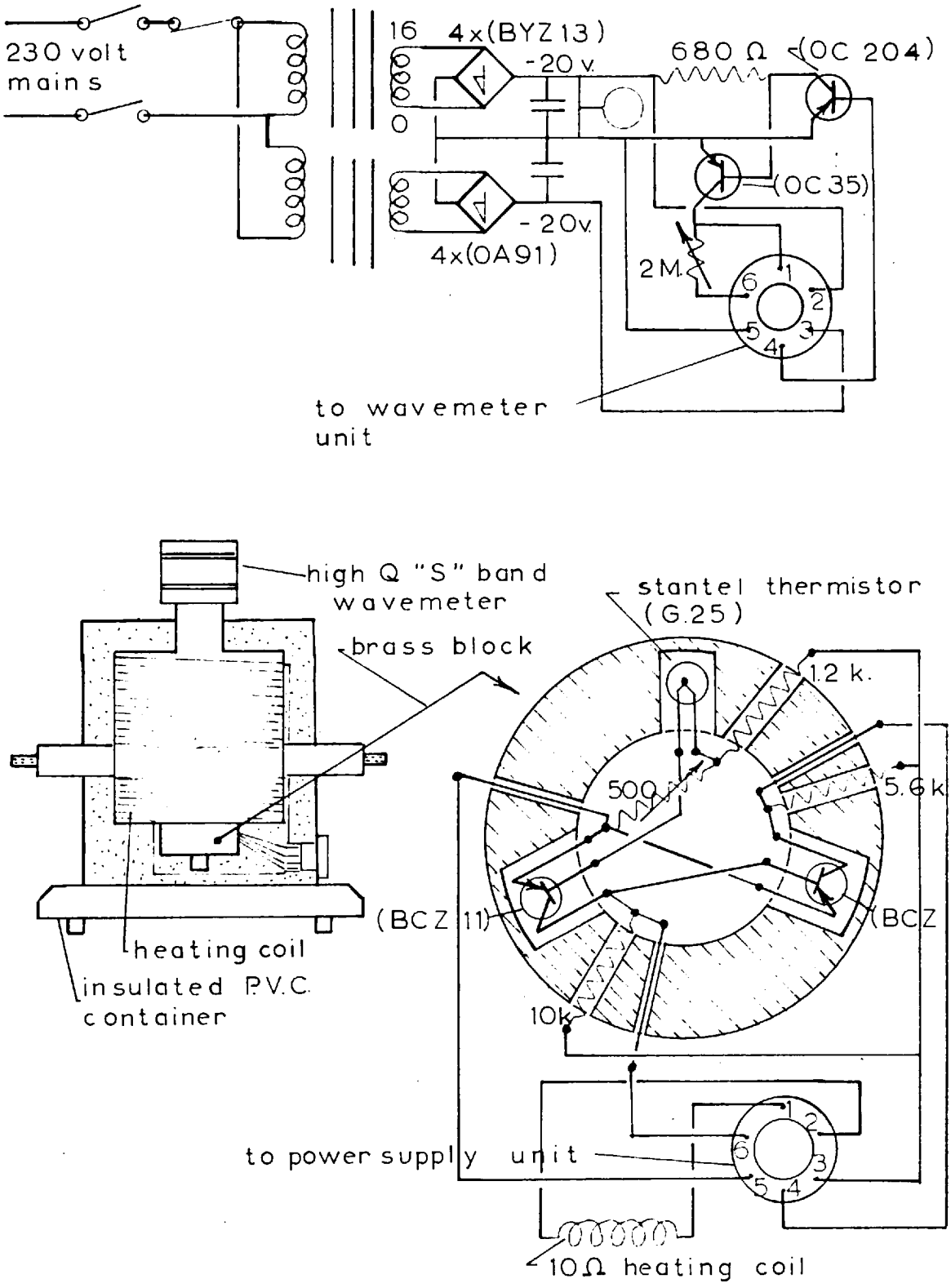

FIG. (4;13;4;1)

Wavemeter temperature stabiliser.

amplifier.

A thermistor was used as the temperature sensing element since it has good response and high output.

The first two stages of the D.C. amplifier were built into the same brass block as the thermistor in an effort to minimise drift due to the transistors themselves. Both transistors and thermistor were mounted in tight fitting holes in the block to insure maximum heat conduction and then the brass block was securely bolted to the wavemeter body. The 10 ohm heating coil was made from 36 S.W.G. enamelled copper wire wound directly on to the wavemeter.

Separate supplies were used for heating coil circuit and for the D.C. amplifier section to minimise instability. In addition a variable feed back line was also incorporated in the design so that the gain of the amplifier could be controlled to a point just below the onset of oscillations.

The wavemeter and brass block, containing the D.C. amplifier were mounted in a P.V.C. container , insulated with expanded polystyrene, such that the calibrated micrometer top just protruded. The D.C. supplies and main regulating transistors were mounted in a separate cabinet.

Performance.

The temperature stabiliser was found to function very effectively giving a temperature variation of less than + or - 0.1 ^{o}C. for a daily room temperature variation of approximately 8 ^{o}C., despite the fact that the wavemeter body was directly coupled to a very large heat sink, formed by the waveguide system. The error in frequency determination due to the temperature variation of the stabiliser could not be detected. Since the wavemeter had an initial heating up time of approximately one hour, the stabiliser was left on continuously.

CHAPTER 5

DETAILED ANALYSIS OF INDIVIDUAL COMPONENTS IN BRIDGE UNIT

5;1 (GENERAL)

As in the case of chapter 4 , a detailed analysis of the individual components constituting the basic microwave bridge unit will now be given. These items will also be considered with reference to:

(a). Reason for inclusion in the system.
(b). Design and construction.
(c). Performance.

5;2 (BRIDGE MAGIC T)

The reasons for developing the system utilising a microwave bridge were as follows;

Firstly, the technique of measurement, being dependent on the determination of a small change in the amplitude and phase of a train .pulses or " echoes " , obtained from an ultrasonic cavity, required that a reference signal be available against which these echoes could be compared. It was also essential that this reference source be extremely stable in amplitude and phase ,with respect to the signal exciting the test cavity and that it occur in the same time phase as the response from the test cavity. Since the test cavity was driven by a modulator-magnetron combination which could not be suitably stabilised it was found desirable to derive the reference signal from the same source , thereby automatically insuring perfect relative amplitude and phase as well as frequency stability.

Another extremely important advantage which was derived from the choice of a bridge system was that since the actual comparison of the test and reference signals was accomplished utilising only passive waveguide elements, all errors due to possible drift or instability in the receiver system were eliminated.

Properties of the Magic T

A magic T is , as shown in FIG.(5;2;1) , a four port hybrid waveguide junction which, when all its arms are properly terminated, has the following properties:(107).

(1). All arms appear matched looking inward into the junction.

(2). Energy incident in arm number 3 will divide and couple equally to arms 1 and 2 with the same phase relationship, but no coupling will exsist to arm number 4.

(3). Energy incident in arm number 4 divides and couples to arms number 1 and 2 with the same amplitude but opposite phase. No coupling to arm number 3 occurs.

(4). Arm number 1 couples equally to arms 3 and 4 but not to 2.

(5). Side arm number 2 couples equally to arms 3 and 4 but not to number 1.

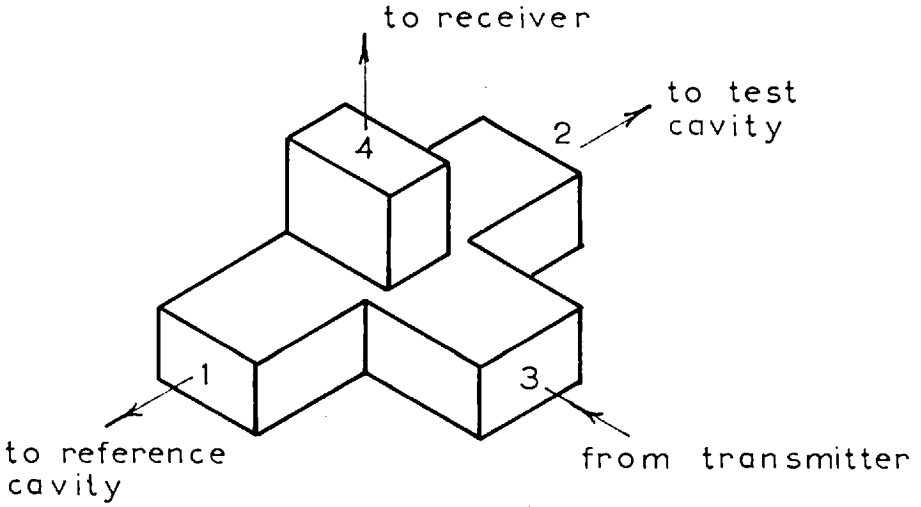

FIG.(5;2;1)

Bridge magic T.

(6). Arms number 1 and 2 couple to arm number 4 with opposite phase relationship.

From the foregoing properties it is evident that the magic T would make a very excellent microwave bridge element when connected to the transmitter, receiver and test and reference cavities in the manner shown in FIG.(5;2;1). This configuration was found to be especially desirable since the receiver was automatically isolated from the high powered transmitter and there was no interaction between the test and reference arms. In addition the comparison of the test and reference signals was actually accomplished in the T junction where bandwidth and isolation from extraneous noise and radiation were excellent. Thus,with reference to FIG.(5;2;1), the sequence was as follows: The high powered magnetron pulse was coupled into arm number 3 of the magic T where the energy was divided equally and with the same phase relationship, between the test and reference cavities , connected to arms 1 and 2 of the junction. Then with the transmitter off the decay or " echo " pattern from each cavity was coupled back into the magic T dividing equally between arms 3 and 4, but with the opposite phase relationship in arm 4 . Therefore when the pulse trains from both cavities were of the same amplitude and phase relationship the components coupled to the receiver or number 4 arm of the T cancelled each other thus giving a null or balanced indication in the receiver system.

From the above description it is evident that under balanced conditions all the energy was coupled back into the transmitter arm and so it was necessary to insert the resonance isolator at this point so that reflections from the transmitter channel would not interfere with bridge balance.

Under low power conditions the receiver system presented a reasonable load for the E plane bridge arms , having a V.S.W.R. of 0.99 . However when the magnetron fired the receiver arm was not well matched due to the ionisation of the T.R. cell. It should be noted here that it was the reflected pulsed power from the microwave cavities during their transient period to resonance that

fired the T.R. cell and not the cross coupling between the transmitter and receiver arms of the bridge. Ideally an isolator should have been inserted in the receiver arm just before the T.R. cell to prevent the power reflected from the ionised cell from coupling back into the microwave bridge. However since this reflected energy occured only during the leading edge of the R.F. pulse only a relatively small amount of energy was involved and so the omission was not a serious one.

5;3 (BRIDGE REFERENCE CHANNEL)

5;3;1 GENERAL

As previously mentioned, the reference channel of the microwave bridge was used to supply a suitable reference to which changes occuring in the test channel could be compared. It was desirable from quartz crystal considerations , which is more fully discussed in section (10;5) , to have the facility to alter attenuation and phase in the reference arm as well as the test arm. Consequently it was essential that all the components in the reference channel be of high electrical quality and possess a high degree of stability and resettability. Since the actual measurement of attenuation and phase shift was made with the components in the test channel it was not required to accurately calibrate the reference arm components.

5;3;2 (PRECISION LEVEL SETTING ATTENUATOR AND PHASE SHIFTER)

Initial experiments using a commercially obtained attenuator and phase shiter showed that these particular items were not satisfactory with respect to their resettability and variation in V.S.W.R. over their range of measurement. Consequently it was necessary to design and construct several attenuators and phase

shifters to meet the required specifications, and to this effect several waveguide sections having carriage mechanisms possessing a very high degree of precision, stability and resetability were developed. These units were then fitted with either well matched attenuating or dielectric vanes, to provide the high precision level setting attenuators and phase shifters required in the system.

In order to achieve the desired accuracy of measurement it was essential that all attenuators be resettable to better than 0.01 db, be highly stable with respect to temperature and humidity, and have a variation in V.S.W.R.,over the operating range of the instrument, of less than 0.045. In addition some units were required to operate at a pulsed power level of some 200 kilowatts . Phase shifter requirements were very similar to the attenuator requirements, except that resetability of 0.01 of a degree was desired. So as not to interfere with attenuation measurements, the variation in insertion loss of all phase shifters , over their range of travel, has to be less than 0.01 db.

In an effort to realise the high degree of resettability imposed on these items, a special carriage mechanism capable of being mechanically reset to better than 0.0001 of an inch,over its whole range of travel, was designed and constructed. This was accomplished by employing a spring loaded,three point , ball suspension , carriage system running on perfectly flat , hardened ground steel V slips, set in a massive base plate. This base plate was then firmly attached to the wave guide section.

The vane support push rods were passed right through the waveguide, thereby enabling the vane to be very stably mounted. In addition any variation in V.S.W.R. resulting from the support rods themselves was eliminated . The waveguide wall thickness, at the point of push rod entry, was increased by $\frac{1}{2}$ inch , which thus formed a circular waveguide far beyond cutoff and hence no detectable radiation

through these holes was observed. A special dielectric material, PolyPenco Q 200:5, was used for the push rods. This material was a cross-linked polystyrene developed for microwave applications, having excellent electrical properties comparable to those of P.T.F.E. In addition this material had high mechanical stability and low moisture absorption as well as good machining properties. The dielectric vanes of the phase shifters were also constructed of this material.

Although the carriage mechanism was driven with a micrometer, actual indication of position was obtained from a dial gauge in an effort to provide still better performance. A transparent dust cover was also provided to insure reliability.

Metalised glass was chosen for the attenuating vane material . This type of vane, being constructed from a low loss glass upon which nichrome was evaporated to a thickness of approximately 100 Angstroms , giving a resistivity of some 200 ohms per square, was highly stable and hence quite satisfactory for this application. The tapers on the leading and trailing edges of the vane were modified experimentally to achieve best performance.

Performance.

All the attenuators and phase shifters constructed in the above manner gave satisfactory performance. Resistability of both devices was better than measurable. Variation in V.S.W.R. of all instruments was found to be well within the tolerance imposed. Typical curves for these constructed devices are given in FIG.(5;3;2;1 and 2).

In order to achieve good temperature stability from the phase shifters the dielectric vanes were constructed from a material having a low dielectric constant, as this would result in a small phase shift for a reasonably large linear displacement , and so any temperature changes , resulting in small displacements or size of vane, would

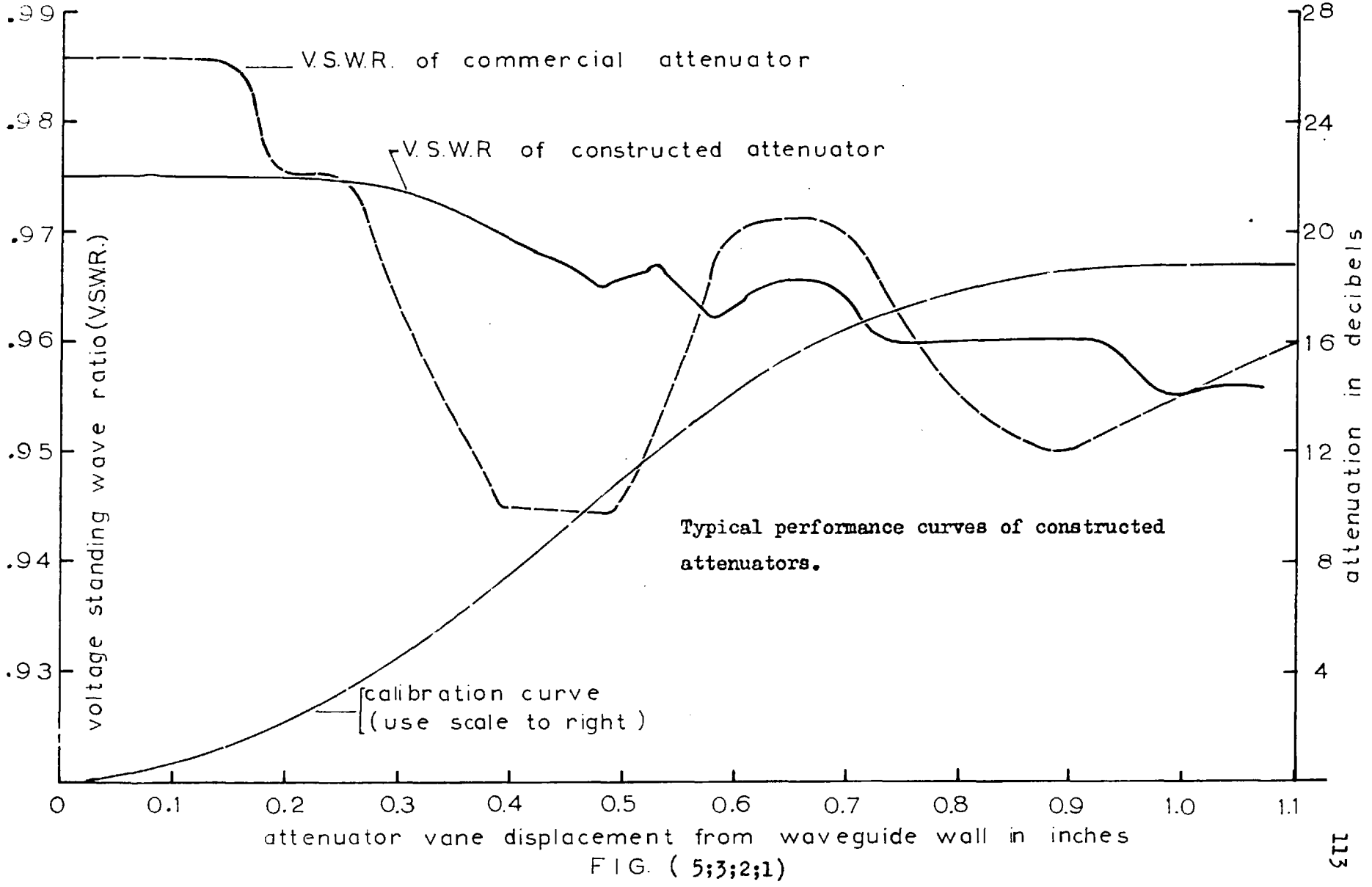

Typical performance curves of constructed attenuators.

FIG. (5;3;2;1)

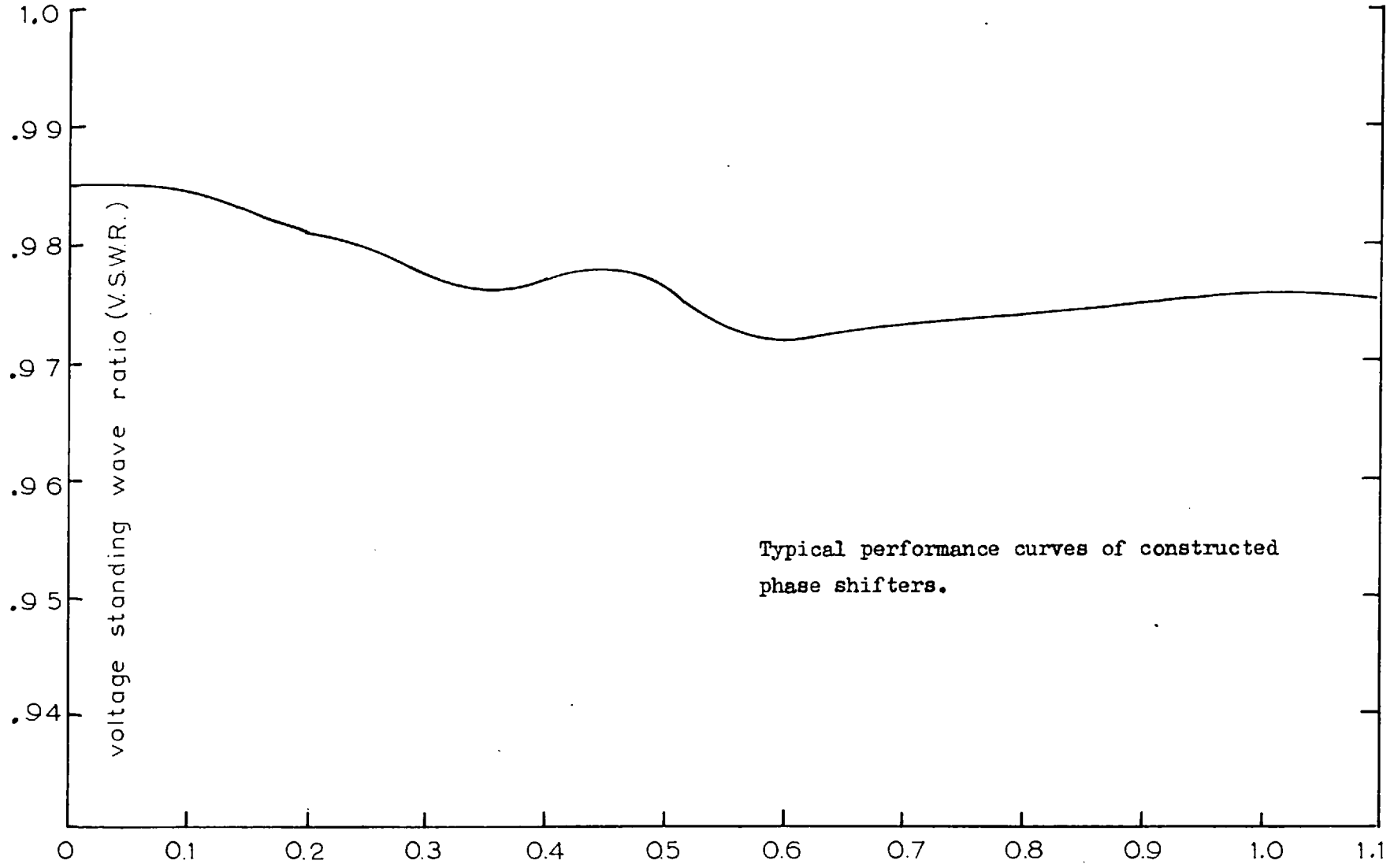

Typical performance curves of constructed phase shifters.

FIG. (5;3;2;2)

have a correspondingly small effect in phase shift.

Due to this low value of vane dielectric constant only about 15o degrees of useful phase shift was obtained from a single unit. Since however a full 360 degrees of level setting phase shift was occasionally required,to compensate for dissimilarities between the two quartz crystals, it was necessary to construct three separate phase shifters for this purpose.

The general technique adopted in the construction of these attenuators and phase shifters is shown in FIG.(5;3;2;3)

5;3;3 (SQUEEZE SECTION PHASE SHIFTER)

A squeeze section was designed and constructed in an attempt to obtain a phase shifter having very high resolution , which could be accurately calibrated and subsequently employed in precise phase differential measurements. A squeeze section type of construction was chosen since it can be made to have negligible V.S.W.R. and variation in insertion loss over its entire range.

The principal behind the squeeze section is extremely simple and can easily be appreciated by considering the expression derived in appendix B for the guide wavelength . Thus from equation (B;4;2;12)

$$\lambda_g = \lambda / \left(1 - (\lambda / 2a)^2 \right)^{\frac{1}{2}} \qquad (B;4;2;12)$$

$$\text{"} = \lambda_o / \left(1 - (\lambda_o / 2a)^2 \right)^{\frac{1}{2}} \qquad (5;3;3;1)$$

since for air dielectric the unbounded wavelength λ is equal to the free space wavelength λ_o.

Clearly it is possible to obtain a phase shift in a given length of waveguide simply by changing the broad waveguide dimension (a), and this in fact is what was done in the squeeze section . The waveguide

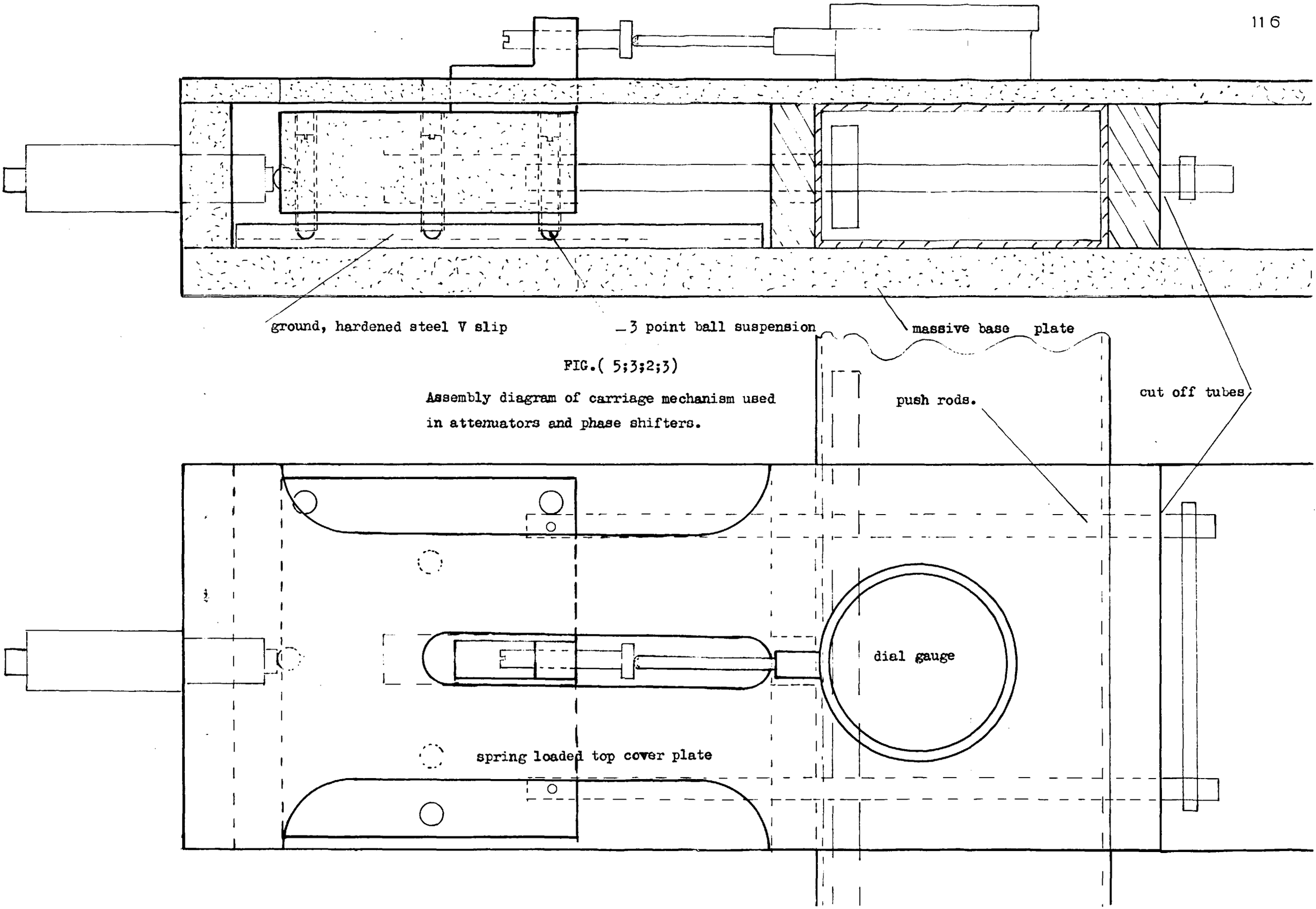

FIG.(5;3;2;3)

Assembly diagram of carriage mechanism used in attenuators and phase shifters.

walls were squeezed together after a long central slot had been cut in both top and bottom surfaces. This squeezing action resulted in a gradual decrease in waveguide dimensions and as a consequence negligible mismatch was introduced .

An estimate of the overall expected phase shift from the device was obtained by assuming that the displacement of the guide wall from its normal position , at any point along the slot, was a linear function of the distance from the beginning of the slot, and then calculating the effective mean waveguide width of the section. This mean waveguide width was subsequently used to determine the wavelength in the squeezed section from equation (5;3;3;1). The expected phase shift was then obtained from the change in the effective electrical length of the section.

The electrical length of the unsqueezed section = L/λ_g

Effective electrical length of squeezed section = L/λ_g'

where λ_g' is the mean squeezed guide wavelength and L is the actual physical length of the slotted section.

Thus the expected phase shift ϕ is given as:

$$\phi = \frac{360\ L}{\lambda_o} \left\{ (1-(\lambda_o/(2a-d/2))^2)^{\frac{1}{2}} - (1-(\lambda_o/2a)^2)^{\frac{1}{2}} \right\} \qquad (5;3;3;2)$$

Now L was made 53 centimeters and d, the slot width, was set at 0.1 55 centimeters. In addition λ_o = 10 cms. and a = 7.2 cms.

Upon substitution of the above value into equation (5;3;3;2) the value of the expected phase shift obtained was .9.53 degrees.

Construction

The technique employed in the construction of the squeeze section is indicated in FIG.(5;3;3;1).

Considerable difficulty was encountered in the construction of this device, the main problem being the instability of the " S " band waveguide wall when the long axial slots were cut in both the top and bottom surfaces. Apparently in the process of manufacture internal stresses are set up within the waveguide as a result of the extrusion. When these stresses were released , during the slotting procedure, the section lost its dimensional stability. Initial attempts at annealing the structure before machining lessened the deformation, however this process made the brass guide extremely rigid and thus of no use for this application. Success was finally achieved by using special " stress relieved " waveguide which had been dimensionally re-established by the manufacturer.

The waveguide wall thickness was also reduced from 0.08 to 0.04 of an inch to lower its moment of inertia and thereby give greater flexibility. The force required to close the 1.55 mm. slot was 220 pounds and this was derived from a large drum micrometer operating through a level system.

Actual waveguide wall displacement from the normal position was measured with a high precision dial gauge.

The entire assembly was mounted in a speoial radiation shield fabricated from number 9 size waveguide.

Performance

Excellent performance was obtained from this squeeze section. The input V.S.W.R. was 0.995 and the variation in V.S.W.R. was undetectable . Mechanical reset accuracy of 0.0004 of an inch was achieved

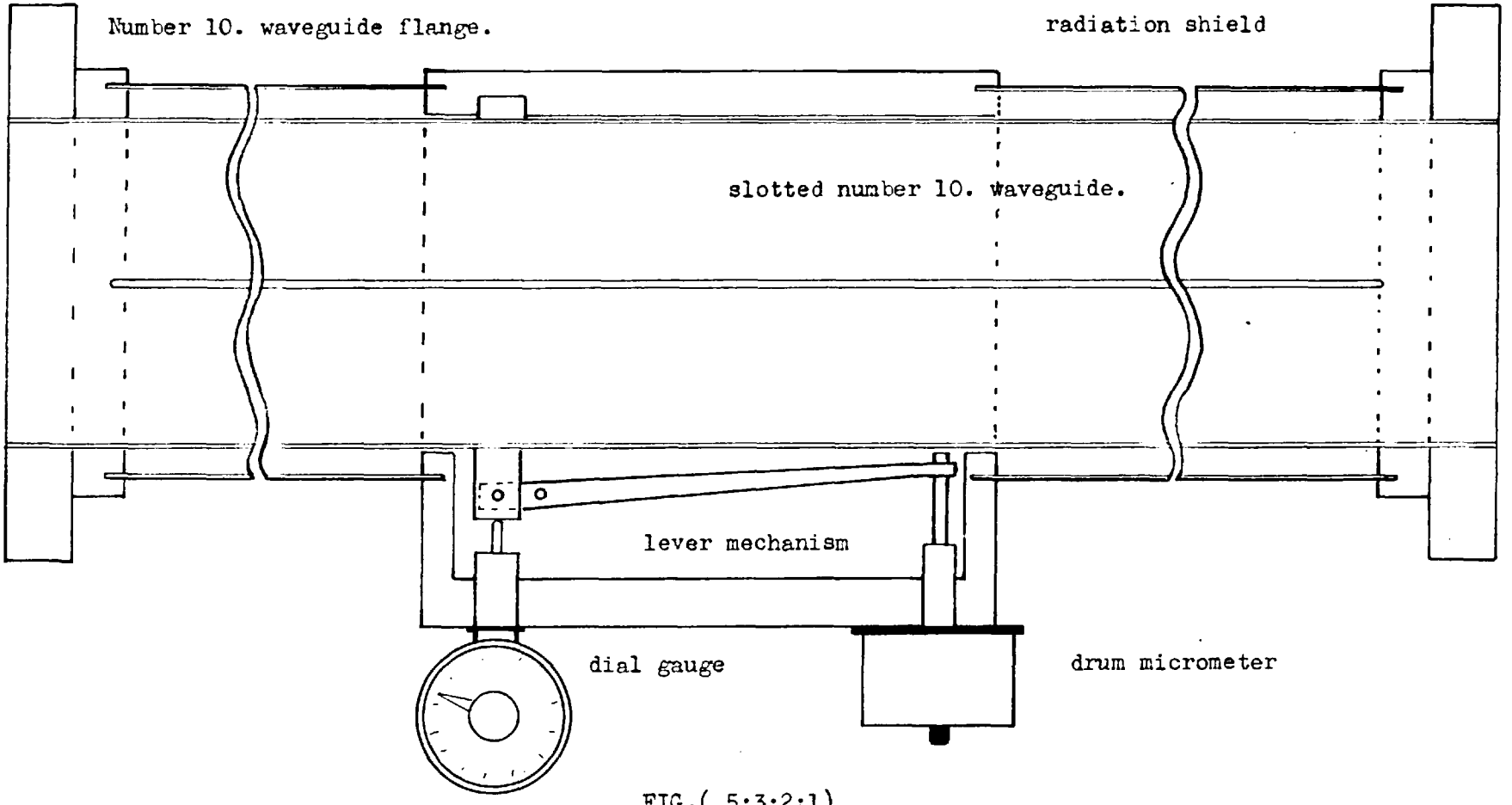

FIG.(5;3;2;1)

Squeeze section phase shifter construction .

giving a phase shift reset accuracy of better than 0.01 of a degree. In addition the variation in insertion loss of the instrument, over its entire range, could not be detected. The radiation shield was found to be effective to -100 db. which was better than that obtained from the choke flanges used in the system.

An overall phase shift variation of some ten degrees was measured , this being in good agreement with the expected estimate of 9.5 degrees.

Actually this phase shifter was not calibrated and used for measurement purposes but rather was inserted in the reference channel of the microwave bridge to compensate for the initial phase shift introduced by the application of the test sample to the test cavity. Utilisation of the section in this manner did not require that it be calibrated but did however impose stringent restrictions on attenuation and V.S.W.R. variations.

5;3;4 (WAVEGUIDE TO COAXIAL LINE TRANSFORMER)

Waveguide to coaxial line transformers were used in both the test and reference channels of the microwave bridge to transform the pulsed electromagnetic energy from the waveguide system into the ultrasonic cavities through short lengths of 50 ohm coaxial cable. Thermostating considerations deemed it essential that these coaxial cables be incorporated into the system to thermally isolate the ultrasonic cavities from the main waveguide system. It was required to stabilise the cavity temperature to + or - 0.02 of a degree centigrade , over a range of -60 ^{o}C. to + 60 ^{o}C. , clearly this could not have been accomplished if direct connection between the cavities and the waveguide channels had been utilised.

These transformers were designed to be tunable by means of a movable shorting plunger of the type described in connection with the lauching section. A four screw stub tuner was also built into the transformer to facilitate matching.

A well matched transformer is desirable at this point in the system so that as little energy as possible is reflected back into the receiver channel of the magic T, during the main transmitter pulse. Any energy reflected into the receiver arm lengthens the receiver recovery time due to greater ionisation of the protective T.R. cell.

Performance

The transformers built were found to easily handle the pulsed power available without sparking. Very fine tuning was also possible with these devices since the shorting plungers were micrometer thread driven and so perfect match was obtained over the band of interest.

5;4 (BRIDGE TEST CHANNEL)

5;4;1 GENERAL

The components in the test channel of the microwave bridge were used to obtain the actual values of differential attenuation and phase shift introduced by the test liquid sample. It follows therefore that unlike the components in the reference channel the test channel components were required to possess a very high accuracy of calibration as well as stability and resettability. In addition, since the technique of measurement invloved the simultaneous adjustment of attenuation and phase shift until bridge balance was achieved, it was essential that the measurement attenuator introduce no phase shift and that the measurement phase shifter introduce no attenuation.

5;4;2 (PRECISION FOUR SCREW TUNER)

Since the rotary attenuator used for differential attenuation measurements had a considerable variation in V.S.W.R. over its range of movement, it was necessary to construct a four screw tuner which could be easily and accurately reset, and to calibrate this device for various attenuator settings.

The construction of the tuner was very simple in that it was similar to the other stub tuners used in the system except that in this case each screw was driven by a micrometer. The screw spacing adopted was approximately $\frac{3}{8}$ of a guide wavelength. This particular spacing was chosen in preference to the normal $\frac{1}{4}$ or $\frac{1}{8}$ wavelength spacing commonly employed in stub tuners, since it can be shown ,(77), that there are certain unfavourable phases of standing waves of moderate amplitude, which require extremely large screw penetrations to achieve a match when $\frac{1}{4}$ or $\frac{1}{8}$ wavelength spacing is adopted. In addition the procedure which must be followed to tune out mismatches with these spacings is very envolved, since both the magnitude and phase of the standing wave is required. When $\frac{3}{8}$ of a wavelength spacing is adopted however it is found that the screw penetration required to tune out a given mismatch is much less and that only the amplitude of the standing wave need be monitored .

5;4;3 (PRECISION ROTARY ATTENUATOR)

Since, as explained in section (5;4;1) , it was essential that the measurement attenuator introduce no phase shift, it was not possible to use a conventional resistive vane attenuator in the test channel because of the phase shift introduced by the displacement of the glass vane in the waveguide. The only satisfactory solution to this problem was found to be utilisation of a rotary attenuator, which although still employing resistive elements can be designed to introduce negligible phase shift over its operating range.

Description of operation

The main body of the rotary attenuator was made from circular waveguide having internal dimensions such that only the dominant $T.E._{11}$ mode would propagate. This section of circular guide was coupled to standard " S " band number 10 rectangular waveguide through transition sections at either end. Since the dominant $T.E._{11}$ mode

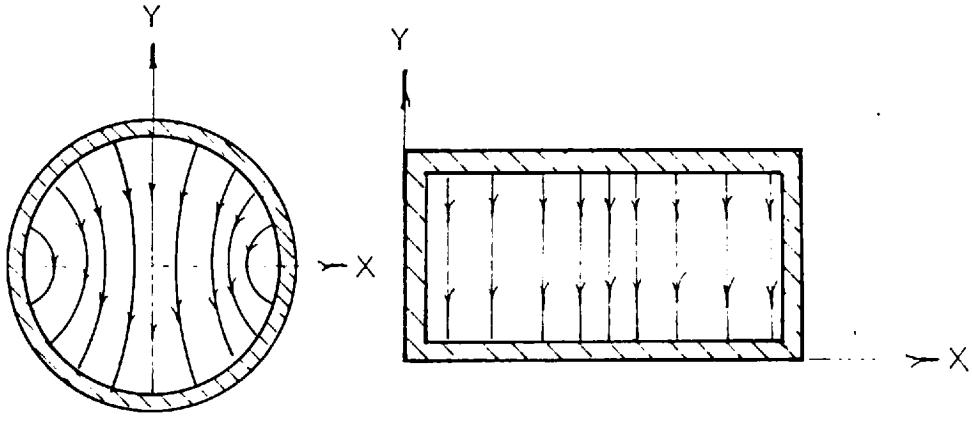

FIG. (5;4;3;1)

Dominant mode field patterns in circular and rectangular waveguides.

field patterns in circular guide are similar to the dominant $T.E._{10}$ mode patterns in rectangular guide, as in shown in FIG.(5;4;3;1), these transition units need be very simple.

The circular section of the attenuator was divided into three parts each having a nichrome coated fibreglass axial vane across its diameter. Both end sections had their attenuating vanes mutually parallel , while the center portion could be rotated through 90 degrees, its angle of rotation relative to the end sections being accurately indicated on a precision scale.

The principal underlying the operation of this device can be easily understood by considering the electric field pattern in circular waveguide as shown in FIG.(5;4;3;1). This electric field pattern may be resolved into two components which are mutually perpedicular and parellel to the x and y axis respectively. If an axial attenuating vane is inserted diametrically across the guide parallel to the x axis, the horizontal electric field component will be completely absorbed, while the vertical or y component will be unaffected. Thus the electric field pattern entering the main part of the rotory attenuator may be considered to be vertically polarised. If the center section of the attenuator is rotated such that its vane makes an angle Θ with with the fixed end vanes, the wave of amplitude E_o emerging from the first transition section will again undergo further polarisation ,due to the rotated vane, the transmitted component being equal to $E_o \cos(\Theta)$. The same process occurs at the tran-

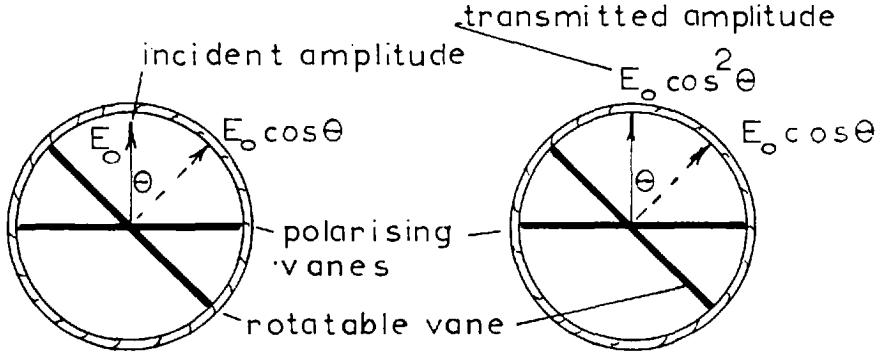

FIG. (5;4;3;2)

Schematic operation of rotary attenuator

sition from the center section to the end section and so the finally emerging wave has an amplitude $E_o \cos^2(\Theta)$. The above is depicted in FIG.(5;4;3;2). It follows therefore that the attenuation of the instrument is given by the relation:

$$A = 40 \log (\sec^2(\Theta)) + C$$

where C is the insertion loss of the instrument resulting from the initial polarisation of the incident wave.

Clearly it is evident that the rotary attenuator is an absolute instrument which does not require calibration , its attenuation being completely determined by the measurement of a physical angle. Another advantage possessed by this device is that there is no dependence on the actual resistivity of the various vanes, provided that there is sufficient attenuation to completely absorb the parallel resolved field component. Similarly the attenuation has no frequency dependence.

It is now possible to appreciate why there is no variation in phase shift with attenuation since the position of the vanes, with respect to the transmitted field component, is always the same.

Performance

Since the attenuator was fitted with a fine anti-backlash drive mechanism it was possible to accurate position the rotating vane. consequently the resetability of the intrument was exceeding high. Thus the accuracy of the device was limited mainly by the marking of the direct reading attenuation scale,being typically better than 0.01 db. over the range used.

Although this rotary attenuator purchased from F.X.R. , was the best of its type commercially available , it was not completely satisfactory in two respects, the first being variation in V.S.W.R. with attenuation and the second, low peak pulsed power handling capacity.

FIG.(5;4;3;3) shows the variation in attenuator match versus attenuation . As explained in section (5;4;2) it was possible to compensate for this failing through the use of a resettable stub tuner.

The low pulsed power capacity of the attenuator however was a much more serious problem which in fact lead to actual failure of the

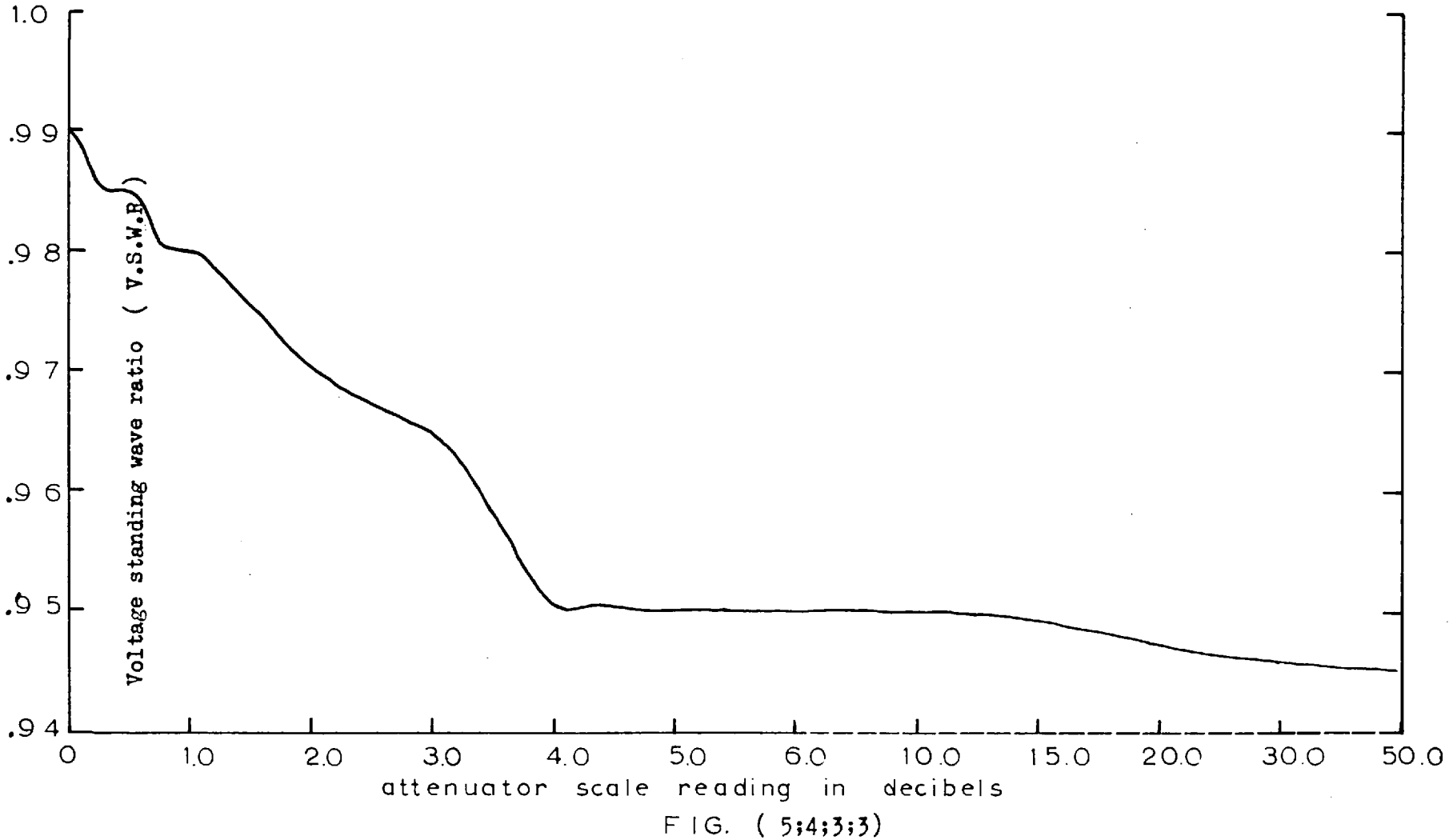

FIG. (5;4;3;3)

Variation in input match of rotory attenuator (F.X.R. S164 A)

nichrome coated fibreglass vanes. Specifications limited the device to two watts mean power but no peak power limit specification could be obtained. Failure however occured at a peak pulsed power of only 30 kilowatts and 0.6 watts mean power. The manufacturer was unable to offer any satisfactory explanation. Since a satisfactory solution to the above problem was not obtained the rotary attenuator, fitted with replacement vanes , was operated under reduced pulse power conditions of approximately 20 to 25 kilowatts.

5;4;4 (PRECISION LEVEL SETTING PHASE SHIFTER)

Another level setting phase shifter of the dielectric vane type was inserted into the measurement channel to help compensate for the unequal acoustic path lengths in the two piezoelectric quartz crystals. This phase shifter was identical to the one described in section (5;3;2).

5;4;5 (PRECISION MEASUREMENT PHASE SHIFTER)

Another dielectric vane phase shifter was utilised as the measurement phase shifter. This instrument was calibrated against a standard at the " Royal Radar Establishment " in Malvern,and has been found to have a reset and differential accuracy of 0.01 degrees over the linear portion of its range.

5;4;6 (WAVEGUIDE TO COAXIAL LINE TRANSFORMER)

The end of the test arm of the microwave bridge was terminated in a waveguide to coaxial line transformer identical to that present in the reference channel. Similarly a short length of 50 ohm coaxial cable was used to connect the test ultrasonic cavity to the waveguide section.

The physical lengths of the individual components comprising both test and reference arms of the microwave bridge were chosen so that the overall length of each of the arms was the same. This was done in an attempt to minimise the introduction of error into the phase measurement, resulting from changes in the electrical lengths of the bridge arms due to variations in ambient room temperature.

CHAPTER 6

DETAILED ANALYSIS OF INDIVIDUAL COMPONENTS IN RECEIVER SYSTEM

6;1 (GENERAL)

The individual components constituting the microwave receiver system will now be discussed in the order in which they appear in the receiver channel , this sequence not necessarily being the order in which they were developed. As in previous cases these components are considered with respect to,reason for inclusion, design and construction and finally performance.

6;2 (90 ^{o} H PLANE BEND)

As explained in section (5;2) the receiver system was coupled to the E plane arm of the bridge magic T . Because of the physical size of the receiver unit it was necessary to change the direction of the waveguide run and to this effect a 90^{o} H plane ,electroformed waveguide bend was inserted at this point.

6;3 (DOUBLE DIRECTIONAL COUPLER)

A double directional coupler was included in the receiver system to enable test signals to be injected for test and alignment purposes. In addition the pulsed power coupled to the receiver arm and the reflected power from the T.R. cell could also be monitored with this device. Since the magic T was well matched no direct coupling exsisted between the transmitter and receiver channels, however transmitter power was reflected back from the ultrasonic cavities into the receiver. As previously indicated, this reflected power arose due to the fact that the ultrasonic cavities had an appreciable Q and consequently appeared as susceptive loads to the transmitter pulse until they became resonant. Obviously the duration of this reflected energy was dependent on the time required for the cavities to assume unity con-

ductance and so was directly proportional to their loaded Q . Since, as explained in section (F;1;2) , there was an optimum loaded cavity Q for the system, the reflected power,as monitored by the double directional coupler, provided a convenient means of determining when this condition had been realised.

Cavity sparking as well as proper functioning of the T.R. cell were also clearly indicated through this monitor system.

Construction

Magnetic coupling through two $\frac{1}{4}$ wavelength spaced holes in the narrow waveguide wall was utilised in the construction of this coupler. Matched terminations were built into the load ends of the auxiliary side arms, while waveguide to coaxial line transformers were placed in the other ends. This particular type of construction resulted in a very compact device.

The size of the holes required for the desired degree of coupling was calculated from the following equation : (108).

$$\text{Coupling} = 20 \log \left\{ \left(\frac{\pi d^3 \lambda_g}{6 a^3 b} - 32.0 \left(1 - \frac{1.71\, d}{\lambda_o} \right)^{\frac{1}{2}} t/d \right) \right\}$$

where a,b and t are the waveguide dimensions with respect to width, height and wall thickness respectively , while d is the diameter of the coupling holes. This formula was originally given by Bethe and assumes two coupling holes in the narrow waveguide wall.

The actual hole size used in the constructed coupler was 1.25 inches and the hole spacing was 1.375 inches. These values gave the following performance for the completed coupler:

Coupling = - 13 db.
Directively = 2o db.
V.S.W.R. in main guide = 0.95

A four screw stub tuner was once again included in the device to eliminate the small V.S.W.R. present.

6;4 (TRANSMIT - RECEIVE , T.R. CELL)

The pulsed transmitter power coupled to the receiver channel as a result of the transient reflections from the test and reference cavities necessitated the incorporation of a protective device in the receiver system. The requirements imposed on this protective device were not only that it should instantaneously and effectively isolate the delicate receiver system from the high powered transmitter pulse but also that it recover completely in time for the receiver to accept the first echo pulse from the cavities . Considering now that the acoustic travel time was only 0.6 microseconds and that the pulse length was 0.35 microseconds , it is evident that the switch was required to clear in only 0.25 microseconds.

The only device capable of withstanding the high pulsed powers and still give adequate receiver protection was found to be an ionisation cell,normally termed (T.R.) cell . Unfortunately no commercial cells were available,operating in this frequency range,which possessed a recovery time any where near what was required. Finally however a specially developed cell was obtained from the A.E.I. laboratories in Lincoln , which was charged with a much larger percentage of water vapour and which consequently had a much faster recovery , at the expense of less isolation and larger initial spike.

This particular T.R. cell, a modified CV 2181, was of the filter type being constructed from three separate cavities coupled through quartz irises and giving a bandpass of approximately 50 megacycles with a loaded Q of 60 . The cell was charged with 4.5 mm. of argon and 12.5 mm. of watervapour.

A one thousand volt negative supply was used to keep the cell " alive " by means of creating a small glow discharge across an electrode gap built into one of the irises. This ion discharge of approximately 100 microamperes did not impair the small signal performance of the unit but did result in much faster cell breakdown under pulsed conditions thereby keeping the spike level within tolerable limits imposed by the delicate varactor diode in the parametric amplifier.

Performance

Accurate determination of cell recovery time under actual system working conditions was not attempted, however observations seem to indicate a recovery time of approximately 0.5 microseconds. This value was considerably below the 0.25 microseconds imposed if the first echo pulse was to be unaffected and so this first echo, although perfectly visible , was not very reliable for measurement purposes..

6;5 (WAVEGUIDE TO COAXIAL LINE TRANSFORMER)

Since the parametric amplifier which followed next in the receiver channel was a coaxial type , a coaxial line to waveguide transformer was inserted immediately susceeding the T.R.cell. This transformer was identical to that described in section (5;3;4).

6;6 (PARAMETRIC AMPLIFIER SYSTEM)

6;6;1 GENERAL

As previously indicated, the relatively low power limitation imposed by both the rotary attenuator and the ultrasonic cavities as well as the poor electromechanical conversion efficiency of the quartz transducers deemed it essential that a highly sensitive

receiver system be developed.

The conventional low noise balanced mixer receiver originally built for this purpose was found to be inadequate and so a non-degenerate , negative resistance , parametric amplifier was incorporated into the system to act as a preamplifier for the main reciver.

As there were a considerable number of auxiliary items of equipment associated with the paramatric amplifier, the complete assembly is discussed under the following topics:

(1). Amplifier signal input and output circuits.
(2). Basic amplifer unit
(3). Amplifier pump circuit.

6;6;2 (PARAMETRIC AMPLIFIER SIGNAL INPUT AND OUTPUT CIRCUITS)

Two strip line Y circulators connected as shown in FIG.(6;6;2;1) constituted the signal input and output circuits of the parametric amplifier.

The first circulator was required since the parametric amplifier used was a single port device and hence circulation was essential to separate input and output signals. In addition, as is explained in appendix (G;3), a circulator was vital if stable operation of the amplifier was to be achieved.

The function of the second circulator was twofold, being firstly to provide a D.C. return for the varactor diode in the parametric amplifier and secondly to function as part of the R.F. varactor switch system, which was incorporated at this point in the receiver channel to provide still further isolation for the balanced mixer receiver. This switch system is more fully discussed in section (6;7).

Strip line construction and inclosed magnetic structure were used in the fabrication of these Y circulators, resulting in very compact units. These circulators, obtained from the Rantex Corporation, were particularly chosen as they had a very large bandwidth and low insertion loss, which made them ideal for parametric amplifier application. The actual performance figures were as follows:

Bandwidth	=	2.5 to 3.5 KMc.
Maximum V.S.W.R.	=	1.2
Minimum isolation	=	20 db.
Insertion loss	=	0.2 db.

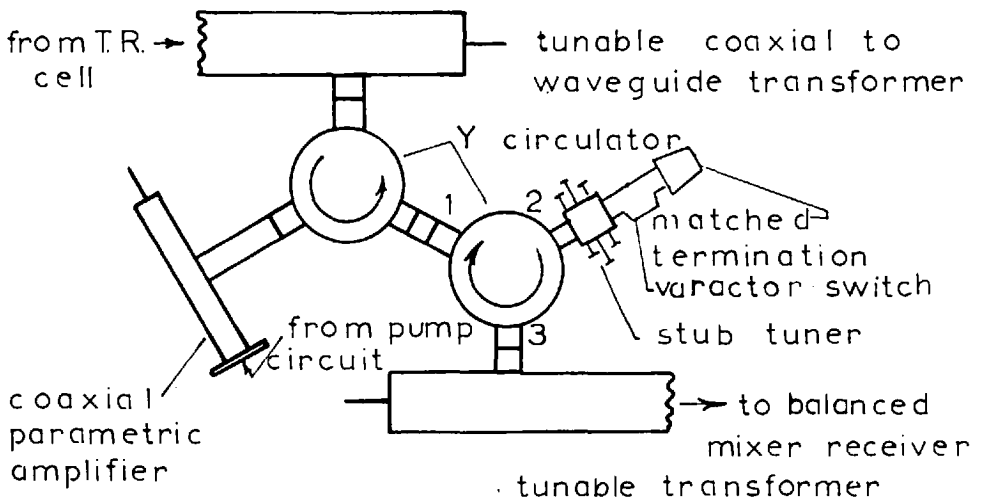

FIG. (6;6;2;1)

Schematic diagram of parametric amplifier input and output circuit.

The actual maximum V.S.W.R. obtained over the system operating range was 1.09 , while the minimum isolation over the same band was found to be 30 db.

It is beyond the scope of this work to consider the theory underlying the operation of these strip line Y circulators, however a complete analysis of this subject has been recently given by Bosma.(78).

6;6;3 (BASIC PARAMETRIC AMPLIFIER UNIT)

The parametric amplifier used in this system was , as is shown in FIG.(6;6;3;1) , a single port coaxial device, the theory of operation of which is given in appendix (G)of this work.

From FIG.(6;6;3;1) it can be seen that the design employed a taper impedance transformer to bring the input and output 50 ohms line impedance down to the optimum impedance level for the varactor, to achieve minimum noise figure. From equation (G;5;13) in appendix G, this optimum impedance ratio is given as:

$$R_g / R_s = \Gamma_1 Q \qquad (G;5;13)$$

where R_g is the input generator impedance, R_s is the series diode resistance , and $\Gamma_1 Q$ is the varactor diode figure of merit.

The varactor used in this amplifier was obtained from Microwave Asscoiates and had the following characteristics:

Type	= MA 4252
Cutoff frequency (f_c)	= 140 KMc.
Static capacitance(C_o)	= 1.09 u u f
Series resistance (R_s)	= 3 ohms
Figure of merit ($_1Q$)	= 5
Γ_1	= 0.33

Inserting the above values into equation (G;5;13) gives the value of the optimum generator input impedance R_g as 15 ohms.

The diode capacitance was resonanted by the inductance of a short length of coaxial line, the end of which extended into an " X " band waveguide, and so served as the pump circuit coupling probe. A tunable short circuiting plunger was built into the pump circuit to facilitate matching of the pump source to the amplifier. The X band waveguide used for the pump circuit was narrowed slightly to insure that it was

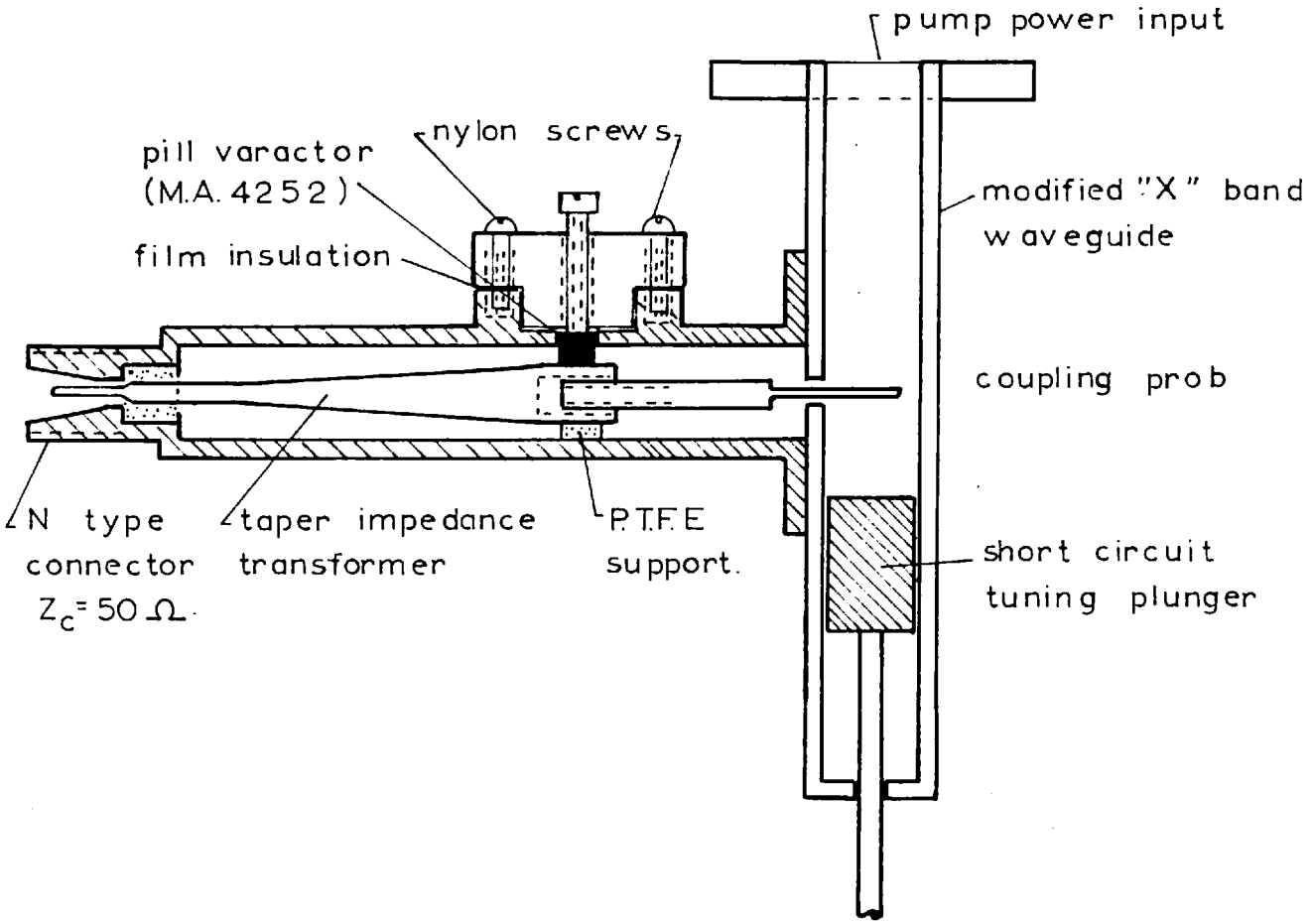

FIG. (6;6;3;1)

Schematic diagram of " S " band coaxial parametric amplifier.

far beyond cut off for the idler frequency, thus confining the idler completely to the amplifier.

An insulating film was inserted between the top, which was connected to one side of the varactor, and the main amplifier body. This was done so that the D.C. rectified diode current could be monitored at will. Special use was made of this facility during initial amplifier alignment, as is explained in appendix (G;6). Under normal operating conditions one of the nylon screws in the top cap was replaced by a brass one thereby completing the D.C. return.

A complete analysis of the operation of this nondegenerate, negative resistance parametric amplifier including bandwidth and noise figure considerations is given in appendix (G).

Performance

Excellent performance was obtained from this coaxial amplifier . An overall single sideband noise figure of approximately 3 db. , under conditions of 20 db. gain and 20 megacycles bandwidth was easily achieved. Of particular advantage was the excellent long term stability possessed by this device, which consequently necessitated only very infrequent realignment.

Up to the present it has not been necessary to replace the varactor diode , it obviously having been given adequate protection by the T.R. cell. No noticable deterioration of operating noise figure has occured after some 700 hours of operation.

6;6;4 (PARAMETRIC AMPLIFIER PUMP CIRCUIT)

Pump frequency power of some 30 milliwatts at a frequency of 9.6 KMc. was derived from a slightly modified, high quality coaxial " X " band oscillator obtained from W.H. Sanders Ltd. This klystron had a frequency stability of one part in ten to the sixth as well as

excellent long term output power stability , both of which were very important if high stability performance of the parametric amplifier was to be achieved. Since variations in the pump power level altered the amplifier operating frequency and also since pump frequency changes drastically affected the amplifier gain, a highly stabilised power supply was used to supply the pump klystron.

A ferrite resonance isolator, a variable attenuator,a stub tuner, a directional coupler and an " X " band wavemeter were also inserted into the pump channel in order to improve stability and facilitate alignment procedures.

6;7;1 (R.F. VARACTOR SWITCH SYSTEM)

A coaxial R.F. varactor switch was incorporated into the receiver system at this point to provide additional isolation for the main waveguide receiver. It was necessary to include this device in the channel since the spike break through associated with the T.R.cell, although not of sufficient amplitude to damage the balanced mixer receiver, was however sufficient to saturate the intermediate frequency amplifiers for a period longer than could be tolerated. As previously described , saturation in any part of the receiver channel for a period in excess of 0.25 microseconds after the trailing edge of the main transmitter pulse meant that the first cavity echo could not be used for measurement purposes. Similarly paralysis of any receiver component for a period of 0.85 microseconds meant that the second as well as the first pulse was obscured , and so on.

This coaxial switch was used in conjunction with the second Y circulator and gated a fraction of a microsecond before the triggering of the main transmitter. In this manner it was possible to obtain an additional 50 db. of isolation in the receiver channel and thereby keep the intermediate frequency amplifiers free of saturation.

The circuit configuration adopted for the switch system is shown in FIG.(6;6;2;1) on page (134), and represents operation of the varactor switch in the " circulator mode ". The switch was used in this particular manner since it is possible to obtain much greater isolation from the combined operation of both switch and circulator then could be achieved from either of the devices used separately.

Description of operation

With reference to FIG.(6;6;2;1) the operation of the switch system was as follows:

For the nonisolation condition the varactor was biased so that the switch unit reflected all energy incident on it , Therefore any power coupled to port number 1 of the second Y circulator was reflected at port 2 on to port number 3 and consequently into the main receiver. For the isolation condition the varactor was then biased so that the switch appeared as a well matched section of line, and so all the energy incident upon port number 2 was absorbed in the matched termination connected in series with the varactor switch.

By inserting a stub tuner just ahead of the varactor switch it was possible to introduce a small reflection into the circulator , of the same magnitude by opposite phase, as the circulator leakage,and so cancell the effective circulator leakage to port number 3. In this manner it was possible to achieve a broad band isolation of 50 db. between the circulator ports 1 and 3. This isolation figure was well in excess of the 20 db.isolation and 30 db. rejection possessed by the circulator and switch separately.

6;7;2 (VARACTOR SWITCH)

As can be seen from FIG.(6;7;1), the varactor switch consisted mainly of a section of coaxial line in which a varactor diode had

been inserted between the central and outer conductors. A fine coiled wire served as the D.C. return for the diode while a large capacitive type choke prevented R.F. radiation. The inductance of the D.C. return was such as to resonate the capacitance assumed by the diode under a + 1.8 volt forward bias, and so the switch appeared as a matched section of transmission line under these conditions. Application of a negative pulse of six volts amplitude to the diode was sufficient to change its effective capacitance from its maximum forward biased value to a very low value such that the switch appeared as a large mismatch , and consequently reflected all power incident upon it.

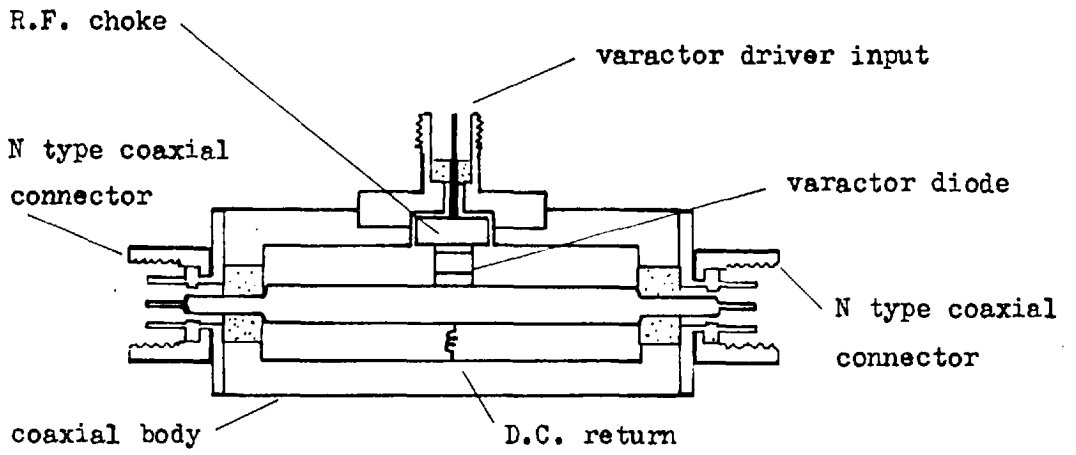

FIG.(6;7;1)

Coaxial varactor switch assembly.

This particular varactor switch used in the system was an experimental model obtained on loan from the Microwave Division of Ferranti in Edinburgh .

6;7;3 (VARACTOR SWITCH PULSER UNIT)

Since it was necessary to gate the switch such that it isolated the receiver just prior to the beginning of the transmitter pulse and subsequently cleared just prior to the return of the first echo pulse,

it was essential that a pulse generator be developed which was capable of switching the varactor from maximum to minimum capacitance in a very small fraction of a microsecond. In addition this pulse generator had to be able to deliver this fast rectangular six volt pulse into a very low impedance load presented by the shunt capacitance of the varactor diode.

Because of the fast rise times and low impedance levels involved it was necessary to use transistors in the construction of the pulser.

FIG.(6;7;3;1) shows the basic circuit used in the pulser. Because of the differentiating network present at the input it was possible to trigger the device from either polarity signals. The device was essentially an emitter coupled emitter-timed monostable multivibrator and as such had several advantages over the conventional bottoming collector-base-coupled monostable circuits, the most significant of which were.

(1). The minimum switching times for a given transistor may be realised.

(2). The rise and fall times of the generated pulses are equal and so the output pulse was symmetrical.

(3). Pulse jitter was minimised.

(4). Recovery time was very rapid.

Transistors 1 and 2 formed the basic monostable unit while Tr_3 acted as the constant current source for the unit. Tr_4 and Tr_5 were simple emitter-follower stages used to progressively lower the output impedance of the basic monostable pulse unit.

The output from Tr_5 was used to drive two separate driver sections such that either positive or negative pulses could be obtained as required. It should be noted here that positive pulses were required to drive the varactor switch when ever it was used as a simple series element, however since the isolation obtained under this series config-

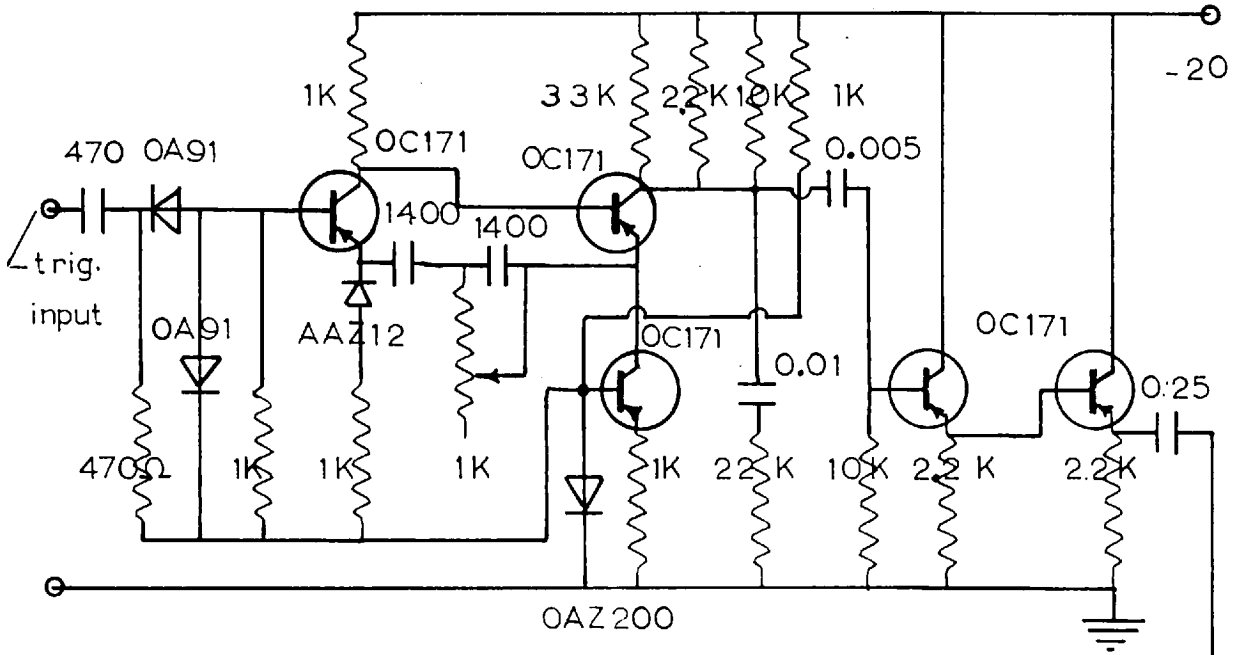

main pulse generator

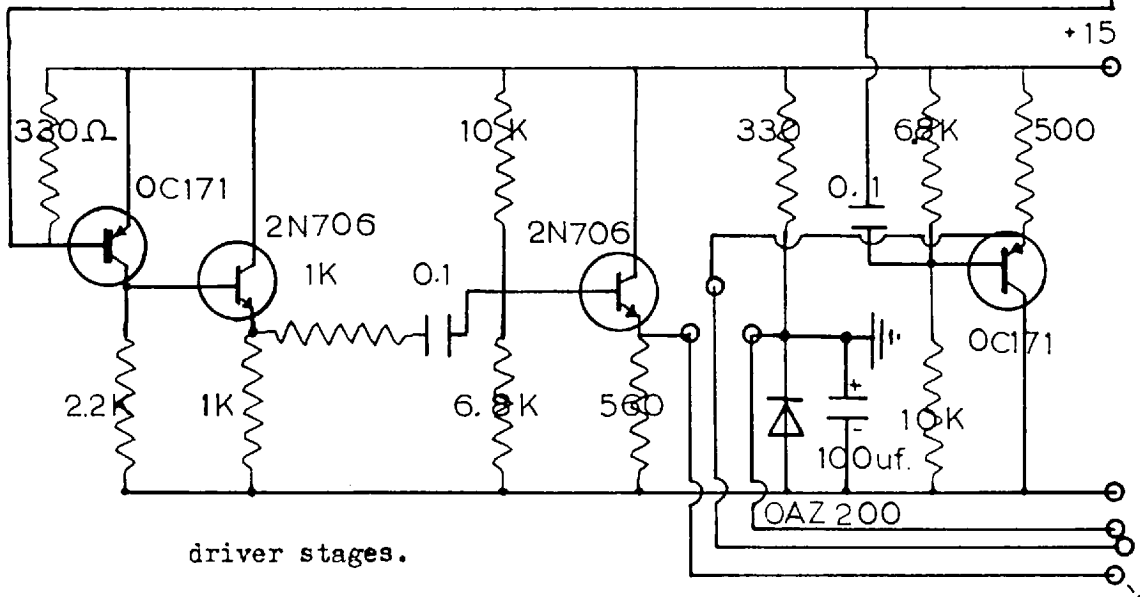

driver stages.

output to
varactor switch.

FIG.(6;7;3;1)

Varactor switch pulser unit.

uration was only 30 db. , compared to the 50 db. derived from the circulator mode type of operation , it was seldom utilised.

The driver stage of the negative output pulse section of this varactor pulser was simply another emitter-follower stage having a very low output impedance. The positive output pulse section on the other hand had a pulse inverting transistor stage coupled to two emitter-follower stages formed from N P N transistors. It was necessary to use a separate positive rail for supplying the output sections of the pulser due to the particular biasing conditions imposed by the varactor diode.

Performance

Excellent output pulses were obtained from the varactor pulser unit, having rise and fall times of 20 nanoseconds and perfectly flat tops. In addition the output impedance level of the pulser was extremely low such that connection of the varactor switch to the pulser did not effect pulse shape. A continuously variable output of 0 to six volts was obtained while the pulse length was adjustable from 0.5 to 2 microseconds.

6;8 (COAXIAL LINE TO WAVEGUIDE TRANSFORMER)

Since the remaining part of the receiver system was built in waveguide it was necessary to include another coaxial line to waveguide transformer at this point. This unit was identical to those previously described.

6;9 (PARAMETRIC AMPLIFIER PERFORMANCE AND ALIGNMENT MONITOR)

As it was occasionally necessary to re-adjust the parametric amplifier and its associated equipment to achieve continued optimum performance, it was desirable that a monitor system be permanently built into the receiver system such that alignment could be made

quickly and under the same conditions in which it would subsequently be used.

The monitoring apparatus incorporated into the waveguide channel at this point consisted of a directional coupler having high directivity and low coupling. A low value of coupling was desirable so as not to upset the operation of either the parametric amplifier or the superheterodyne receiver. One end of the auxiliary side arm of this directional coupler was properly terminated ,while the opposite end was connected to a broad band crystal mount. This crystal mount was used in conjunction with a high gain selective amplifier as a broad band detector for alignment of the amplifier.

6;10 (FERRITE RESONANCE ISOLATOR)

Another ferrite resonance isolator identical to that described in section (4;12), was inserted next in the receiver channel. This isolator functioned to protect the parametric amplifier from any local oscillator power coupled back from the following balanced mixer. In addition this unit served to isolate the amplifier from any impedance changes in the output circuit. Such impedance variations are a result of slight changes in the mixer crystal R.F. impedances with corresponding variations in local oscillator drive. Much greater impedance variations occur when ever the mixer crystals are changed. Obviously if the local oscillator drive fails or if either crystal was damaged, the resultant impedance variation was extremely large.

6;11 (BALANCED MIXER SYSTEM)

6;11;1 GENERAL

As is well known best performance can be obtained from conventional superheterodyne receivers only if balanced mixing is utilised to eliminate local oscillator noise.

This noise is derived from the spurious signals accompanying the

local oscillator signal and which are generated by the electron beam within the local oscillator. Although the electron beam possesses noise currents at all frequencies, only those within a certain band are strongly coupled, this band being determined by the loaded Q of the oscillator cavity. Moreover only those noise components centered around the signal and image frequencies will cause deterioration in receiver noise figure since it is only these components that produce intermediate frequencies within the bandwidth of the intermediate frequency amplifiers. This situation is depicted in FIG.(6;11;1;1).

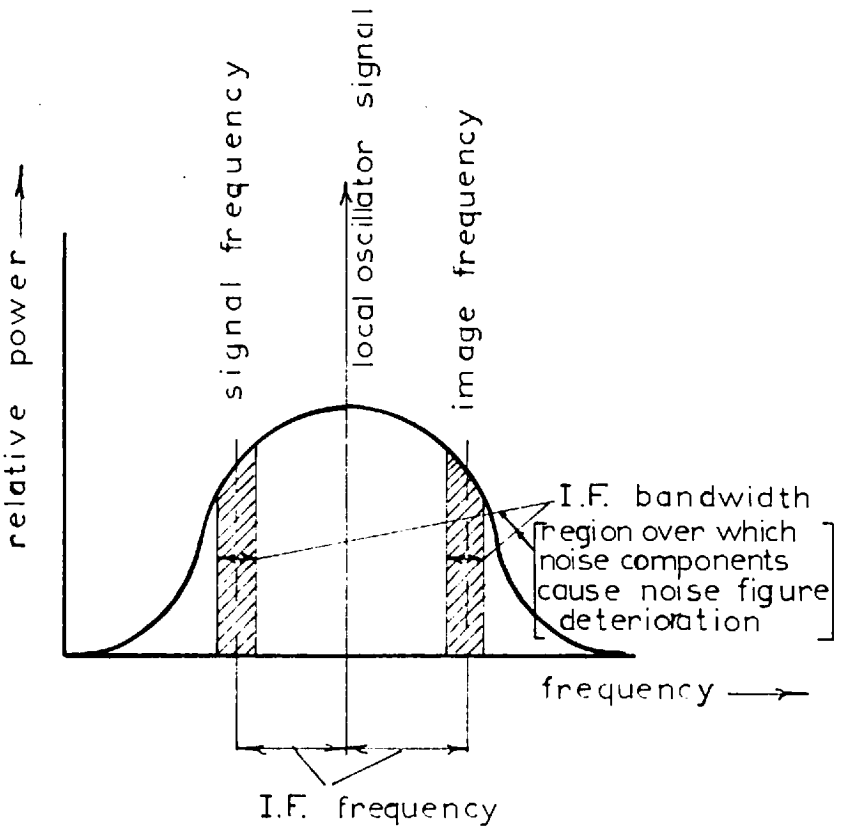

FIG. (6;11;1;1)

Schematic representation of local oscillator noise components contributing to noise figure deterioration of superheterodyne receiver.

6;11;2) (BALANCED MIXER MAGIC T)

It is possible to construct a balanced mixer in several different ways, however best performance can be obtained if a magic T is used as the balancing unit.

Upon connection of the magic T as shown in FIG.(6;11;2;1) , it is found that,provided the two mixer mounts are fitted with opposite polarity crystals, the two intermediate frequency components,presented at the mixer output terminals , are in phase and therefore add, while the noise components produced by the local oscillator are out of phase and cancel . It follows therefore that if the two mixer outputs are simply connected together a large improvement in noise figure will result.

Several other advantages were obtained from the utilisation of a

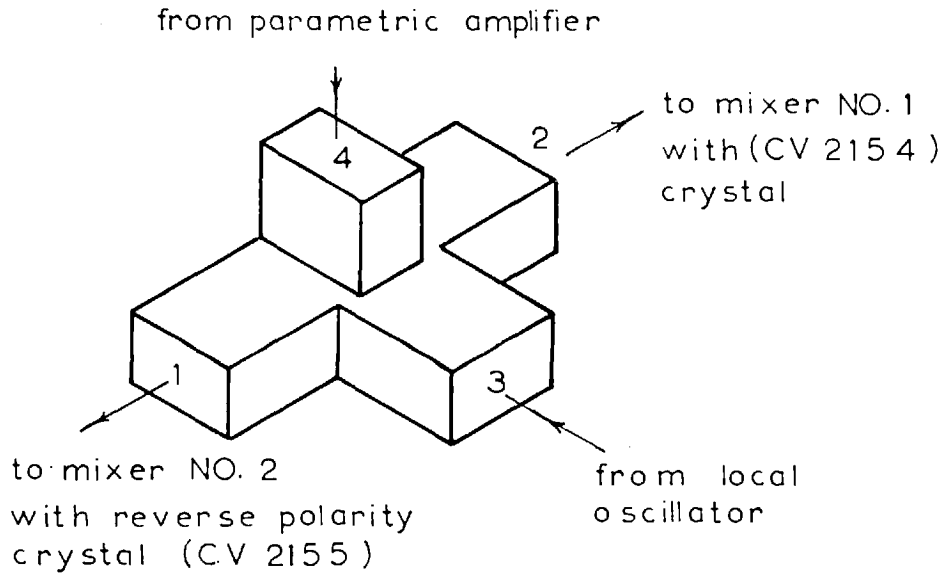

FIG. (6;11;2;1)

Balanced mixer magic T connection.

magic T for the balanced mixer as follows:

(1). Less local oscillator power is required.

(2). No interaction between local oscillator circuit and signal frequency occurred thus giving freedom from loss of signal power.

(3). Reasonably large variations in crystal admittances were permissible,without deterioration in performance,as there was no cross coupling between the two mixers. Any power reflected from the mixers was coupled back into the well padded local oscillator channel and there absorbed and also into the signal channel, fitted with an isolator, and consequently also absorbed.

(4). The magic T balanced mixer did not respond to intermediate frequency signals derived by the interaction of frequencies in the signal channel. It follows therefore that the receiver was not susceptible to interference from frequencies that were not at the signal or image frequency sidebands of the local oscillator . This particular feature was of special significance in this system application where the receiver was built in close proximity to intense radiation from the high powered modulator.

6;11;3 (LOCAL OSCILLATOR CHANNEL)

The required local oscillator drive of approximately one milliwatt was obtained from an inexpensive low voltage reflex klystron. This klystron had an output of 150 milliwatts and so a variable attenuator was inserted in series. The insertion of some 15 db. of attenuation into the local oscillator channel was a desirable feature since it effectively made the arm appear as a well matched load to any mixer unbalance, and also acted as a stabilising influence on the local oscillator.

6;11;4 (MIXER CHANNELS)

Because of the physical construction and dimensions of the magic T and mixer mounts, it was necessary to insert two 90 degree H plane

bends into each mixer arm to enable the I.F. mixer outputs to be obtained in close proximity. This was required since the mixer outputs had to be coupled to the grid of the head I.F. amplifier with as little addition of cable capacitance as possible if the optimum noise figure and bandwidth were to be achieved. This aspect was of particular importance in this application since the mixer mounts were found to have an inordinately large shunt capacitance.

A four screw tuner was also inserted in each mixer channel to compensate for large variations in the R.F. admittances of the mixer crystals used.

Commercial fixed tuned mixer mounts of the conventional bar and post design were employed in the receiver. These units were designed for coaxial type CV 2154 and CV 2155 mixer crystals, having an equivalent noise temperature of 1.5 times and conversion loss of approximately 6 db . Under local oscillator drive conditions such that the rectified crystal current was 0.5 milliamperes, the crystals developed an I.F. impedance of 450 ohms. The mixer mount characteristicswere as follows:

Shunt capacitance(at 30 Mcs)	= 17 uuf
V.S.W.R. (no crystal)	= 30
V.S.W.R. (with crystal at 0.5 ma)	= 1.9
Bandwidth	= 20 Mcs.

6;12 (INTERMEDIATE FREQUENCY (I.F.) AMPLIFIERS)

6;12;1 (HEAD AMPLIFIER)

Having achieved a condition where the mixer outputs were separated by only five inches it was possible to fix a small screened box directly over the mixer output terminals and then to mount the head amplifier inside thereby eliminating lead cables completely. This head amplifier consisted of a single low noise triode having an autotransformer input

section to accomplish optimum impedance transformation from the balanced mixer outputs to its grid. The balanced mixer output impedance was measured,on a bridge at 30 Mcs. , to be approximately 200 ohms and 35 uuf, under 0.5 milliamperes rectified crystal current conditions. To achieve lowest noise figure the optimum grid input impedance of the particular valve used in the head amplifier was specified by the manufacturers as 600 ohms. Transformer coupled negative feed back was used to insure amplifier stability.

FIG.(6;12;1;1) shows the circuit of the head amplifier, which gave the following performance figures:

Gain	= 10 db.
Bandwidth	= 10 Mcs.
Center frequency	= 30 Mcs.
Noise figure	= 1.4 db.
Output impedance	= 50 ohms.

As is evident from the above figures, the noise figure obtained was indeed excellent. In addition the amplifier was extremely stable breaking into oscillation only when local oscillator drive to the mixer crystals was removed. This onset of instability upon loss of mixer crystal drive was to be expected since the I.F. impedance of the mixer crystals is a function of the rectified current and hence upon loss of the local oscillator drive the amplifier no longer had the proper input impedance presented to it.

This head amplifier was obtained from the Electronics Division of Ferranti in Edinburgh .

6;12;2 (CRYSTAL CURRENT MONITOR)

Since, as was indicated above, the I.F. input impedance presented to the head amplifier is a function of the rectified crystal current and also since there is an optimum value of the input impedance for

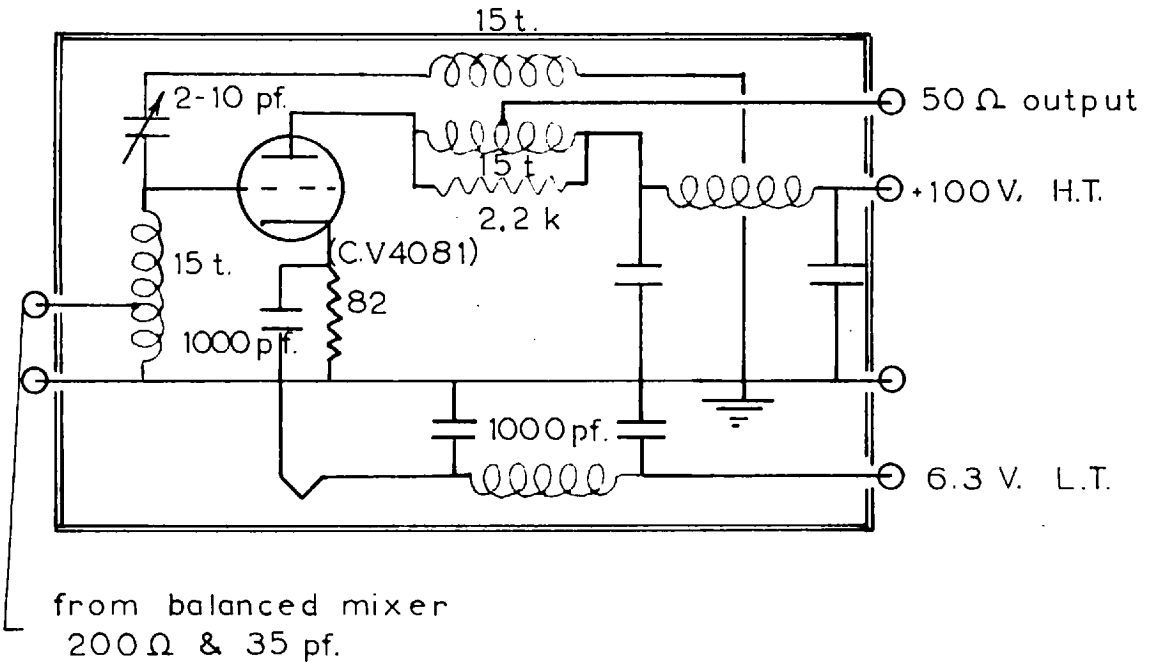

FIG. (6;12;1;1) **Head I.F. Amplifier**

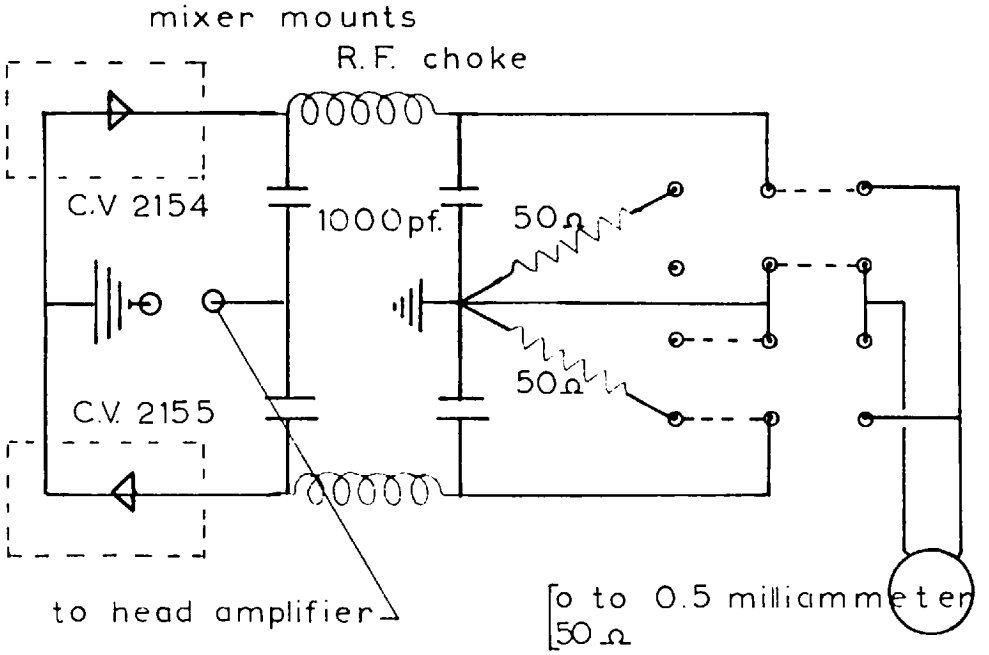

Crystal current monitor

FIG. (6;12;2;1)

lowest noise figure performance, it was desirable to have the facility to monitor either crystal drive at will. To accomplish the above a small crystal current monitor was constructed having the circuit shown in FIG.(6;12;2;1). A crystal current return impedance of 50 ohms was used which was the upper limit advisable if lowest noise figures were to be attained. The device was constructed so that it could be directly coupled to the shielding box containing the head amplifier.

6;12;3 (SECOND INTERMEDIATE FREQUENCY AMPLIFIER)

The circuit diagram of the second I.F. amplifier used in the system is shown in FIG.(6;12;3;1). This unit was coupled to the output of the head amplifier, and in fact due to its compactness , resulting from its printed circuit construction, was bolted directly to the screened box containing the head amplifier. In this manner any external pick up was minimised.

This amplifier, also obtained from Ferranti's, had the following specifications:

Noise figure	= 4 db.
Bandwidth	= 10 Mcs.
Gain	= 40 db.
Frequency	= 30 Mcs.
Output impedance	= 50 ohms.

6;12;4 (THIRD INTERMEDIATE FREQUENCY AMPLIFIER)

A third and final I.F. amplifier obtained from Decca Radar Ltd., was inserted in the amplifier chain. This device developed 50 db. gain under 10 Mcs. bandwidth. The circuit of this strip is given in FIG.(6;12;4;1).

Second intermediate frequency amplifier

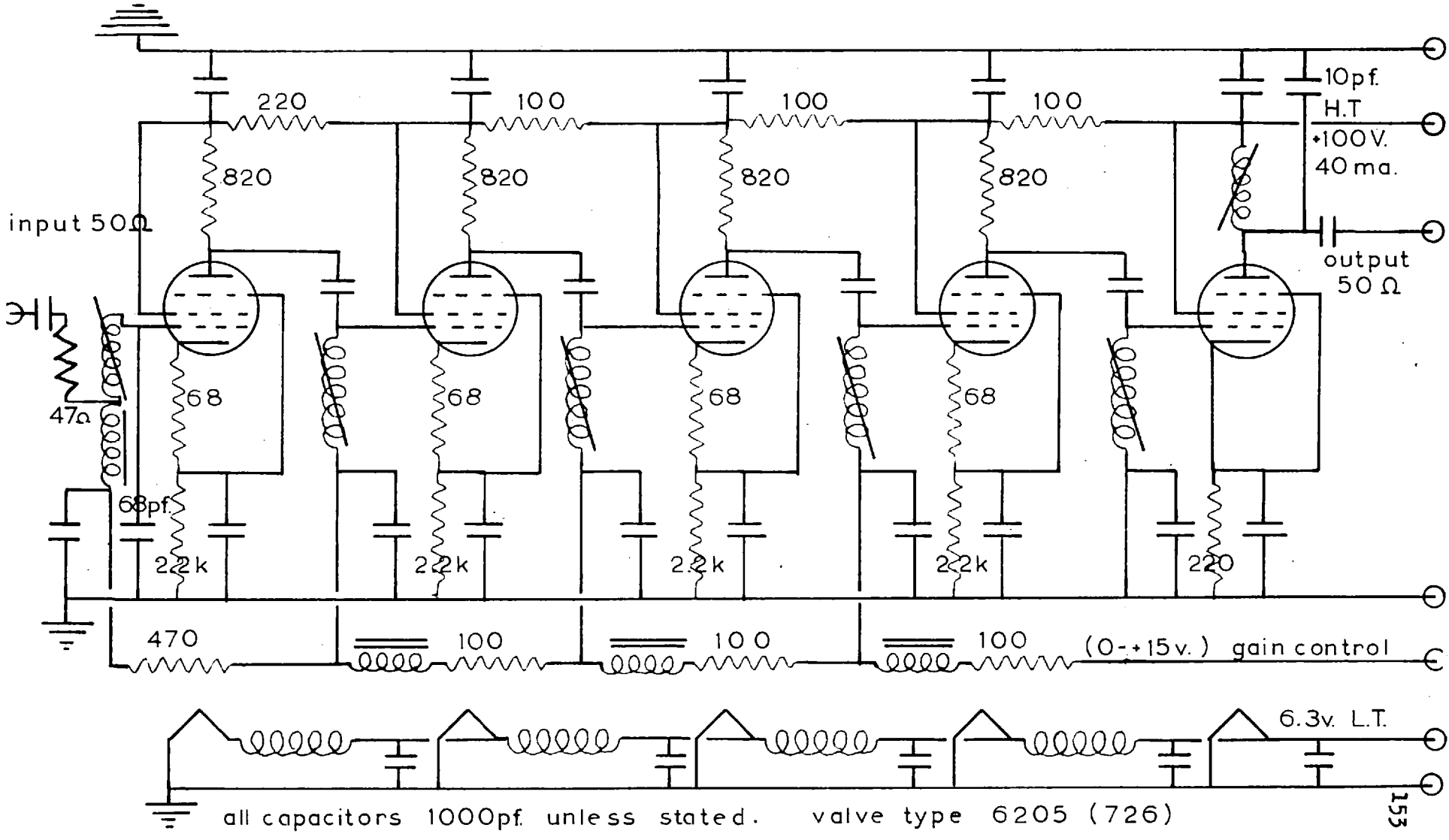

FIG.(6;12;3;1)

Third intermediate frequency amplifier

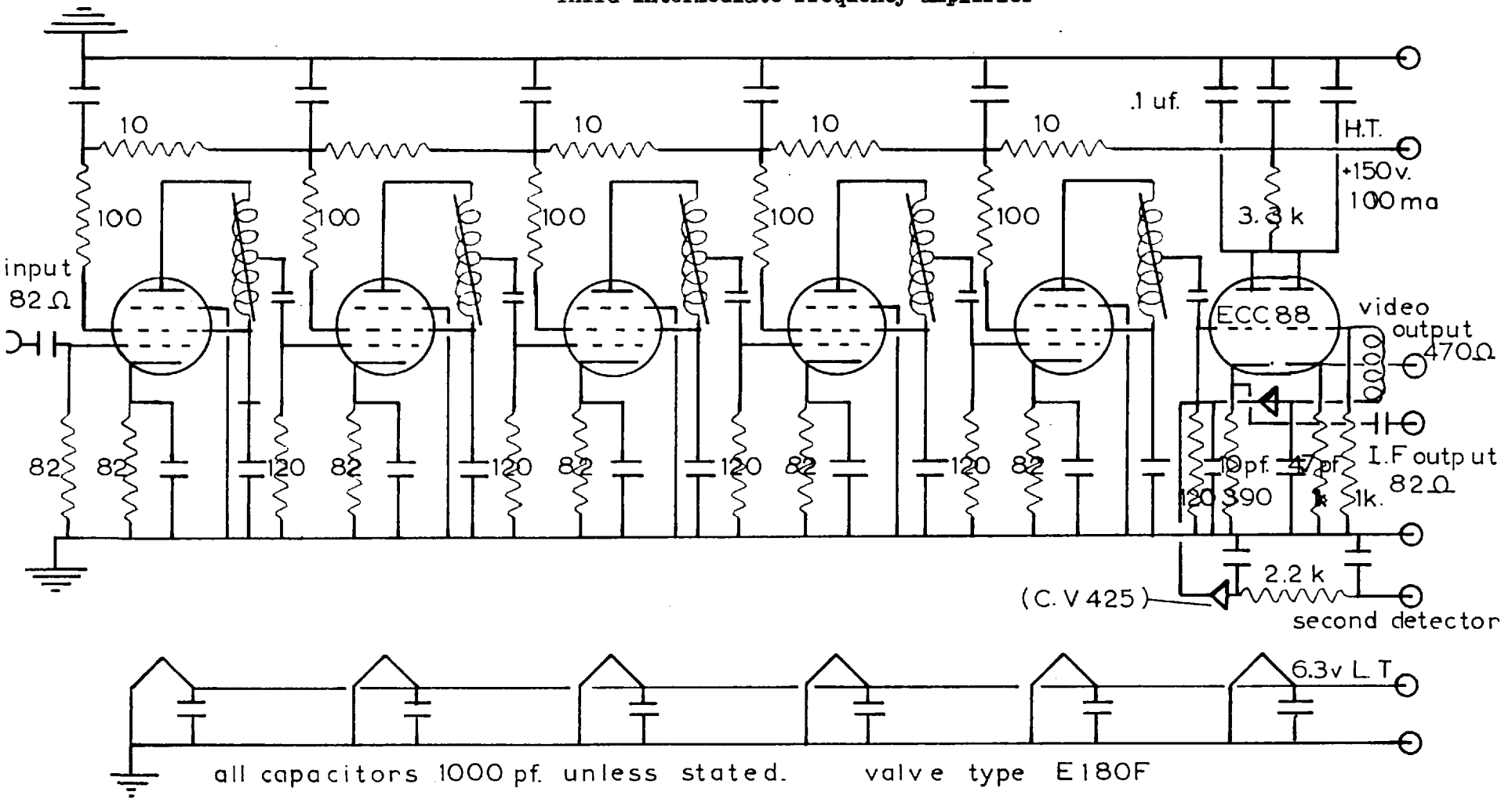

FIG. (6;12;4;1)

6;13 (RECEIVER SYSTEM NOISE FIGURE)

Now that all the individual components effecting the performance of the receiver system have been considered , it is possible to determine the overall noise figure of the complete receiver unit.

The combined noise figure of the intermediate frequency amplifiers may be obtained from equation (H;1;9) of appendix (H). Thus:

$$F_{13} = F_1 + \frac{F_2 - 1}{G_1} + \frac{F_3 - 1}{G_2 G_1} \qquad (H;1;9)$$

and upon inserting the appropriate values into the above equation:

$$F_{13} = 1.38 + \frac{2.5 - 1}{10} + \frac{3 - 1}{10^5} = 1.53$$

$$= 1.85 \text{ db.}$$

Now the overall noise figure of the balanced mixer unit may be obtained from equations(H;1;5 and 9) since:

$$F_{\text{balanced mixer}} = F_{\text{crystal}} + \frac{F_{13}}{G_{\text{mixer crystal}}}$$

and

$$F_{\text{crystal}} = \frac{T_e}{T_o} + 1 \qquad (H;1;5)$$

where T_e is the equivalent noise temperature of the crystal. From section (6;11;4) the mixer crystal characteristics are as follows:

$$G_{\text{mixer crystal}} = -6 \text{ db}$$

$$T_e = 1.5\ T_o$$

Thus

$$F_{\text{balanced mixer}} = 2.5 + 1.53/\tfrac{1}{4} = 8.63 = 9.3 \text{ db.}$$

Finally the overall receiver system noise figure including the 3db. parametric amplifier is obtained as:

$$F_{\text{overall}} = 2 + 8.63/100 = 2.0862 = 3.03 \text{ db.}$$

From the foregoing calculations it is evident that the overall receiver system noise figure was essentially that of the parametric amplifier.

It is also possible to calculate of the overall receiver system sensitivity by using equation (H;2;1) . So :

$$S_i = F_{overall} (K T_o B) \qquad (H;2;1)$$

therefore $S_i = 2.086 \times 4 \times 10^{-15} \times 10 = 8.34 \times 10^{-14}$ watts.

and so the receiver should be able to detect less than one tenth of a micro-microwatt of R.F. energy, and this in fact was experimentally verified.

6;14 (OSCILLOSCOPE)

The final item of equipment comprising the receiver unit of the experimental system was a 585 Tektronix oscilloscope fitted with a high gain L type preamplifier. The receiver I.F. output was displayed directly without demodulation, since it was found that a much higher accuracy of bridge balance could be ascertained in this manner. This can be appreciated by considering that bridge balance was indicated by a null, which means that the receiver pulse amplitude as displayed on the C.R.T. became zero. Now if there was a zero base line shift of the receiver, which usually was the case especially for the first few echoes displayed, the exact determination of zero pulse amplitude was very difficult to judge when only the demodulated envelope was present. However in the case of the undemodulated wave form, the balance condition was clearly indicated when the displayed I.F. pulse degenerated to a single line. Whether this single line was straight or not was of no particular significance.

CHAPTER 7

DETAILED DISCUSSION OF INDIVIDUAL COMPONENTS IN MICROWAVE ULTRASONIC TRANSDUCER UNIT

7;1 (GENERAL)

The individual components comprising the basic microwave ultrasonic transducer unit are now discussed under the same three headings of :

(1). Reason for incorporation in system.

(2). Design and construction.

(3). Performance.

7;2 (RESONANT MICROWAVE CAVITIES)

7;2;1 GENERAL

The main function of the microwave cavities was to transform the pulsed electromagnetic radiation from the magnetron into an R.F. electric field which was then instantaneously applied across the faces of a B.C. cut piezoelectric quartz crystal. The intense electric field produced in this manner generated a mechanical wave within the quartz medium , the actual mechanism of such generation being given in appendix (D;8). page (282) of this work.

Several cavities were constructed in the process of investigation of the best type suited for this particular application. All the cavities however were of the re-entrant type, having the piezoelectric crystal placed within the re-entrant gap.

A detailed development of the cavity theory is given in appendix (F) page ,(301), and so will not be considered here, this section being restricted to a discussion of the particular cavity configurations investigated.

7;2;2 (CAVITY NUMBER ONE)

FIG.(7;2;2;1) is an assembly drawing of the first cavity built to investigate the possibility of microwave ultrasonic generation in quartz crystals at room temperature.

From the diagram it is evident that the crystal was placed completely inside a symmetrical cavity and in this respect is different to the asymmetrical configurations used by others, (79) , in which one end of the crystal was brought completely out of the cavity. This internal crystal type of construction was imposed by virtue of the high acoustical transmission losses in the quartz medium, being approximately 20 db. per centimeter.

The selection of a symmetrical configuration although not absolutely vital,from the standpoint of crystal excitation, was to be prefered to the asymmetrical case as less radial component of electric field was developed. It has been found that the existence of a radial component of electric field can cause unwanted modes to be generated in the crystal which interfere with the desired mode and consequently results in an undesirable acoustic decay pattern.

The cavity was made tunable to accommodate slight variations in crystal dimensions, the crystal being held in position by a special P.T.F.E. shielding ring employed in an attempt to prevent flashover along the crystal surface.

Complete success was achieved with this cavity with respect to the basic aim of microwave ultrasonic generation at room temperature, however attempts at utilising this design for actual viscoelastic measurements were not successful. The reason for this lack of success arose from the fact that the technique of measurement required that the crystal surfaces be loaded with the test liquid and since the crystal was contained completely inside the cavity it was necessary to introduce this liquid through hollow electrodes. Unfortunately the introduction of only a minute quantity of test liquid to the crystal surfaces detuned the cavity to such an extent that resonance could not

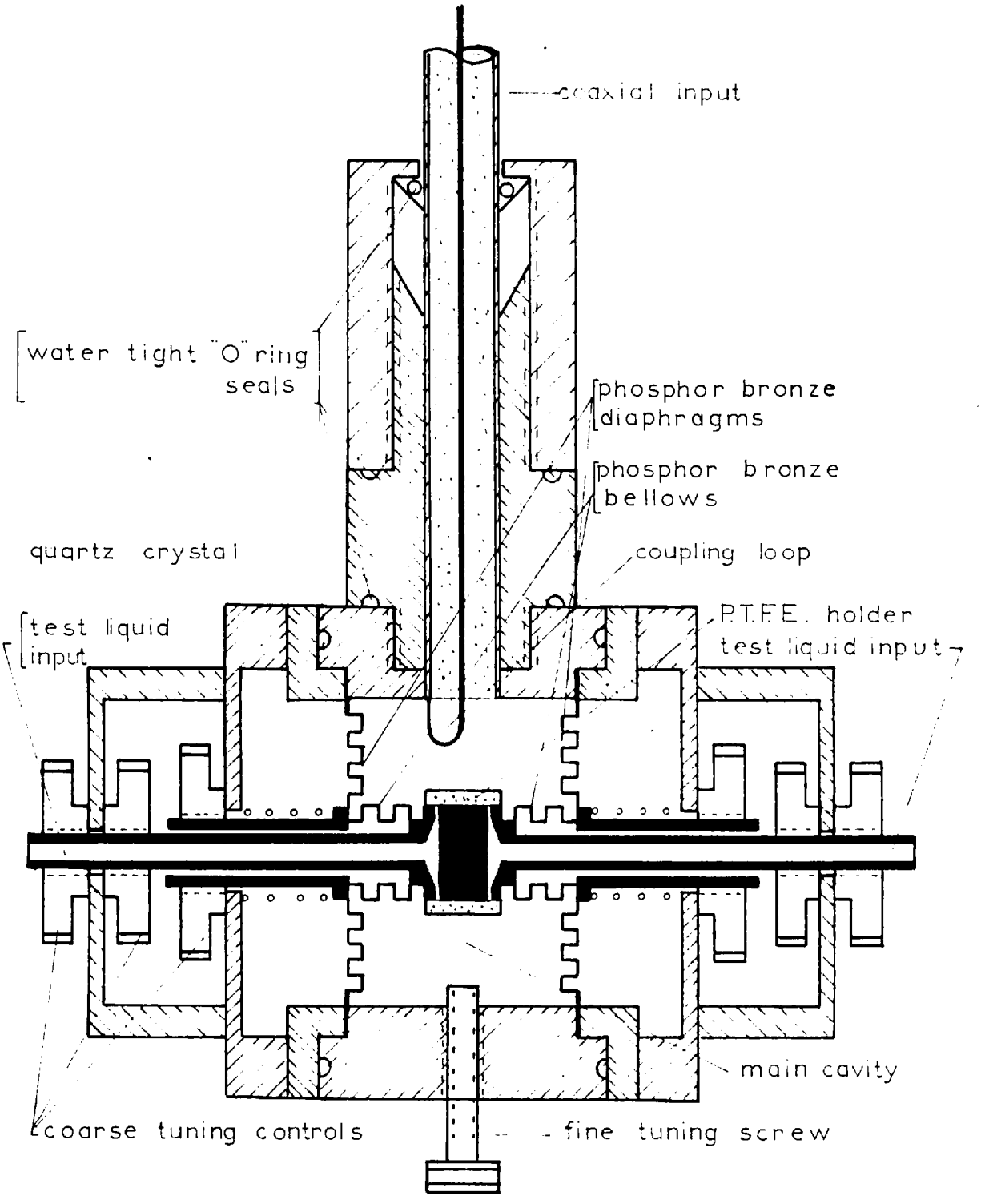

FIG. (7;2;2;1)

Microwave cavity number one.

be re-established with the limited tuning range available.

Various attempts at overcoming this difficulty such as plating the crystal surfaces with a thin evaporated metallic film, were unsuccessful and consequently the cavity was abandoned and another design developed.

7;2;3 (CAVITY NUMBER TWO)

In the second cavity design an effort was made at overcoming or minimising the previous detuning problem by attempting to reflect an electrical short circuit across the face of the crystal and thereby lessen the field strength immediately behind the crystal, where the test liquid would be placed.

In order to accomplish the above it was necessary to construct another larger cavity , the original being much to small to accommadate the necessary alteration s to be made to the inner cavity electrodes. As in the case of cavity number one, this cavity also supported a **hybrid** coaxial T.E.M. mode.

As can be seen from FIG.(7;2;3;1) the unit was essentially a circular tube with an adjustable,capacitively coupled,choke type, shorting plunger inserted in either end. The configuration was in reality two $\frac{3}{4}$ wavelength coaxial cavities coupled back to back. The inner posts were mounted on the end plungers and spring mounted so as to maintain the gap constant regardless of the end plunger position. This arrangement provided extreme flexibility, giving the cavity a very wide tuning range.

Tunable short circuited coaxial lines having a high characteristic impedance were built inside the hollow inner cavity electrodes.

A special P.T.F.E. sleeve arrangement was again used to hold the quartz crystal and to provide adequate flashover protection, without straining the crystal.

Test liquid was introduced to the crystal surfaces through a

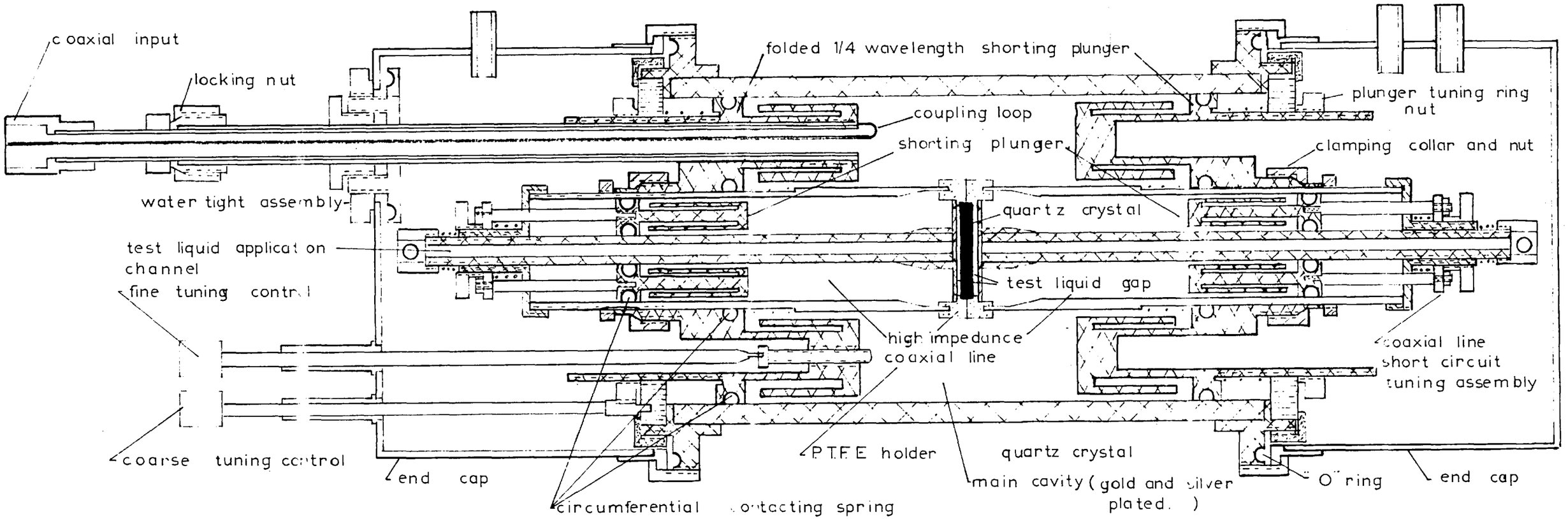

FIG. (7;2;3;1)

Microwave cavity number two

small hole in the center of the inner coaxial section.

The cavity was loop coupled and made water and air tight for thermostating and controlled atmosphere considerations.

Unfortunately very little success was achieved with this design the main reason being the existence of higher order coaxial modes in the cavity due to its large physical size. Various tests were performed on the cavity and in fact the TE_{11} mode was identified as being present from its characteristic field polarisation pattern.

Another undesirable aspect of this particular design was the very poor transforming efficiency. This was found to result from the $\frac{3}{4}$ wavelength construction, in that a large percentage of the electrical energy in the cavity was stored in the coaxial section rather than in the electrode gap region. Obviously only electrical energy stored in the cavity gap could be utilised in the electromechanical conversion process. This particular aspect is considered at length in appendix (F).

7;2;4 (CAVITY NUMBER THREE)

As a result of the inadaptability of the first cavity and the multimoding of the second a third cavity was designed and constructed. This design was different from the previous two in that it supported a hybrid radial mode rather than the former coaxial T.E.M. mode.

A complete analysis of this cavity operation and design is given in appendix (F;2) on page (320), while the actual construction adopted is shown in FIG.(7;2;4;1).

The flashover problem was conveniently overcome by making the crystal much larger than the electrode diameter. In this design only a few drops of test liquid were required for a test, these being placed on a specially shaped microscope cover glass. which was held in position just back of the crystal surface. Application of the liquid to the crystal surface was accomplished merely by activation of a small push

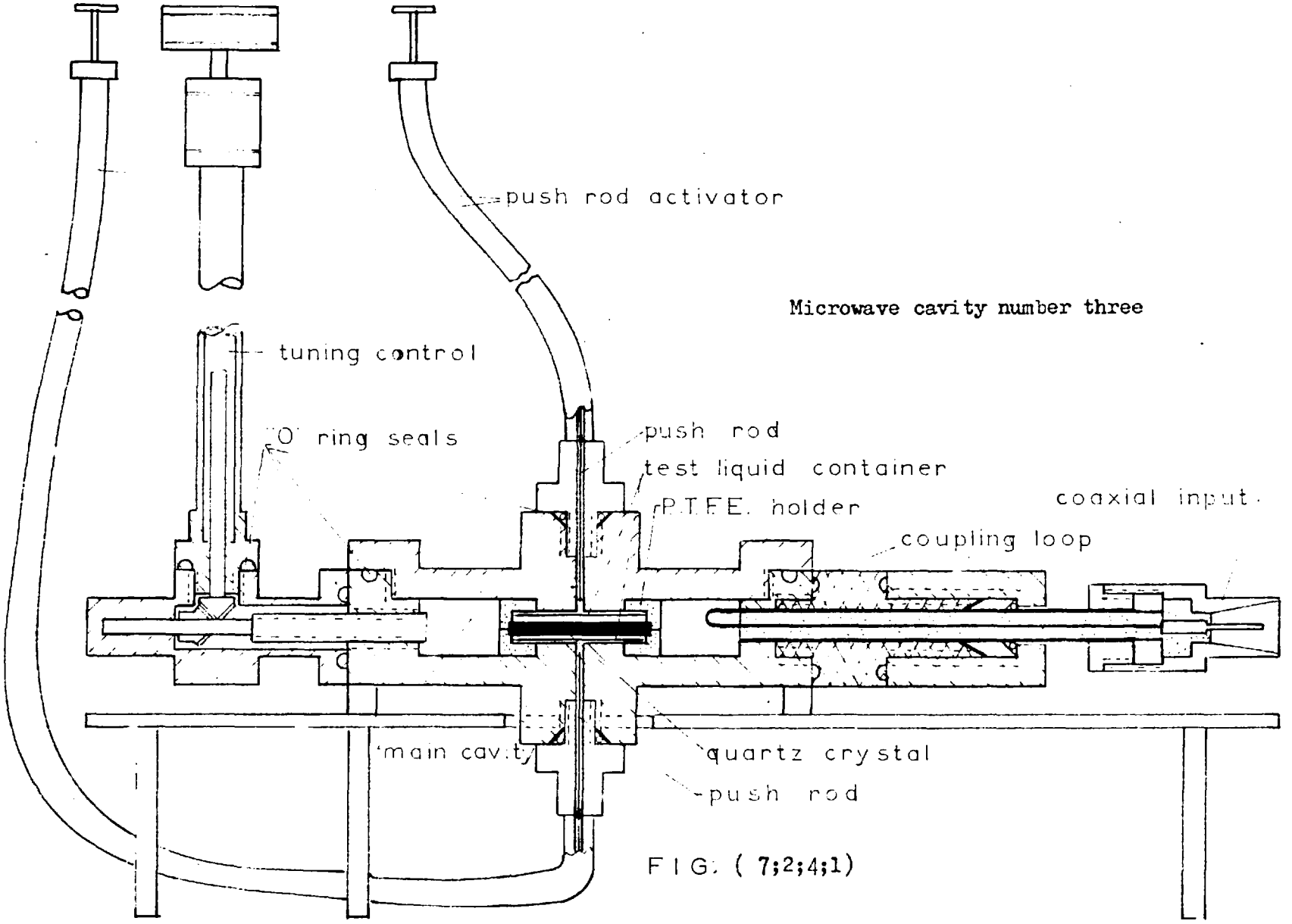

Microwave cavity number three

FIG. (7;2;4;1)

rod device which moved the cover slide against the crystal, at this point capillary action completely and uniformly covered the crystal surface.

A slight dish or depression was etched into the cover glasses to insure that sufficient film thickness was always present at the crystal surface.

As in the previous cases, the crystal was held in position by a P.T.F.E. ring designed to subject the crystal to minimum strain.

The top cover glass was held in position by surface tension, as a small amount of the test liquid was placed between the P.T.F.E. holding ring and the back of the cover glass such that when pushed together the glass was held quite firmly.

This technique of having the liquid sample always inside the cavity was devised in an attempt to reduce the detuning effect of test sample application . In addition it was felt that there was less likelihood of a temperature differential existing between the sample and the crystal since, being in such close proximity, they were subjected to merely the same thermal conditions.

An additional advantage derived from the above configuration was that only a minute quantity of test sample was required, this aspect being of considerable importance when dealing with specially prepared synthetic samples which are difficult to obtain.

The main disadvantage of the design of cavity number three was that the technique of supporting the test sample just above the crystal surface often lead to a condition where the liquid accumulated in the center of the glass dish and hence caused a field pattern disturbance. These field perturbations resulted in changes in the accustic decay pattern of the crystal and thereby introduced error into the measurement. A much more objectionable feature associated with this liquid accumulation was that occasionally a drop was formed of sufficient depth as to prematurely load the top surface of the crystal. This occurrence naturally rendered the test invalid.

7;2;5 (CAVITY NUMBER FOUR)

In an attempt at eliminating the objectionable features of cavity number three, a fourth unit was constructed. This new cavity shown in FIG.(7;2;5;1) was of essentially the same design as number three except that a complete modification was made to the liquid application system.

A liquid and vacuum tight P.T.F.E. container was developed to inclose the crystal and so arranged as to permit application of a slight film of the sample to both top and bottom surfaces. This test liquid was sucked into the cavity, from an external reservoir, through special connecting lines, and allowed to fill the 0.005 of an inch gap left on either side of the crystal. This technique made it possible to inject most liquids into the cavity for measurement, the only limit being set by very viscous liquids of static viscosity in excess of 500 poise which were too viscous to be sucked into the small gaps within a reasonable length of time.

Unlike the other radial cavity in which retuning was accomplished by means of a radial screw inserted through the cavity wall, tuning in this design was by means of altering the length of the re-entrant posts. In this manner it was possible to achieve a large tuning range and still maintain symmetry. It was found necessary to build choke type short circuits into the electrode posts to eliminate contact resistance problems. As in previous designs this unit was made water and air tight.

The main advantages possessed by the radial design cavities, were high,gap electrical energy storage efficiency , and relative freedom from radial electric field components.

The main disadvantage on the other hand was that it was necessary to introduce the test sample into the cavity thereby creating the possibility of error due to possible disturbance of the electric field distribution over the crystal surface.

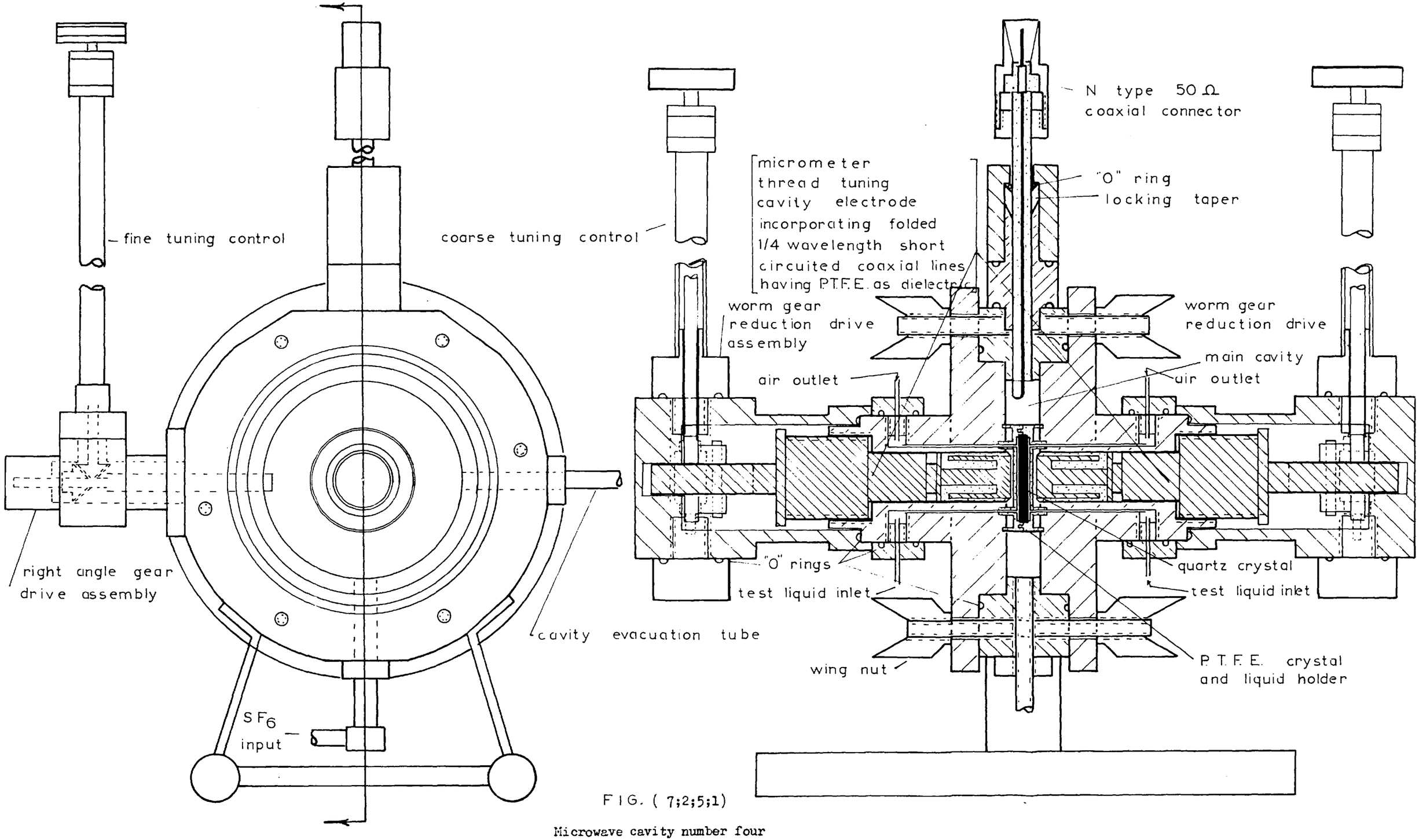

FIG. (7;2;5;1)

Microwave cavity number four

By proper selection of the system operating repetition frequency it was possible to eliminate all possible error in the measurement arising from dielectric heating of the test liquid. This aspect is fully considered in section (10;5) of this work.

7;2;6 (CAVITY NUMBER FIVE)

A fifth cavity configuration was investigated in an attempt at eliminating the detuning and slight field pattern variations present to some degree in the fourth design.

As is evident from FIG.(7;2;6;1), the main part of the fifth cavity was essentially that of the previous number three and four radial types, however in this case the crystal diameter was reduced to the same value as its length and inserted completely within the cavity wall, such that its upper surface was just flush with the inside of the cavity top. With this type of construction it was possible to arrive at a condition where very little electric field was present at the opposite crystal surface, since the hole in which the crystal was placed acted as a circular waveguide far beyond cut off. It follows therefore that application of the test liquid to the external crystal surface would have negligible effect on the cavity itself and this in fact was found to be the case.

The very serious problem of flashover was finally solved by simply placing a 0.002 of an inch , large diameter, ruby mica disk over the crystal.

Unfortunately although superior from the test liquid point of view, this cavity configuration resulted in extremely poor electro-mechanical conversion. This was to be expected since not only had the active generating crystal surface been reduced from two large surfaces to one very small surface, but the acoustic travel path length had been doubled,as the acoustic wave had to transit the crystal twice for each echo. As a result of the above only four echoes

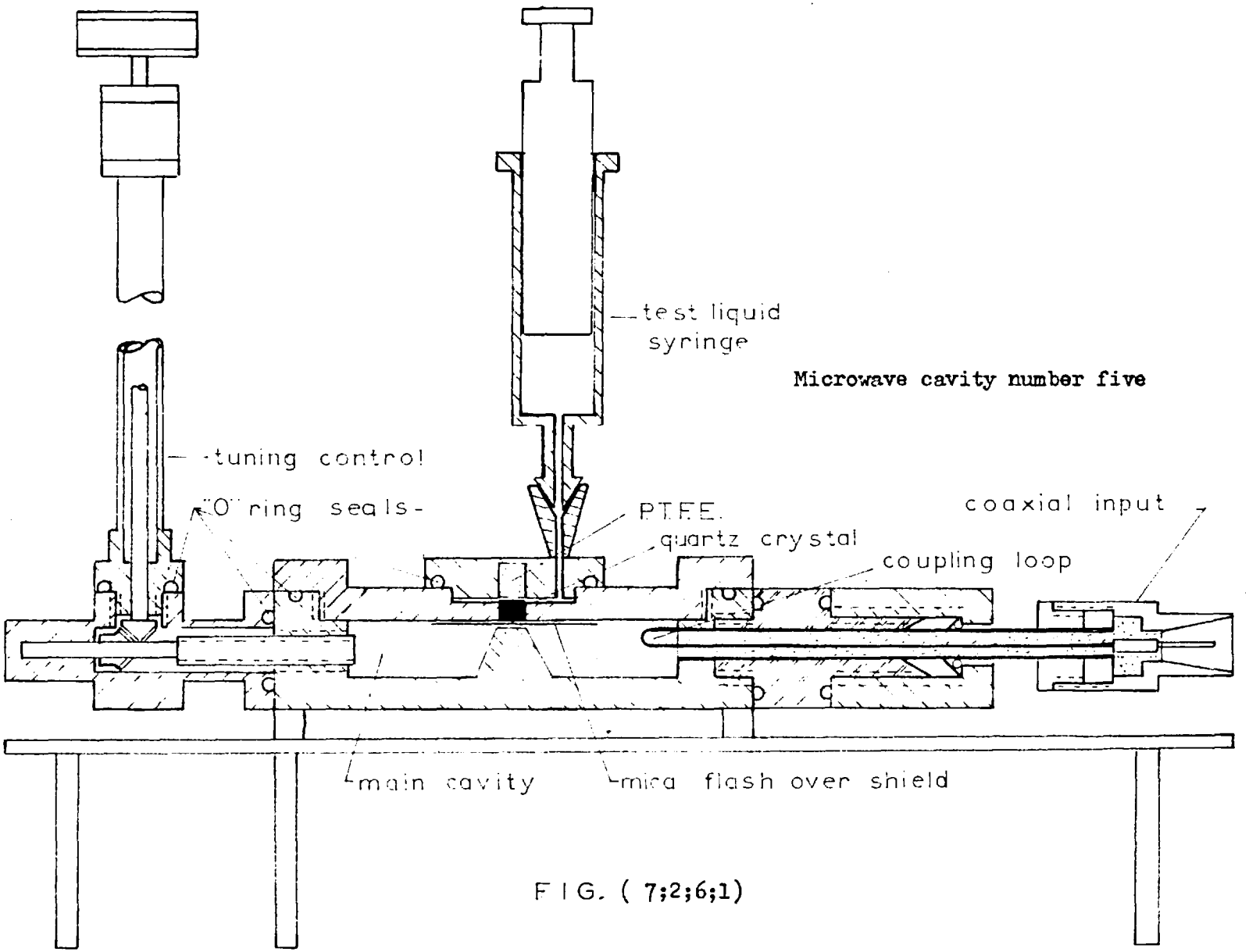
test liquid
syringe
Microwave cavity number five
tuning control
'O' ring seals
PTFE.
quartz crystal
coaxial input
coupling loop
main cavity
mica flash over shield

FIG. (7;2;6;1)

could be observed above noise level and this was far too few to be useful, consequently cavity number five was not used for measurement purposes.

7;3 (MICROWAVE CAVITY CALCULATIONS)

7;3;1 GENERAL

The various aspects of cavity performance developed in appendix (F) is now considered for cavity designs number one to three , so that the relative merits of each configuration may be determined.

7;3;2 (COAXIAL CAVITY NUMBER ONE)

The first cavity constructed had the following dimensions with reference to FIG.(F;1;1).

$b = 1.39$ cms. , $a = 0.375$ cms. , $d = 0.15$ cms. , $\mathcal{E}_{r_1} = 4.7$, $\lambda_o = 10$ cms.

$\beta_o = 0.628$ $\quad k_{c_1} = 1.3634$ $\quad x_1 = k_{c_1} a = 0.51128$

$J_1(x_1) = 0.2428$ $\quad J_o(x_1) = 0.9356$

Resonant cavity length l

From equation (F;1;4;19b)

$$\frac{J_1(x_1)}{J_o(x_1)} \tan(2\pi l/\lambda_o) \ln(b/a) a\left(\frac{\mathcal{E}_{r_1}}{d}\right)^{1/2} = 1$$

and so $l = 0.79166$ cms.

Maximum electric field in cavity gap

From equation (F;1;4;21)

$$E_o = (\mu_o/\mathcal{E}_o\mathcal{E}_{r_1})^{\frac{1}{2}} H_o \frac{\cos(\beta_o l)}{a\ J_1(x_1)} = (\mu_o/\mathcal{E}_o)^{\frac{1}{2}} H_o 4.447$$

From equation (F;1;4;11)

$$E_{z(r=a)} = \frac{H_o}{a}(\mu_o/\varepsilon_o\varepsilon_{r_1})^{\frac{1}{2}}\cos(\beta_o L)\,\frac{J_o(x_1)}{J_1(x_1)} = 0.9356\ E_o$$

and so

$$E_{z(\text{average}} = 0.96784\ E_o$$

Magnetic energy storage in coaxial region

From equation (F;1;4;27)

$$W_{s(m)}\,\frac{2}{\mu_o} = H_o^2\pi\ln(b/a)\left(1+\frac{\sin(2\beta_o L)}{2\beta_o}\right) = H_o^2\ 6.02108$$

coaxial region

Magnetic energy storage in gap region

From equation (F;1;4;32)

$$W_{s(m)}\,\frac{2}{\mu_o} = H_o^2\pi d\cos^2(\beta_o L)\left\{1-\frac{2J_o(x_1)}{x_1J_1(x_1)}+\frac{J_o^2(x_1)}{J_1^2(x_1)}\right\} = H_o^2 0.2820$$

gap region

Magnetic energy dissipation in coaxial region

From equation (F;1;4;28)

$$W_{\text{diss}}^{\sigma\delta} = H_o^2\left(\left(1+\frac{\sin(2\beta_o L)}{2\beta_o}\right)\left(\frac{1}{b}+\frac{1}{a}\right)+2\ln(b/a)\right)$$

coaxial region

$$" \quad = H_o^2\ 23.8044$$

Magnetic energy dissipation in gap region

From equation (F;1;4;34)

$$W_{\text{diss}}^{\sigma\delta} = H_o^2\cos^2(\beta_o L)\left\{1-\frac{2J_o(x_1)}{x_1J_1(x_1)}+\frac{J_o^2(x_1)}{J_1^2(x_1)}\right\} = H_o^2 1.880$$

Cavity unloaded Q

From equation(F;1;4;35)

$$Q_{un} = \frac{2}{\delta}\left(\frac{W_{s(m)}\frac{2}{\mu_o}+W_{s(m)}\frac{2}{\mu_o}}{\text{coax.}\qquad\text{gap.}}\right) = 1963.2$$

$$\left(\frac{}{W_{\text{diss}}^{\sigma\delta}+W_{\text{diss}}^{\sigma\delta}}\right)$$

coax. gap.

Electrical energy storage in coaxial region

From equation (F;1;5;4)

$$W_{s(e)\,\text{coax.}}\,\frac{2}{\mu_o} = H_o^2 \ln(b/a)\left(l - \frac{\sin(2\beta_o l)}{2\beta_o}\right) = H_o^2\ 0.4960$$

Electrical energy storage in gap region

From equation (F;1;5;5)

$$W_{s(e)}\,\frac{2}{\mu_o} = H_o^2 \cos^2(\beta_o l)\left(1+\frac{J_o^2(x_1)}{J_1^2(x_1)}\right) = H_o^2\ 5.7678$$

Gap region electrical energy storage efficiency

From equation (F;1;5;7)

$$\eta_{(e)\ gap} = \frac{(\ W_{s(e)\ gap}\ )}{W_{s(e)_{gap}} + W_{s(e)_{coax.}}} = 92.07\ \%$$

7;3;3 (COAXIAL CAVITY NUMBER TWO)

The second cavity dimensions were as follows:

a= 1.5 cms. , b= 4.5 cms. , d= 0.15 cms. $\varepsilon_{r_1} = 4.7, \lambda_o = 10$cms.

$\beta_o = 0.628$, $k_{c_1} = 1.3634$ $x_1 = k_{c_1} a = 2.045$

$J_1(x_1) = 0.5734$ $J_o(x_1) = 0.2035$

Since this second cavity was of the same type as number one the same equations apply and therefore:

Resonant cavity length l = 0.02369 cms.

Since the cavity length required for resonance in this case was so small it was necessary to increase the cavity length by $\frac{1}{2}$ of a wavelength, thus the final cavity length was = 5.02369 cms.

Maximum electric field in cavity gap $E_o = (\mu_o/\varepsilon_o)^{\frac{1}{2}} H_o\ 0.53568$

Magnetic energy storage in coaxial region $W_{s(m)}\,\frac{2}{\mu_o}\,{}_{coax.} = H_o^2\ 17.4204$

Magnetic energy storage in gap region $W_{s(m)}\,\frac{2}{\mu_o}\,{}_{gap.} = H_o^2\ 0.3670$

Magnetic energy dissipation in coaxial region $W_{diss}^{\sigma\delta}\,{}_{coax.} = H_o^2\ 20.9577$

Magnetic energy dissipation in gap region $W_{diss}^{\sigma\delta}\,{}_{gap.} = H_o^2\ 0.3670$

Unloaded cavity Q $Q_{un} = 6069.77$

Magnetic energy storage efficiency $\eta_{s(m)}\,{}_{gap.} = 2.063\ \%$

Electric energy storage in coaxial region $W_{s(e)}\,\frac{2}{\mu_o}\,{}_{coax.} = H_o^2\ 17.2569$

Electric energy storage in gap region $W_{s(e)}\,\frac{2}{\mu_o}\,{}_{gap.} = H_o^2\ 0.5304$

Gap electric energy storage efficiency $\eta_{s(e)}\,{}_{gap.} = 3.0\ \%$

7;3;4 (RADIAL CAVITY NUMBER THREE)

The radial cavity dimensions were as given below:

$b' = 0.813$ cms. , $r_1 = 0.635$ cms. , $d=b = 0.305$ cms. $\mathcal{E}_{r_1} = 4.7$

$\mathcal{E}_{r_2} = 1.0$, $\beta_o = 0.628$, $k_{c_1} = 1.3634$, $x_1 = k_{c_1} r_1 = 0.86577$

$J_1(x_1) = 0.3936$, $J_o(x_1) = 0.8213$, $k_{c_2} = 0.62831$ $x_2 = k_{c_2} r_1 = 0.39898$

$\alpha = 0.37515$

The above dimensions refer to FIG.(F;2;1) , where the crystal fills only the gap region.

Resonance condition

From equation (F;2;2;3)

$$ct(x_2y_2) = \frac{b'}{b}(\varepsilon_{r_1}/\varepsilon_{r_2})^{\frac{1}{2}} \frac{J_1(x_1)}{J_o(x_1)} + k_{c_1} \frac{b'}{\pi} \ln\left(\left(\frac{1-\alpha^2}{4\alpha}\right)\left(\frac{1+\alpha}{1-\alpha}\right)^{\frac{1}{2}(\alpha+1/\alpha)}\right)$$

" = 2.9988

Since the above equation is a transcendental equation it is best solved graphically . From FIG.(7;3;4;1) the range of values of $(y-x)$ which satisfy the equation $ct(x_2,y_2) = 2.99$ are found to lie between 0.4 and 1.2), thus minimum and maximum values of y_2 are approximately 0.8 and 1.6 respectively, while the corresponding mimimum and maximum values of (y_2/x_2) are 2.0 and 4.0.

Using these approximate upper and lower limits of (y_2/x_2) along with FIG.(7;3;4;1) it is possible to obtain more accurate limits of (y_2-x_2) as 0.48 and 0.7 . These new limits may again be used to determine better approximations of the minimum and maximum values of (y_2/x_2), which are 2.20 and 2.76 respectively. At this point it is best to accurately calculate the value of the function $ct(x_2,y_2)$ for selected values of (y_2/x_2) between the limits of 2.20 and 2.76 , as shown in FIG.(7;3;4;2)

$x_2 = 0.39898$

y_2/x_2	y_2	$J_o(y_2)$	$N_o(y_2)$	$ct(x_2,y_2)$
2.0				3.475
1.9	0.759	0.8667	-0.127	3.780
2.2	0.878	0.8157	-0.0120	3.02
2.4	0.956	0.7890	-0.050	2.67

FIG.(7;3;4;2)

in the above calculation x_2 is a known quantity since k_{c_2} is known,

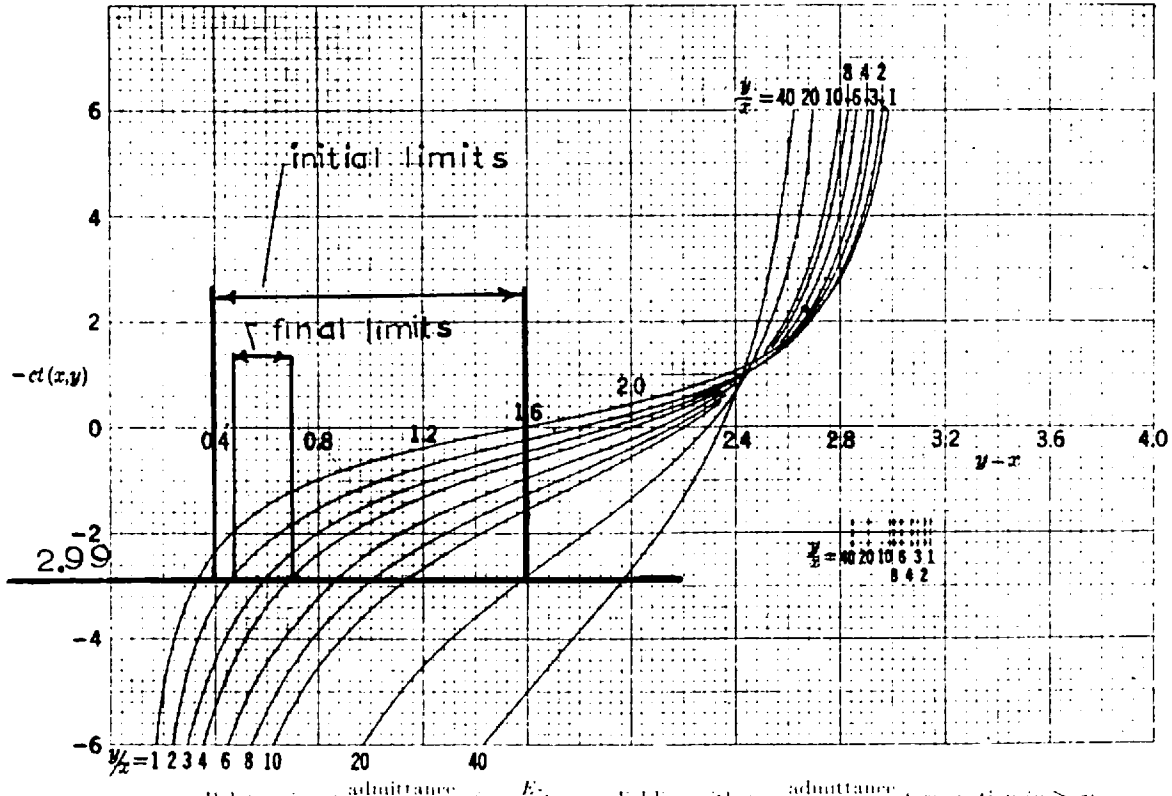

- Relative input $\frac{\text{admittance}}{\text{impedance}}$ of an $\frac{E}{H}$-type radial line with zero $\frac{\text{admittance}}{\text{impedance}}$ termination ($y > x$).

FIG (7:3:4:1)

Graphical solution to radial cavity resonance equation

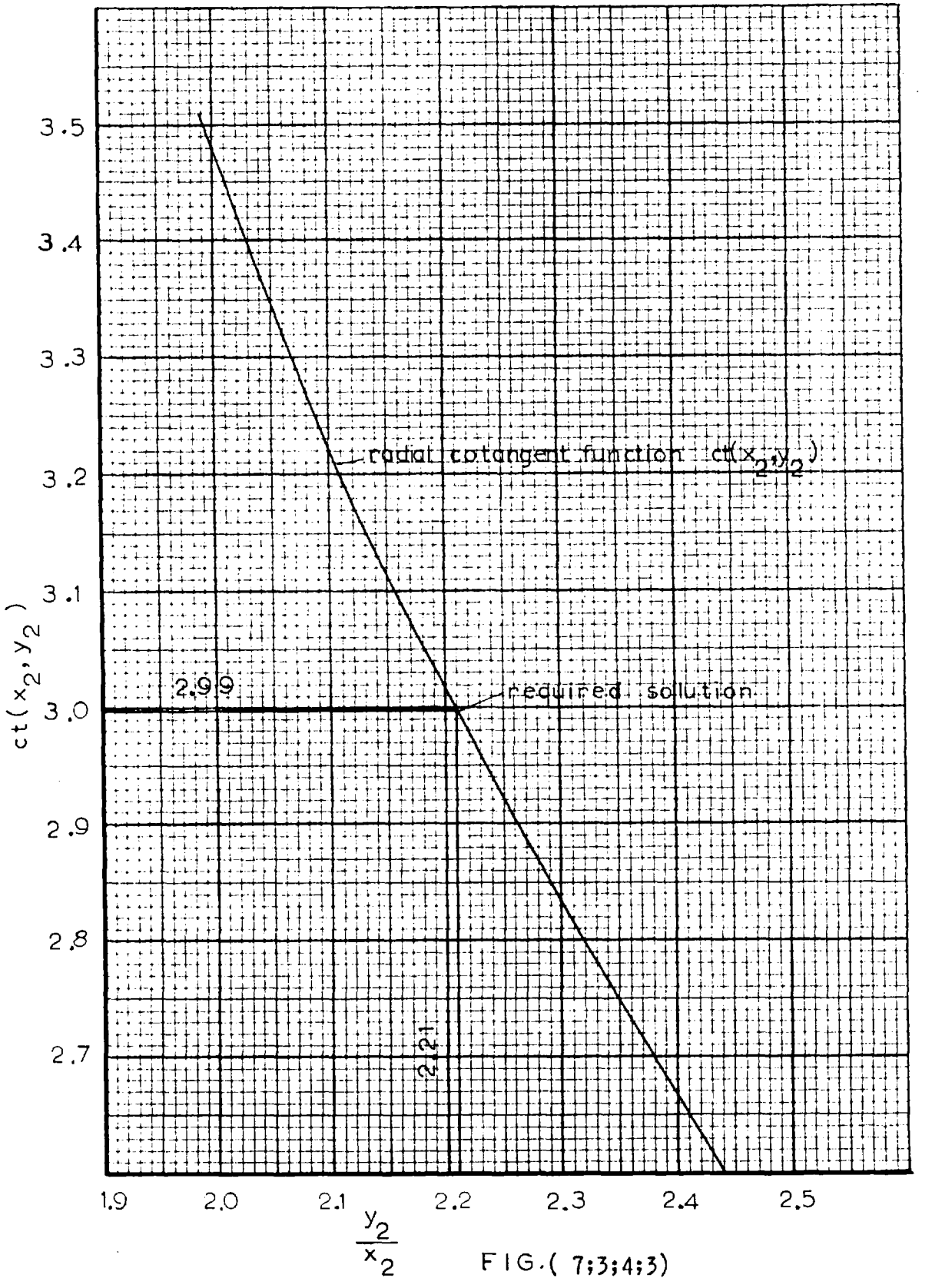

FIG.(7;3;4;3)

and the function $ct(x_2,y_2)$ is given by equation (B;4;4;31) of appendix (B) as:

$$ct(x_2,y_2) = \frac{J_1(x_2)\,N_o(y_2) - N_1(x_2)\,J_o(y_2)}{J_o(x_2)\,N_o(y_2) - N_o(x_2)\,J_o(y_2)}$$

where
$$J_1(x_2) = 0.1960$$
$$J_o(x_2) = -1.781$$
$$N_1(x_2) = 0.964$$
$$N_o(x_2) = -0.606$$

The calculated values of the function $ct(x_2,y_2)$ are then plotted as shown in FIG.(7;3;4;3) and the intersection of the curve with the line $ct(x_2,y_2) = 2.99$ gives the required solution as $y_2/x_2 = 2.210$.

Thus $y_2 = 0.8817$

but also $y_2 = k_{c_2} r_2 = k_{c_2} r_o$

and so finally $r_2 = 1.4033$ cms.

Consequently the required outer cavity diameter required for resonance was .2.8o4 cms or 1.1o5 inches.

Having now all the cavity dimensions it is possible to calculate its performance. Thus:

<u>Maximum electric field in cavity gap.</u>

From equation (F;2;2;12)

$$E_o = \frac{H_o}{r_o}(\mu_o/\varepsilon_o\varepsilon_{r_1})^{\frac{1}{2}}\,\frac{cs(x_2,y_2)}{J_1(x_1)} = H_o(\mu_o/\varepsilon_o)^{\frac{1}{2}}1.678$$

where
$$cs(x_2,y_2) = \frac{y_2}{2}\left(N_o(y_2)J_1(x_2) - J_o(y_2)N_1(x_2) \right) = 2.0119$$

now
$$E_{z(r=r_1)} = E_o\ J_o(x_1) = 0.8213\ E_o$$

and so the average value of the electric field in the cavity gap is

$$E_{z(\text{average})} = 0.910\ 25\ E_o$$

Magnetic energy storage in gap region

From equation (F;2;3;1)

$$W_{s(m)\ \text{gap}} \frac{2}{\mu_o} = H_o^2 \left(\frac{r_1}{r_o}\right)^2 cs^2(x_2,y_2)\pi d \left\{1 - \frac{2J_o(x_1)}{x_1 J_1(x_1)} + \frac{J_o^2(x_1)}{J_1^2(x_1)}\right\}$$

$$" = H_o^2\ 0.423$$

Magnetic energy storage in second radial line

From equation (F;2;3;11)

$$W_{s(m)\ \text{radial line}} \frac{2}{\mu_o} = \frac{(H_o k_2)^2 \pi^3 b'}{4} \left(A^2(\text{IV}) + B^2(\text{V}) - AB(\text{VI})\right)$$

$$" = H_o^2\ 3.7496$$

where the symbols (IV), (V) and (VI) represent the functions given in equations (F;2;3;7 , 8 and 10) respectively and A,B are as given by equation (F;2;3;6).

Magnetic energy dissipation in gap region

From equation (F;2;3;3)

$$W_{\text{diss}(m)\ \text{gap}}^{\sigma\delta} = H_o^2\ 2.77497$$

Magnetic energy dissipation in second radial line

From equation (F;2;3;13)

$$W_{\text{diss}(m)\ \text{radial line}}^{\sigma\delta} = H_o^2\ 8.2428$$

Unloaded cavity Q

From equation (F;2;3;14)

$$Q_{un} = 3024.32$$

Gap magnetic energy storage efficiency

From equation (F;1;5;1)

$$\eta_{\substack{(m)\\gap}} = 10.16\ \%$$

Gap electrical energy storage

From equation (F;2;4;4)

$$W_{\substack{s(e)\\gap}} \frac{2}{\mu_o} = H_o^2\ 4.25044$$

Electrical energy storage in second radial line

From equation (F;2;4;13)

$$W_{\substack{s(e)\\radial\ line}} \frac{2}{u_o} = H_o^2\ 0.2020$$

Gap electrical energy storage efficiency

From equation (F;2;4;14)

$$\eta_{\substack{(e)\\gap}} = 95.5\ \%$$

7;3;5 (COMPARISON OF CAVITY PARAMETERS)

Cavity number	one	two	three
Maximum gap electric field $E_o(\mu_o/\varepsilon_o)^{\frac{1}{2}}H_o$	4.447	0.535	1.678
Minimum gap electric field x E_o	0.936	0.295	0.82o
Average gap electric field x E_o	0.97	0.647	0.910
Gap magnetic energy storage	4.47 %	2.o6 %	10.16 %
Gap electric energy storage	92.o7%	3.o %	95.5%
Cavity unloaded Q (theoretical)	1963.2	6069.7	3024.3

Examination of the above table reveals why the second cavity design was inefficient since only 3% of the electrical energy was stored in the gap region. The above figures also indicate that the radial design was superior to either of the two coaxial cavities.

7;3;6 (MODIFIED RADIAL CAVITY HAVING LARGE CRYSTAL)

The solution to the resonance equation for the modified radial cavity shown in FIG.(F;2;1;4) is now considered.

The effective dielectric constant of the gap region is found from equation (F;2;1;11) using the following cavity parameters.

$\mathcal{E}_{r(1)} = 4.65$, $\mathcal{E}_{r(2)} = 1$, $\mathcal{E}_{r(3)} = 2$, $d_1 = 0.120"$, $d_2 = 0.010"$

$d_3 = 0.050"$, $d_{t(1)} = 0.180"$

thus

$$\mathcal{E}_{r(1)(eff)} = 2.96$$

Similarly for region A of the short circuited radial section:

$d_1 = 0.120"$, $d_2 = 0.10"$, $d_3 = 0.190"$ $d_{t(A)} = 0.320"$

and so:

$$\mathcal{E}_{r(A)(eff)} = 2.45$$

Now region B gives:

$d_1 = 0.120"$, $d_2 = 0.010"$, $d_3 = 0.050"$, $d_4 = 0.140"$

therefore: $\mathcal{E}_{r(B)(eff)} = 1.595$

while for region C:

$$\mathcal{E}_{r(C)(eff)} = 1.39$$

and finally for region D:

$$\mathcal{E}_{r(D)(eff)} = 1.0$$

Now the other cavity dimensions , with reference to FIG.(F;2;1;4), were:

$r_1 = 0.250"$, $r_1' = 0.2812"$, $a = 0.3612"$, $b = 0.475"$, $c = 0.537"$

$d = 0.5687"$

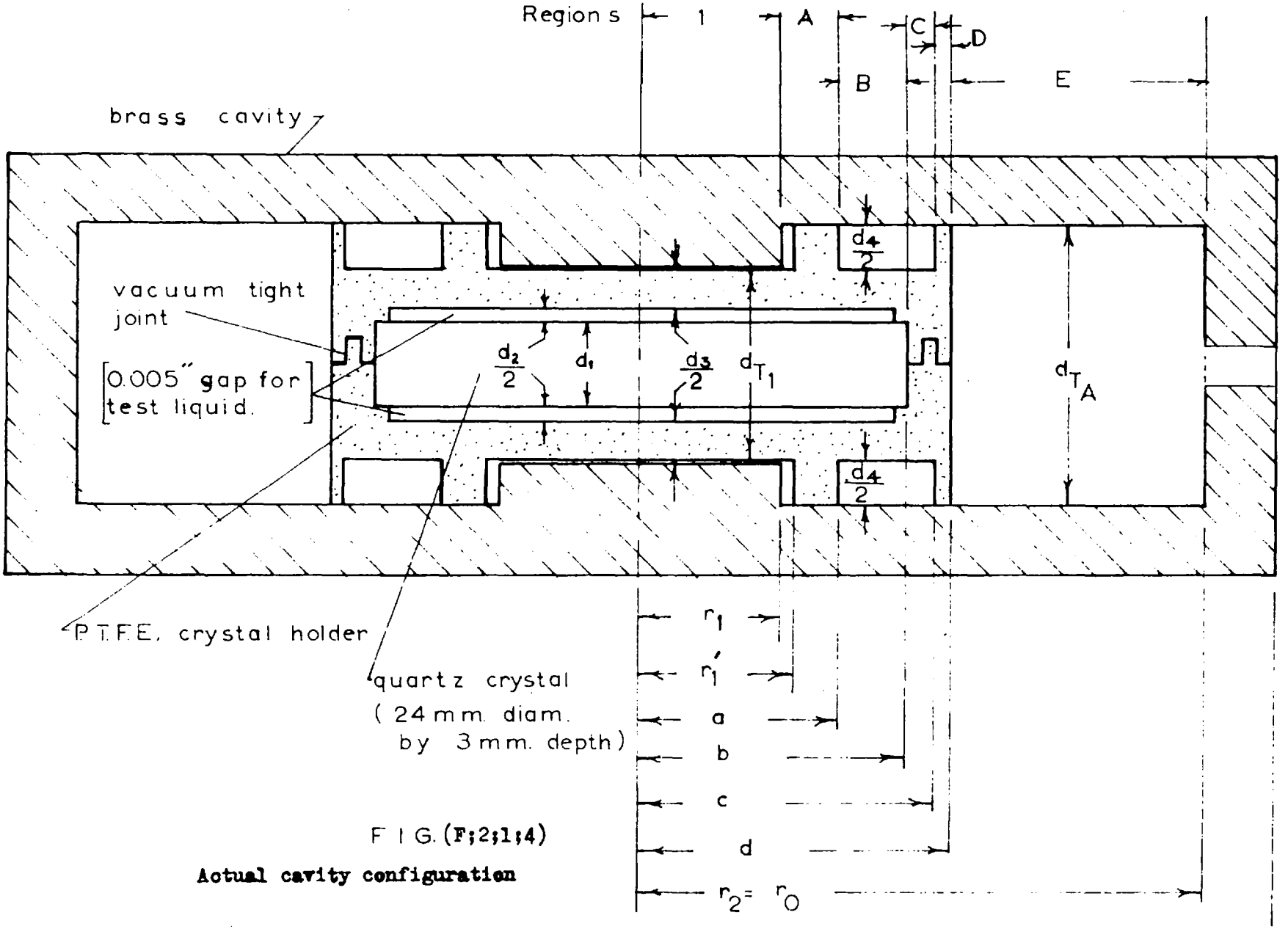

FIG. (F;2;1;4)

Actual cavity configuration

Now from equation (F;2;1;19)

$$\mathcal{E}'_{r(eff)} = 1.775$$

and so finally from (F;2;1;20)

$$\mathcal{E}_{r(2)(eff)} = \left(\frac{r_2^2 + 0.72}{r_2^2 - 0.404} \right)$$

Now:

$$x_1 = k_1 r_1 = \beta_o \left(\mathcal{E}_{r_{(1)(eff)}} \right)^{\frac{1}{2}} r_1 = 0.687$$

and so the resonance equation (F;2;1;10) becomes:

$$ct(x_2,y_2) = \frac{b'}{b} \left\{ \frac{\mathcal{E}_{r_{(1)(eff)}}}{\mathcal{E}_{r_{(2)(eff)}}} \right\}^{\frac{1}{2}} \left\{ \frac{J_1(x_1)}{J_o(x_1)} \right\} + \frac{k_1 b'}{\pi} \ln \left\{ \left(\frac{1-\alpha}{4\alpha} \right) \left(\frac{1+\alpha}{1-\alpha} \right)^{\frac{1}{2}(\alpha + 1/\alpha)} \right\}$$

$$" = 1.116 \left\{ \frac{r_2^2 = 0.404}{r_2^2 = 0.72} \right\}^{\frac{1}{2}} + 0.1086 = \Phi$$

Since as before the above resonance equation is transcendental it is best solved graphically. To accomplish this, selected values of r_2 are picked and the corresponding values of $(ct(x_2,y_2)$ and Φ are calculated, and plotted as shown in FIG.(7;3;6;1).

The intersection of the two functions $(ct(x_2,y_2)$ and Φ give the required solution. when $r_2 = 2.22$ cms. and hence the outer cavity diameter required for resonance was 4.44 cms = 1.75 inches.

The technique of specifying an effective dielectric constant for the various cavity regions was experimentally verified to be accurate to approximately five.percent.

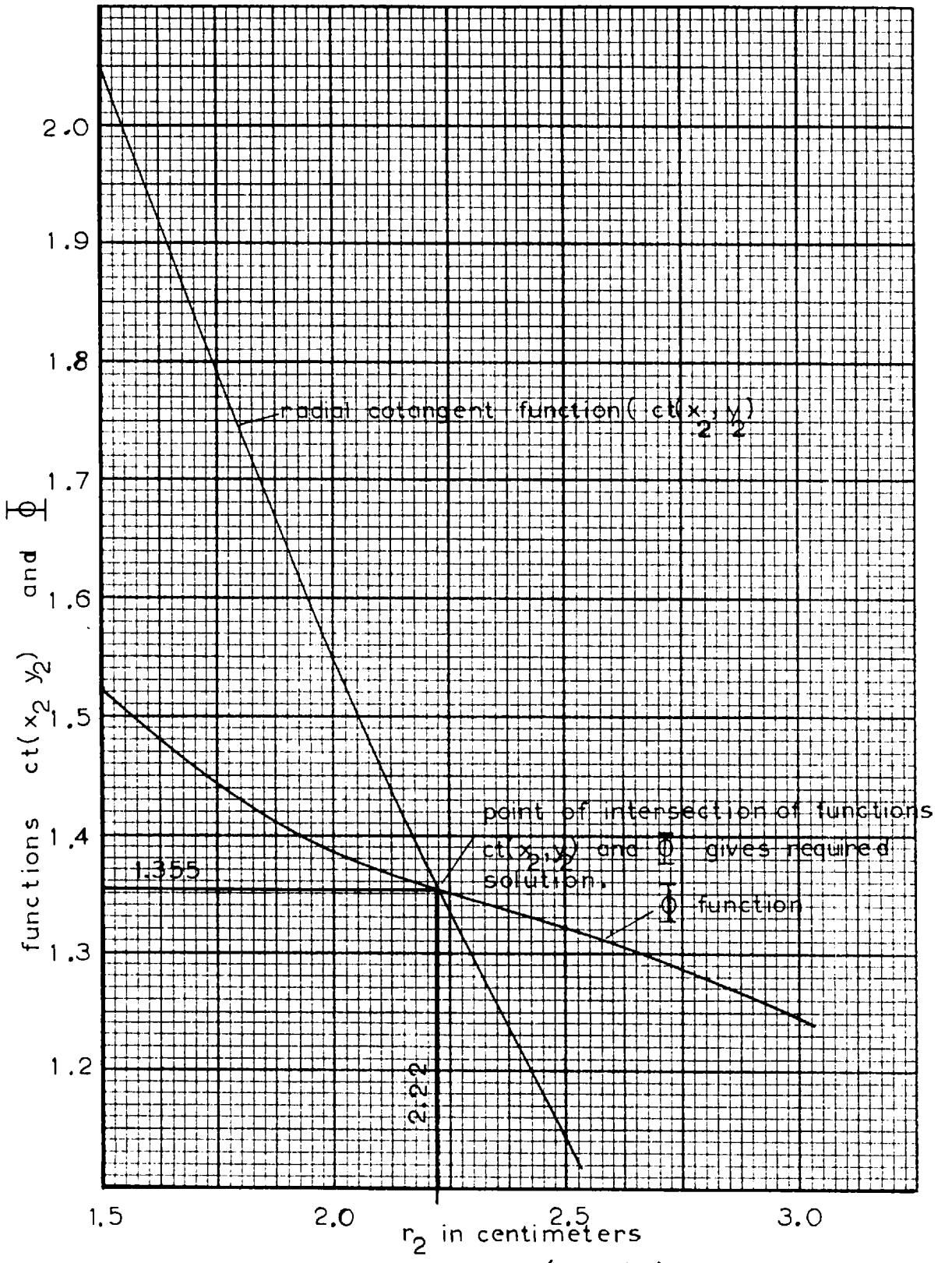
2.0
1.9
1.8
1.7
1.6
1.5
1.4
1.3
1.2
functions ct(x2 y2) and Φ
radial cotangent function(ct(x2, y2)
point of intersection of functions
ct(x2,y2) and Φ gives required
solution.
Φ function
1.355
2.22
1.5
2.0
2.5
3.0
r2 in centimeters

FIG. (7;3;6;1)

7;4 (QUARTZ CRYSTAL TRANSDUCER)

7;4;1 GENERAL

The ultrasonic transducer used in this system was, as previously mentioned, a piezoelectric single quartz crystal. This material was actually crystalline silicon dioxide having a trigonal trapezohedral structure . The Z or optical axis was an axis of three fold symmetry. The I.R.E. standard crystallographic axes are shown in FIG.(7;4;1;1), for the natural occurring crystal.

Because of its symmetry the crystal was found to have only six independent elastic constants, two piezoelectric constants and two dielectric constants. These constants are given in FIG.(7;4;1;2), along with other crystal parameters.

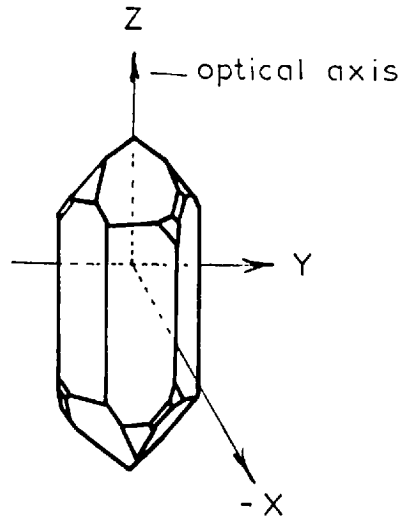

FIG. (7;4;1;1)

I.R.E. standard crystallographic axes for quartz.

FIG.(7;4;1;2)

Elastic constants for quartz

C_{ijkl} =

	11 (1)	22 (2)	22 (3)	23 (4)	13 (5)	12 (6)
11	8.683	0.709	1.19343	-1.8064	o	o
22	0.709	8.683	1.19343	1.8064	o	o
33	1.193	1.193	10.594	o	o	o
23	-1.8064	1.8064	o	5.8267	o	o
13	o	o	o	o	5.826	-1.8064
12	o	o	o	o	-1.8064	3.9871

From Koga (Phys, Rev. 109 , 1958 P.1467) $\times 10^{10}$ newtons/m^2

Piezoelectric constants for quartz

e_{ijk} =

	11	22	33	23	13	12
11	17.5	-17.5	o	-4.07	o	o
22	o	o	o	o	4.07	-17.5
33	o	o	o	o	o	o

$\times 10^{-12}$ ampere second/m^2

Dielectric constants for quartz

εr_{ij} =

	11	22	22
11	4.5o	o	o
22	o	4.5o	o
33	o	o	4.7o

Expansion coefficients

α_{ij} =

	11	22	33
11	14.3	o	o
22	o	14.3	o
33	o	o	7.8

$\times 10^{-6}$/°C

Elastic -temperature coefficients for quartz (101)

Tc_{ijkl} =

	11	22	33	23	13	12
11	-46.5	-33oo	-7oo	+9o	o	o
22	-33oo	-46.5	-7oo	-9o	o	o
33	-7oo	-7oo	-2o5	o	o	o
23	+9o	-9o	o	-166	o	o
13	o	o	o	o	-166	+9o
12	o	o	o	o	+9o	+164

$\times 10^{-6}$/°C

The density of quartz= 2.65 grams/ cm^3 .

7;4;2 (CHOICE OF CRYSTAL CUT)

The requirements imposed on the crystal cut were as follows:

(1). Crystal had to support a pure shear mode so that mode conversion and/or interference did not occur upon reflection.

(2). Axis of energy propagation had to coincide with the direction of elastic wave phase velocity propagation for cavity re-excitation considerations.

(3). Crystal cut had to be so arranged that excitation conditions necessary for the required mode did not excite any other mode.

It can be shown through the use of equations (D;2;20 and D;3;13) of appendix D , that the first of the above requirements was satisfied by anyY crystal cut. (109). Here a Y cut is meant to signify that the axis of phase velocity propagation is rotated about the X axis in the YZ plane.

It is also a simple matter to show from equations (D;4;1 to 3) that the second requirement was also satisfied when the crystal cut was arranged such that the angle of rotation of the wave normal was $31^{\circ}\ 30'$ or $-58^{\circ}29'\ 11''$ as indicated in FIG.(7;4;2), the first cut being termed an AC cut , while the second was a BC cut.

In this work only the BC crystal cut was used since it was found experimentally that this cut had a much lower acoustic attenuation than the AC.

To investigate whether or not condition three could be satisfied it was necessary to consider equation (D;8;10) of appendix (D) page(286). Thus:

$$u_k = \frac{j}{\Gamma_s} \frac{e_{ijm}}{C_{ijkl}} E_m \; e^{j(\omega t - \Gamma_s x_l)} \qquad (D;8;10)$$

where u_k is the particle displacement, e_{ijm} is the piezoelectric constant

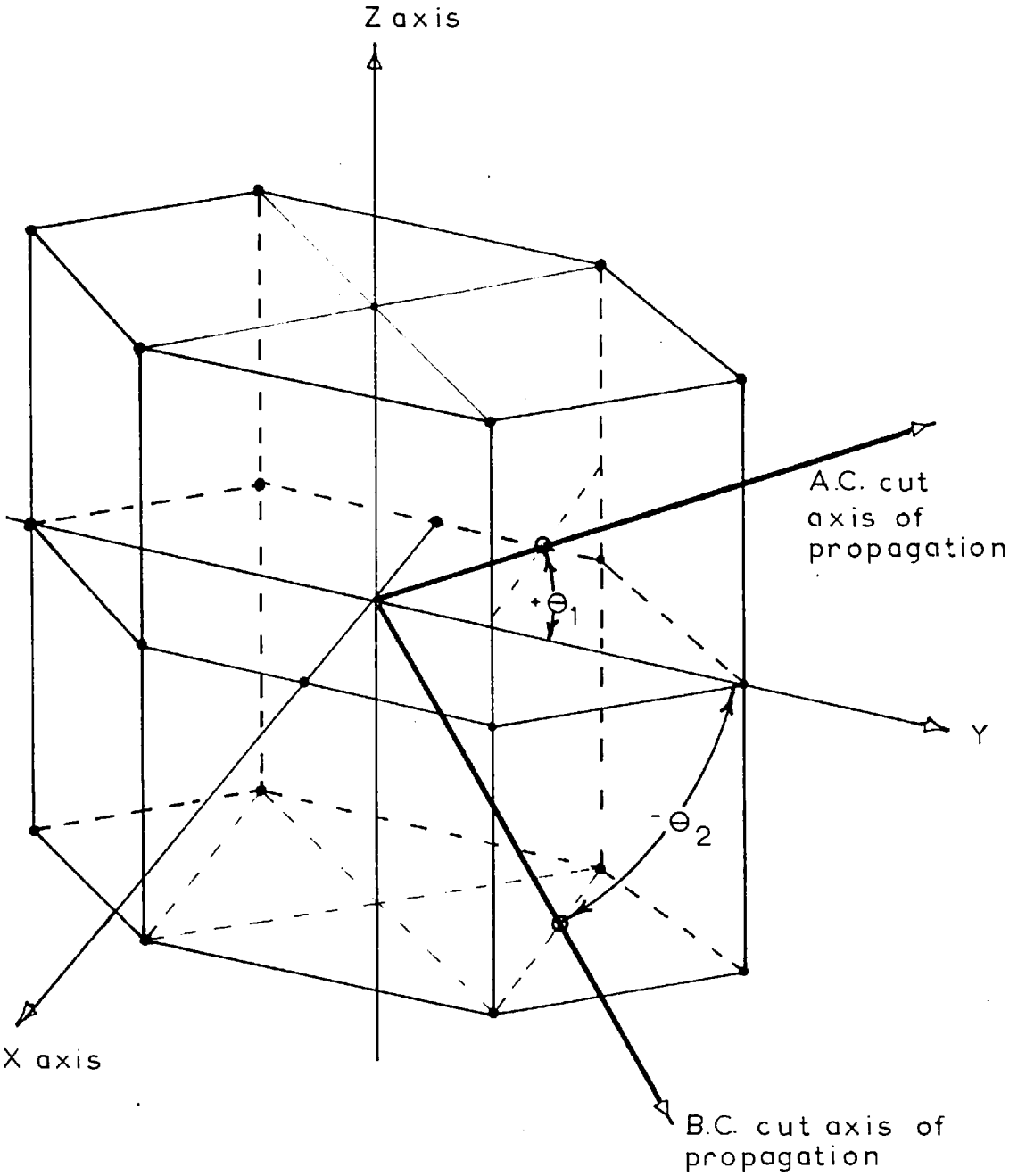

FIG. (7;4;2;1)

Diagram of rotated Y cuts in quartz crystal.

tensor, C_{ijkl} is the elastic constant tensor , while E_m is the applied electric field. For a rotated crystal orientation it is necessary to use the rotated crystal constants, which are derived from appendix (D;6) and FIG.(7;4;1;2), and are as follows for the BCcut:

Rotated constants for BC cut quartz

		11	22	33	23	13	12
C'_{ijkl}	11	8.683o	2.6698	-0.7681	0.6o41	o	o
	22	2.6698	10.4588	-0.8139	-0.7167	o	o
	33	-0.7681	-0.8139	12.8112	-0.952o	o	o
	23	0.6o41	-0.7167	-0.952o	3.8228	o	o
	13	o	o	o	o	2.8792	o
	12	o	o	o	o	o	6.9319
		(x 10^{1o} newtons/ m^2)					
e'_{ijk}	11	16.67	-1.77	-15.o2	-6.o8	o	o
	22	o	o	o	o	-6.625	-6.1o5
	33	o	o	o	o	-1o.685	-9.855
		(x 10^{-12} ampere seconds/ m^2)					
ε'_{ij}	11	4.5o	o	o			
	22	o	4.65	-0.o89			
	33	o	-0.o89	4.55			
α'_{ij}	11	14.3	o	o			
	22	o	9.56	-2.88			
	33	o	-2.88	12.51			
		(x 10^{-6}/ ^oC)					

at constant strain

FIG.(7:4:2:2:)

(Rotated constants after J. Richter (110)).

Now expanding equation (D;8;10) and inserting the appropriate rotated constants from the table above, noting that for the rotated cut n= 2' it is found that only u_1 exists ,which indicates that only one pure shear mode is present.

Thus it can be seen that the BC cut fulfilled all the initial requirements and thus was used exclusively in this work.

7;4;3 (CRYSTAL CALCULATIONS)

Having thus specified the crystal orientation it is possible to calculate the velocities and the direction of particle displacements by inserting the appropriate elastic constants into equations (D;2;22 and 23).

Now since $\theta = -58^{\circ}\ 29'\ 10''$ and propagation is in the YZ plane

$$L = 0 \quad , m = 0.5227 \ , n = -0.8524$$

where L, m and n are the direction cosines of the wave normal as given in FIG.(D:2;1) on page(26o).

Thus the " Christoffel Constants" of equations (D;2;12 to 19) become:

$$h_{11} = 6.93210 \times 10^{11} \text{ dynes/ cm}^2$$
$$h_{22} = 4.99580 \quad "$$
$$h_{33} = 9.28637 \quad "$$
$$h_{23} = -2.633685 \quad "$$
$$h_{12} = h_{13} = 0$$

and so the velocity determinant of equation (D;2;22) is:

$$\begin{vmatrix} h_{11} - \rho C^2 & 0 & 0 \\ 0 & h_{22} - \rho C^2 & h_{23} \\ 0 & h_{23} & h_{33} - \rho C^2 \end{vmatrix} = 0$$

and so $C_1 = (h_{11} / \rho)^{\frac{1}{2}} = 5.1145 \times 10^5$ cm/ sec.

while $C_2 = (h_{22}+h_{33}+(h_{22}+h_{33})^2-4(h_{22}h_{33}-(h_{23})^2))$

$" = 6.30597 \times 10^5$ cm/ sec.

similarly $C_3 = 3.7588 \times 10^5$ cm/ sec.

The particle displacement direction cosines $\alpha_i, \beta_i \gamma_{,i}$ of each of the foregoing modes can be found as indicated in appendix (D;2), thus for mode one:

$$\frac{\alpha_1}{(h_{22}-h_{11})(h_{33}-h_{11})-(h_{23})^2} = \frac{\beta_1}{0} = \frac{\gamma_1}{0}$$

which indicates that the first mode is a pure shear mode having a particle displacement parallel to the x axis..

In a similar manner the second mode particle displacement direction cosines are:

$$\frac{\alpha_2}{0} = \frac{\beta_2}{(h_{11}-\rho C_2^2)(h_{23}-\rho C_2^2)} = \frac{\gamma_2}{(h_{11}-\rho C_2^2)(h_{23})}$$

and therefore the angle between the Y axis and the direction of particle displacement is 64° 33'. Finally the deviation ψ_2 between the wave normal and the particle displacement can be determined from equation (D;2;25) and so:

$$\psi_2 = 6.5^\circ$$

which indicates that C_2 corresponds to a quasi-longitudinal mode of propagation.

Now since , as explained in appendix (D;2), the three mode displacements are mutually perpendicular , the particle displacements of the third mode is known and as such is a quasi-shear mode.

The sonic operational wavelength in the quartz crystal used under conditions of pure shear mode propagation may be determined since the velocity of propagation is now known. So:

$$\lambda_s = C_1 / f = 1.70466 \times 10^{-4} \text{cms.} = 1.7046 \text{ microns.}$$

Obviously since the acoustic wavelength was so small, very stringent conditions were imposed on the crystal surfaces. The crystals used had highly polished faces, flat to less than one tenth of a wavelength and parallel to better than three seconds of arc. It follows that with such a small sonic wavelength within the crystal any slight strains applied to the crystal would seriously effect the acoustic transmission and hence it was essential that the crystal be very delicately held and completely at thermal equilibrium if any useful measurements were to be obtained.

It is also possible to determine the characteristic impedance of the quartz crystal medium. Thus from equation (D;7;23) :

$$Z_c = \rho_c C_1 = 1.355 \times 10^6 \text{ grams/sec.cm}^2$$

Now having all the pertinent crystal parameters for the rotated BC cut , the value of the electromechanical coupling coefficient is, from equation (D;9;5) page (287):

$$K^2 = \frac{e_{122}^2}{C_{1212}\,\varepsilon_{22}}$$

and imposing the conditions of pure shear mode propagation along the rotated or Y' axis with particle displacement along the X' axis gives:

$$K^2 = \frac{e_{122}'^2}{C_{1212}'\,\varepsilon_{22}'} = 1.30654 \times 10^{-3}$$

In the above equation the primes denote rotated constants.

7;4;4 (ACOUSTIC ATTENUATION IN QUARTZ)

The mechanism of acoustic attenuation in quartz is still not completely understood although theoretical calculations of expected attenuation giving the right order of magnitude have been derived by Bommel and Dransfield assuming a phonon- phonon interaction mechanism. (81).

The acoustic attenuation versus temperature characteristic for a typical quartz transmission line, supporting a shear mode, is given in FIG.(7;4;4;1). From the diagram it is clear that the loss mechanism undergoes a transition at approximately 30 degrees Kelvin and hence the difficulty in using quartz at room temperature and high frequencies is that the acoustic loss is exceedingly high.

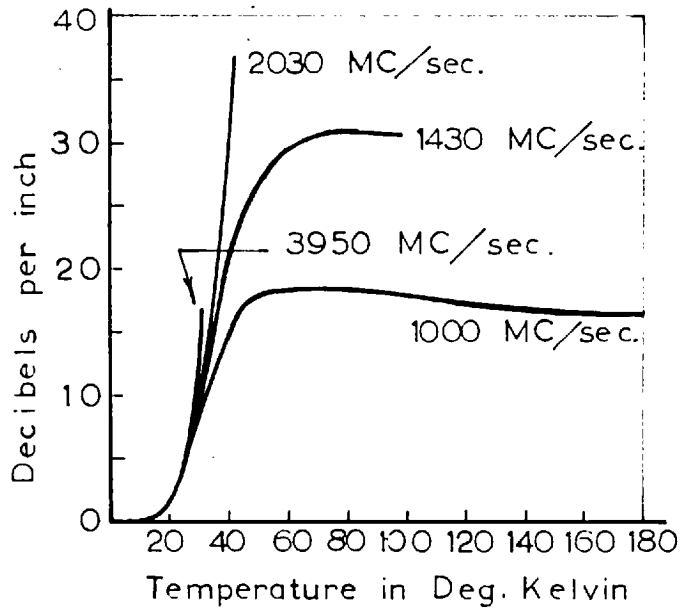

FIG. (7;4;4;1)

Temperature dependence of attenuation in crystal quartz for shear waves . after Bommel and Dransfeld (Phy.Rev. Let. April 1959)

Initially at the outset of this project no published information was available with regard to the acoustic attenuation to be expected at room temperature and 3000 Mcs. operating frequency. Bommel and Dransfeld (82), had published the results of their investigations of attenuation in several crystal cuts in this frequency range but only below the transition temperature, as indicated in FIG.(7;4;4;1). Similarly Jacobson (83), reported generation of acoustic waves in crystal quartz up into the " X " band region , under very low temperature conditions, however above 77°K he could detect no propagation.

An estimate of what the room temperature acoustic loss might be at " S " band was obtained from extrapolation of experimental attenuation results obtained previously in this department (84) for crystal quartz,in the frequency range of 100 to 1000 Mcs. The value derived from such extrapolation was 40 db./ cm. for an X cut disk but it was felt that the situation would improve with the BC cut.

The actual values of acoustic attenuation in BC crystal quartz at 3000 Mcs., measured with this developed system were found to range between 14.5 to 25 db. per centimeter. That there should be such a wide spread was initially difficult to comprehend however this variation was later found to be a function of the crystal surface condition.

Initially only one crystal,out of a group of eight identical crystals obtained commercially,was found to perform satisfactorily with respect to conversion efficiency and shape of decay pattern. Several of the other crystals were observed to give only a few echoes with poor nonexponential decays, while the remainder produced no response what so ever. Apparently perfect crystals obtained from another source were also found to be useless in the same manner.

Since the manufacturers were unable to indicate a solution to the problem and also since at least two good crystals were vitally required for the operation of the system, an attempt was made to determine why apparently identical perfect crystals exhibited such

different performance.

It was felt that since the excitation process was mainly a surface effect, as is explained in appendix (D;8), the active depth being of atomic dimensions, any severe crystal surface damage,resulting in the process of manufacture, would seriously deteriorate performance and perhaps still not be detectable optically. Thus the crystal surfaces were etched in Hydrofluoric acid to remove any damaged crystal molecules present and then a fine polish applied to render the surfaces accurately flat and parallel once more. This treatment was found to have an almost unbelievably beneficial effect on the crystals, transforming even the previously most useless crystals into units having performance surpassing anything previously attained.

The measured acoustic absorption of these treated crystals was found to be up to five db. less than the best untreated ones. It follows therefore that since the surface conditions have such a marked effect on the decay pattern for a particular crystal, it is doubtful if the values obtained experimentally for the acoustic absorption of a material,merely by plotting the slopeof its decay pattern, are of any **significance.**

7;5 (GENERAL MICROWAVE ULTRASONIC TRANSDUCER CALCULATIONS)

Calculation of the general overall performance of the microwave ultrasonic transducer is now made for typical operating conditions. Only the radial cavity design is considered as only it was used for measurement purposes. The operational unloaded cavity Q is specified at 200 while the pulsed input power is set at 20 kilowatts.

Electromechanical conversion efficiency

From equation (D;9;12)

$$\eta_o = \left(\frac{K^2 Q_{un} \lambda_s \eta_{e(gap)}}{2\pi d} \right)^2 = 2.037 \times 10^{-9} = -86.91 \text{ db.}$$

Pulsed acoustic power

From equation (D;9;10)

$$P_s = (\eta_o)^{\frac{1}{2}} \; P_{in} = 0.90305 \quad \text{watts}$$

Average gap electric field

From equation (F;1;3;2)

$$E_{z_{(average)}} = \left\{ \frac{P_{in} \eta_{e(gap)} Q_{un}}{(\varepsilon_o \varepsilon_{r_{(1)}} r_1^2 \pi^2 f d)} \right\}^{\frac{1}{2}} = 2.124 \times 10^6 \text{ volts/m}$$

Maximum gap electric field

From equation (F;1;3;2) and table (7;3;5)

$$E_{z_{(max.)}} = 2.3327 \times 10^6 \text{ volts / meter.}$$

Sonic energy density. (stored)

From equation (D;9;3)

$$W_s = \frac{e_{122}^2}{2 C_{1212}} (E_{z_{(max)}})^2 = 6.301 \times 10^{-8} \quad \frac{\text{newtons meters}}{m^3}$$

Maximum pulsed sonic energy flux density

$$\text{Sonic flux density (max. pulsed)} = W_s \; C_1 = 7.5021 \times 10^2 \text{ watts/ } m^2$$

where C_1 is the velocity of propagation of the pure mode acoustic shear wave.

Maximum particle displacement

From equation (D;8;9)

$$u_{1(max)} = \frac{e_{122}}{\nabla_s C_{1212}} E_{z_{(max)}} = \frac{e_{122} \lambda_s}{C_{1212} \; 2\pi} E_{z_{(max)}}$$

$$" \quad = \quad 5.5738 \times 10^{-13} \quad \text{meters}$$

Maximum shear strain

From equation (D;1;26 and D;8;8)

$$S_{xy'(max)} = -\Gamma_s \; u_{1\,(max)} = \frac{-2\pi}{\lambda_s} u_{1(max)}$$

$$S_{12'(max)} = 2.0544 \times 10^{-6}$$

Maximum shear strain rate

The shear strain rate is obtained by differentiation of the shear strain expression with respect to time. Now under the assumed time dependence of $e^{j\ t}$ the maximum shear rate becomes:

$$\text{Maximum shear rate} = j\omega\Gamma_s \; u_{1(max)}$$

$$= 3.8725 \times 10^{4} \quad \text{sec.}^{-1}$$

The maximum particle displacement velocity

The particle displacement velocity is obtained from time differentiation of equation (D;8;10). Thus:

$$\text{Maximum particle displacement velocity} = j\omega\, u_{1(max)}$$

$$" \qquad = 1.0506 \times 10^{-2} \text{ m/sec.}$$

Maximum particle acceleration

The particle acceleration is obtained by taking the second time differential of equation (D;8;10). Thus:

$$\text{Maximum particle acceleration} = \omega^2 \, u_{1(msx)}$$

$$" \qquad = 1.9804 \times 10^{8} \text{ m/sec.}^2$$

Discussion

Examination of the foregoing calculations of section (7;5) reveals that the electromechanical conversion efficiency obtained under practical operating conditions was exceedingly poor and therefore imposed a variety of restrictions on the design of the system which in turn necessitated a much higher degree of system complexity than would other wise have been the case.

The previous calculations also indicate that the maximum sonic energy flux density achieved in the quartz crystals was well within the accepted linearity limit of 1×10^{5} watts / m^2.

It is also interesting to note that the peak particle acceleration experienced by the quartz crystal was extremely high being approximately 2×10^{7} g, where g is the gravitational acceleration.

The maximum shear strain rate produced in the crystal was also high being almost 4×10^{4} sec^{-1}. However since the actual particle strain was only 2×10^{-6}, the usually observed phenomenon of reduction in viscosity with high shear rate was not observed.

Chapter 8

AUXILIARY ITEMS OF EQUIPMENT

8;1 (THERMOSTATING BATH)

In order to realise the high degree of temperature stability necessary for accurate measurements, it was found desirable to construct a thermostating bath into which both ultrasonic cavities could be immersed. The general construction of the bath is given in FIG.(8;1;1).

Extremely good temperature stability was obtained with this device. The cyclic temperature variation resulting from the on-off operation of the pump was measured to be + or - 0.01 of a degree centigrade, while the long term variation was found to be +or - 0.03°C. Such performance was obtained by having the pump output placed directly on the contact thermometer bulb. A slight modification was made to the Sunvic control relay , as shown in FIG.(8;1;2), so that the bath could be used either for heating or cooling. For cold operation the heat exchanger coil was placed in a refrigeration unit.

8;2 (NOISE SOURCE)

A waveguide noise source was also constructed so as to provide an easy and reliable method of determining the overall system noise figure from time to time and thus insure that optimum performance was being achieved.

This noise source was of the conventional gas discharge type in which a small D.C. electric field was maintained along the axis of a long slender tube, resulting in the acceleration of electrons. These excited electrons exchanged energy through elastic collisions and thus gave rise to a random distribution of velocities. Inelastic collisions between electrons and gas molecules resulted in ionisation by which the supply of electrons to the positive column was maintained. Basically it was the free electrons in the discharge column , having relatively

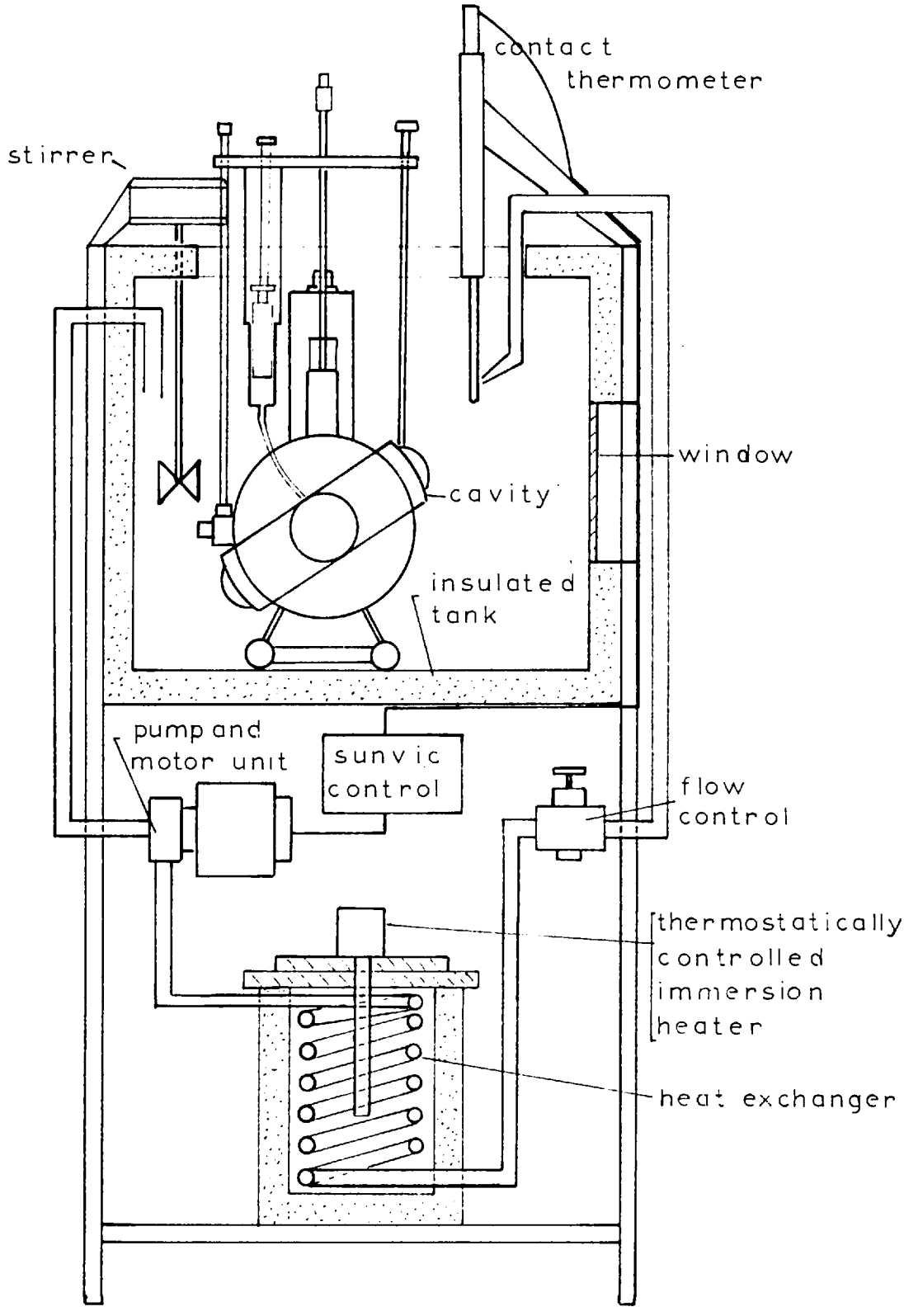

FIG. (8;1;1)

Schematic diagram of thermostating bath.

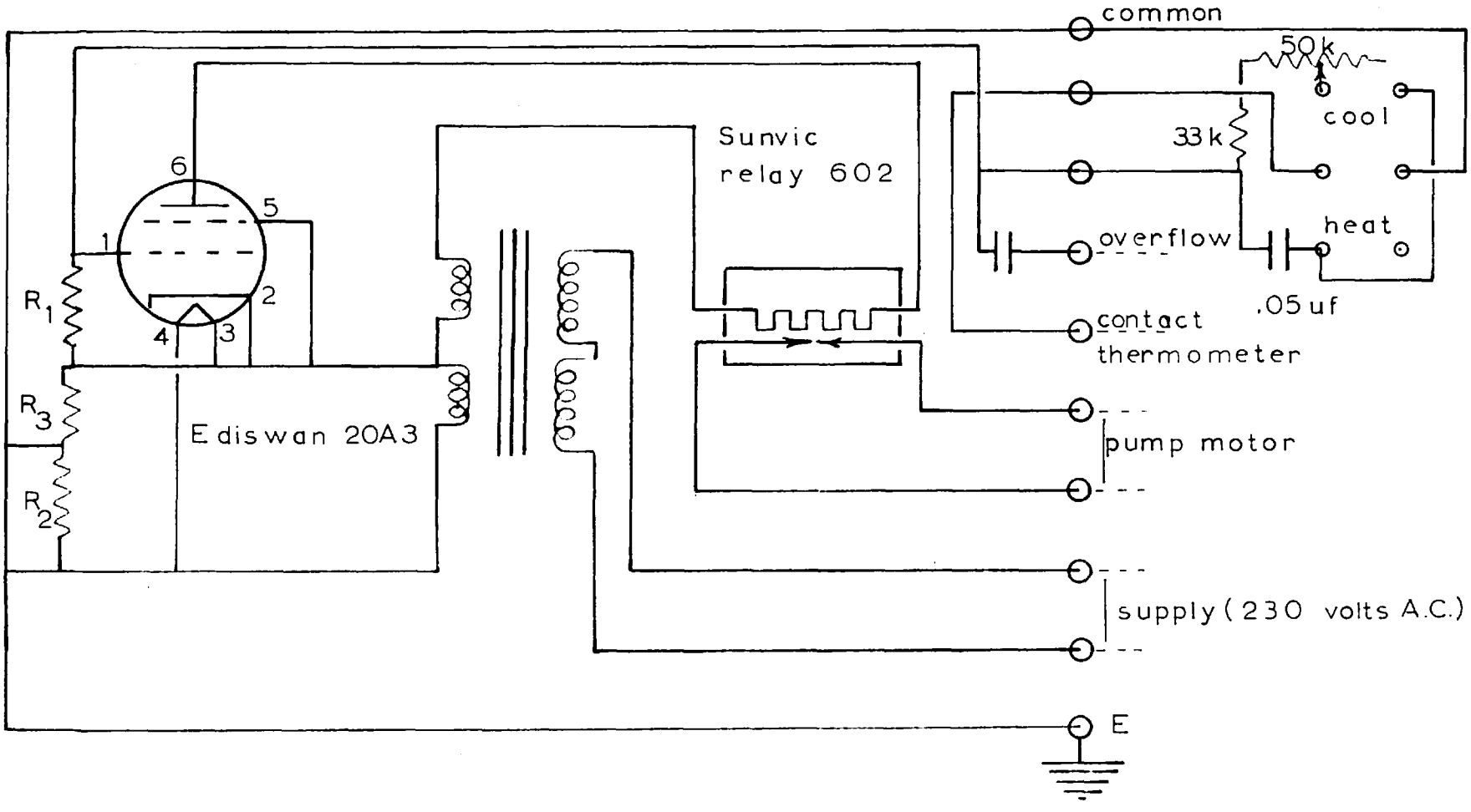

FIG. (8;1;2)

Sunvic electronic control relay used in thermostating bath system.

small mass, which were the chief sources of noise at microwave frequencies. It follows therefore that matching to the plasma could be considered as matching to an electron **cloud**, in which the randomness of the electron velocity distribution, produced noise. (1o2,1o3.1o4).

A D.C. potential of some 60 volts was found to be sufficient to maintain a stable discharge of 180 milliamperes in the CV1881 argon gas tube utilised. It was necessary however to supply an initial impulse of approximately 2000 volts to strike the discharge, this voltage spike being generated within the noise source power supply shown in FIG.(8;2;1). Due to the negative resistance characteristic of the discharge it was necessary to insert a ballast resistor in series with the noise tube to maintain the discharge current at 180 milliamperes.

It was found experimentally that provided the discharge current was kept above a critical level of 150 milliamperes, the device was very stable and in addition both R.F. conductance of the plasme and its effective temperature showed negligible variation for large changes in operating current. In addition the CV1881 is found to have a noise output only slightly effected by ambient temperature. Thus it is evident that the argon filled gas tube was ideally suited as a standard microwave noise source.

The basic parameters of the CV1881 noise tube are given below:

Gas filling	= argon
Gas pressure	= 30 mm Hg.
Optimum operating current	= 180 ma.
Effective noise temperature	= 11,000 ^{o}K
Noise output	= 15.7 db. above thermal
Noise output variation	= -0.005 db./ ma.

The technique adopted in the construction of the noise tube mount is shown in FIG.(8;2;2).

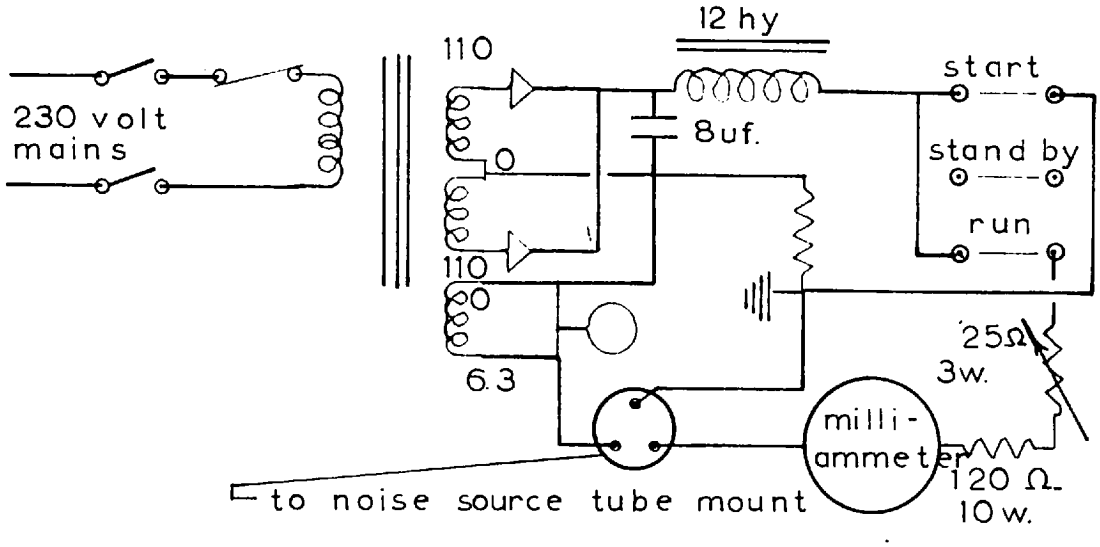

Noise tube power supply

FIG. (8;2;1)

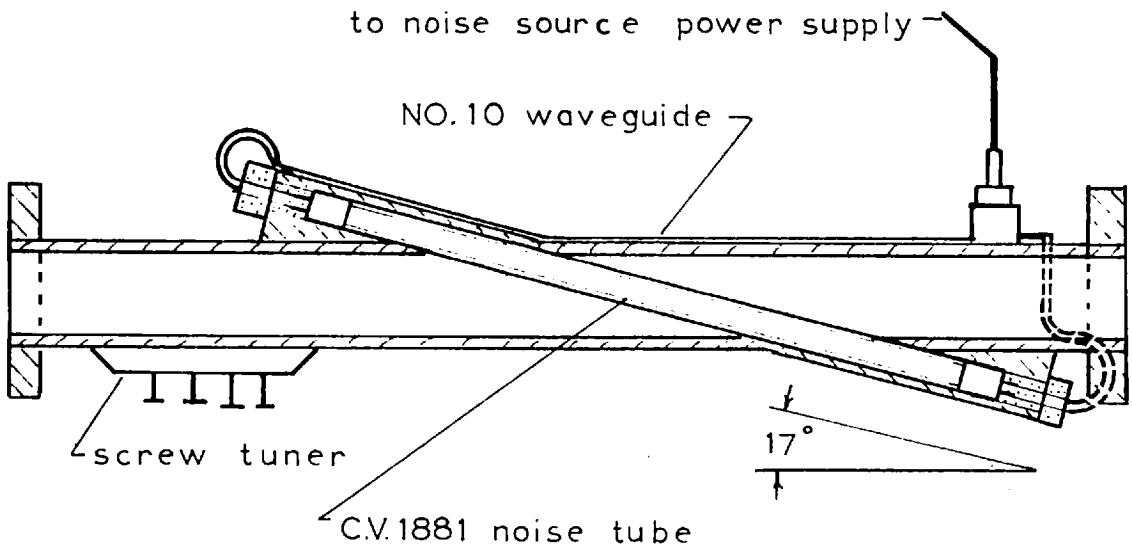

Noise tube " S " band waveguide mount.

FIG. (8;2;2)

CHAPTER 9

THEORY AND MATHEMATICS OF MEASUREMENT

9;1 (GENERAL CONSIDERATIONS)

In appendix (D) it is shown that when an acoustic shear wave of amplitude B_1 , propagating in a medium (a), is incident normally upon an interface between medium (a) and a second medium (b), the amplitude B_2 of the reflected shear wave component is given by the relation:

$$B_2 = B_1 \left\{ \frac{Z_{o(a)} - Z_{o(b)}}{Z_{o(a)} + Z_{o(b)}} \right\} = B_1 \, (\underline{\rho}) \qquad (D;7;27)$$

where $Z_{o(a)}$ and $Z_{o(b)}$ are the characteristic impedances of mediums a and b respectively, while $(\underline{\rho})$ is the complex reflection coefficient.

Considering now the case of a microwave ultrasonic transducer arrangement as shown in FIG.(9;1;1) , in which one end of the piezo-electric quartz crystal is brought outside of the resonant cavity, and neglecting the intrinsic acoustic attenuation of the quartz rod, it can be seen that after the initial excitation of the shear wave B_1 the cavity is periodically re-excited with amplitudes ηB_2 , ηB_3 , ηB_4 etc. Here η is meant to represent the one way electromechanical conversion of equation (D;9;10).

Now since $B_2 = B_1 \, (\underline{\rho})$, and $B_3 = B_2 \, (\underline{\rho})$, while $B_4 = B_3 \, (\underline{\rho})$ etc., it is obvious that $B_3 = B_1 \, (\underline{\rho})^2$ and $B_4 = B_1 \, (\underline{\rho})^3$ and so on, since for all practical purposes 100 % reflection occurs at the free crystal surface inside the cavity. The justification for assuming that 100 % internal reflection is achieved at the inside free surface arises from the fact that since η is so small (ie: -43 db.) negligible power is coupled out of the mechanical wave upon cavity re-excitation.

If initially the outer crystal surface is unloaded the reflection coefficient ($\underline{\rho}$) is equal to unity and so $B_1=B_2=B_3=B_4$ etc. Thus if a plot is made of the relative decrease in the amplitude of the cavity response in dbs. , against echo, upon application of a test liquid of characteristic impedance $Z_{o(b)}$, to the outer crystal surface, a straight line is obtained having a slope equal to the absolute value of ($\underline{\rho}$). Similarly plotting the relative phase shift of the response yields the phase angle associated with ($\underline{\rho}$).$=\rho\angle\phi$

The characteristic impedance of the test liquid may be expressed as :

$$Z_{o(b)} = Z_L = R_L + j\,X_L$$

while the characteristic impedance of the quartz medium becomes:

$$Z_{o(a)} = Z_c = \rho_c\, C_1 = 1.3554 \times 10^6 \text{ gram/sec. cm}^2$$

from equation (D;7;23) and page (188) of section (7;4;3).

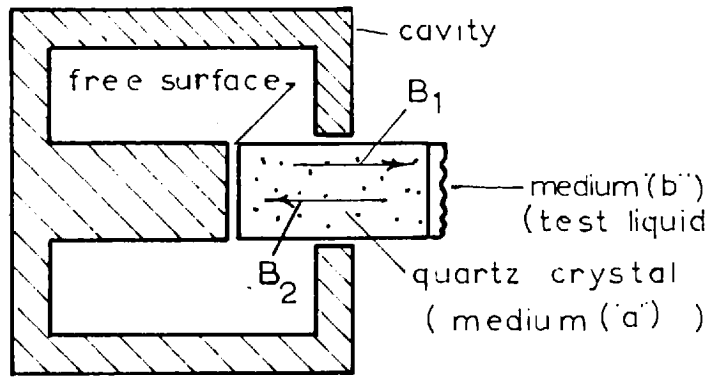

FIG.(9;1;1)

Simplified ultrasonic transducer configuration

Upon inserting the above characteristic impedance expressions into equation (D;7;27) it can be shown that:

$$R_L = Z_c\left(\frac{1-\rho^2}{1+\rho^2+2\rho\cos(\phi)}\right) \cong Z_c\left(\frac{1-\rho}{1+\rho}\right) \quad \text{when } \phi \cong 0$$

$$X_L = Z_c\left(\frac{-2\rho\sin(\phi)}{1+\rho^2+2\rho\cos(\phi)}\right) \qquad \text{gram/ sec.cm}^2$$

and so the real and imaginary parts of the test liquid impedance are known.

From the foregoing it is evident that for the simplified cavity configuration of FIG.(9;1;1) the analysis is straight forward, however in the actual cavities used the situation is more complicated in that the loaded crystal surface is also the generating surface.

It is clear from appendix (D;8) that any damping of the crystal surface results in less acoustic generation, however this change in the initial excitation level need cause no problem since it is only the slope of the decay pattern which is of importance and thus any increase or decrease in the overall excitation level is of no consequence.

As previously indicated, the amount of acoustic energy coupled out of the mechanical wave upon cavity re-excitation is negligible and so only the energy transmitted into the terminating test liquid has any noticable effect on the acoustic decay pattern .

There remains therefore only to investigate the mechanism of excitation and reflection to determine whether in fact the cavity re-excitation is proportional to (ρ) .

In appendix (D;8) it is indicated that the exact mechanism of surface excitation of these piezoelectric crystals is somewhat in doubt. The concept of an effective plane of generation located a small distance $dx/2$ inside the surface giving rise to two travelling wave components agrees well with the observation that a free surface produces twice the acoustic generation as a bonded surface, however since the phase of these two components is the same, the distance $dx/2$

must in the limit be zero. The problem therefore arises as to what mechanism should be assumed for purposes of reflection coefficient calculation.

Considering first the case where $dx/2 = 0$, which means that excitation and reflection occur at the same point, the situation is as given in FIG.(9;1;2). A shear wave of amplitude B_1 is incident normally upon the quartz-liquid interface. Since the plane of excitation is assumed to be exactly at this interface, the cavity is

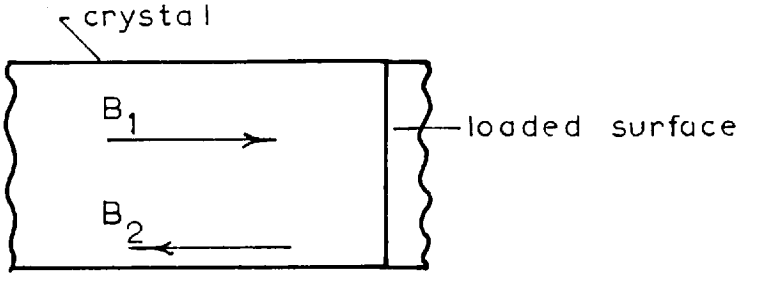

FIG. (9;1;2)

Case one, where plane of excitation and reflection are coincident.

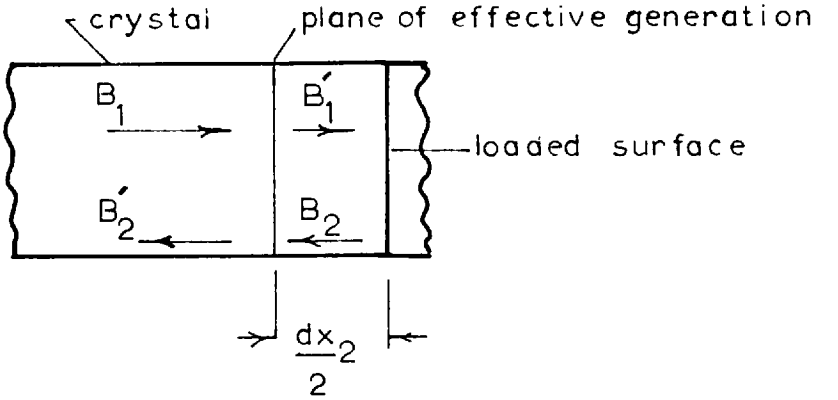

FIG. (9;1;3)

Case two, where plane of excitation is inside plane of reflection.

re-excited by an amount equal to $\eta \underline{\beta} B_1$ while the amplitude of the reflected wave is simply $(\underline{\rho})\ B_1$. Obviously the same process occurs at the other surface and so the cavity is periodically re-excited with amplitudes $2\eta B_1(\underline{\rho})$, $2\eta B_1(\underline{\rho})^2$, $2\eta B_1(\underline{\rho})^3$ . . etc., and so it can be seen that case one is equivalent to the previous open ended cavity case.

Consideration is now given to case two where, as shown in FIG.(9;1;3) the effective plane of generation is located a distance $dx_2/2$ inside the crystal surface. The incident acoustic wave of amplitude B_1 upon reaching the effective plane of generation, excites the cavity by an amount ηB_1 and then travels on to the interface where it is partially transmitted and reflected back along its original path. The amplitude of the reflected component is still $(\underline{\rho})\ B_1$ and upon crossing the effective plane of generation it again re-excites the cavity. Thus the total cavity excitation is proportional to $2\ B_1(1+(\underline{\rho})\ )$ and so it follows that the cavity is periodically re-excited with an amplitude proportional to:

$$2\eta\ B_1(1+(\underline{\rho})\ ) = \underline{C}$$

$$2\eta\ B_1(1+(\underline{\rho})\ )(\underline{\rho}) = \underline{C}\ (\underline{\rho})$$

$$2\eta\ B_1(1+(\underline{\rho})\ )(\underline{\rho})^2 = \underline{C}\ (\underline{\rho})^2$$

$$2\eta\ B_1(1+(\underline{\rho})\ )(\underline{\rho})^3 = \underline{C}\ (\underline{\rho})^3$$

Clearly the absolute value of $(\underline{\rho})$ may again be obtained by finding the slope of the cavity response plotted in dbs. against echo number. Similarly the phase angle ϕ associated with $(\underline{\rho})$ may again be determined by plotting the relative phase shift of the cavity response against echo number.

Thus it may be seen that provided actual measured quantities of attenuation and phase shift are plotted against echo number and the slope of the curves used to determine (ρ) and ϕ, no error should be introduced regardless of the exact process of excitation and reflection.

9;2 (TYPICAL MEASUREMENT)

The measured values of attenuation and phase shift for a typical measurement are shown plotted in FIG.(9;2;1 and 2).

The slope of the differential attenuation and phase shift curves give the magnitude and phase of the complex reflection coefficient as follows:

From FIG.(9;2;1) the attenuation per reflection due to the application of the test liquid is found to be $2(0.34) = 0.68$ db. It is necessary to multiply by two since the signal has to pass the attenuator twice . Similarly from FIG.(9;2;2) the phase shift per reflection introduced by the test liquid is given as $2(0.77) = 1.54^{\circ}$.

Thus:

$$- 0.68 = 20 \log (\rho)$$

and so

$$(\rho) = 10^{-0.34} = 0.9247$$

while

$$\phi = 1.54^{\circ}$$

The real and imaginary parts of the liquid shear impedance are then calculated from the equations in section (9;1)as:

$$R_L = Z_c \left(\frac{1-\rho^2}{1+\rho^2 + 2\rho\cos(\phi)} \right) = 1.355 \times 10^6 \frac{(1-0.925)}{(1+0.925)}$$

$$R_L = 53.02 \times 10^3 \text{ gram/ sec. cm}^2 \text{ (mechanical ohms).}$$

and

$$X_L = Z_c \left(\frac{-2\rho\sin(\phi)}{1+\rho^2 + 2\rho\cos(\phi)} \right) = 23.59 \times 10^6 \text{ gram/sec.cm}^2$$

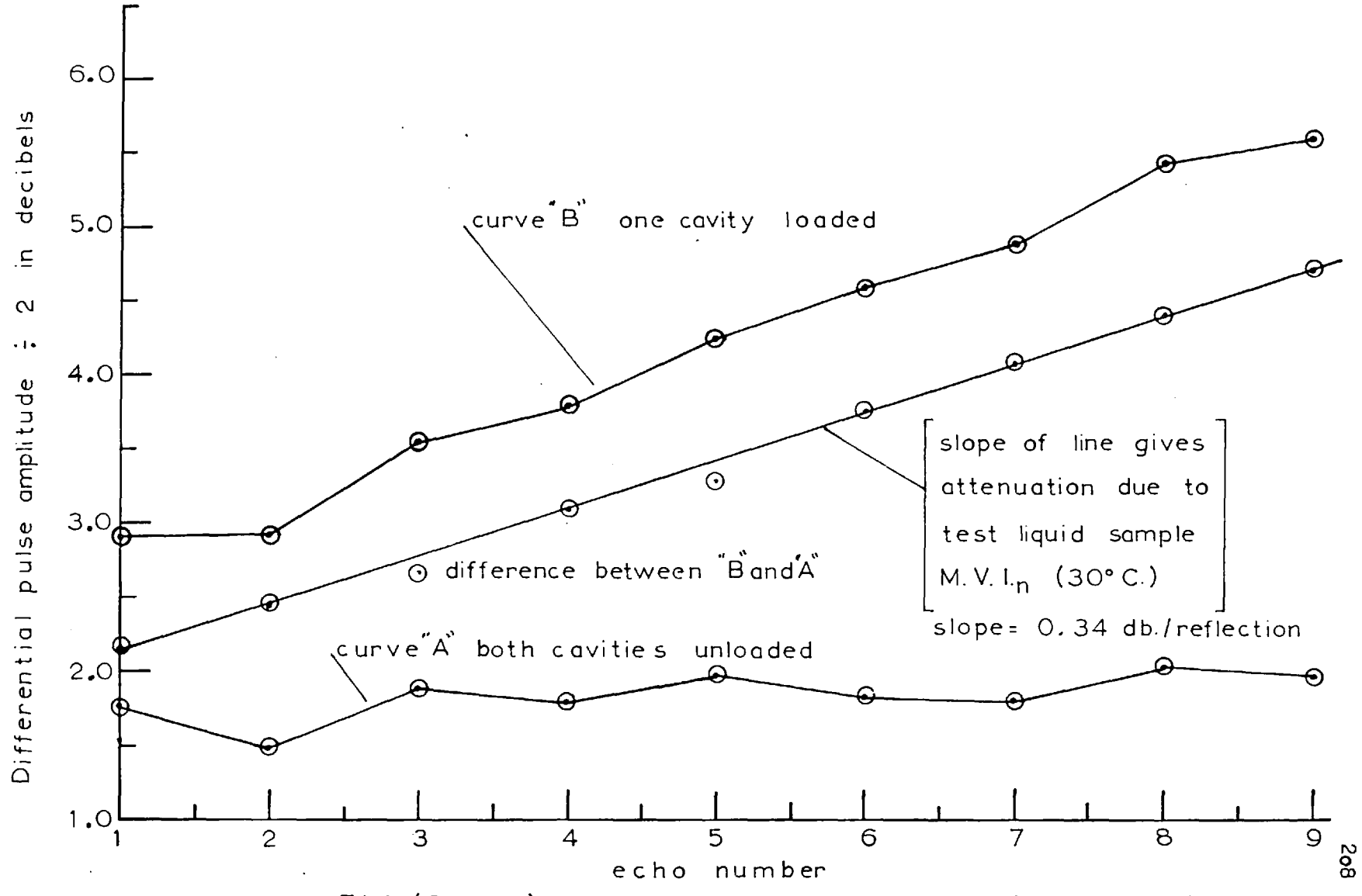

FIG. (9:2:1) **Typical differentical attenuation measurement.**

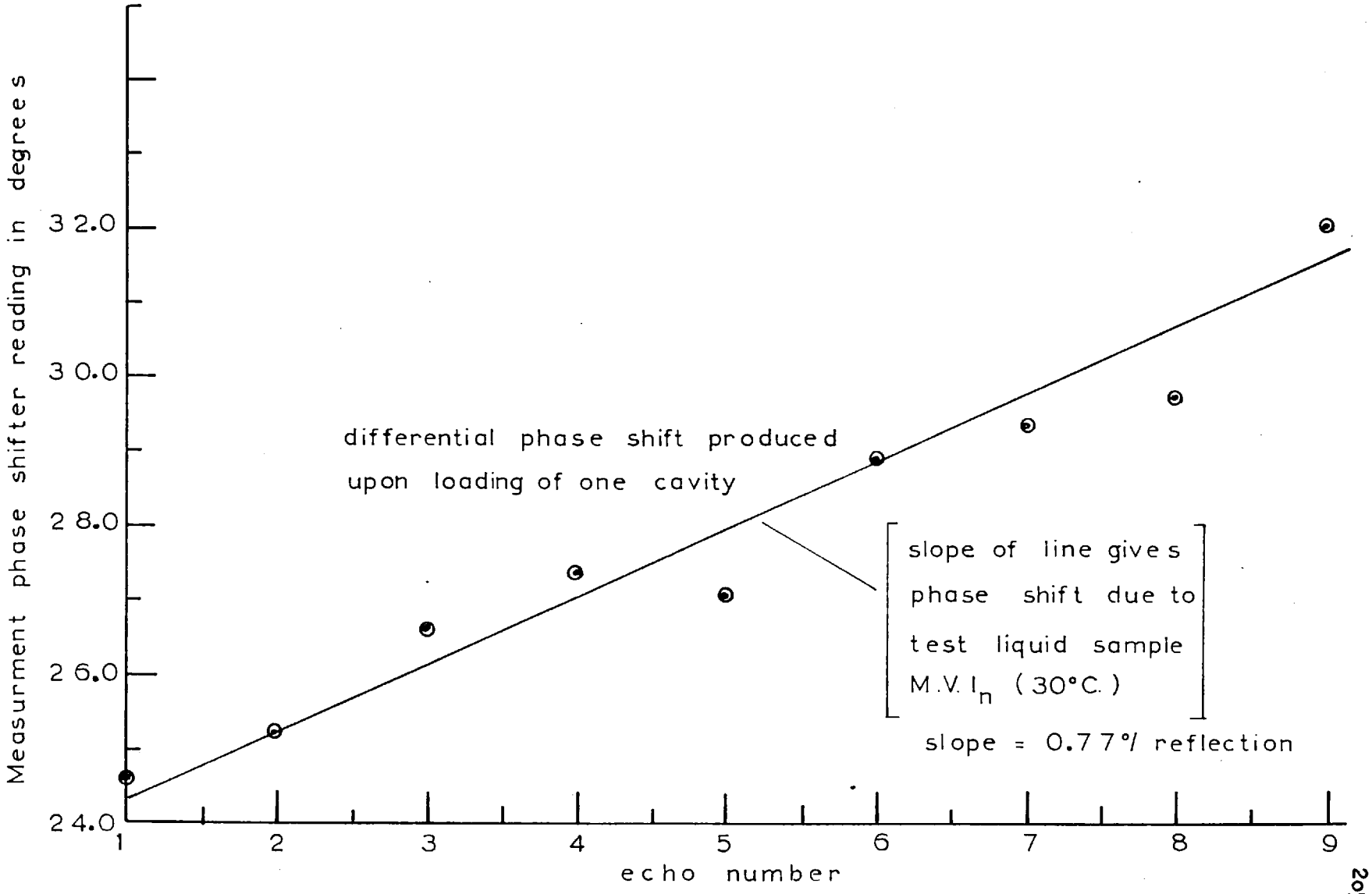

FIG (9;2;2) **Typical differential phase shift measurement.**

CHAPTER 10

SYSTEM ACCURACY CONSIDERATIONS

10;1 (GENERAL)

The various factors which could conceivably influence the system measurement accuracy are now considered, through the analysis of the four basic units of section (3;1).

10;2 (TRANSMITTER CONSIDERATIONS)

The factors pertaining to the microwave transmitter which might have had an effect on system accuracy were:

(1). Fluctuations in pulsed power output.

(2). Drift in magnetron operating frequency.

(3). Frequency pulling, ie: variation in transmitter frequency during output pulse.

(4). Output pulse shape.

Due to the bridge type construction adopted in the design of the system, fluctuations in the transmitter output pulsed power were common to both test and reference channels and so provided the quartz crystal transducers were operated in a linear range , no errors should have been introduced. The general transducer calculations of section (7;5) reveal that in fact the crystals were operated well within their linearity limit, however even if this had not been the case, error would still not be introduced unless the degree of nonlinearity in either crystal was much different.

Drift in the magnetron operating frequency was again common to both test and reference cavities and thus provided the resonant cavities had the same Q , no error should have been present. The quartz crystal calculations of section (7;4;3) indicate that the velocity of acoustic propagation within the quartz crystal was independent of frequency and consequently no trouble should have been experienced from this quarter.

Obviously magnetron frequency pulling may be regarded in the same manner as operating frequency drift and so should have negligible effect on system performance.

Since the system relied on pulse cancellation for its operation any factor which effected the degree to which such cancellation could be resolved was bound to strongly influence measurement accuracy. If both test and reference crystals had been perfectly identical in their frequency response the particular shape of the transmitter pulse would have been of no consequence. However since in practice this condition could not be achieved, it was found that the trailing and leading edges of the cavity echoes could not be cancelled and only the flat center portion of the pulses could be utilised in the measurement process. Nevertheless excellent pulse cancellation resolution was achieved provided the R.F. pulse had a very flat top. Thus it was necessary that the magnetron output pulse be flat topped, and this condition , as is explained in section (4;6) , was in fact realised.

10;3 (MICROWAVE BRIDGE CONSIDERATIONS)

There are two types of imperfections normally encountered in magic T's these being impedance mismatch looking into one or more of the bridge arms, and T asymmetry.

The first of the above two imperfections does not normally cause any trouble since it can be corrected for by the use of a stub tuner on arms 3 and 4 of the four port junction, (with reference to FIG.(5;2;1) . T asymmetry , resulting from nonuniformity of construction or slight misplacement of the post,used to match the H plane arms , cannot be completely corrected for by a stub tuner. This asymmetry results in unequal power division between arm 1 and 2, from arm number 3 as well as between 3 and 4 , from arm 2 , and between 3 and 4 from number 1. Obviously asymmetry which effects power division between the side arms will lead to a false indication of bridge balance, however since the technique of measurement involved

cancellation of signals before and after a specific occurrence the effect of unequal power division between the junction arms was of no consequence. This can be more fully appreciated by considering that the bridge was merely used to compare the relative amplitude and phase change to two signals and so the particular amplitude of either of the signals was unimportant since only the change was of interest.

Thus it is evident that slight imperfections in the bridge T did not restrict the accuracy of measurement.

The only requirement imposed on the bridge system as a whole was that there be no undue variation in match in either the test or reference channel during a particular pulse cancellation sequence. This condition thus demanded that the attenuators and phase shifters utilised in the measurement be of a high quality . In order to be able to achieve the desired accuracy of measurement of + or - 0.01 db. of relative attenuation change the maximum variation in V.S.W.R. tolerable in either channel was 0.09. As there were two elements which had to be varied during a measurement, the maximum tolerable variation in their respective V.S.W.R 's was therefore 0.05 , since for certain unfavourable phase conditions the individual V.S.W.R 's multiply.

10;4 (RECEIVER SYSTEM CONSIDERATIONS)

Since the receiver system was used mainly as a null detector in the measurement sequence any drift or instability in the unit presented no limitation on system accuracy. The only requirement of the receiver unit was that it have adequate bandwidth and sensitivity. It was found that a bandwidth of at least 20 Mcs. was required to achieve the desired pulse cancellation resolution . Such a wide bandwidth was very difficult to obtain due to the relatively narrow bandwidth of the waveguide mixer mounts and intermediate frequency amplifiers.

10;5 (MICROWAVE ULTRASONIC TRANSDUCERS)

The three main items associated with the ultrasonic transducers which could have influenced the system accuracy were:

(1). Resonant Cavities.

(2). Quartz crystals.

(3). Test liquid.

10;5;1 (RESONANT CAVITY CONSIDERATIONS)

The resonant cavity sources of possible error were:

(1). Too high a cavity Q.

(2). Resonant frequency drift.

(3). Change in Q during measurement sequence.

Clearly if the cavity Q was too high the R.F. pulse shape would be seriously distorted and this would in turn make pulse cancellation resolution difficult, resulting in loss of measurement accuracy. In section (F;1;2) it was found that the maximum loaded Q permissible for good pulse response is 273 and since in practice the cavity Q's obtained were less than this value no difficulty should have been experienced.

Slight resonant frequency drift of the cavities resulting from temperature variations of the cavity body should not have had any significant effect on the system accuracy since both units were affected to the same degree. Similarly any slight R.F. heating in the cavities tended to cancell out as well. The actual R.F. heating energy presented to each cavity may be determined from the product of the mean R.F. power level incident on the cavities and the time factor of a test sequence. Thus:

Mean incident R.F. power = pulsed power x pulse length x pulse repetition frequency.

and for typical operating conditions of 20 kilowatts this becomes:

Mean incident R.F. power = 7×10^{-3} watts/ cycle/sec.

Now assuming a pulse cancellation sequence of 2 minutes and a system pulse repetition frequency of 15 cycles/ sec., the cavity R.F. heating energy is:

R.F. heating energy = 2.998 gram-calories .

Considering the case where no heat is lost to the surroundings it is found that for a cavity mass of one pound of brass, having a specific heat of 0.0743 calories/ gram/ ^{o}C., the temperature rise of the cavity at the end of the test sequence is:

$$T_{rise.} = \frac{2.998}{2.2 \times 10^{3} \times 0.743} = 1.83477 \quad {}^{o}C. \times 10^{-2}$$

Since in actual fact the cavity mass was many times that assumed and also since the outer surface of the cavity was held at a constant temperature, as a result of immersion in the thermostating bath, it may be safely concluded that resonant frequency drifts of the cavities due to R.F. heating of the cavity body were negligible.

Clearly a change in cavity Q during an actual pulse cancellation sequence, lasting some two minutes would seriously upset the measurement, however there is no reason to suspect that such a phenomenon could occur. Variation in cavity Q from one test run to another or from one cancellation sequence to another, which may occur when the test liquid is inserted into the cavity, should have had no significant effect on the measurement accuracy as a result of the low electro-mechanical conversion efficiency. This aspect had the effect of rendering the acoustic wave within the crystal almost completely insensitive to any exterior electrical condition.

10;5;2 (QUARTZ CRYSTAL CONSIDERATIONS)

The major sources of possible error associated with the piezo-electric quartz crystals were as follows:

(1). Dissimilar frequency response of both test and reference crystals.

(2). Strains set up in crystal by support and liquid application mechanism.

(3). Nonunifrom acoustic decay pattern.

(4). Temperature differential between crystal and test liquid sample.

(5). Acoustic heating effects in crystal

(6). R.F. heating effects in crystal.

As previously mentioned, the dissimilar response of the two crystals was a limitation only in that it necessitated that the transmitter pulse shape be much more flat topped than would otherwise have been the case.

It has been found that even very slight pressure on the crystal results in a serious deterioration of the acoustic decay pattern and hence it was necessary to develop special holders which introduced the very minimum of strain to the crystal. The situation was very much improved in the radial cavity design where the crystal diameter was much larger than the excited region beneath the posts, since any edge strains had much less effect on the central region.

It was pointless to attempt measurements with crystals which did not have a uniform acoustic decay pattern. This was so because a nonuniform or nonexponential decay pattern indicated that there was wave interference within the crystal itself and hence application of a liquid to the crystal surface altered the degree of this interference as well as absorbed some of the acoustic energy. The result observed therefore upon test liquid application was a combination of both liquid and crystal effects and consequently the measurement was meaningless.

Since strains are easily generated within a crystal due to a nonuniform temperature distribution , it was necessary to allow a period

of some two hours to elapse before commencing the recancellation sequence, so that equilibrium could be established after application of the test liquid.

The R.F. heating power present in the quartz crystal may be found from the product of the power flow through the crystal and its loss tangent. Thus:

$$\text{R.F. crystal heating power} = \text{Mean cavity power} \times \eta_{e(gap)} \times \text{loss tangent.}$$

The loss tangent for quartz is known to be 1×10^{-4} and so for a pulsed power input of 2×10^{4} watts the crystal R.F. heating is:

$$\text{R.F. crystal heating power} = 6.685 \times 10^{-7} \text{ watts/ cycle/ sec.}$$

Now assuming a cavity Q_{un} of 200 the acoustic heating power in the crystal may be obtained from equation (D;9;12).

$$\text{Acoustic crystal heating power} = \text{Mean cavity power} \times \eta_{e(gap)} \times \eta$$
$$= 3.1606 \times 10^{-7} \text{ watts/cycle/sec.}$$

and so the total crystal heating power is:

$$\text{Total crystal heating power} = 9.845 \times 10^{-7} \text{ watts/cycle/sec.}$$

Now for the two minute cancellation sequence at a system repetition frequency of 15 cycles per second , the total crystal heating energy was:

$$\text{Total crystal heating energy} = 4.2320 \times 10^{-4} \text{ gram-calories.}$$

It is now possible to calculate the temperature rise of the crystal from its mass and specific heat. Thus:

$$\text{Crystal temperature rise} = 6.7241 \times 10^{-4} \ ^{o}C.$$

Having calculated the temperature rise of the crystal it is a simple matter to determine the phase shift resulting from such a temperature change by considering the expansion coefficients for the BC cut crystal given in FIG.(7;4;2;2) on page (187). The only dimensional change of interest is in the x_2' or y direction and so the expansion coefficient to be used is:

$$\alpha'_{22} = 9.56 \times 10^{-6} / {}^{o}C.$$

The axial expansion for the three millimeter thick crystal is found to be $= 1.9284 \times 10^{-9}$ cms. and so the phase shift due to the thermal expansion of the quartz disk was:

$$\text{Phase shift} = 4.0838 \times 10^{-3} \text{ degrees}$$

which is well within the imposed accuracy limit of 0.01 degrees.

It is now necessary to consider the temperature variation of the crystal elastic constants to determine what phase shift arises from a change in the velocity of propagation. The velocity of propagation for the pure shear mode in this BC cut crystal is from section (7;4;3):

$$C_1 = (h_{11} / \rho)^{\frac{1}{2}}$$

The elastic-temperature coefficient applicable to this situation is determined from FIG.(7;4;1;2) and equation (D;2;14) assuming that the elastic-temperature coefficients for the rotated cuts have the same dependence as the rotated elastic constants . Thus

$$\tau_{h_{11}} = \tau_{c_{66}} m^2 + \tau_{c_{55}} n^2 + \tau_{c_{56}} 2mn$$

$$= 3.9 \times 10^{-6} {}^{o}C.$$

Now the velocity equation may be written as:

$$C_1 = \left(\frac{h_{11}}{\rho} \left(1 + \tau_{h_{11}} (\theta - \theta_o) \right) \right)^{1/2}$$

where $\tau_{h_{11}}$ is the temperature coefficient of h_{11} and $(\theta - \theta_o)$ is

the crystal temperature change.

Taking the differential of the foregoing equation with respect to temperature gives:

$$\frac{dC_1}{d(\theta - \theta_o)} = \tfrac{1}{2}\left\{ \frac{h_{11}}{\rho}\left(1 + \gamma_{h_{11}}(\theta - \theta_o) \right) \right\}^{-\frac{1}{2}} \frac{h_{11}}{\rho}\gamma_{h_{11}}$$

and so dC_1 is the change in velocity of propagation due to the crystal temperature change $(\theta - \theta_o)$

The fractional change in propagation velocity is then:

$$\frac{dC_1}{C_1} = \frac{\gamma_{h_{11}}\, d(\theta - \theta_o)}{2(1 + \gamma_{h_{11}}(\theta - \theta_o))}$$

and therefore the fractional change in sonic wavelength is given by the same expression. Thus:

$$\Delta\lambda_s/\lambda_s = 1.31120 \times 10^{-9}$$

Finally the phase shift resulting from the temperature change may be found from the expression:

$$\text{Phase shift} = 360\,(\Delta\lambda_s/\lambda_s) \times \text{number of wavelengths in crystal}$$

$$= 360\,(\Delta\lambda_s/\lambda_s)\; d/\lambda_s = 8.3299 \times 10^{-4} \text{ degrees.}$$

Obviously therefore any phase changes due to heating of the quartz crystal were much too small to be of any significance and as such did not effect the system accuracy.

10;5;3 (TEST LIQUID CONSIDERATIONS)

Since the test liquid sample was injected inside the cavity both acoustic and dielectric heating effects must be considered in determining the temperature rise of the test sample.

The sonic energy transmitted into the test liquid sample was normally very small being of the order of less than 20 % corresponding to a reflection coefficient of approximately 0.9. Assuming a 20 % transmission the acoustic heating power in the liquid is simply:

Acoustic liquid heating power = acoustic crystal heating power

x 0.20

$= 6.3212 \times 10^{-8}$ watts/cycle/sec.

Now assuming a liquid film depth of 5×10^{-3} cms. and an area the same as the crystal, with a specific heat of 0.8 and a density of unity, the temperature rise of the test sample for two minutes of operation at 15 cycles per second is:

Temperature rise of test liquid due to acoustic heating = 1.4964×10^{-3} °C.

Clearly the acoustic heating in the test liquid may be neglected since in practice the liquid film was much thicker than that assumed and in addition heat was conducted away by the crystal and crystal holder arrangement as well as by the liquid application mechanism.

Considering now the dielectric heating of the test sample it is possible to determine the ratio of the power loss in the liquid film to that lost in the quartz crystal with the aid of FIG.(10;5;3;1), which is meant to represent a situation where a power P_{in} is flowing through two dielectrics , one representing the quartz crystal and the other the liquid film. Each dielectric is characterised by a complex dielectric to signify loss.

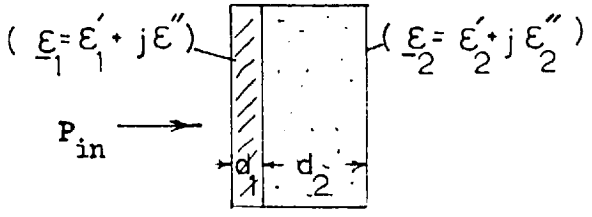

FIG.(10;5;3;1)

The power lost in region one may be obtained by considering the power flow through the section. Thus:

$$P_{L\,(1)} = \frac{P_{in}}{Z_T} \quad Z_1 \tan(\delta_1)$$

while for region two:

$$P_{L(2)} = \frac{P_{in}}{Z_T} \quad Z_2 \tan(\delta_2)$$

where Z_T is the total impedance of the combined liquid film and crystal configuration and is approximately equal to:

$$Z_T = 1 \,/\, j\omega C = \frac{d_1 \varepsilon'_2 + d_2 \varepsilon'_1}{j\omega \varepsilon'_1 \varepsilon'_2}$$

while Z_1 is the impedance of the film and is given by :

$$Z_1 = 1/\, j\omega C_{(1)} \cong \frac{d_1}{j \varepsilon'_1 \omega} \qquad \text{since } \varepsilon''_1 \ll \varepsilon'_1$$

similarly $$Z_2 = 1/\, j\ C_{(2)} = \frac{d_2}{j \varepsilon'_2 \omega} \qquad \text{since } \varepsilon''_2 \ll \varepsilon'_2$$

Thus: $$\frac{P_{L(1)}}{P_{L(2)}} \cong \frac{\tan(\delta_1)\ d_1 \varepsilon'_2}{\tan(\delta_2)\ d_2 \varepsilon'_1}$$

where $\tan(\delta_1) = \varepsilon''_1 / \varepsilon'_1$ and $\tan(\delta_2) = \varepsilon''_2 / \varepsilon'_2$

For a typical test liquid having a loss tangent of 1×10^{-3} and film thickness of 5×10^{-3} cms. , the above loss ratio becomes:

$$P_{L(1)} \,/\, P_{L(2)} = 0.2583$$

and so it is seen that the heating power in the liquid film is much less than in the quartz crystal.

Finally the temperature rise of the liquid may be determined, and therefore assuming the same power input to the cavity the temperature rise is = 1.9329×10^{-4} °C., which is negligible.

From the foregoing calculations it can be seen that the heating effects in the ultrasonic transducers are extremely small and therefore should not restrict the system accuracy . Moreover since both test and reference cavities were identical all the heating effects, other than that of the test liquid, were common to both channels and therefore tended to cancel .

10;6 (DISCUSSION)

From the previous analysis of the various system components it would appear that from the electronic and microwave side of the apparatus a relative attenuation and phase shift measurement accuracy of $\pm$ 0.01 db. and $\pm$ 0.01 ° should have been achieved and this in fact was experimentally verified. When the acoustic side of the system was included the pulse cancellation resolution and reset accuracy was found to be approximately $\pm$ 0.02 db. and $\pm$ 0.05 ° for the first six or seven echoes having good signal to noise ratio. Test to test reproducibility of this order was also obtained provided two conditions were satisfied. These conditions were firstly, that the waveguide system temperature remain constant during the pulse cancellation procedure and secondly that the magnetron operating frequency remain constant over the whole of the measurement sequence. The first condition was to be expected since changes in waveguide temperature result in changes in the electrical length of the test and reference channels thereby introducing phase shift into the bridge system. . The second oondition, which is difficult to achieve, was believed to stem from two factors the first being unequal acoustic path lengths in the two quartz crystals and secondly , imperfections in the quartz

transducer surfaces and interior.

The test and reference crystals used in the system were found to differ in physical length by approximately 25 sonic wavelengths and consequently any slight variation in the system operating wavelength was amplified 25 times at each transit through the crystal thereby introducing a progressively increasing phase shift error with increasing echo number. It should be possible to completely eliminate this type of error through the utilisation of two crystals having the same physical length.

The second factor,which was believed to be responsible for the frequency dependence of the system repeatability, was felt to arise from the condition that the crystal surfaces or bulk material were not completely uniform such that upon incidence at a generating surface , the acoustic wave did not produce a wave front of uniform phase over the surface. Consequently a slight variation in the operating wave length , resulting from frequency drift of the magnetron, produced a variation in the phase distribution of the acoustic wave over the crystal surface and thereby altered the effective phase and amplitude of the cavity re-excitation. This particular occurrence was found especially troublesome in that to eliminate the possible introduction of error it was necessary to perform the two cancellation sequences , separated in time by approximately two hours, at the same frequency $\pm$ approximately 10 kc/s.

Since it was not possible to measure or reset the magnetron frequency to this accuracy an attempt was made to stabilise the temperature and driving conditions of the magnetron so that its operating frequency would remain constant for the required two hour period. Only limited success was achieved in this line however, the main problem being the difficulty in stabilising the high powered modulator.

CHAPTER 11

RESULTS

The actual liquid shear impedance measurement accuracy obtained with this experimental microwave ultrasonic system is now considered.

Test measurements were performed on four selected liquids , the mechanical behaviour of which was well known. These selected test liquids were , M.V.I. , H.V.I. , L.V.I. and M.S.(200/1000) oils, the first three having been completely investigated by J.Barlow,(114) and the last by G. Harrison ,(115)

Since the shear mechanical properties of these liquids were measured in the frequency range of 10 Kc/s.to 80 Mc/s. it was necessary to invoke the reduction principle technique in order to obtain reference data for the 3000 Mc/s. measurements.

The original experimental universal curves obtained by Barlow and Harrison, for the four test liquids, are given in FIG.(11;1 to 4) along with the experimental values of the real and imaginary components of the liquid shear impedance measured with this 3000 Mc/s. system. The actual numerical values of the measured and reference test liquid shear impedances are given in FIG.(11;5) along with the percentage discrepancy and reproducibility.

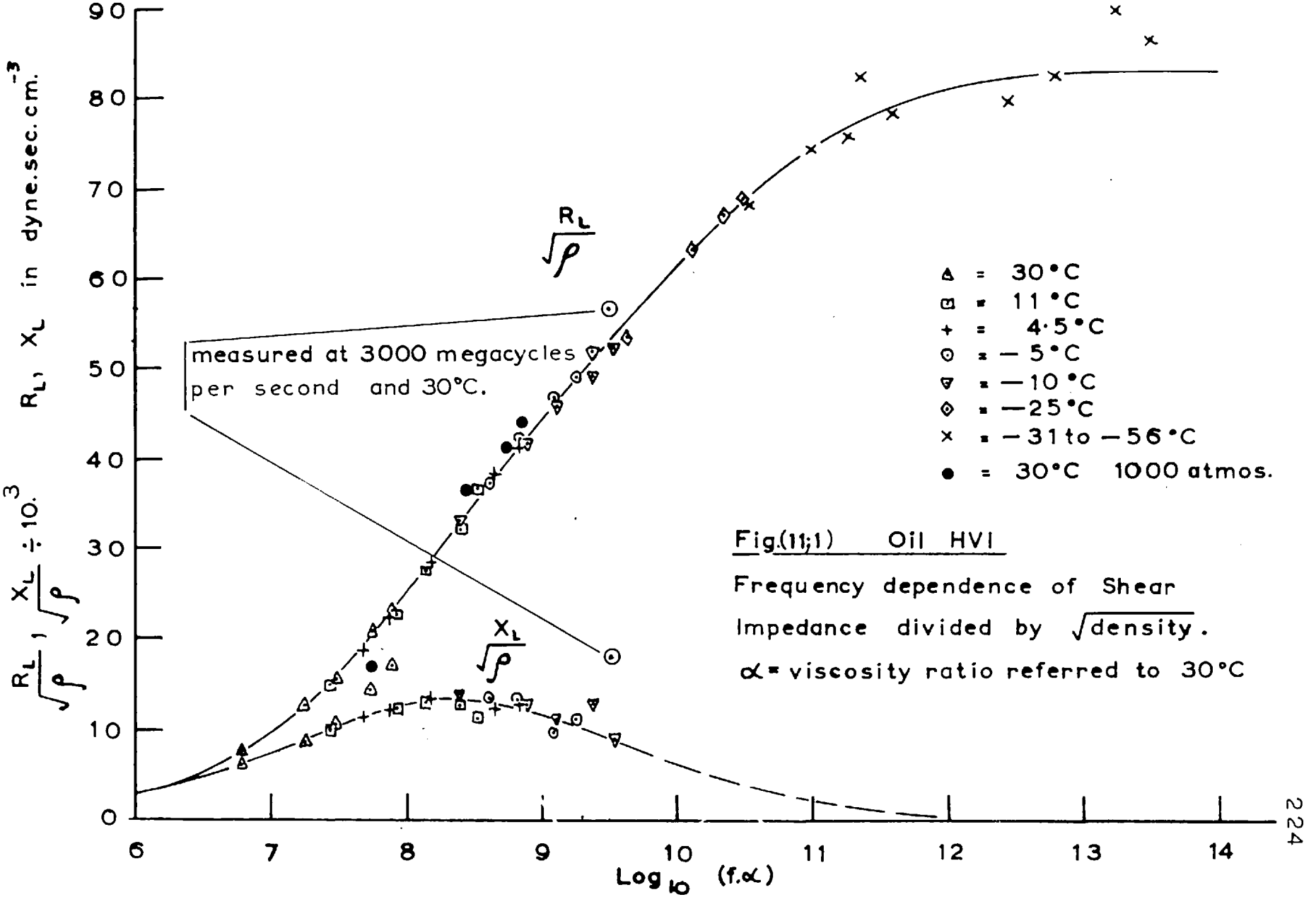

Fig.(11;1) Oil HVI

Frequency dependence of Shear Impedance divided by $\sqrt{\text{density}}$.

α = viscosity ratio referred to 30°C

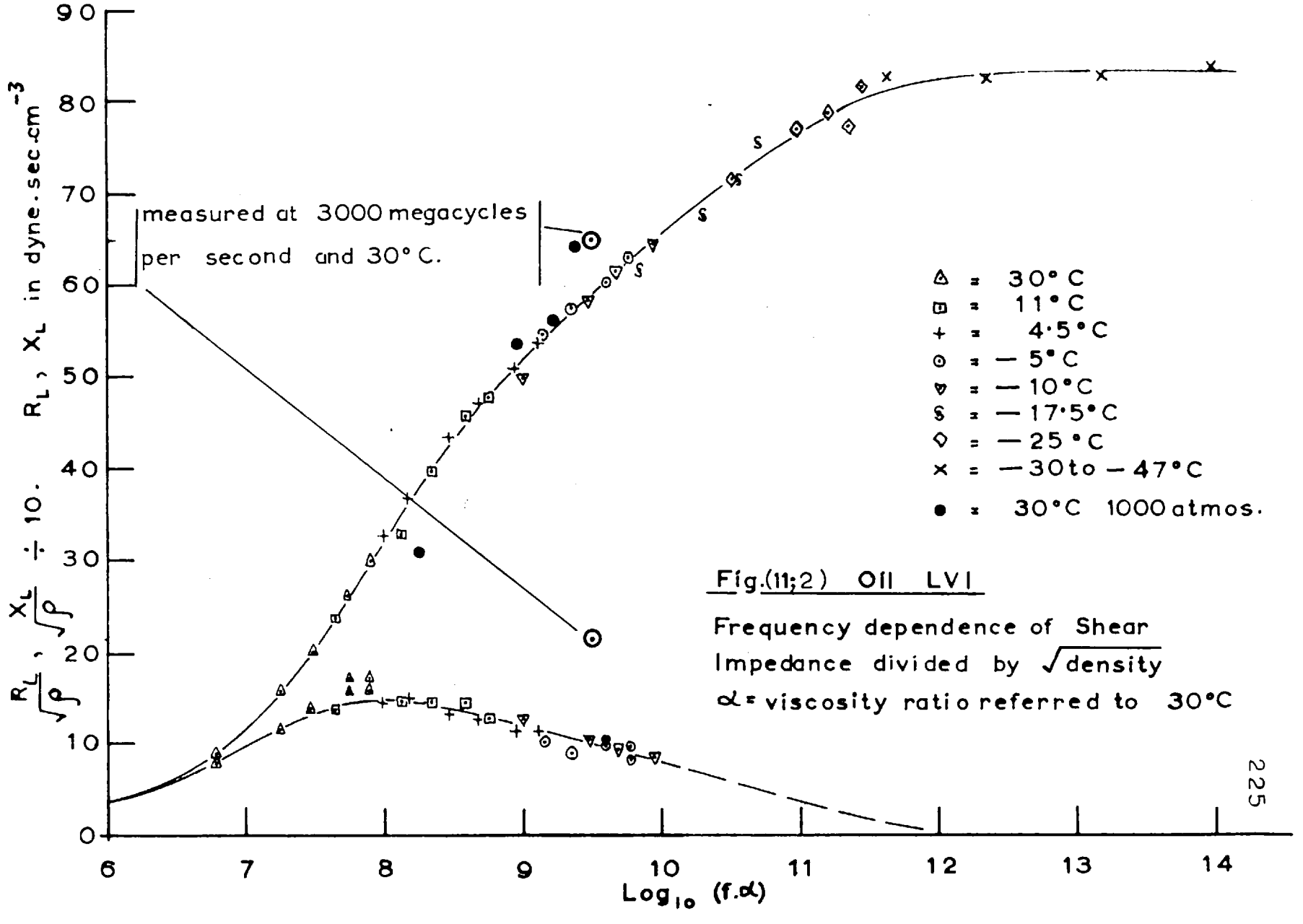

Fig.(11;2) Oil LVI

Frequency dependence of Shear Impedance divided by $\sqrt{\text{density}}$

α = viscosity ratio referred to 30°C

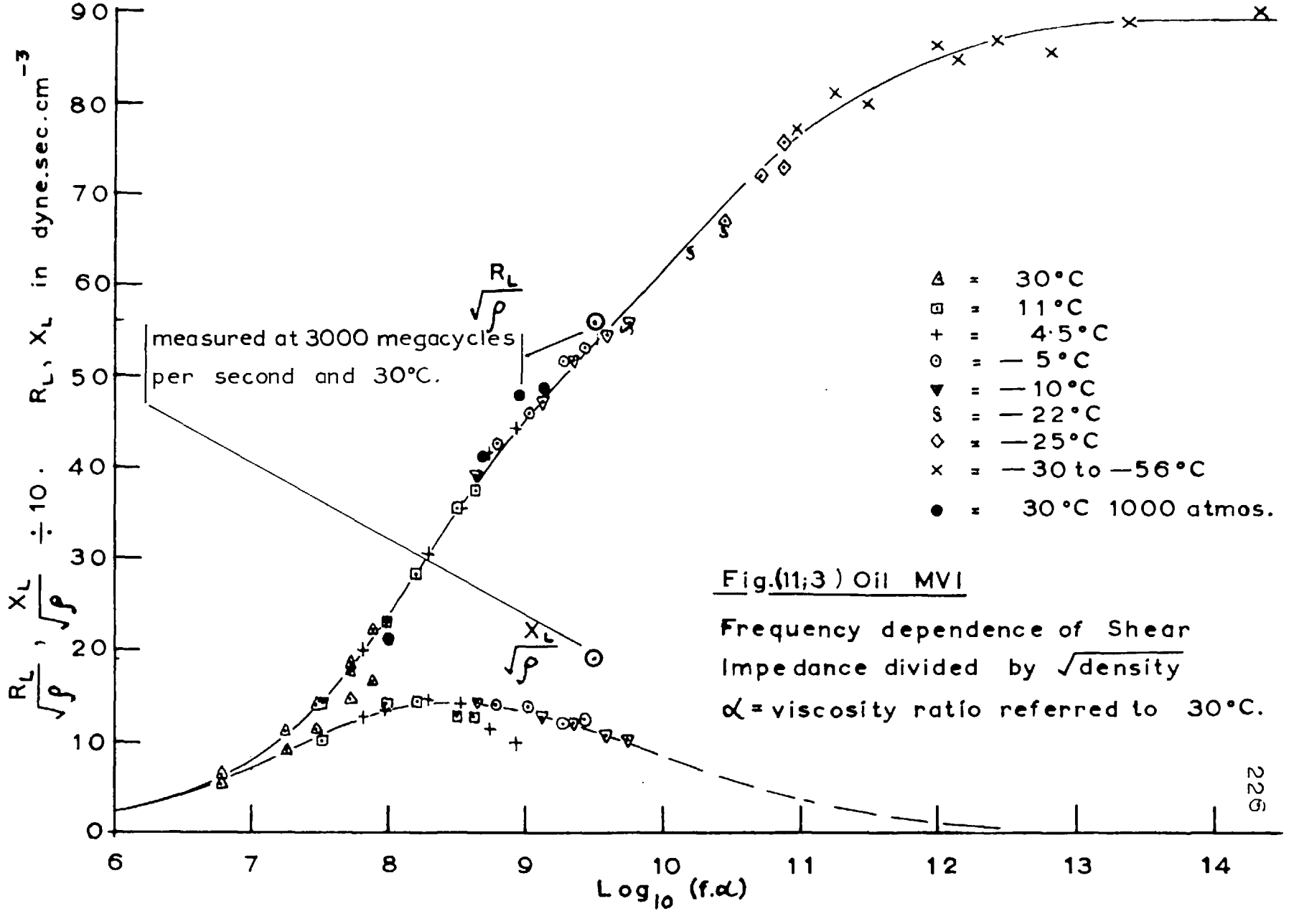

Fig.(11;3) Oil MVI

Frequency dependence of Shear Impedance divided by $\sqrt{\text{density}}$

α = viscosity ratio referred to 30°C.

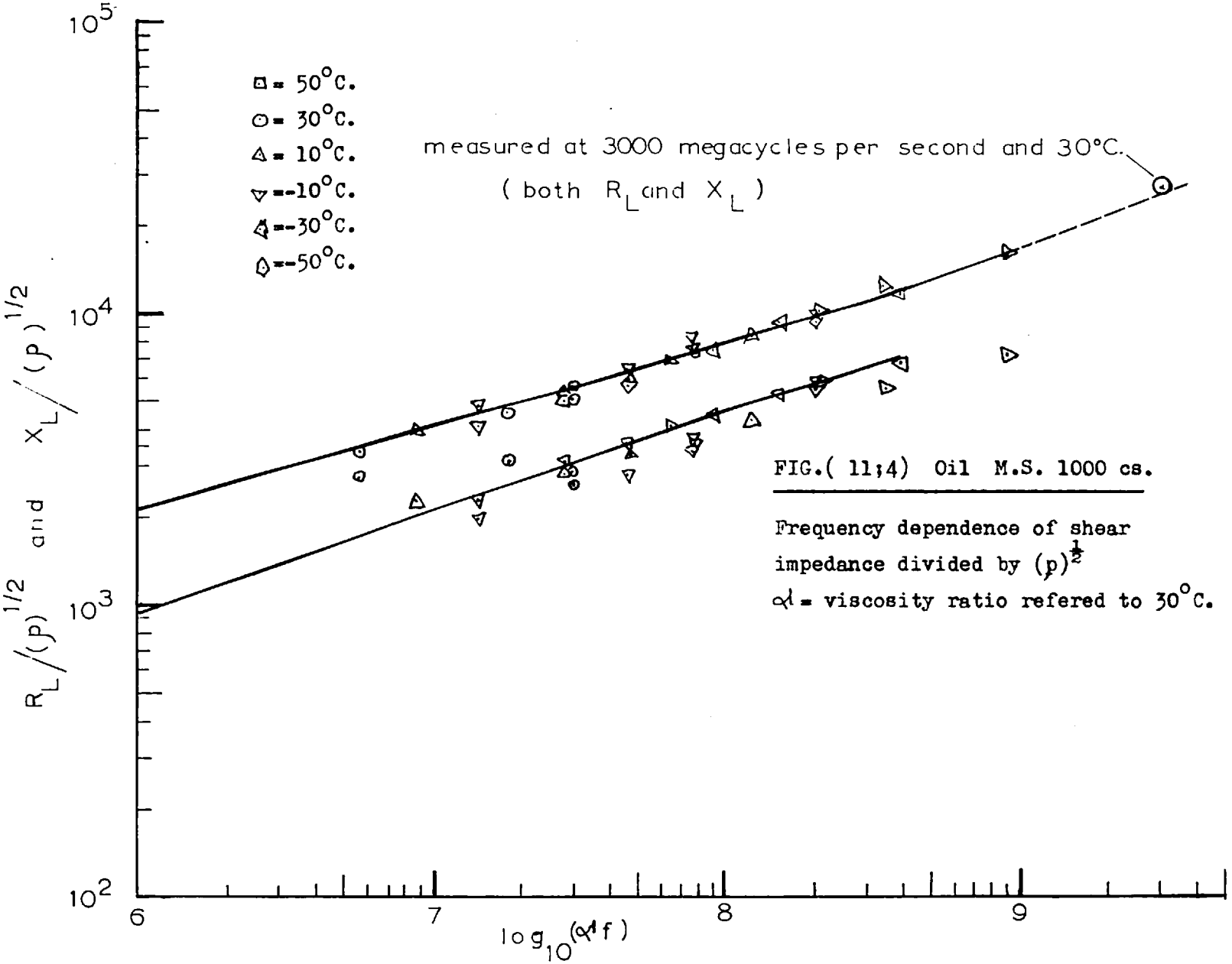

FIG.(11;4) Oil M.S. 1000 cs.

Frequency dependence of shear impedance divided by $(p)^{\frac{1}{2}}$

α = viscosity ratio refered to 30°C.

11;1 (NUMERICAL RESULTS)

Researcher	Parameter	M.S./200	H.V.I.	M.V.I.	L.V.I.
Barlow	density (grams/cm^3) at 30°C.		0.874	0.895	0.932
"	viscosity (poise)		3.54	2.08	4.52
"	$R_L \times 10^3 \left(\frac{\text{dynes.sec.}}{\text{cm.}^3}\right)$		49.6	50.6	57.3
"	$X_L \times 10^3 \left(\frac{\text{dynes.sec.}}{\text{cm.}^3}\right)$		8.6	10.4	9.7
Harrison	density (grams/cm^3) at 30°C.	0.963			
"	viscosity (poise)	8.96			
"	$R_L \times 10^3 \left(\frac{\text{dynes.sec.}}{\text{cm}^3}\right)$	23.85			
"	$X_L \times 10^3 \left(\frac{\text{dynes.sec.}}{\text{cm.}^3}\right)$	12.38			
Author	$R_L \times 10^3 \left(\frac{\text{dynes.sec.}}{\text{cm.}^3}\right)$	25.0	53.0	53.5	62.4
"	$X_L \times 10^3 \left(\frac{\text{dynes.sec.}}{\text{cm.}^3}\right)$	25.0	17.1	18.3	20.8
"	reproducibility in R_L	± 5 %	± 3.3 %	± 2 %	± 2.5 %
"	reproducibility in X_L	± 5 %	± 10 %	± 5 %	± 10 %
"	discrepancy in R_L	+ 6 %	+ 8 %	+ 5 %	+ 8 %
"	discrepancy in X_L	+ 102 %	+ 99 %	+ 81 %	+ 115 %

FIG.(11; 5)

As can be seen from the curves in FIG.(11;1 to 4) , reasonable agreement was achieved between the real part of the liquid shear impedance measured at 3000 Mc/s. and the univeral curves of the four test liquids. This close agreement would seem to indicate ,firstly that the system developed was capable of producing sensible results, and secondly that the reduction principle was valid up to this frequency range , for these particular liquids.

The results obtained for the imaginary liquid impedance components were however not nearly so encouraging since it was found that in each case the measured quantities were approximately twice too large. It was not possible to account for this factor of 2 in the theory of the measurement technique or in the calibration of the measurement phase shifter, although both aspects were carefully reconsidered. Nevertheless despite the inability to find a satisfactory explanation for the error of approximately one hundred percent in the phase measurement, it was felt that the discrepany was too consistent to be a coincidence.

The numerical values of FIG.(11;5) indicate that there was a five to eight percent positive discrepancy in the real part of the liquid impedance for all four of the reference liquids measured. The value and sign of this discrepancy however was found to be consistent with that obtained from similar measurements performed on the same oils but at 1000 Mc/s.(112).

It is possible to explain this small discrepancy by assuming that the quartz crystals used in both the 1000 and 3000 Mc/s experimental systems, are not exactly rotated Y cuts. It has been shown,(113) , that if the cut of the crystal is such that the Y' or wave normal axis departs from the YZ crystallographic plane by only one minute, an error of several percent is introduced into the shear impedance measurement. In addition it is found that the sign of this systematic error is always positive.

Although itis preferrable to be able to obtain the imaginary component of the liquid shear mechanical impedance,it is not absolutely essential since at this frequency level most of the liquids measured are found to be well into the relaxation region and consequently the imaginary part of the impedance is small.

11;2 (DISCUSSION)

From the tabulated results of FIG.(11;5) , it is evident that the developed microwave ultrasonic system was capable of a relatively high accuracy of measurement and reproducibility with respect to the real part of the liquid shear impedance. The percentage reproducibility figures given were the extreme values obtained under wide variations in ambient room temperature and without stabilisation of the high powered modulator power supply .

It was observed that whenever the temperature variations of the waveguide system were small,during the measurement sequence, the measurement reproducibility increased accordingly such that typical values of $\pm$ 1.5 to 2 % in R_L reproducibility were readily achieved.

Reasonable consistency in the phase was however much more difficult to achieve in that it was seldom that a straight line plot of relative phase shift versus echo number was obtained. Consequently it was usually necessary to adopt a best fit curve approach , which correspondingly introduced inconsistency.

As explained in section(10;6) this phase measurement inconsistency was believed to arise from changes in the system operating frequency. Theoretically small changes in the system operating frequency should not have introduced any significant error into the measurement provided that the two piezoelectric quartz crystals were perfect and identical, however since in practice this condition could not be completely attained it was to be expected that the system phase measurement accuracy would exhibit some frequency dependence.

It should be possible to completely eliminate the phase measurement error arising from the dissimilarity of approximately 25 acoustic wavelengths between the lengths of the test and reference quartz transducer crystals by obtaining two crystals which were processed and polished simultaneously . It can easily be shown that with the two crystals used in the system a change in the transmitter operating frequency during a pulse cancellation sequence of only 1 part in 10^5 introduced an error in the phase measurement of 10 % on the first echo, 20 % on the second, 30 % on the third and so forth.

It should also be possible to obtain crystals in which the variation in their acoustic decay pattern with frequency is negligible. This could most probably be accomplished by applying the hydrofluoric acid etch and repolish technique described in section(7;4;4) to a particular crystal several times , so as to finally obtain a crystal having high quality surfaces.

Alternatively it should be possible to substantially increase the phase measurement reproducibility and accuracy by stabilising the magnetron frequency over the time period of a particular measurement. The main difficulty in the stabilisation of the magnetron frequency is that very slight changes in the driving voltage applied to the magnetron result in relatively large variations in its operating frequency. For example it may be shown that a change in the mains supply voltage to the modulator of only 0.26 % results in a change in magnetron operating frequency of 1 part in 10^5 which , as indicated above, can result in a large accumulative phase measurement error of approximately 100 % on the tenth echo.

Another possible solution to the above problem is to use a tuneable magnetron as transmitter and to reset the operating frequency prior to each pulse cancellation sequence, provided of course that a magnetron frequency monitor having adequate resolution could be devised.

Another technique which would probably increase the system measurement accuracy is to arrange that the test liquid sample is introduced into both cavities simultaneously but that only one of the crystals has its faces actually loaded. This could be accomplished by placing a thin P.T.F.E. sheath around one of the crystals such that the test liquid did not wet its surfaces. This particular technique would have the advantage that any slight field disturbance, caused by the introduction of the test liquid,would be common to both test and reference cavities and hence the effects would tend to cancel . In addition since the Q of both cavities would be effected by the same amount pulse cancellation would be better. This last aspect is of appreciable importance when very lossy liquids are to be measured.

Within the last two years several reports have been published concerning the development of a highly efficient , high frequency electromechanical transducer, utilising a single YIG,(yttrium-iron garnet) crystal. (1o6).

This material has been found to be some 80 db. more efficient than the piezoelectric quartz crystals used in this system. Consequently incorporation of these transducers into this present experimental system would eliminate the need for a high powered transmitter as a low powered signal generator would suffice. In addition many more usable echoes would be obtained and therefore system measurement would improve correspondingly.

Since the YIG. transducer conversion efficiency does not have a strong frequency dependence it should be feasible to develop an experimental system similar to that described in this work, but operating at a much higher frequency. Present indications are that the upper operating frequency limit of such a system will be set not by the transducer conversion efficiency but rather by the extremely high tolerance imposed on the crystal surface finish and parallelism.

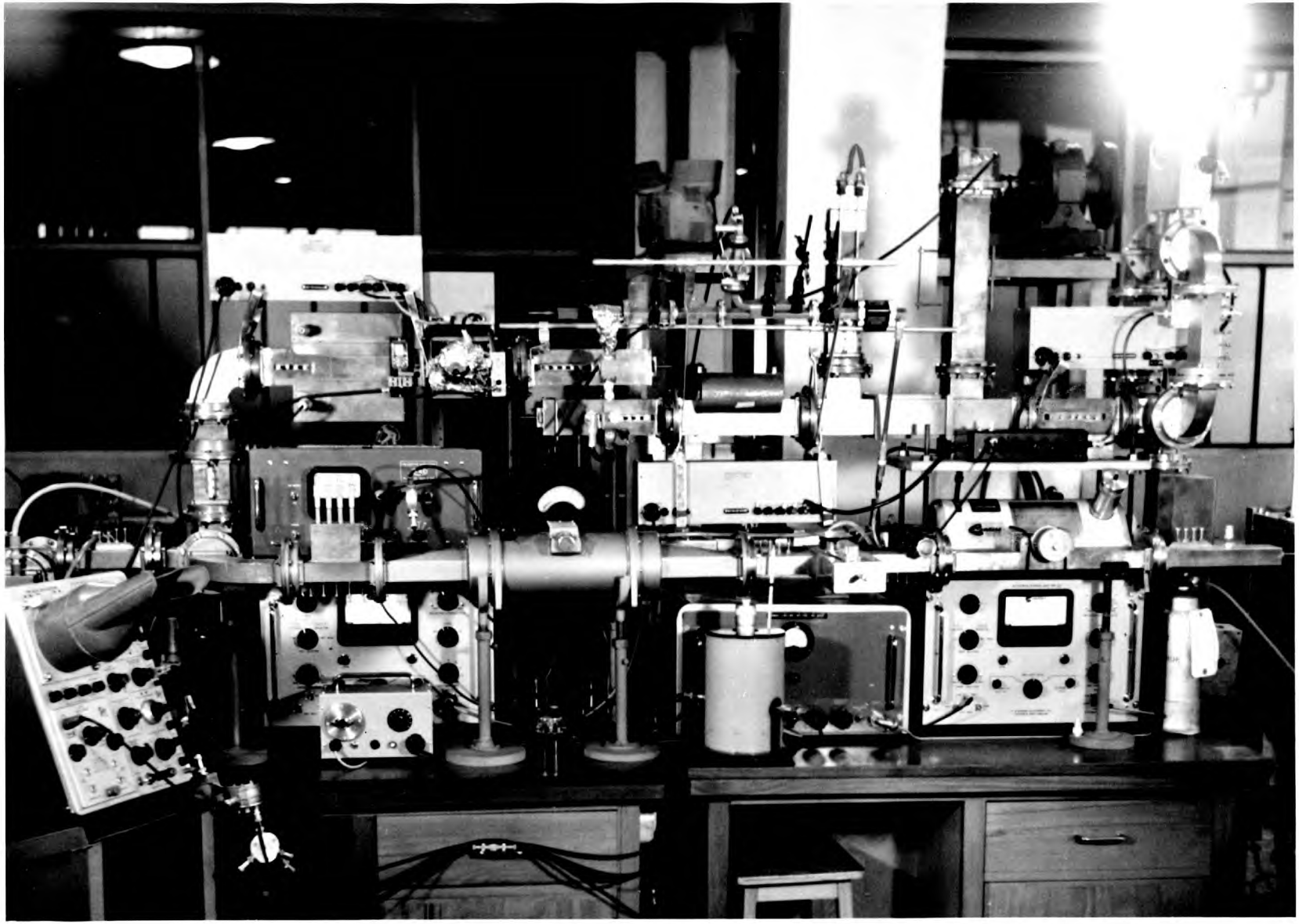

GENERAL VIEW OF EXPERIMENTAL SYSTEM

PART III

" EXPERIMENTAL SYSTEM THEORY "

Part III of this work consisting of appendices A to H, contains all the theory pertinent to the design , construction and operation of the individual components in the microwave ultrasonic experimental system.

APPENDIX A

A:1 (THE OPERATOR ∇)

In subsequent appendices reference will periodically be made to the operator " ∇ " (del) and to its successive operations upon vector quantities. Some of the more important of these successive applications of the operator will therefore be summarised here without proof, adequate proof being amply available in the literature. (1).

The Vector Operator ∇ (del) is defined as:

$$\nabla = \underline{i}\frac{\partial}{\partial x} + \underline{j}\frac{\partial}{\partial y} + \underline{k}\frac{\partial}{\partial z} \qquad (A:1)$$

where $\underline{i}$, $\underline{j}$ and $\underline{k}$ are unit vectors in the right handed cartesian coordinate system and correspond to the x, y, and z coordinate axes respectively.

Some of the more important operations are as follows:

$$\nabla_x(\nabla_x\underline{A}) = \nabla(\nabla_\cdot\underline{A}) - \nabla^2\underline{A} \qquad (A:2)$$

$$\nabla_\cdot(u\underline{A}) = u(\nabla_\cdot\underline{A}) + \underline{A}_\cdot(\nabla u) \qquad (A:3)$$

$$\nabla_x(u\underline{A}) = u(\nabla_x\underline{A}) + (\nabla u)_x\underline{A} \qquad (A;4)$$

$$\nabla_\cdot(\underline{A}_x\underline{B}) = \underline{B}_\cdot(\nabla_x\underline{A}) - \underline{A}_\cdot(\nabla_x\underline{B}) \qquad (A:5)$$

$$\nabla(\underline{A}_\cdot\underline{B}) = \underline{A}_x(\nabla_x\underline{B}) + (\underline{A}_\cdot\nabla)\underline{B} + \underline{B}_x(\nabla_x\underline{A}) + (\underline{B}_\cdot\nabla)\underline{A} \qquad (A;6)$$

$$\nabla_x(\underline{A}_x\underline{B}) = (\underline{B}_\cdot\nabla)\underline{A} - (\underline{A}_\cdot\nabla)\underline{B} - \underline{A}(\nabla_\cdot\underline{B}) \qquad (A;7)$$

$$\nabla_x(\nabla u) = 0 \qquad (A;8)$$

$$\nabla_\cdot(\nabla_x\underline{A}) = 0 \qquad (A;9)$$

where $(\underline{A}_\cdot\underline{B}) = \underline{i}\left(A_x\frac{\partial B_x}{\partial x} + A_y\frac{\partial B_x}{\partial y} + A_z\frac{\partial B_x}{\partial z} \right) +$

$$+ \underline{j}\left(A_x \frac{\partial B_y}{\partial x} + A_y \frac{\partial B_y}{\partial y} + A_z \frac{\partial B_y}{\partial z} \right)$$

$$+ \underline{k}\left(A_x \frac{\partial B_z}{\partial x} + A_y \frac{\partial B_z}{\partial y} + A_z \frac{\partial B_z}{\partial z} \right) \qquad \text{(A:10)}$$

In the above expressions the " dashed" symbols denote vector quantities while the undashed symbols signify scalar values. In addition the term $(\nabla \cdot \underline{A})$ stands for the dot product while $(\nabla_x \underline{A})$ is meant to represent the cross product.

For the cylindrical coordinate system we have:

$$\nabla_r \underline{\phi} = \frac{\partial \phi}{\partial r} \qquad \text{(A;11)}$$

$$\nabla_\theta \underline{\phi} = \frac{\partial \phi}{\partial \theta} \qquad \text{(A;12)}$$

$$\nabla_z \underline{\phi} = \frac{\partial \phi}{\partial z} \qquad \text{(A:12)}$$

and $$\nabla \cdot \underline{A} = \frac{1}{r}\frac{\partial (r A_r)}{\partial r} + \frac{1}{r}\frac{\partial A_\theta}{\partial \theta} + \frac{\partial A_z}{\partial z} \qquad \text{(A:14)}$$

$$\nabla^2 \underline{\phi} = \frac{1}{r}\frac{\partial}{\partial r}\left(r \frac{\partial \phi}{\partial r}\right) + \frac{1}{r^2}\frac{\partial^2 \phi}{\partial \theta} + \frac{\partial^2 \phi}{\partial z^2} \qquad \text{(A:14)}$$

$$(\nabla_x \underline{A})_r = \frac{1}{r}\frac{\partial A_z}{\partial \theta} - \frac{\partial A_\theta}{\partial z} \qquad \text{(A;16)}$$

$$(\nabla_x \underline{A})_\theta = \frac{\partial A_r}{\partial z} - \frac{\partial A_z}{\partial r} \qquad \text{(A;17)}$$

$$(\nabla_x \underline{A})_z = \frac{1}{r}\left\{ \frac{\partial (r A_\theta)}{\partial r} - \frac{\partial A_r}{\partial \theta} \right\} \qquad \text{(A;18)}$$

APPENDIX B

ELECTROMAGNETIC WAVES

It is desirable at this point to develop the general case of electromagnetic wave propagation in terms of vector analysis. Once having expressed the interaction of charges and their mutual energy in terms of the five field vectors ($\underline{E}$, $\underline{B}$, $\underline{D}$, $\underline{H}$, and $\underline{J}$) specific boundary conditions will be applied and thus solutions will be obtained for the particular cases of propagation of interest in this work: ie: electromagnetic wave propagation in coaxial lines, circular waveguides, rectangular waveguides and radial waveguides.

B:1 (FIELD VECTOR SYMBOLS AND UNITS)

In this section the rationalised M.K.S. system of units will be adopted, and in this system the five field vectors and associated constants are as follows.

SYMBOL	NAME	UNITS
$\underline{E}$	electric intensity	volts per meter
$\underline{B}$	magnetic induction	webers per meter sq.
$\underline{D}$	electric displacement	coulombs per meter sq.
$\underline{H}$	magnetic intensity	amperes per meter
$\underline{J}$	current density	amperes per meter sq.
σ	electric conductivity	mhos per meter
ε	dielectric permittivity	farads per meter
μ	magnetic permeability	henery per meter
ε_o	permittivity of free space	farads per meter
μ_o	permeability of free space	henery per meter
ρ_v	charge density	coulombs per meter cu.
C	velocity of propagation	meters per second.
C_o	free space propagation velocity	meters per second
μ_r	relative permeability	dimensionless
ε_r	relative permittivity	dimensionless

B:2 (ELECTROMAGNETIC EQUATIONS OF STATE)

Applying Gauss's theorem to electrostatics we find that

$$\nabla \cdot \underline{D} = \rho_v \qquad (B;2;1)$$

and when applied further to magnetic fields the relationship

$$\nabla \cdot \underline{B} = 0 \qquad (B;2;2)$$

is found to exsist.

Faraday's and Lenz's law of electromagnetic induction specify that:

$$\nabla \times \underline{E} = -\frac{\partial \underline{B}}{\partial t} \qquad (B;2;3$$

while Ampere's law for electromotive force stipulates the condition that:

$$\nabla \times \underline{H} = \underline{J} + \frac{\partial \underline{D}}{\partial t} \qquad (B;2;4)$$

For a homogeneous isotropic medium the following additional relations prevail:

$$\underline{D} = \varepsilon \underline{E} \qquad (B;2;5)$$

$$\underline{B} = \mu \underline{H} \qquad (B;2;6)$$

$$\underline{J} = \sigma \underline{E} \qquad (B;2;7)$$

The above equations are collectively termed " Maxwell's Equations and as such in aggregate form the basis of a comprehensive electromagnetic theory.

B;3 (THE WAVE EQUATION)

Having specified the complete set of field equations which are self consistent, it is possible to manipulate them to obtain a general expression of their interdependence, the result of which is given here in the form of the general electromagnetic wave equation..

$$\nabla^2 \underline{H} = \mu \varepsilon \frac{\partial^2 \underline{H}}{\partial^2 t} + \mu \sigma \frac{\partial \underline{H}}{\partial t} \qquad (B;3;1)$$

The three field vectors $\underline{H}$,$\underline{E}$ and $\underline{J}$ satisfy equations of the same form and further more if a time dependence restriction of the form $e^{j\omega t}$ is specified, which encompasses the sphere of interest in this work, one can simplify the wave equations considerably as follows.

$$\nabla^2 \underline{E} = -\mu\varepsilon\omega^2 \underline{E} + j\mu\sigma \underline{E}\,\omega \qquad (B;3;2)$$

$$\nabla^2 \underline{H} = -\mu\varepsilon\omega^2 \underline{H} + j\mu\sigma \underline{H}\,\omega \qquad (B;3;3)$$

$$\nabla^2 \underline{J} = -\mu\varepsilon\omega^2 \underline{J} + j\mu\sigma \underline{J}\,\omega \qquad (B;3;4)$$

where $\underline{H} = H_o\, e^{j\omega t}$ (B;3;5)

and $\underline{E} = E_o\, e^{j\omega t}$ (B;3;6)

in the above expressions ω is the angular frequncy , e the Naperian logarithmic base and j the square root of minus one.

Similarly Maxwell's equations simplify to :

$$\nabla_x \underline{E} = -j\mu\omega \underline{H} \qquad (B;3;7)$$

$$\nabla_x \underline{H} = \underline{J} + j\omega\varepsilon \underline{E} \qquad (B;3;8)$$

$$\nabla_\cdot \underline{D} = 0 \qquad (B;3;9)$$

$$\nabla_\cdot \underline{B} = 0 \qquad (B;3;10)$$

The form of the equations (B;3;9 and 10) is a consequence of the stipulation that propagation be restricted to homogeneous , loss free dielectric media contained within uniform metallic boundaries of infinite length.

B;4 (SOLUTIONS TO THE WAVE EQUATIONS)

B:4:1 (T.E.M. MODES IN COAXIAL CYLINDERS)

Consideration will now be given to the above equations for conditions for propagation between coaxial cylinders. The boundary conditions imposed are that only transverse fields exsist and hence with reference to FIG.(B;4;1;1) :

$$\underline{E}_z = \underline{H}_z = \underline{H}_r = \underline{E}_\theta = 0 \qquad (B;4;1;1)$$

Applying the above boundary conditions to the simplified equations of section (B;3) and taking due account of the form of the curl of a vector in the cylindrical coordinate system :ie: equations (A;11) to (A;18), one obtains the following results.

$$\frac{\partial E_r}{\partial z} = - j\mu\omega H_\phi \qquad (B;4;1;2)$$

$$\frac{\partial H_\phi}{\partial z} = - (\sigma + j\omega\varepsilon) E_r \qquad (B;4;1;3)$$

$$\frac{\partial^2 E_r}{\partial z^2} = - j\mu\omega(\sigma + j\omega\varepsilon) E_r = 0 \qquad (B;4;1;4)$$

$$\frac{\partial^2 H_\phi}{\partial z^2} = - j\mu\omega(\sigma + j\omega\varepsilon) H_\phi = 0 \qquad (B;4;1;5$$

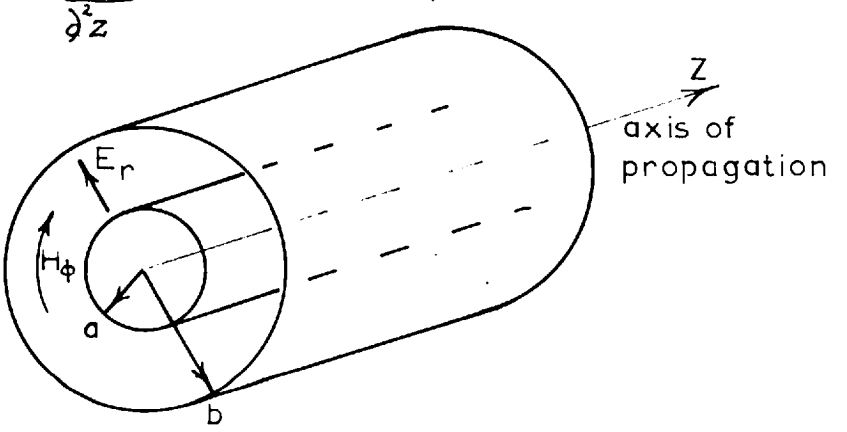

FIG.(B;4;1;1) **Coaxial waveguide**

Equation (B;4;1;4) is a homogeneous second order differential equation with constant coefficients and has a solution of the form

$$E_r = E_o\, e^{-\Gamma z} \qquad (B;4;1;6)$$

where E_o is an amplitude coefficient and may be taken as real, while Γ, the propagation constant is found to satisfy the relation:

$$\Gamma = \alpha + j\beta = (j\mu\omega\sigma - \omega^2\mu\varepsilon)^{\frac{1}{2}} \qquad (B;4;1;7)$$

Here α is the attenuation constant and β is the phase constant. The phase velocity C_p is given by :

$$C_p = \omega/\beta \qquad (B;4;1;8)$$

while the wavelength λ_g is determined by the expression:

$$\lambda_g = \frac{2\pi}{\beta} = \lambda \qquad (B;4;1;9)$$

here it is seen that for T.E.M. mode operation the guide wavelength is equal to the unbounded wavelength.

The solution to equation (B;4;1;5) is found to be:

$$H_\phi = - \frac{\Gamma}{j\mu\omega} E_r \qquad (B;4;1;10)$$

and thus the wave impedance Z_w becomes:

$$Z_w = \left((j\mu\omega) / (\sigma + j\omega\epsilon) \right)^{\frac{1}{2}} \qquad (B;4;1;11)$$

Similarly the other field components are found to be :

$$H_\phi = \frac{H_o}{r} \qquad (B;4;1;12)$$

where $$H_o = \frac{I_o}{2\pi} \qquad (B;4;1;13)$$

and I_o may be considered to be the mode current.

B:4;2 (PROPAGATION IN RECTANGULAR WAVEGUIDE)

Attention will now be given to the solution of the field and wave equations for conditions of propagation in a uniform rectangular metallic waveguide, shown in FIG.(B;4;2;1) , containing a homogeneous lossless dielectric. The equation of section (B;4) still apply and as such it is found that two different modes of propagation are possible within such a configuration, and are designated as T.M.or T.E. modes corresponding to the condition that the magnetic or electric field components are purely transverse. For the case of interest here,discussion will be restricted to the T.E. or H modes of propagation .

The wave equation which is found to apply in this case is:

$$\frac{\partial H_z}{\partial^2 x} + \frac{\partial^2 Hz}{\partial^2 y} + k_c^2 H_z = 0 \qquad (B;4;2;1)$$

where $$k_c^2 = \gamma^2 + \omega^2 \mu \varepsilon = \gamma^2 + k^2 \qquad (B;4;2;2)$$

here k_c is meant to represent the cut off wave number.

The solution of the above wave equation is of the form:

$$H_z = \cos(k_x x)\cos(k_y y) \qquad (B;4;2;3)$$

where k_x and k_y, the x and y coordinate wave numbers respectively, satisfy the relations:

$$k_x = n\pi/a \quad \text{and} \quad k_y = m\pi/b \qquad (B;4;2;4)$$

where n and m are integers or zero.

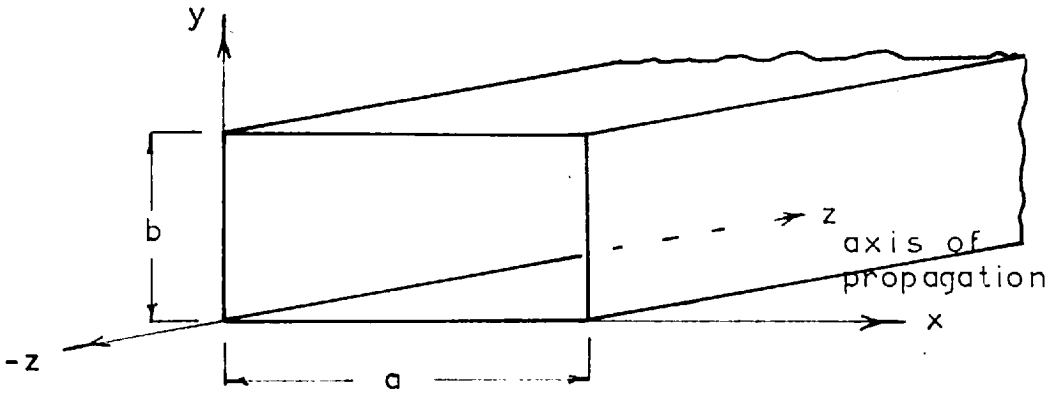

FIG. (B;4;2;1) **Rectangular waveguide.**

The subscripts n and m denote the particular mode of operation, the lowest or dominant mode being the $T.E._{10}$ and is the mode which is of interest in this work.

For the dominant mode of propagation equation (B;4;2;3) becomes:

$$H_z = \cos(\pi x/a) \qquad (B;4;2;5)$$

and in a similar manner the other field components are found to be:

$$H_y = E_x = 0 \qquad (B;4;2;6)$$

$$H_x = j\frac{2a}{\lambda_g}\sin(\pi x/a) \qquad (B;4;2;7)$$

$$E_y = -\frac{j2a}{\lambda_g} Z_w \sin(\pi x/a) \qquad (B;4;2;8)$$

and here $$Z_w = \frac{\lambda_g}{\lambda} \left(\mu / \varepsilon \right)^{\frac{1}{2}} \qquad (B;4;2;9)$$

It can be shown through the use of equation (B;4;2;2) that for dominant mode conditions the cut off angular frequency ω_c is given by

$$\omega_c = \frac{\pi}{\mu a \varepsilon} \qquad (B;4;2;10)$$

and so the cut off wavelength becomes:

$$\lambda_c = 2a \qquad (B;4;2;11)$$

where a is the waveguide width as shown in FIG.(B;4;2;1).

It can also be shown that the guide wavelength is given by:

$$\lambda_g = \lambda / \left(1-(\lambda / \lambda_c)^2 \right)^{\frac{1}{2}} \qquad (B;4;2;12)$$

B:4:3 (PROPAGATION IN CIRCULAR WAVEGUIDES)

For propagation in cylindrical waveguide it is necessary to transform the wave equation into its cylindrical coordinate form. Thus through the use of equation (A;15) and equations (B;3;2 to 4) one finds that the wave equation becomes:

$$\frac{\partial^2 \underline{E}}{\partial^2 r} + \frac{1}{r}\frac{\partial \underline{E}}{\partial r} + \frac{1}{r^2}\frac{\partial^2 \underline{E}}{\partial \theta^2} + k_c^2 \underline{E} = 0 \qquad (B;4;3;1)$$

and similarly for $\underline{H}$ and $\underline{J}$.

T.M. MODES

Considering first the transverse magnetic or "E" modes, for which $\Pi_z = 0$ one finds that equation (B:4:3;1) becomes :

$$\frac{\partial^2 E_z}{\partial^2 r} + \frac{1}{r}\frac{\partial E_z}{\partial r} + \frac{1}{r^2}\frac{\partial^2 E_z}{\partial \theta^2} + k_c^2 E_z = 0 \qquad (B;4;3;2)$$

The above equation applies to the case where the waveguide is filled with a perfect dielectric and propagation is taken in the Z direction as indicated in FIG.(B:4;3;1).

The solution of equation (B;4;3;2) by separation of variables technique yields the result:

$$E_z = e^{j\alpha\theta} J_\alpha(k_c r) + e^{j\alpha\theta} N_\alpha(k_c r) \qquad (B;4;3;3)$$

where J_α is a Bessel function of the first kind and order α while N_α is a Bessel function of the second kind. The second part of the solution of E_z is however rejected on physical grounds since it has a singularity at r=0. Thus the final solution is simply:

$$E_z = e^{j\alpha\theta} J_\alpha(k_c r) \qquad (B;4;3;4)$$

Application of the boundary condition specify that :

$$J_\alpha(k_c a) = 0 \qquad (B;4;3;5)$$

and so $$k_c = \frac{t\alpha n}{a} \qquad (B;4;3;6)$$

where $t\alpha n$ is the nth. root of the Bessel function of order α .

The cut off conditions are determined as previously and are found to give; $$\omega_c^2 = \frac{(t\alpha n)^2}{\mu\varepsilon a^2} \qquad (B;4;3;7)$$

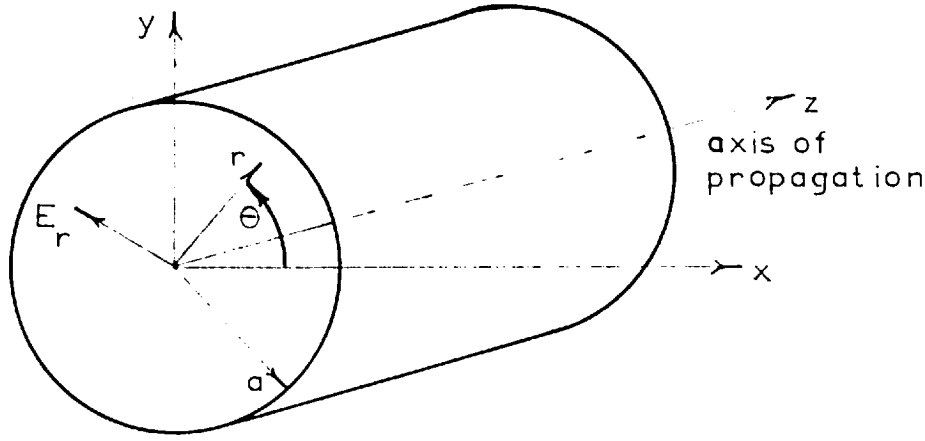

FIG. (B;4;3;1) **Cylindrial waveguide.**

The remaini ng field vectors may be determined in terms of E_z through utilization of the remaining Maxwell equations suitably modified for the cylindrical coordinate system through equations (A;11 to 18).

Thus one obtains for T.M. modes:

$$H_r = \frac{\chi \omega \varepsilon}{r k_c^2} J_\chi(k_c r)\ e^{j\chi\theta} \qquad (B;4;3;8)$$

$$H_\theta = -\frac{j \omega \varepsilon}{k_c} J'_\chi(k_c r)\ e^{j\chi\theta} \qquad (B;4;3;9)$$

$$E_r = Z_e H_\theta \qquad (B;4;3;10)$$

$$E_\theta = -Z_e H_r \qquad (B;4;3;11)$$

where $$Z_e = \gamma / j\omega\varepsilon \qquad (B;4;3;12)$$

T.E. MODES

In a similar manner it can be shown that for conditions of T.E. mode propagation the field vectors are given by the equations:

$$H_z = J_\chi(k_c r)\ e^{j\chi\theta} \qquad (B;4;3;13)$$

$$E_\theta = \frac{j\mu\omega}{k_c} J'_\chi(k_c r)\ e^{j\chi\theta} \qquad (B;4;3;14)$$

$$E_r = \frac{\mu \omega}{r k_c^2} J_\chi(k_c r)\ e^{j\chi\theta} \qquad (B;4;3;15)$$

$$H_r = \frac{E_\theta}{Z_h} \qquad (B;4;3;16)$$

$$H_\theta = E_r / Z_h \qquad (B;4;3;17)$$

where $$Z_h = j\mu\omega/\gamma \qquad (B;4;3;18)$$

also $$\lambda_c = 2\pi / k_c \qquad (B;4;3;19)$$

The dominant mode in circular waveguide is the $T.E._{11}$ mode since first root of the equation $J'_\chi(k_c a) = 0$ occurs at 1.841 and this is the smallest root of J'_χ or J_χ. Thus for the dominant mode of propagation $k_c = s_{11}/a = 1.841/a \qquad (B;4;3;20)$

B:4;4 (PROPAGATION IN NONUNIFORM RADIAL WAVEGUIDE.)

Unfortunately unlike the case of uniform wave propagation in which all the field components are derivable from a single component , radial waveguide field components cannot be formulated into a transverse field representation, and hence it is necessary to use a scalar superposition of modes to completely specify the field patterns.

Montgomery (2) has shown that for the case where $H_z=0$ the remaining field components of a radial transmission line of height b are given as follows: (with reference to FIG.(B;4;4;1)

T.M. MODES

$$E_z = -\frac{\epsilon_n}{b} V_1' \cos(n\pi/b) \cos(m\theta) \qquad (B;4;4;1)$$

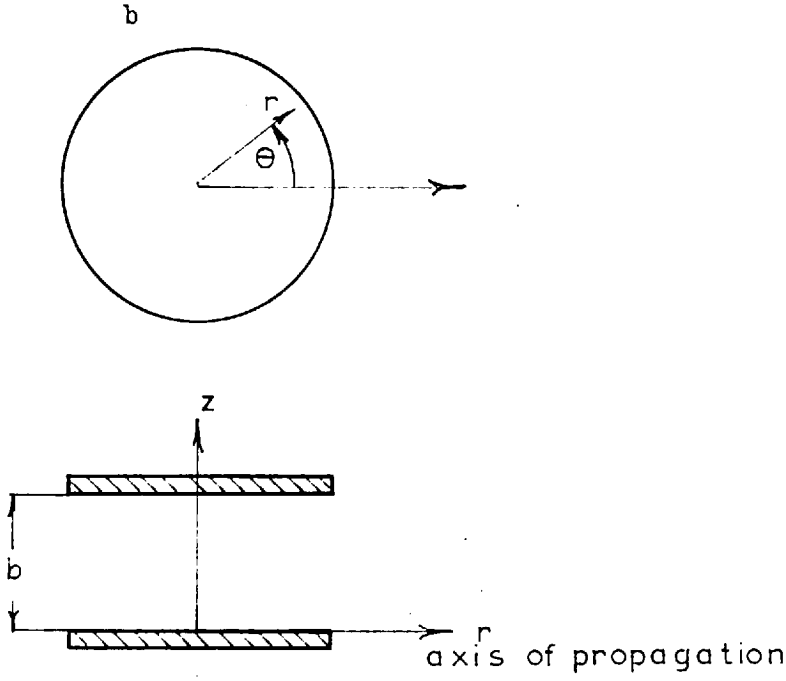

FIG. (B;4;4;1) **Radial waveguide**

$$E_\theta = -\frac{\epsilon_n}{\Gamma^2 b} V_1' (m/r)(n\pi/b) \sin(n\pi z/b) \sin(m\theta) \qquad (B;4;4;2)$$

$$H_\theta = \frac{\epsilon_m}{2\pi r} I_1' \cos(n\pi z/b) \cos(m\theta) \qquad (B;4;4;3)$$

where $$\Gamma^2 = k^2-(n\pi/b)^2 = k^2 - k_c^2 \qquad (B;4;4;4)$$

and $$k = (\omega^2 u \varepsilon)^{\frac{1}{2}} = 2\pi/\lambda \qquad (B;4;4;5)$$

is the unbounded wave number.

In the above expressions m and n , the mode indices , are determined by the angular aperture and height of the cylindrical ez cross-section of the radial guide. V_1' and I_1' are the mode voltage and current respectively which characterise the amplitude of the electric and magnetic fields of an "E" mode and b corresponds to the guide height. In addition $\epsilon_n = 1$ for n=0 and $\epsilon_n = 2$ for n 1 .

T.E.MODES

For T.E. modes the expressions become:

$$H_z = \frac{\epsilon_n I_1'}{b} \sin(n\pi/b) \sin(m\theta) \qquad (B;4;4;6)$$

$$H_\theta = \frac{\epsilon_n I_1'}{r^2 b} (m/r) (n\pi/b) \cos(n\pi z/b) \cos(m\theta) \qquad (B;4;4;7)$$

$$E_\theta = \frac{\epsilon_m V_1'}{2\pi r} \sin(n\pi z/b) \sin(m\theta) \qquad (B;4;4;8)$$

Montgomery (3) and Marcuvitz (4) have shown that it is possible to obtain the " Simplified Radial Transmission Line Equations " by eliminating $\underline{E}$ and $\underline{H}$ from the cylindrical coordinate form of Maxwell's equations and substituting into equations (B;4;4;2 to 8), which, when further simplified to cover the case where only one mode is allowed to exsist, that being the lowest "E" mode,where both m and n are zero, are found to be:

$$\frac{dV}{dr} = -jkZ_o I \qquad (B;4;4;9)$$

and $$\frac{dI}{dr} = -jkY_o V \qquad (B;4;4;10)$$

where $$Z_o = 1/Y_o = \frac{b}{2\pi r} (\mu/\varepsilon)^{\frac{1}{2}} \qquad (B;4;4;11)$$

These radial transmission line equations differ from the uniform line equations in that the propagation constant and characteristic

impedance Z_o are functions of the radial dimension r.

Eliminating I from equations (B;4;4;9 to 11) gives the wave equation:

$$\frac{1}{r}\frac{d}{dr}\left(r\frac{dV}{dr}\right) + k^2 V = 0 \qquad (B;4;4;12)$$

The above equation is similar to the wave equation dealt with earlier in the section on propagation in cylindrical waveguide and as such has a solution of the form:

$$V_{(r)} = A\, J_o(k r) + B\, N_o(k r) \qquad (B;4;4;13)$$

and upon evaluation of the constants by suitable application of the boundary conditions one finds that :

$$V_{(r)} = V_{(r_o)}\, Cs(x,y) - jZ_{o(r_o)}\, I_{(r_o)}\, Sn(x,y) \qquad (B;4;4;14)$$

and similarly it is found that:

$$Z_{o(r)} = \frac{(Z_{o(r_o)}\, I_{(r_o)}\, cs(x,y) - jV_{(r_o)}\, Sn(x,y))}{I_{(r)}} \qquad (B;4;4;15)$$

where

$$Cs(x,y) = (J_1(y)\, N_o(x) - N_1(y)\, J_o(x))(\pi y/2) \qquad (B;4;4;16)$$

$$cs(x,y) = (N_o(y)\, J_1(x) - J_o(y)\, N_1(x))(\pi y/2) \qquad (B;4;4;17)$$

$$Sn(x,y) = (J_1(y)\, N_1(x) - N_1(y)\, J_1(x))(\pi y/2) \qquad (B;4;4;18)$$

$$sn(x,y) = (J_o(y)\, N_o(x) - N_o(y)\, J_o(x))(\pi y/2) \qquad (B;4;4;19)$$

and

$$Z_{o(r)} = \frac{Z_i\, b}{2\pi r} \qquad (B;4;4;20)$$

$$Z_{o(r_o)} = \frac{Z_i\, b}{2\pi r_o} \qquad (B;4;4;21)$$

here Z_i is the intrinsic impedance and is given by :

$$Z_i = (\mu/\epsilon)^{\frac{1}{2}} \qquad (B;4;4;22)$$

also $x = (k r)$ and $y = (k r_o)$ (B;4;4;23)

For the dominant mode of propagation:ie: "E" mode where m and n are zero , the field equations of (B:4;4;1 to 3) become:

$$E_{z(r)} = \frac{- V_{(r)}}{b} \qquad (B;4;4;24)$$

$$E_{\theta} = 0 \qquad (B;4;4;25)$$

$$H_{\theta(r)} = \frac{I_{(r)}}{2\pi r} \qquad (B;4;4;26)$$

and so $$H_{\theta(r_o)} = I_{(r_o)} / 2\pi r = H_o / r \qquad (B;4;4;27)$$

where H_o is the maximum value of the magnetic field .

From the above equations it is evident that the dominant mode is a T.E.M. mode.

The normalised relative admittance $Y'_{(r)}$ is defined as:

$$Y'_{(r)} = Y_{(r)} / Y_{o(r)} = \frac{Z_{o(r)} \; I_{(r)}}{V_{(r)}} \qquad (B;4;4;28)$$

which is the absolute admittance at a radius (r) divided by the characteristic admittance at the same radius.

Appropriate substitutions yield the following:

$$Y'_{(r)} = \frac{j + Y'_{(r_o)} \; Z_i(x,y) \; ct(x,y)}{Ct(x,y) + j \; Y'_{(r_o)} \; Z_i(x,y)} \qquad (B;4;4;29)$$

where $$Y'_{(r_o)} = \frac{Z_{o(r_o)} \; I_{(r_o)}}{V_{(r_o)}} = Y_{(r_o)} / Y_{o(r_o)} \qquad (B;4;4;30)$$

and $$ct(x,y) = \frac{J_1(x) \; N_o(y) - N_1(x) \; J_o(y)}{J_o(x) \; N_o(y) - N_o(x) \; J_o(y)} \qquad (B;4;4;31)$$

$$Ct(x,y) = \frac{J_1(y) \; N_o(y) - N_1(y) \; J_o(x)}{J_1(x) \; N_1(y) - N_1(x) \; J_1(y)} \qquad (B;4;4;32)$$

also $$Z_i(x,y) = \frac{J_o(x)\, N_o(y) - N_o(x)\, J_o(y)}{J_1(x)\, N_1(y) - N_1(x)\, J_1(y)} \qquad (B;4;4;33)$$

and as before $x=(k\ r)$ and $y=(k\ r)$

where (y-x) is termed the electrical length of the radial transmission line. In the above equations $Y_{o(r_o)}$ is meant to represent the characteristic line admittance at the plane $r=r_o$ and similarly $Z_{o(r_o)}$ signifies the characteristic impedance at $r= r_o$.

Having obtained a relative admittance expression for a radial transmission line it is now possible to examine some of the characteristics of such a system in comparison to a uniform transmission line (5).

(a) The relative input admittance $Y'_{(r)}$ of a radial line supporting an E mode and having its output short circuited at the plane $r=r_o$ is found to be :

$$Y'_{(r)} = - j\ ct(x,y) \qquad (B;4;4;34)$$

(b) The relative input admittance of a radial line with an open circuit at its output is given by:

$$Y'_{(r)} = j\ /\ Ct(x,y) \qquad (B;4;4;35)$$

(c) The relative input admittance of an infinite radial E type line is given by the equation:

$$Y'_{(r)} = \frac{j + Z_i(x,y)\ ct(x,y)}{Ct(x,y) + j\ Z_i(x,y)} \qquad (B;4;4;36)$$

From the above equation it is evident that the input admittance of a radial line is not generally equal to the characteristic admittance $Y_{o(r)}$ and that it is complex. More over the relative admittance of the line is not the same looking in opposite directions.

APPENDIX C

(GENERAL TRANSMISSION LINE EQUATIONS)

For completeness the more important transmission line equations used in this work will be summarised here without proof.

C:1 (COAXIAL LINE RELATIONS)

The series impedance of a transmission line is given as:

$$Z = R + j X = R + j\omega L \qquad (C;1;1)$$

while the shunt admittance is:

$$Y = G + j B = G + j\omega C \qquad (C;1;2)$$

The characteristic impedance is defined as:

$$Z_o = (Z/Y)^{\frac{1}{2}} \qquad (C;1;3)$$

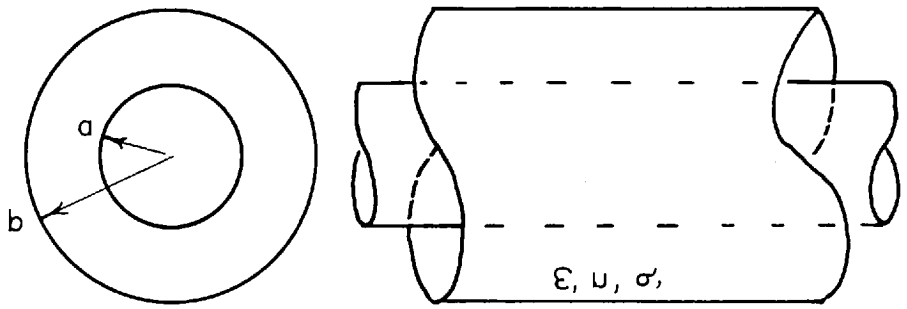

FIG. (C;1;1) **Coaxial transmission line**

and the propagation constant is given as:

$$\Gamma = (Y Z)^{\frac{1}{2}} \qquad (C;1;4)$$

For a loss less coaxial transmission line the series inductance and shunt capacitance are given by the relations:

$$L = \frac{\mu}{2\pi} \ln(b/a) \qquad (C;1;5)$$

$$C = \frac{2\pi\varepsilon}{\ln(b/a)}$$

and thus the propagation constant Γ becomes:

$$\Gamma = \alpha + j\beta = 0 + j\omega (\mu\varepsilon)^{1/2} \qquad (C;1;6)$$

while the phase velocity C_p is:

$$C_p = \omega/\beta = C_o / (\mu_r \varepsilon_r)^{\frac{1}{2}} \qquad (C;1;7)$$

where C_o is the free space propagation velocity.

Finally the characteristic impedance of a lossless coaxial line becomes:

$$Z_o = 60.0 \left(\mu_r / \epsilon_r \right)^{\frac{1}{2}} \ln(b/a) \qquad (C;1;8)$$

When standing waves are present on a transmission line the reflection coefficient ρ is determined by the relation:

$$\rho = \frac{Z_r - Z_o}{Z_r + Z_o} \qquad (C;1;9)$$

and the standing wave ratio " r " is given by the equation:

$$\text{" r "} = \frac{1 + \rho}{1 - \rho} \qquad (C;1;10)$$

The complex impedance seen at a point, a distance l back from the terminating impedance Z_r, on a transmission line is found to be:

$$Z_{(-l)} = Z_o \left(\frac{Z_r + j\, Z_o \tan(\beta l)}{Z_o + j\, Z_r \tan(\beta l)} \right) \qquad (C;1;11)$$

APPENDIX D

ELASTIC WAVES

at this point it is desirable to consider various aspects of elastic wave propagation in solid bodies, this topic being of paramont importance to the theory of measurement in this system.

D:1 (STRESS - STRAIN COMPONENTS)

Consider FIG.(D:1;1) which is intended to represent the free body diagram of an elemental volume, being part of an infinite, homogeneous but not necessarily isotropic medium. The force R , which is centrally located on face ABCD is meant to represent the effect of all the stresses acting on face ABCD . For conditions of equilibrium it is necessary to introduce a couple to account for stress variations across the face, however in the limit as the elemental area tends to zero the couple can be neglected since it varies as the cube of the face dimension.

Similarly as dA approaches zero,R will be proportional to the area of the face ABCD and so may be considered as the stress on face ABCD , where stress is here defined as the force per unit area. The positive sense of R is taken as directed outward.

Now R can be resolved into three axial stress components as T_{x,x_2} , T_{y,x_2} , T_{z,x_2} , where , following the standard subscript designation, the first letter indicates the stress component while the second denotes the face upon which this stress acts.

The stress components pertaining to the other cube faces are found to be:

T_{x,y_1}	T_{y,y_1}	T_{z,y_1}	for face OABE	(D;1;1)
T_{x,y_2}	T_{y,y_2}	T_{z,y_2}	for face CFGD	(D;1;2)
T_{x,z_1}	T_{y,z_1}	T_{z,z_1}	for face OADG	(D;1;3)

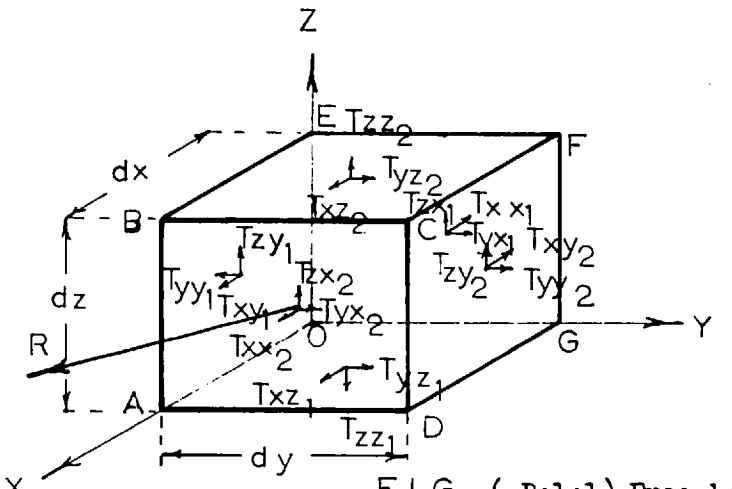

FIG. (D;1;1) **Free body diagram**

and

T_{x,z_2}	T_{y,z_2}	T_{z,z_2}	for face BCFE	(D:1:4)
T_{x,x_1}	T_{y,x_1}	T_{z,x_1}	for face OEFG	(D:1;5)

A summation of all the components in each of the coordinate directions gives the resultant force in that direction and so for the x direction one obtains:

$$F_x = \left(T_{x,x_2} - T_{x,x_1} \right) dydz + \left(T_{x,y_2} + T_{x,y_1} \right) dxdz + \left(T_{x,z_2} + T_{x,z_1} \right) dxdy \qquad (D;1;6)$$

but now $$T_{x,x_2} = - T_{x,x_1} + \frac{\partial (T_{x,x})}{\partial x} dx \qquad (D;1;7)$$

and similar expressions exsist for T_{x,y_2} and T_{x,z_2} such that equation (D;1;6) may be written as:

$$F_x = \left(\frac{\partial}{\partial x} T_{x,x} + \frac{\partial}{\partial y} T_{x,y} + \frac{\partial}{\partial z} T_{x,z} \right) dxdydz \qquad (D;1;8)$$

similarly for the other coordinate directions one finds that:

$$F_y = \left(\frac{\partial}{\partial x} T_{y,x} + \frac{\partial}{\partial y} T_{y,y} + \frac{\partial}{\partial z} T_{y,z} \right) dxdydz \qquad (D;1;9)$$

$$F_z = \left(\frac{\partial}{\partial x} T_{z,x} + \frac{\partial}{\partial y} T_{z,y} + \frac{\partial}{\partial z} T_{z,z} \right) dxdydz \qquad (D;1;10)$$

It can be shown from limiting conditions of rotational equilibrium (6) that:

$$\begin{aligned} T_{x,y} &= T_{y,x} \\ T_{x,z} &= T_{z,x} \\ T_{y,z} &= T_{z,y} \end{aligned} \qquad (D;1;11)$$

and so the complete set of stress components may be written in matrix form as follows:

$$\begin{vmatrix} T_{x,x} & T_{x,y} & T_{x,z} \\ T_{x,y} & T_{y,y} & T_{y,z} \\ T_{x,z} & T_{y,z} & T_{z,z} \end{vmatrix} = \begin{vmatrix} T_{11} & T_{12} & T_{13} \\ T_{12} & T_{22} & T_{23} \\ T_{13} & T_{23} & T_{33} \end{vmatrix} = \begin{vmatrix} T_1 & T_6 & T_5 \\ T_6 & T_2 & T_4 \\ T_5 & T_4 & T_3 \end{vmatrix} \qquad (D;1;12)$$

In the final condensed notation :

$$1=11,\ 2=22\ ,\ 3=33\ ,\ 4=23,\ \ 5=13,\ \ 6=12\ . \qquad (D;1;13)$$

The above stress components may be expressed in tensor notation as follows:

$$T_{ij} = \begin{vmatrix} T_1 & T_6 & T_5 \\ T_6 & T_2 & T_4 \\ T_5 & T_4 & T_3 \end{vmatrix} \qquad (D;1;14)$$

It should be noted at this point that tensor notation is introduced sparingly in this analysis, the reason for any such inclusion being the ease with which the elastic and piezoelectric constants for rotated axes can be derived from the principal crystalographic axes by simple tensor transformation formulae. The general tensor character of the stress and strain tensors will therefore not be considered here, however a comprehensive treatment is available in the literature. (8), (9).

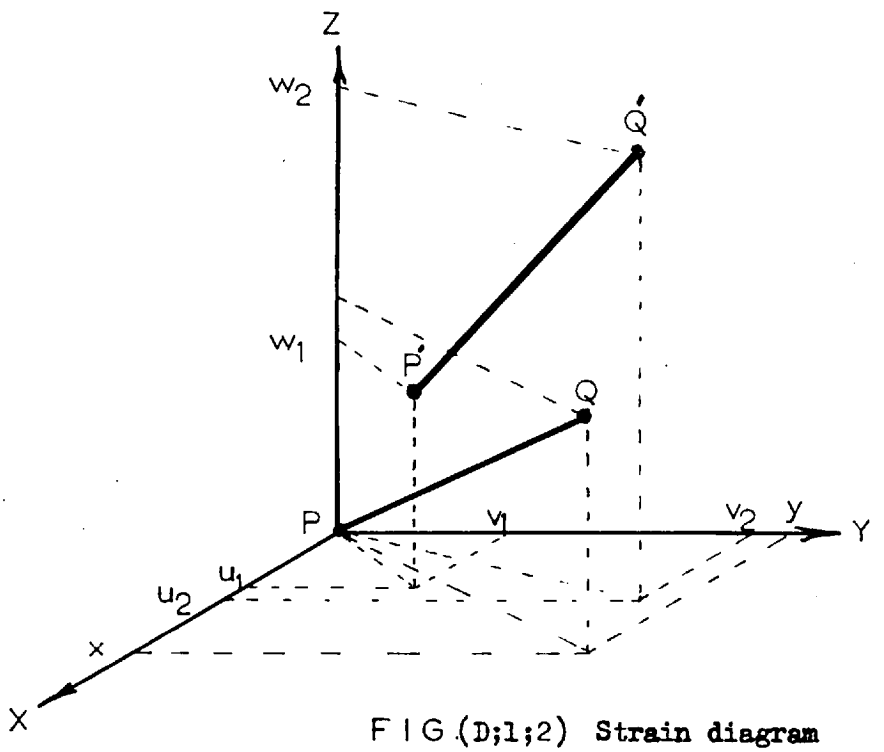

FIG.(D;1;2) **Strain diagram**

In order to develop a strain matrix, where strain is defined as per-unit elongation, it is best to consider the classical case of the change in length and position of a line due to applied stress. Thus, with reference to FIG.(D;1;2),the relative positions of two points,P and Q , on a line , after undergoing translation and rotation as a result of applied stress are P' and Q' respectively. The points P'and Q' have respective coordinates u_1, v_1, w_1 and $x+u_2, y+v_2, z+w_2$.

The displacement of Q' may also be given by:

$$u_2 = u_1 + \frac{\partial u}{\partial x} x + \frac{\partial u}{\partial y} y + \frac{\partial u}{\partial z} z \qquad (D;1;15)$$

$$v_2 = v_1 + \frac{\partial v}{\partial x} x + \frac{\partial v}{\partial y} y + \frac{\partial v}{\partial z} z \qquad (D;1;16)$$

$$w_2 = w_1 + \frac{\partial w}{\partial x} x + \frac{\partial w}{\partial y} y + \frac{\partial w}{\partial z} z \qquad (D;1;17)$$

since in a homogeneous medium the strain is a continuous function of the coordinates.

The net change in thelength of the line in three dimentions is thus obtained by finding the difference between the two point displacements, and so one has:

$$\delta x = x \frac{\partial u}{\partial x} + y \frac{\partial u}{\partial y} + z \frac{\partial u}{\partial z} \qquad (D;1;18)$$

$$\delta y = x \frac{\partial v}{\partial x} \quad y \frac{\partial v}{\partial y} \quad z \frac{\partial v}{\partial z} \qquad (D;1;19)$$

$$\delta z = x \frac{\partial w}{\partial x} \quad y \frac{\partial w}{\partial y} \quad z \frac{\partial w}{\partial z} \qquad (D;1;20)$$

The terms $\partial u/\partial x$, $\partial v/\partial y$, $\partial w/\partial z$ are the per-unit elongations and as such are defined as the linear coordinate strains and designated as:

$$S_{x,x} = \partial u / \partial x = S_{11} \qquad (D;1;21)$$

$$S_{y,y} = \partial v / \partial y = S_{22} \qquad (D;1;22)$$

$$S_{z,z} = \partial w / \partial z = S_{33} \qquad (D;1;23)$$

The other strain components,known as the "shear strains", are given as:

$$S_{y,z} = \partial w / \partial y + \partial v / \partial z = S_4 \qquad (D;1;24)$$

$$S_{x,z} = \partial u / \partial z + \partial w / \partial x = S_5 \qquad (D;1;25)$$

$$S_{x,y} = \partial v / \partial x + \partial u / \partial y = S_6 \qquad (D;1;26)$$

The rotational coefficients are found to be:

$$2\omega_x = \partial w/\partial y - \partial v/\partial z \qquad (D;1;27)$$

$$2\omega_y = \partial u/\partial z - \partial w/\partial x \qquad (D;1;28)$$

$$2\omega_z = \partial v/\partial x - \partial u/\partial y \qquad (D;1;29)$$

The above equations may be verified by inspection of FIG.(D;1;3).

If a strain condition occurs in which $\omega_x = \omega_y = \omega_z = 0$ the deformation is irrotational and is defined as " pure strain ".

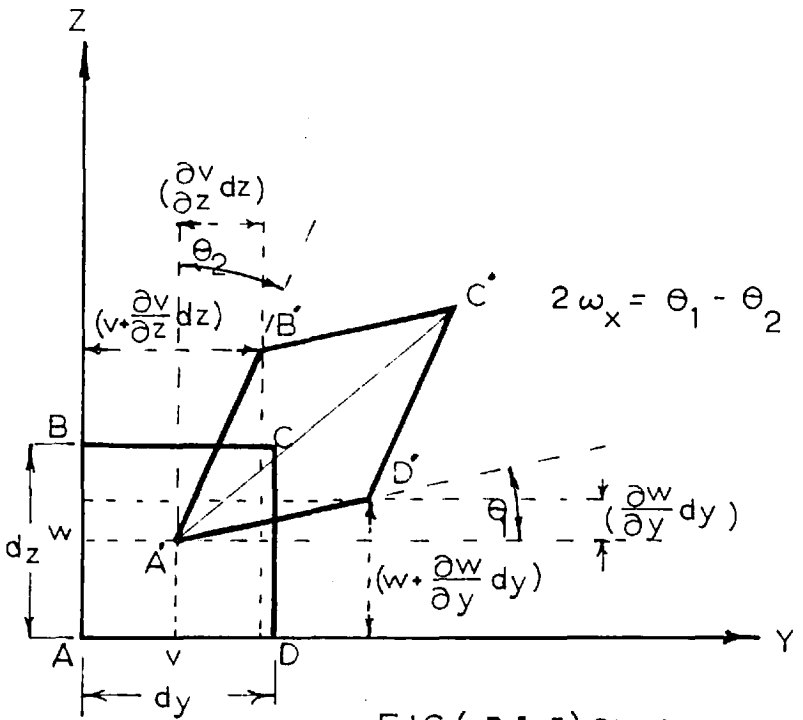

FIG(D;1;3) Strain components

Unfortunately equations (D;1;24 to 26) are of such a nature as not to permit their inclusion in a strain tensor, however it can be shown (7) that if the substitutions $S_4 = 2S_{23}$, $S_5 = 2S_{13}$, and $S_6 = 2S_{12}$ are made, a strain tensor can indeed be formulated as follows:

$$S_{ij} = \begin{vmatrix} S_{x,x} & \frac{S_{x,y}}{2} & \frac{S_{x,z}}{2} \\ \frac{S_{x,y}}{2} & S_{y,y} & \frac{S_{y,z}}{2} \\ \frac{S_{x,z}}{2} & \frac{S_{y,z}}{2} & S_{z,z} \end{vmatrix} = \begin{vmatrix} S_{11} & S_{12} & S_{13} \\ S_{12} & S_{22} & S_{23} \\ S_{13} & S_{23} & S_{33} \end{vmatrix} = \frac{\partial u_i}{\partial x_j} \qquad (D;1;30)$$

STRESS VS STRAIN

Provided the applied stresses are of such magnitude that the resultant strains do not exceed the elastic limit of the medium, it is found that Hooke's Law applies and so each individual stress component is expressible in terms of a linear function of the six strain components. Generally the relationship is written as follows:

$$\begin{array}{llllllll} T_{11}=T_1= & C_{11}S_1+ & C_{12}S_2+ & C_{13}S_3+ & C_{14}S_4+ & C_{15}S_5+ & C_{16}S_6 \\ T_{22}\ T_2= & C_{21}S_1 & C_{22}S_2 & C_{23}S_3 & C_{24}S_4 & C_{25}S_5 & C_{26}S_6 \\ T_{33}\ T_3 & C_{31}S_1 & C_{32}S_2 & C_{33}S_3 & C_{34}S_4 & C_{34}S_5 & C_{36}S_6 \\ T_{23}\ T_4 & C_{41}S_1 & C_{42}S_2 & C_{43}S_3 & C_{44}S_4 & C_{45}S_5 & C_{46}S_6 \\ T_{13}\ T_5 & C_{51}S_1 & C_{52}S_2 & C_{53}S_3 & C_{54}S_4 & C_{55}S_5 & C_{56}S_6 \\ T_{12}\ T_6 & C_{61}S_1 & C_{62}S_2 & C_{63}S_3 & C_{64}S_4 & C_{65}S_5 & C_{66}S_6 \end{array} \qquad (D;1;31)$$

where the C's are the elastic proportionality constants between two particular stress and strain components in the absence of any other strains. The above equation may be written in condensed tensor notation as:

$$T_i = C_{ij}\, S_j \qquad \begin{array}{l} i= 1,2,3,,, 6 \\ j= 1,2,3,,, 6 \end{array} \qquad (D;1;32)$$

where C_{ij} represents the elastic constant tensor. According to the Enstein convention , a repeated subscript indicates summation over the subscript.

More generally equation (D;1;32) is written as :

$$T_{ij}= C_{ijkl}S_{kl} \qquad (D;1;33)$$

and i,j,k, and l may take the values from 1 to 3

It has been shown,(13),(14), that as a consequence of the medium internal energy being a perfect differential one has that:

$$C_{ijkL} = C_{jikL} = C_{ijLk} = C_{jiLk} \quad ,,, \text{ etc.} \qquad (D;1;34)$$

The above condition reduces the general case number of independent elastic constants in equation (D;1;31) from 36 to 21. Any symmetries present in the particular medium in question will result in a further reduction of independent elastic constants. (15).

D:2 (GENERAL EQUATIONS OF MOTION IN ANISOTROPIC MEDIA)

Having derived the force equations applicable to an elemental volume of a homogeneous infinite medium in section (D;1), it is now possible to develop the equations of motion for the element by invoking Newton's second law. Thus we have:

$$F_x = \rho \frac{\partial^2 u}{\partial^2 t} \, dV \qquad (D;2;1)$$

$$F_y = \rho \frac{\partial^2 v}{\partial^2 t} \, dV \qquad (D;2;2)$$

$$F_x = \rho \frac{\partial^2 w}{\partial^2 t} \, dV \qquad (D;2;3)$$

which when combined with equations (D;1;8 to 10) lead to :

$$\rho \frac{\partial^2 u}{\partial^2 t} = \frac{\partial T_{11}}{\partial x} + \frac{\partial T_{12}}{\partial y} + \frac{\partial T_{13}}{\partial z} \qquad (D;2;4)$$

$$\rho \frac{\partial^2 v}{\partial^2 t} = \frac{\partial T_{21}}{\partial x} + \frac{\partial T_{22}}{\partial y} + \frac{\partial T_{23}}{\partial z} \qquad (D;2;5)$$

$$\rho \frac{\partial^2 w}{\partial^2 t} = \frac{\partial T_{31}}{\partial x} + \frac{\partial T_{32}}{\partial y} + \frac{\partial T_{33}}{\partial z} \qquad (D;2;6)$$

where ρ is the medium density .

In tensor form the above equations become:

$$\rho \frac{\partial^2 u_i}{\partial^2 t} = \frac{\partial}{\partial x_j} T_{ij} \, dV \qquad (D;2;7)$$

which is the elastic wave equation.

Here the tensor indices i and j , assume the values from one to three.

Equation (D;2;7) may also be expressed in terms of the strains by virtue of equation (D;1;32) , therefore:

$$\rho \frac{\partial^2 u_i}{\partial^2 t} = \frac{\partial}{\partial x_j} C_{ijkl} S_{kl} \qquad (D;2;8)$$

where $i,j,k,l, = 1,2,3.$

Equations (D;2;7 and 8) are quite general and as such apply to both anisotropic and isotropic media, however in order to be able to apply the equations to a situation in which the direction of propagation "S" is not along one of the crystallographic axes, it is best to express the component stresses and strains in terms of the direction cosines l,m and n, (16),(17),(18) , where l is the cosine of the angle between "S" and the X axis , m the cosine of the angle between "S" and the Y axis and similarly n represents the cosine of the angle between "S" and the Z axis.

From the above definition and FIG.(D:2:1) it follows that:

$$s = lx + my + nz \qquad (D;2;9)$$

and so equations (D;1;21 to 26) become:

$$S_{11} = l \frac{\partial u}{\partial s} \qquad 2S_{23} = m \frac{\partial w}{\partial s} + \frac{\partial v}{\partial s} n$$

$$S_{22} = m \frac{\partial v}{\partial s} \qquad 2S_{13} = n \frac{\partial u}{\partial s} + \frac{\partial w}{\partial s} l \qquad (D;2;10)$$

$$S_{33} = n \frac{\partial w}{\partial s} \qquad 2S_{12} = l \frac{\partial v}{\partial s} + \frac{\partial u}{\partial s} m$$

It is now possible to express equations (D;2;4 to 6) in terms of "S" by appropriate substitutions of equation (D;2;10) into (D;1;31) and so one has that: (19),(20) :

$$\rho C^2 \frac{\partial^2 u}{\partial^2 s} = h_{11}\frac{\partial^2 u}{\partial^2 s} + h_{12}\frac{\partial^2 v}{\partial^2 s} + h_{13}\frac{\partial^2 w}{\partial^2 s} \qquad (D;2;11)$$

$$\rho C^2 \frac{\partial^2 u}{\partial^2 s} = h_{12}\frac{\partial^2 u}{\partial^2 s} + h_{22}\frac{\partial^2 v}{\partial^2 s} + h_{23}\frac{\partial^2 w}{\partial^2 s} \qquad (D;2;12)$$

$$\rho C^2 \frac{\partial^2 u}{\partial^2 s} = h_{31}\frac{\partial^2 u}{\partial^2 s} + h_{32}\frac{\partial^2 v}{\partial^2 s} + h_{33}\frac{\partial^2 w}{\partial^2 s} \qquad (D;2;13)$$

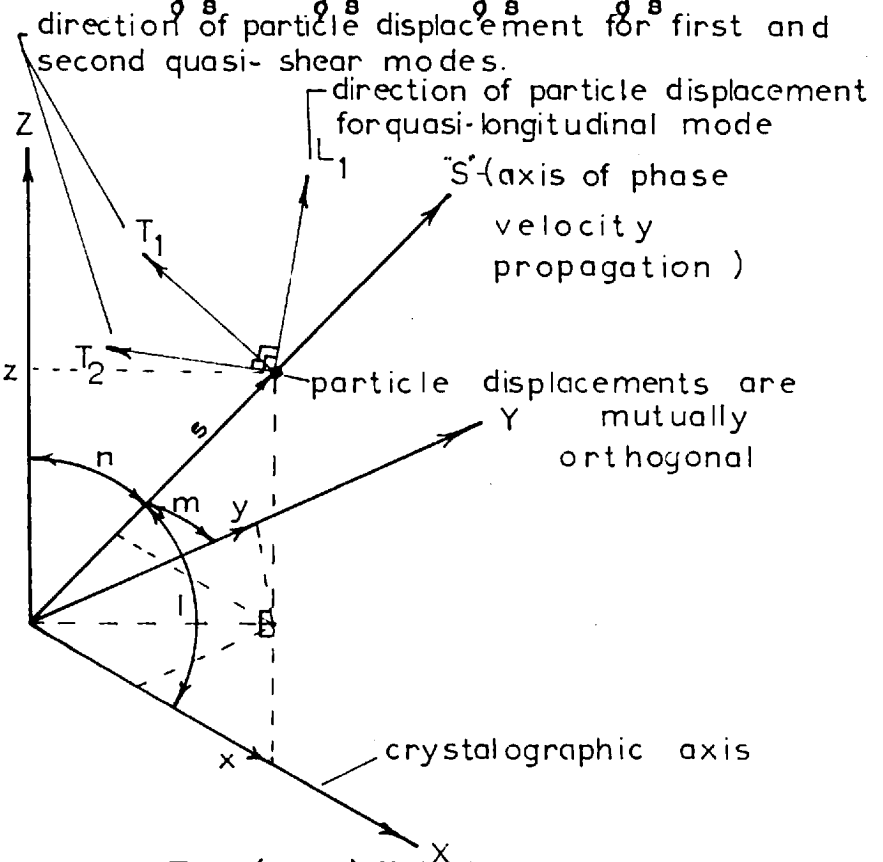

FIG.(D;2;1) **Mode diagram**

where C is the velocity of phase propagation and where the terms in (h) , known as Christoffel's constants , are given by the following expressions:

$$h_{11} = l^2C_{11} + m^2C_{66} + n^2C_{55} + 2mnC_{56} + 2nlC_{15} + 2mlC_{16} \qquad (D;2;14)$$

$$h_{12} = h_{21} = l^2C_{16} + m^2C_{26} + n^2C_{45} + mn(C_{46}+C_{25}) + nl(C_{14}+C_{56}) + lm(C12+C56) \qquad (D;2;15)$$

$$h_{13} = h_{31} = l^2C_{15} + m^2C_{46} + n^2C_{35} + mn(C_{45}+C_{36}) + nl(C_{13}+C_{55}) + lm(C_{14}+C_{56}) \qquad (D;2;16)$$

$$h_{23} = h_{32} = l^2C_{56} + m^2C_{24} + n^2C_{34} + mn(C_{44}+C_{23}) + nl(C_{36}+C_{45}) + lm(C_{25}+C_{46}) \qquad (D;2;17)$$

$$h_{22} = l^2C_{66} + m^2C_{22} + n^2C_{44} + 2mnC_{24} + 2nlC_{46} + 2mlC_{26} \qquad (D;2;18)$$

$$h_{33} = l^2C_{55} + m^2C_{44} + n^2C_{33} + 2mnC_{34} + 2nlC_{35} + 2mlC_{45} \qquad (D;2;19)$$

Equations (D;2;11 to 13) may be expressed in matrix form as:

$$\begin{vmatrix} h_{11}-\rho c^2 & h_{12} & h_{13} \\ h_{12} & h_{22}-\rho c^2 & h_{23} \\ h_{13} & h_{23} & h_{33}-\rho c^2 \end{vmatrix} \begin{vmatrix} u'' \\ v'' \\ w'' \end{vmatrix} = 0 \qquad (D;2;20)$$

where u'', v'', w'', denote the second differential of u,v and w with respect of the propagation direction "S".

Following Kelvin (21) , a plane wave solution of the form

$$u,v,w, = (P\alpha, Q\beta, R\gamma,) e^{j(\omega t - \Gamma_s s)} \qquad (D;2;21)$$

is assumed, where $\Gamma_s = \alpha + j\beta$ is the propagation constant similar to that defined in the section on electromagnetic wave propagation, and P,Q,R, are the unit displacement vectors associated with a plane wave of normal (l , m , and n). α , β , and γ are the direction cosines of the particle displacement.

Equation (D;2;20) contains a set of linear simultaneous homogeneous equations and as such has a nontrivial solution only when the determinant of the ceofficients becomes zero.(22). Therefore:

$$\begin{vmatrix} h_{11}-\rho C^2 & h_{12} & h_{13} \\ h_{12} & h_{22}-\rho C^2 & h_{23} \\ h_{13} & h_{23} & h_{33}-\rho C^2 \end{vmatrix} = 0 \qquad (D;2;22)$$

It is evident from the symmetry of the above equation that three solutions of C are possible since the determinant has three real roots. Consequently , in general, three distinct propagation velocities will exsist corresponding to three different propagating waves, all having the same direction of propagation but different velocity and direction of particle displacement. In general none of the waves will have its particle displacement parallel or perpendicular to the direction of propagation, however if one of the three waves does have its particle displacement co-incident with the direction of phase velocity propagation , ie; longitudinal mode, it is found that the two remaining waves have their particle displacements perpendicular to the axis of propagation and hence are shear modes. The above is a consequence of the fact that the displacements of the three modes are mutually orthogonal (23).

Non perpendicular or non parallel directions of particle displacement, with respect to the phase velocity normal, depicts a condition of quasi-shear and quasi-longitudinal mode propagation. This situation is shown in FIG.(D;2;1).

It can also be shown that as a consequence of the condition that the system of wave equations are homogeneous and linearly dependent, the ratio of the component particle displacement directions of each of the waves is equal to the ratio of their co-factors in the determinant of equation (D;2;22),(22). Thus one obtains the relationship:

$$\alpha_i/(h_{22}-\rho c_i^2)(h_{33}-\rho c_i^2)-h_{23}^2 = \beta_i/(h_{23}h_{13})-h_{12}(h_{33}-\rho c_i^2)$$

$$= \gamma_i/(h_{12}h_{23})-h_{13}(h_{22}-\rho c_i^2) \qquad (D;2;23)$$

and also: $l^2+m^2+n^2 = \alpha^2+\beta^2+\gamma^2 = 1 \qquad (D;2;24)$

The deviation ψ_i of any of the mode displacements from the wave normal is given by the expression:

$$\cos(\psi_i) = l\alpha_i + m\beta_i + n\gamma_i \qquad (D;2;25)$$

D;3 (ENERGY FLOW IN ANISOTROPIC ELASTIC MATERIALS)

The acoustic energy flow associated with a given propagating elastic wave is defined as the product of the elastic stored energy and the velocity of propagation. In general this may be expressed, for an anisotropic medium, as:

$$P_u = -\left(T_{11}\frac{\partial u}{\partial t} + T_{12}\frac{\partial v}{\partial t} + T_{13}\frac{\partial w}{\partial t} \right) \qquad (D;3;1)$$

$$P_v = -\left(T_{21}\frac{\partial u}{\partial t} + T_{22}\frac{\partial v}{\partial t} + T_{23}\frac{\partial w}{\partial t} \right) \qquad (D;3;2)$$

$$P_w = -\left(T_{31}\frac{\partial u}{\partial t} + T_{32}\frac{\partial v}{\partial t} + T_{33}\frac{\partial w}{\partial t} \right) \qquad (D;3;3)$$

and $$\underline{P} = \left(P_u^2 + P_v^2 + P_w^2 \right)^{\frac{1}{2}} \qquad (D;3;4)$$

The resultant of the above energy flux components may be considered to be the mechanical Poynting Vector.

In tensor notation equation (D;3;4) becomes:

$$P_i = -T_{ij}\frac{\partial u_j}{\partial t} \qquad (D;3;5)$$

It has been shown (26) that although the direction of phase velocity propagation of all three possible elastic waves in an anisotropic medium is the same, the elastic energy flux associated with these waves is not generally collinear with this direction. More over the three waves in general have energy flux vectors which are all different from one another. This situation is depicted in FIG.(D;3;1) given originally by Mossgrave. (26).

The diagram of FIG.(D;3;1) is meant to represent the three beams of elastic wave energy radiated from a source at O and propagating through an anisotropic medium. The line S represents the common phase velocity propagation direction, and the distances t_1, t_2, t_3, are respectively proportional to the phase velocities of modes 1, 2, and 3. The angles ξ_1, ξ_2, ξ_3, indicate the deviation of energy flux from the wave normal S. Wave fronts are taken as parallel to the surface AOB . Mossgrave has also indicated that upon reflection at the free surface CDE the energy ray travels back along its original oblique

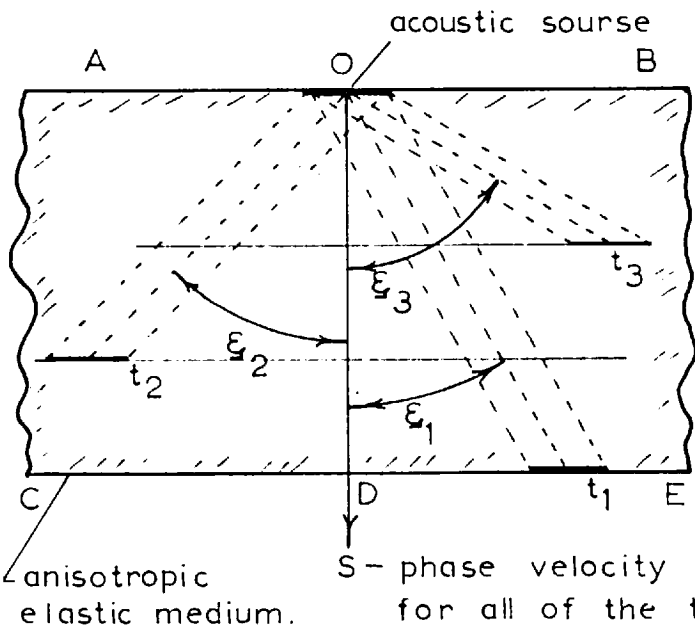

F I G. (D;3;1) **Energy propagation diagram**

path, such that the deviation angle ξ_i is not accumulative.

From consideration of equations (D;3;1 to 3) it is evident that generally the x,y,and z components of the mechanical Poynting Vector will not be proportional to the magnitude of the particle displacement in that direction and hence the resultant energy flux will not have the same direction cosine as the wave normal, thereby giving rise to off-axis energy propagation.

D:4 (ELASTIC WAVE PROPAGATION IN PIEZOELECTRIC MEDIA)

In the preceding section elastic wave propagation in anisotropic media has been analysed resulting in the derivation of equations from which all the desired information may be obtained. For the case in question in this work however one finds that the material which is utilised , namely crystal quartz , is not only anisotropic but piezoelectric as well. It is therefore necessary to investigate the effect which this pie zoelectric phenomenon has upon elastic wave propagation within the material and hence to determine what modifications have to be made to the equations of section (D;3).

The analysis given here is basically that given by Kyame.(27).

To analyse the situation it is required to simultaneously find a solution to Mawwell's equations concerning electromagnetics and Newton's equations of motion.

From thermodynamic considerations it is possible to derive the mechanical and electrical equations of state applicable to the situation. (28) . Thus one has:

$$T_{ij} = C_{ijkl}\, S_{kL} - e_{ijm}\, E_m \qquad (D;4;1)$$

and

$$D_k = e_{ijk}\, S_{ij} + \mathcal{E}_{mk}\, E_m \qquad (D;4;2)$$

where $i;j;k;l;m = 1,2,3.$

The forgoing equations apply for adiabatic conditions and negligible conductivity. Where C_{ijkl} is the elastic constant tensor for constant electric field and e_{ijk} represents the piezoelectric constant tensor while $\mathcal{E}_{mk}$ is the dielectric permittivity tensor.

Assuming an infinite medium and taking the x or 1 axis as the direction of propagation one finds that for plane wave conditions the equations become.

$$T_{il} = C_{ilkl}\, S_{kl} - e_{ilm}\, E_m \qquad (D;4;3)$$

$$D_k = e_{ilk}\, S_{il} + \mathcal{E}_{im}\, E_m \qquad (D;4;4)$$

since $$\partial / \partial y = \partial / \partial z = 0 \qquad (D;4;5)$$

Applying the above assumed propagation conditions to Maxwell's equations of section (B;2) and further stipulating the condition that the medium be magnetically isotropic one finds that:

$$\frac{\partial D_1}{\partial t} = 0 \,, \quad \frac{\partial D_2}{\partial t} = \frac{\partial H_3}{\partial x_1} \,, \quad \frac{\partial D_3}{\partial t} = -\frac{\partial H_2}{\partial x_1} \qquad (D;4;6)$$

and:

$$\frac{\partial B_1}{\partial t} = 0 \,, \quad \frac{\partial B_2}{\partial t} = -\frac{\partial E_3}{\partial x_1} \,, \quad \frac{\partial B_3}{\partial t} = \frac{\partial E_2}{\partial x_1} \qquad (D;4;7)$$

Now substituting the expression for $\partial T_{ij} / \partial x_j$ obtainable from (D;4;3) into the equation of motion (D;2;7) taking due account of the direction of propagation, one observes that :

$$\rho \frac{\partial^2 u_i}{\partial^2 t} = \frac{\partial T_{il}}{\partial x_1} = C_{ilkl} \frac{\partial^2 u_k}{\partial^2 x_1} - e_{ilm} \frac{\partial E_m}{\partial x_1} \qquad (D;4;8)$$

also $$\frac{\partial^2 E_2}{\partial^2 x_1} = \mu \frac{\partial}{\partial t} \left(\frac{\partial H_3}{\partial x_1} \right) \quad \text{from (D;4;7)} \qquad (D;4;8)$$

and so upon combining with (D;4;6) one has:

$$\partial^2 E_2 / \partial^2 x_1 = \mu \, \partial^2 D_2 / \partial^2 t \qquad \text{(D;4;10)}$$

or $$\partial^2 E_p / \partial^2 x_1 = \mu \, \partial^2 D_p / \partial^2 t$$

Using the above expressions in conjunction with equation (D;4;4) and remembering that:

$$S_{kl} = \partial u_k / \partial x_1$$

it follows that:

$$\frac{\partial^2 E_p}{\partial^2 x_1} = \mu \frac{\partial^2}{\partial^2 t} \left(e_{ilp} \frac{\partial u_i}{\partial x_1} + \varepsilon_{mp} E_m \right) \qquad \text{(D;4;11)}$$

where $i:j:k = 1,2,3$.

and $p = 2,3$

It is possible to obtain an expression for E_1 from (D4;4) and so upon elimination of E_1 from equation (D;4;11) one has:

$$\frac{\partial^2 E_p}{\partial^2 x_1} = \mu \frac{\partial^2}{\partial^2 t} \left(e'_{ilp} \frac{\partial u_i}{\partial x_1} + \varepsilon'_{qp} E_q \right) \qquad \text{(D;4;12)}$$

where $$e'_{ilp} = e_{ilp} + \frac{\varepsilon_{1p} e_{ill}}{\varepsilon_{11}} \qquad \text{(D;4;13)}$$

and $$\varepsilon'_{qp} = \varepsilon_{qp} + \frac{\varepsilon_{1p} \varepsilon_{q1}}{\varepsilon_{11}} \qquad \text{(D;4;14)}$$

and also where

$$i = 1,2,3 \quad \text{but} \quad p:q = 2,3$$

Similarly eliminating E_1 from equation (D;4;8) gives the modified elastic wave equation as follows:

$$\rho \frac{\partial^2 u_i}{\partial^2 t} = C'_{ilkl} \frac{\partial^2 u_k}{\partial^2 x_1} - e'_{ilq} \frac{\partial E_q}{\partial x_1} \qquad (D;4;15)$$

where now: $$C'_{ilkl} = C_{ilkl} + \frac{e_{ill}\, e_{llk}}{\varepsilon_{11}} \qquad (D;4;16)$$

the above primed coefficients are usually refered to as " stiffened" coefficients.

Inspection of equations (D;4;12 and D;4;15) reveals that there are five coupled wave equations to be solved since ,i:k=1,2,3, and p:q=2,3.

If a plane wave solution of the form:

$$u_i = \hat{u}_i\, e^{\,j(\omega t - \Gamma x_1)} \qquad (D;4;17)$$

and $$E_p = \hat{E}_p\, e^{\,j(\omega t - \Gamma x_1)} \qquad (D;4;18)$$

is assumed , one finds that the wave equations simplify considerably to:

$$\Gamma^2 C'_{ilkl}\, u_k - \rho\omega^2 u_i + j\Gamma e'_{ilq} E_q = 0 \qquad (D;4;19)$$

and $$j\mu\Gamma\omega^2 u_i e'_{ilp} + \Gamma^2 E_p - \mu\omega^2 \varepsilon'_{qp} E_q = 0 \qquad (D;4;20)$$

where as before: i:k = 1,2,3 and q:p= 2,3

In the assumed solutions of (D;4;17and 18) the symbol ^ signifies the maximum value.

Expanding equations (D;4;19 and 20) and arranging in matrix form results in the following:

$$\begin{vmatrix} (\Gamma^2 C'_{1111}-\rho\omega^2) & (\Gamma^2 C'_{1112}) & (\Gamma^2 C'_{1113}) & (j\Gamma e'_{211}) & (j\Gamma e'_{311}) \\ (\Gamma^2 C'_{1211}) & (\Gamma^2 C'_{1212}-\rho\omega^2) & (\Gamma^2 C'_{1213}) & (j\Gamma e'_{221}) & (j\Gamma e'_{321}) \\ (\Gamma^2 C'_{1311}) & (\Gamma^2 C'_{1312}) & (\Gamma^2 C'_{1313}-\rho\omega^2) & (j\Gamma e'_{231}) & (j\Gamma e'_{331}) \\ (j\mu\Gamma\omega^2 e'_{211}) & (j\mu\Gamma\omega^2 e'_{212}) & (j\mu\Gamma\omega^2 e'_{213}) & (\Gamma^2-\mu\omega^2\varepsilon'_{22}) & (-\mu\omega^2\varepsilon'_{32}) \\ (j\mu\Gamma\omega^2 e'_{311}) & (j\mu\Gamma\omega^2 e'_{312}) & (j\mu\Gamma\omega^2 e'_{313}) & (-\mu\omega^2\varepsilon'_{23}) & (\Gamma^2-\mu\omega^2\varepsilon'_{33}) \end{vmatrix} \begin{vmatrix} u_1 \\ u_2 \\ u_3 \\ E_2 \\ E_3 \end{vmatrix} = 0$$

(D;4;21)

As in the previous case, a nontrivial solution of this set of five linear homogeneous equations exsists only when the determinant of the coefficients vanishes. The solution of this determinant will obviously give rise to a fifth order equation in $(\omega/\Gamma)^2 = C$. Thus it is evident that there will in general be five possible phase velocities and hence five different propagating waves in a piezoelectric medium . The above is the result of the piezoelectric coupling effect, and this can easly be seen to be the case by allowing the piezoelectric coefficients in the determinant of equation (D;4;21) to vanish.

This gives:

$$\begin{vmatrix} (\Gamma^2 C'_{1111}-\rho\omega^2) & (\Gamma^2 C'_{1112}) & (\Gamma^2 C'_{1113}) & 0 & 0 \\ (\Gamma^2 C'_{1211}) & (\Gamma^2 C'_{1212}-\rho\omega^2) & (\Gamma^2 C'_{1213}) & 0 & 0 \\ (\Gamma^2 C'_{1311}) & (\Gamma^2 C'_{1312}) & (\Gamma^2 C'_{1313}-\rho\omega^2) & 0 & 0 \\ 0 & 0 & 0 & (\Gamma^2-\mu\omega^2\varepsilon'_{22}) & (-\mu\omega^2\varepsilon'_{32}) \\ 0 & 0 & 0 & (-\mu\omega^2\varepsilon'_{23}) & (\Gamma^2-\mu\omega^2\varepsilon'_{33}) \end{vmatrix} = 0 \quad \text{(D;4;22)}$$

Inspection of the above equation reveals that the original five by five determinant has become separated into a three by three, and a two by two determinant. The 3 by 3 part is of the same form as that obtained for elastic wave propagation, along the x axis in anisotropic

media except that the " stiffened " elastic coefficients are used. One expects therefore to obtain the velocities of the acoustic waves from this determinant. Similar consideration reveals that the two by two portion of equation (D;4;22) gives the phase velocities of electromagnetic waves propagating through the medium. It is therefore apparent that the presence of piezoelectricity in a medium serves to couple the elastic and electromagnetic waves. Kyame,(29), has indicated that this coupling effect gives rise to two classes of propagation, ie: fast elastic waves, which are in reality mechanical deformations accompanying the electromagnetic waves, and slow electromagnetic waves which can be considered as being the electromagnetic field variations associated with the elastic disturbance.

Using equation (D;4;22) Kyame has shown that the piezoelectric coupling effects, under the conditions used in this work, give rise to only very small modifications to the pure acoustic phase velocities.(29). In fact if one uses the 3 by 3 determinant in equation (D;4;22) along with the stiffened elastic coefficients in evaluating the phase velocities, it is found that the error introduced by neglecting the rest of the determinant , is given by the square of the ratio of the acoustic to the electromagnetic phase velocities in the medium.(30). For the situation considered in this work the correction term is found to be approximately 1×10^{-9} , which is far less that the uncertainty in the original experimental determination of the elastic constants of the crystal. If only the unstiffened elastic constants are used in the calculations the error introduced is still only of the order of one percent. For all subsequent velocity calculations the medium will be considered to be purely anisotropic and not piezoelectric and hence the unstiffened elastic constants will be used.

D;5 (ELASTIC CONSTANTS FOR ROTATED AXES)

Often it is found necessary to determine the elastic constants of a medium in a coordinate system different from the crystallographic coordinate system, in which the elastic constants are usually specified. The above can be accomplished quite readily through the use of tensor transformation formulae.

Generally the elastic constants may be expressed as a tensor of the fourth rank and thus one expects to have 81 terms in the expression. However due to the condition of symmetry , ie; equation (D;1;34), only 21 of the terms are independent and so the tensor is usually written as:

$$C_{ijkL} = C_{ij} = \begin{vmatrix} C_{11} & C_{21} & C_{31} & C_{41} & C_{51} & C_{61} \\ C_{12} & C_{22} & C_{32} & C_{42} & C_{52} & C_{62} \\ C_{13} & C_{23} & C_{33} & C_{43} & C_{53} & C_{63} \\ C_{14} & C_{24} & C_{34} & C_{44} & C_{54} & C_{64} \\ C_{15} & C_{25} & C_{35} & C_{45} & C_{55} & C_{65} \\ C_{16} & C_{26} & C_{36} & C_{46} & C_{56} & C_{66} \end{vmatrix} \qquad (D;5;1)$$

where in the contracted tensor notation:

1=11	4=23	
2=22	5=13	
3=33	6=12	and i:j= 1,2,3,4,5,6.

From tensor theory one has the transformation formulae as:

$$C''_{ijkL} = \frac{\partial'' x_i}{\partial x_i} \frac{\partial'' x_j}{\partial x_j} \frac{\partial'' x_k}{\partial x_k} \frac{\partial'' x_L}{\partial x_L} (C_{ijkL}) \qquad D;5;2)$$

where C''_{ijkL} represents the tensor of modified elastic constants pertaining to the x" coordinate system. Mason ,(30), has given a simple table form for calculating the results of the operations indicated by equation (D;5;2)

D:6 (ELASTIC CONSTANTS FOR QUARTZ WITH ROTATED "Y" CUT)

In this work the only crystal cuts of interest are the so called rotated Y cuts, which correspond to the axis of the wave normal being rotated about the X axis in the YZ plane.

For quartz , the non zero elastic constants are as follows:

$$
\begin{aligned}
&C_{1111} = C_{11} && C_{1313} = C_{2323} = C_{55} = C_{44} \\
&C_{1122} = C_{2211} = C_{12} && C_{1212} = C_{66} = (C_{11} - C_{12})/2 \\
&C_{1133} = C_{3311} = C_{13} && C_{2222} = C_{22} \\
&C_{1123} = C_{2311} = C_{14} && C_{2223} = C_{2322} = C_{24} = C_{42} \\
&C_{3333} = C_{33} && C_{1213} = C_{1312} = C_{65} = C_{56} = C_{14} = -C_{24}
\end{aligned}
\qquad (D;6;1)
$$

From the above definition it is obvious that the direction cosines for the rotated Y cut are:

$$l = o \quad , \; m=\cos(-\theta)=\cos(\theta), \quad n=\cos(90-\theta)=\sin(-\theta) \qquad (D;6;2)$$

Upon substitution of (D;6;1 and 2) into equation (D;5;2) and expanding one arrives at the following expressions: (32).

$$
\begin{aligned}
C''_{11} &= C_{11} \\
C''_{22} &= C_{22}m^4 + C_{33}n^4 + 2(2C_{44}+C_{23})m^2n^2 + 4C_{24}nm^3 + 4C_{34}n^3m \\
C''_{33} &= C_{22}n^4 + C_{33}m^4 + 2(2C_{44}+C_{23})m^2n^2 - 4C_{24}n^3m - 4C_{34}nm^3 \\
C''_{44} &= C_{44} + (C_{22}+C_{33}-4C_{44}-2C_{23})n^2m^2 + 2(C_{24}-C_{34})(nm^3-n^3m) \\
C''_{55} &= C_{55}m^2 + C_{66}n^2 - 2C_{56}nm \\
C''_{66} &= C_{55}n^2 + C_{66}m^2 + 2C_{56}mn \\
C''_{12} &= C_{12}m^2 + C_{13}n^2 + 2C_{14}mn \\
C''_{13} &= C_{12}n^2 + C_{13}m^2 - 2C_{14}mn \\
C''_{14} &= C_{14}(m^2-n^2) + (C_{13}-C_{12})mn
\end{aligned}
$$

and

$$C''_{23} = C_{23}(m^2+n^2) + (C_{22}+C_{33}-4C_{44})m^2n^2 + 2(C_{24}-C_{34})(n^2-m^2)mn$$

$$C''_{24} = C_{24}m^2 - C_{34}n^2 - 3n^2m^2(C_{24}-C_{34}) + ((C_{33}n^2 - C_{22}m^2 + (C_{23}+2C_{44})\cdot (m^2-n^2)\ )\ mn$$

$$C''_{34} = -C_{24}n^4 + C_{34}m^4 + 3n^2m^2(C_{24}-C_{34}) + ((C_{33}m^2 - C_{22}n^2 - (C_{23}+2C_{44})\cdot (m^2-n^2)\ )\ mn$$

$$C''_{56} = C_{56}(m^2-n^2) + (C_{55}-C_{66})mn$$

$$C''_{15} = C''_{16} = C''_{25} = C''_{26} = C''_{35} = C''_{36} = C''_{45} = C''_{46} = 0$$

(D;6;3)

The transformation equations for the dielectric and expansion coefficients are as follows:

$$\alpha''_{11} = \alpha_{11} \qquad \varepsilon''_{11(r)} = \varepsilon_{11(r)}$$

$$\alpha''_{22} = \alpha_{22}m^2 + \alpha_{33}n^2 \qquad \varepsilon''_{22(r)} = \varepsilon_{22(r)}m^2 + \varepsilon_{33(r)}n^2$$

$$\alpha''_{33} = \alpha_{22}n^2 + \alpha_{33}m^2 \qquad \varepsilon''_{33(r)} = \varepsilon_{22(r)}n^2 + \varepsilon_{33(r)}m^2$$

$$\alpha''_{23} = mn(\alpha_{22} - \alpha_{33}) \qquad \varepsilon''_{23(r)} = mn(\varepsilon_{22(r)} - \varepsilon_{33(r)})$$

$$\alpha''_{12} = \ ''_{13} = 0$$

(D;6;4).

D:7 (REFLECTION AND REFRACTION OF ELASTIC WAVES)

At this point it is of interest to consider the reflection and refraction of elastic waves at an interface. Consideration will first be given to the isotropic media case.

In general it is found that an elastic waves impinging upon a slipfree boundary will give rise to the generation of four other waves, two of which will be reflected, while the other two will be refracted. One of the reflected and refracted components is a shear wave and the other is found to be a compressional wave. (33).

To illustrate the above consider FIG.(D;7;1), depicting a plane compressional wave of amplitude A_1 propagating in the XY plane through an isotropic medium of density ρ_a . This elastic wave is then incident upon an interface , represented by the YZ plane , at an angle θ. The amplitudes and wave normals of the reflected compressional and shear waves are given as A_2, θ_2 and A_3, θ_3 respectively and similarly the refracted longitudinal and transverse waves propagating in medium (b) are designated by A_4, θ_4 and A_5, θ_5 .

For conditions of equilibrium it is necessary that the normal and tangential particle displacements and stress be continuous. These conditions are represented symbolically as:

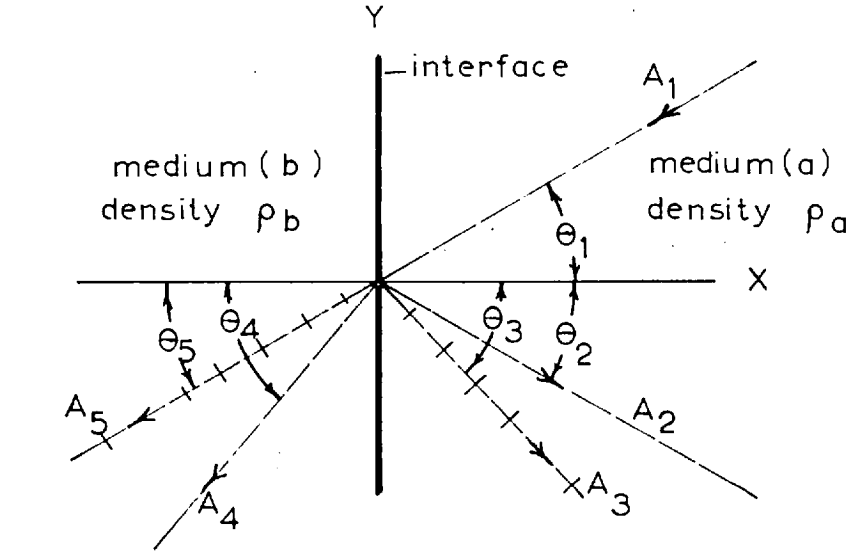

— — — represents longitudinal waves

+ + + represents shear waves

FIG.(D;7;1)

$$\sum u_a = \sum u_b \qquad \sum (T_{xx})_a = \sum (T_{xx})_b$$

$$\sum v_a = \sum v_b \qquad \sum (T_{xy})_a = \sum (T_{xy})_b$$

$$\sum w_a = \sum w_b \qquad \sum (T_{zx})_a = \sum (T_{zx})_b \qquad (D;7;1)$$

where u,v,w refer to the particle displacements in the x,y,and z directions , and the subscripts a and b denote the particular medium.

The equations of (D;7;1) may be written in a different form through the use of equations (D;1;31 and 32) . And so :

$$\sum (\lambda \Delta + 2\mu \frac{\partial u}{\partial x})_a = \sum (\lambda \Delta + 2\mu \frac{\partial u}{\partial x})_b \qquad (D;7;1;d)$$

$$\sum (\mu (\frac{\partial v}{\partial x} + \frac{\partial u}{\partial y}))_a = \sum (\mu (\frac{\partial v}{\partial x} + \frac{\partial u}{\partial y})_b \qquad (D;7;1;e)$$

$$\sum (\mu (\frac{\partial w}{\partial x} + \frac{\partial u}{\partial z}))_a = \sum (\mu (\frac{\partial w}{\partial x} + \frac{\partial u}{\partial z}))_b \qquad (D;7;1;f)$$

where λ and μ are the two independent elastic constants of an isotropic medium and are usually known as Lame's constants, while Δ is the cubical dilatation and is given as :

$$\Delta = S_{11} + S_{22} + S_{33} \qquad (D;7;2)$$

For an isotropic medium Lame's constants are as follows:

$$\lambda = C_{12} = C_{13} = C_{21} = C_{23} = C_{31} = C_{32}$$

$$\mu = C_{44} = C_{55} = C_{66} = (C_{11} - C_{12}) / 2 \qquad (D;7;3)$$

and $$\lambda + 2\mu = C_{11} = C_{22} = C_{33}$$

Knott, Macelwane and Sohon,(33), have shown that the conditions which apply to the reflection and refraction of light also applies in this case. Therefore one has from Snell's Law:

$$\frac{\sin(\theta_1)}{C_1} = \frac{\sin(\theta_2)}{C_2} = \frac{\sin(\theta_3)}{C_3} = \ , \ , \ , = \frac{\sin(\theta_i)}{C_i} \qquad (D;7;4)$$

where C_i is the propagating velocity of the elastic wave,of amplitude A_i.

Now considering the first three parts of (D;7;1) in the light of equation (D;7;4), one may write:

$$(A_1-A_2)\cos(\theta_1)+ A_3\sin(\theta_3)- A_4\cos(\theta_4)-A_5\sin(\theta_5)= 0 \qquad (D;7;5)$$

and

$$(A_1+A_2)\sin(\theta_1)+ A_3\cos(\theta_3)- A_4\sin(\theta_4)+ A_5\cos(\theta_5)= 0 \qquad (D;7;6)$$

also from (D;7;1;d) :

$$(A_1+A_2)C_1\cos(2\theta_3)-A_3C_3\sin(2\theta_3)-A_4C_4(\rho_b/\rho_a)\cos(2\theta_5)-A_5C_5(\rho_b/\rho_a)\cdot \cdot\sin(2\theta_5) = 0 \qquad (D;7;7)$$

similarly from (D;7;1;e) :

$$\rho_a C_3^2\left[(A_1-A_2)\sin(2\theta_1)-A_3(C_1/C_3)\cos(2\theta_3)\right]-\rho_b C_5^2\left[(C_1/C_4)A_4\sin(2\theta_4)- A_5(C_1/C_5)\cos(2\theta_5)\right]= 0 \qquad (D;7;8)$$

By appropriate substitutions of equations (D;7;4) into the above four equations, a set of four simultaneous equations is obtained, which when solved, gives the relative amplitudes of the reflected and refracted waves in terms of the amplitude of the incident wave.

For the case of reflection and refraction of incident shear waves consider FIG.(D:7:2), depicting a shear wave of amplitude B_1 incident upon an interface YY , at an angle ϕ_1. The reflected and refracted components are specified as in the previous case. Here it is necessary to investigate two seperate situations, namely when the incident wave particle displacement is perpendicular or parallel to the Z axis, since the polarisation of the incident wave determines whether or not a mode conversion will result. When the incident shear waves particle displacement is parallel to the z axis no mode conversion exsists and hence no refracted or reflected compressional waves are present. (34)

Considering first the case of **parallel** particle displacement, t-here is only one reflected and one refracted shear wave, so that one has :

$$\phi_1 = \phi_2$$

Also $$\sin(\phi_5) \,/\, \sin(\phi_1) = C_5/C_1 \qquad (D;7;9)$$

Now from (D;7;1;c):

$$B_1 + B_2 - B_5 = 0$$

and so one has from (D;7;1;f):

$$\rho_a \sin(2\phi_1)(B_1 - B_2) - B_5 \rho_b \sin(2\phi_5) = 0 \qquad (D;7;10)$$

and so B_2 and B_5 can be determined in terms of B_1, the incident shear wave amplitude.

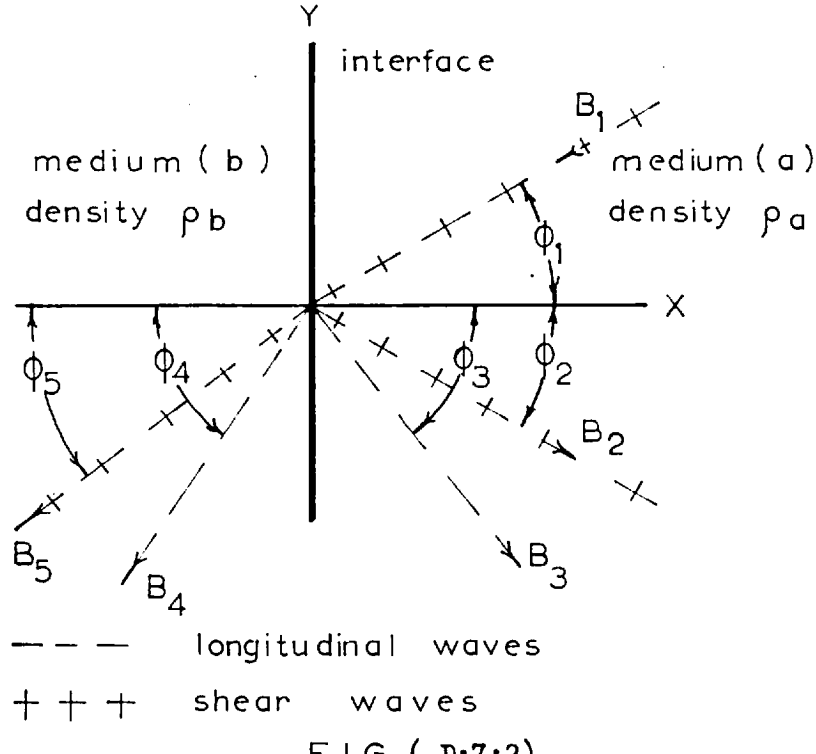

FIG. (D;7;2)

When the incident shear wave polarisation is such that the part-icle displacement is in the XY plane, four waves are in general gener-

ated as shown in FIG.(D;7;2). Upon applying the appropriate boundary conditions to the equations of (D;7;1) one arrives at the equations:

$$(B_1-B_2)\sin(\phi_1)+B_3\cos(\phi)+B_4\cos(\phi)-B_5\sin(\phi_5) = 0 \qquad (D;7;11)$$

and $$(B_1+B_2)\cos(\phi_1)+B_3\sin(\phi_3)-B_4\sin(\phi_4)-B_5\cos(\phi_5)= 0 \qquad (D;7;12)$$

also $$C_2(B_1+B_2)\sin(2\phi_1)-B_3C_3\cos(2\phi_1)+B_4C_4(p_b/p_a)\cos(2\phi_5)-B_5C_5(p_b/p_a)\cdot \sin(2\phi_5) = 0 \qquad (D;7;13)$$

and $$p_aC_2\{(B_1-B_2)\cos(2\phi_1)-B_3(C_1/C_3)\sin(2\phi_3)\}-p_bC_5\{(C_5/C_4)B_4\sin(2\phi_4)+B_5\cos(2\phi_5)\} = 0 \qquad (D;7;14)$$

Here again the amplitude of the reflected and refracted waves can be determined in terms of the incident wave amplitude, from the above equations.

SPECIAL CASE OF NORMAL INCIDENCE

A (NORMALLY INCIDENT LONGITUDINAL WAVE)

For the special case of normal incidence the equations developed previously in section (D;7;) are considerably simplified. One has for the longitudinal case that:

$$\theta_1 = \theta_2 = \theta_4 = 0$$

and so equation (D;7;5) becomes:

$$(A_1-A_2) - A_4 = 0 \qquad (D;7;15)$$

similarly for (D;7;6):

$$(A_3+A_5) = 0 \qquad (D;7;16)$$

also (D;7;7) simplifies to:

$$(A_1+A_2)C_1 - A_4C_4 \left(\rho_b/\rho_a \right) = 0 \qquad (D;7;17)$$

and so (D;7;8) reduces to:

$$-\rho_a C_3^2 A_3 (C_1/C_3) + A_5 (C_1/C_5) \rho_b C_5^2 = 0 \qquad (D;7;18)$$

From the above equations one finds that:

$$A_5 = A_3 = 0$$

and also that:

$$A_2 = A_1 \frac{(\rho_b C_4 - \rho_a C_1)}{(\rho_b C_4 + \rho_a C_1)} \qquad (D;7;19)$$

and:

$$A_4 = A_1 \frac{(2\rho_a C_1)}{(\rho_b C_4 + \rho_a C_1)} \qquad (D;7;20)$$

Thus it can be seen that for a normally incident compressional wave only one reflected and one refracted wave are generated.

Usually the product ρC, being the product of density and velocity of acoustic phase propagation, is defined as the characteristic mechanical impedance of the medium. Thus equations (D;7;19 and 20) may be written as:

$$A_2 = A_1 \frac{(Z_{o(b)} - Z_{o(a)})}{(Z_{o(b)} + Z_{o(a)})} \qquad (D;7;21)$$

and

$$A_4 = A_1 \frac{(2\, Z_{o(a)})}{(Z_{o(b)} + Z_{o(a)})} \qquad (D:7:22)$$

where

$$Z_{o(a)} = \rho_a C_a \qquad (D:7:23)$$

and is the characteristic impedance of medium a .

It is possible now to define a mechanical reflection coefficient such that:

$$\underset{\sim}{\rho} = A_2/A_1 = \frac{Z_{o(b)} - Z_{o(a)}}{Z_{o(b)} + Z_{o(a)}} \qquad (D;7;24)$$

Equation (D;7;24) is of the same form as the voltage reflection coefficient normally associated with electrical transmission lines, and as such is of special significance in this work as it indicates that the mechanical impedance of a medium may be determined in terms of the mechanical impedance of another medium merely by measurement of the reflection coefficient. It should be noted here that in general $Z_{o(a)}$ and $Z_{o(b)}$ are complex and so $\underset{\sim}{\rho}$ will be complex.

B (NORMALLY INCIDENT SHEAR WAVE)

For conditions of a normally incident shear wave it may be shown that once more no mode conversion occurs and thus no compressional waves are produced. The equations (D;7;11 to 14) simplify to :

$$B_1 + B_2 - B_5 = 0 \qquad (D;7;25)$$

and

$$p_a C_1 (B_1 - B_2) - p_b C_5 B_5 = 0 \qquad (D;7;26)$$

which in turn give:

$$B_2 = B_1 \frac{(Z_{o(a)} - Z_{o(b)})}{(Z_{o(a)} + Z_{o(b)})} = B_1 (\underset{\sim}{\rho}) \qquad (D;7;27)$$

and

$$B_5 = B_1 \frac{(2 Z_{o(a)})}{(Z_{o(a)} + Z_{o(b)})} \qquad (D;7;28)$$

Equation (D;7;27) may be used to give the magnitude of the reflected wave when the interface is a free surface, by setting $p_b = 0$. Thus one can see that complete acoustic reflection is achieved at a free

surface.

In the foregoing analysis it has been found that for the general case of reflection and refraction in isotropic media, ten wave components must be considered in the complete solution. The situation is naturally more complicated when anisotropic materials are involved since, as was shown in section (D;2) , three independent modes may exsist in such media. It follows therefore that to satisfy all possible boundary conditions at the interface, for the reflection and refraction of elastic waves in anisotropic materials,will involve the determination of fifteen separate propagating components. Clearly this is an extremely complicated problem and as such will not be considered here.

In this work, elastic wave propagation in anisotropic materials is restricted to pure mode and normal incidence conditions. These restrictions immediately simplify the problem to one resembling that just considered, so that the equations developed pertaining to the acoustic impedance and reflection coefficients , etc. apply. (34)

D:8 (EXCITATION OF ELASTIC WAVES)

The mechanism by which the acoustic waves are generated in piezoelectric crystals will now be considered. For this analysis any coupling between elastic and electromagnetic disturbances will be neglected. The exciting conditions are depicted in FIG.(D;8;1) . Here the piezoelectric crystal is placed between the posts of a re-entrant cavity, across which an R.F. electric field $\underline{E}$ exsists. This electric field is assumed to have no axial dependence and only time dependence of the form $e^{j\omega t}$. Plane wave conditions are also assumed, this assumption being quite valid since the crystal dimensions are very much larger than the sonic wavelength. For the same reason the quartz medium is considered as being infinite.

The wave equation applicable to this situation is given by (D;-4;8) . Since one is concerned only with propagation in one direction, this equation may be simplified accordingly. Taking the x_2 or Y axis as the wave normal one has:

$$p \frac{\partial^2 u_i}{\partial^2 t} - C_{i2k2} \frac{\partial^2 u_k}{\partial^2 x_2} = - e_{i2m} \frac{\partial E_m}{\partial x_2} \qquad (D;8;1)$$

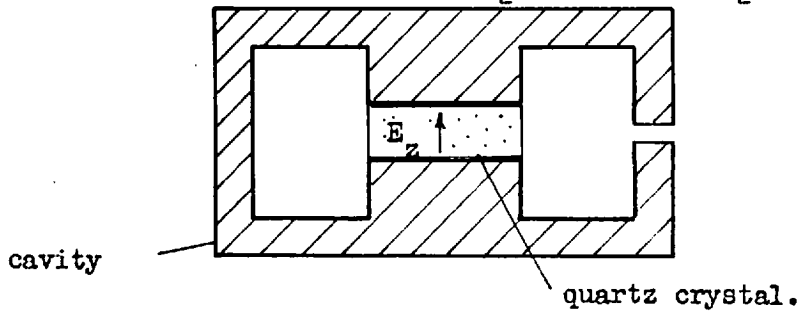

FIG. (D:8:1)

which may be written in the form:

$$\frac{\partial^2 u_k}{\partial^2 x_2} - \frac{1}{c^2} \frac{\partial^2 u_i}{\partial^2 t} = \frac{\partial}{\partial x_2} \left(\frac{e_{i2m} E_m}{C_{i2k2}} \right) \qquad (D;8;2)$$

where C, the acoustic propagation velocity, is given as:

$$C = (C_{i2k2} / p)^{\frac{1}{2}} \qquad (D;8;3)$$

Equation (D;8;2) clearly represents a set of nonhomogeneous wave equations in which the driving force, or source of sound is the gradient in the piezoelectric stress.

Jacobson , (35) , has shown that much qualitative information about the process of excitation can be obtained if one develops the solution to the nonhomogeneous wave equation in terms of Green's function $\underline{G}$.

where: $$\underline{G} = \frac{G(x_2 - x_{2(o)})}{\omega} = \frac{j}{2\Gamma} e^{-j(\omega t \mp \Gamma (x_2 - x_{2(o)})} \qquad (D;8;4)$$

ie: (-)for $x_2 > x_{2(o)}$

(+)for $x_2 < x_{2(o)}$

and $x_{2(o)}$ represents the origin.

and so the particle displacement u_i is given in terms of a travelling wave having origin at $x_{2(o)}$.

Jacobson has further extended the use of Green's solution to the investigation of the behaviour of the generation process under pulsed conditions , by determining the solution to the wave equation in terms of the integral representation of the Dirac delta function. Using this approach Jacobson has found it possible to analyise the effect of various boundary conditions upon the acoustic generation mechanism, the results of such analysis being as follows:

(a) Generation of sound occurs only when there is a sharp gradient or discontinuity in the piezoelectric stress.

(b) For a free crystal surface, the generation zone extends only to an infinitesimal depth (dx_2) due to the fact that the piezoelectric stress $(e_{i2m} / C_{i2k2})\, E_m$ undergoes a transition from zero in air to a finite constant value,in the crystal, in a distance of only a few atomic cells. The foregoing is illustrated in FIG.(D;8;2).

In FIG:(D:8:2) the interface between a piezoelectric and a non-piezoelectric medium is represented by the vertical line at $(x_{2(o)}-dx_2)$. The region dx_2 is meant to signify the small zone in which the piezoelectric generation occurs. The gradient in the piezoelectric stress is depicted by the dashed line and as such indicates, a zero component in the nonpiezoelectric medium, a sharp gradient in the transition region and a constant value throughout the remainder of the piezoelectric material.

(c) If a pulse of axial electric field is applied parallel to the x_2 axis, two step function displacements are produced, both travelling along x_2 but in opposite direction. If medium (1) has the same mechanical impedance as medium (2) both waves will travel indefinitely in the $+x_2$ and $-x_2$ directions. However if the mechanical impedance of medium (1) is zero, ie: free surface, the negative travelling component

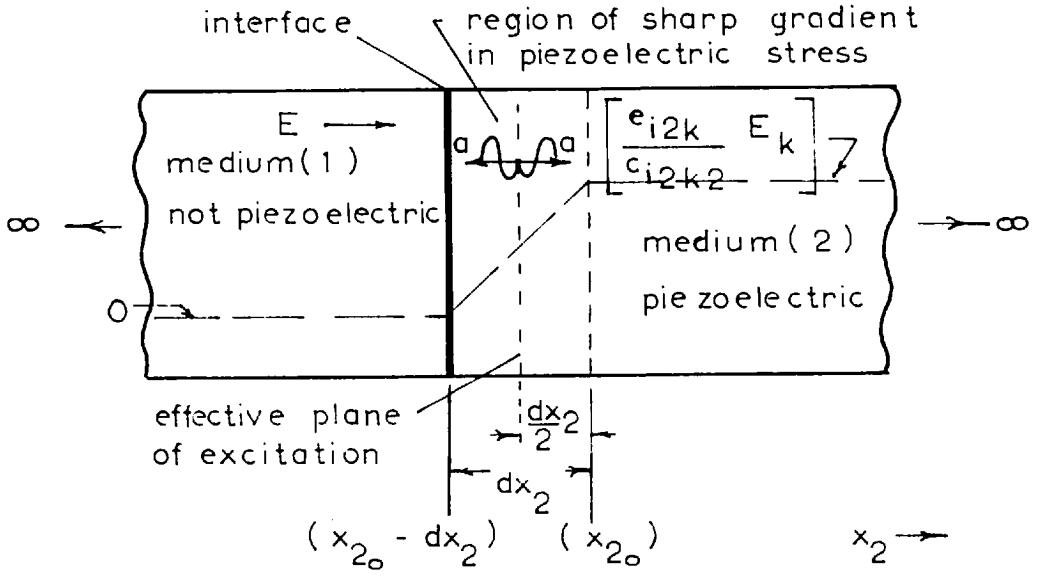

FIG.(D;8;2)

will be completely reflected and hence one has two waves propagating towards the right. As the region dx_2 approaches zero the phase of both waves will be the same and consequently one has,in effect,a single elastic wave of double amplitude propagating in medium (2). It follows therefore that a free surface results in twice the sonic energy

generation. If on the other hand medium (1) is not air but another substance such as a liquid, as is the case in this work, the effect will be intermediate between the two previously described cases, being dependent on the magnitude of the reflection coefficient at the interface.

Assuming that **dx = 0** and that the interfaceoccurs at $x_{2(o)}$ one has the following :

$$(e_{i2m} / C_{i2k2}) E_{m\ (1)} = 0 \qquad (D;8;5)$$

since (e_{12m}) is zero for medium one.

also: $$(e_{i2m} / C_{i2k2}) E_{m\ (2)} \neq 0 \qquad (D;8;6)$$

Mode type

It is possible to determine what modes will be generated within a given material by considering equation (D;4;1) and applying the boundary conditions. Thus for the direction of propagation indicated in FIG.(D:8;2):

$$T_{i2} = C_{i2k2} \frac{\partial u_k}{\partial x_2} - e_{i2m} E_m \qquad (D;4;1)$$

Considering now the free surface case, it is evident that the stress must vanish at $x_{2(o)}$. And so:

$$C_{i2k2} \frac{\partial u_k}{\partial x_2} = e_{i2m} E_m \qquad (D;8;7)$$

Now if a solution having spatial dependence of the form $e^{-j \nabla_s x_2}$ is assumed , the above equation simplifies to:

$$-j \nabla_s u_k C_{i2k2} = e_{i2m} E_m \qquad (D;8;8)$$

where Γ_s is meant to signify the sonic propagation constant.

Solving for the particle displacement gives:

$$u_k = \frac{j}{\Gamma_s} \frac{e_{i2m}}{C_{i2k2}} E_m \qquad (D;8;9)$$

Inserting the assumed time dependence of E_m and the spacial dependence of u_k one obtains generally:

$$u_k = \frac{j}{\Gamma_s} \frac{e_{ijm}}{C_{ijkl}} \hat{E}_m e^{j(\omega t - \Gamma_s x_1)} \qquad (D;8;10)$$

where ^ signifies maximum value with respect to time. In the above equation E_m is assumed to be constant across the crystal surface, however in practice this is not the case and hence the average value of E_m has to be used.

Equation (D;8;10) is identical with that given by Jacobson in his analysis using Green's function solution to the wave equation.(35), and when expanded gives the modes generated within the medium, for a specific exciting electric field.

D;9 (ELECTROMECHANICAL CONVERSION EFFICIENCY)

It is convenient at this point to investigate the efficiency of conversion from electromagnetic to elastic energy.

The sonic energy density W_s ,stored in a unit elastic element,is defined as the product of stress and strain, thus:

$$W_s = \tfrac{1}{2} \left(C_{ijkl} \frac{\partial u_k}{\partial x_l} \cdot \frac{\partial u_i}{\partial x_j} \right) \qquad (D;9;1)$$

Assuming plane wave propagation along the x_2 axis , as in FIG.(D;8;2), with particle displacement parallel to the x_1 axis and also specifying spatial dependence of the form $e^{-\Gamma_s x_2}$, one finds that equation(D;9;1) becomes:

$$W_{s(2)} = -\tfrac{1}{2} \left(C_{1212} \Gamma_s^2 u_1^2 \right) \qquad (D;9;2)$$

which when combined with equation (D;8;10) yields:

$$W_{s(2)} = \frac{e_{122}^2}{2\, C_{1212}} \left(\hat{E}_2 \right)^2 \qquad (D;9;3)$$

Now the average stored electrical energy within the same unit volume is given by :

$$W_{e(2)} = \tfrac{1}{2} \left(\hat{E}_2 \right)^2 \varepsilon_{22} \qquad (D;9;4)$$

and so the ratio of the stored sonic and electric energy, usually referred to as the square of the electromechanical coupling coefficient (K), is given as:

$$K^2 = W_{s(2)} / W_{e(2)} = \frac{e_{122}^2}{C_{1212}\, \varepsilon_{22}} \qquad (D;9;5)$$

The mechanical energy flux for the unit element is obtained from equation (D;3;5) as:

$$P_{s_{(2)}} = - T_{12} \frac{\partial u_1}{\partial t} = - C_{1212} \frac{\partial u_1}{\partial x_2} \cdot \frac{\partial u_1}{\partial t} \qquad (D;9;6)$$

When the assumed time and space dependence is inserted into the above equation , one obtains the average value of the energy flux per unit cross sectional area.

$$P_{s_{(2)}} = \frac{\omega K^2 \varepsilon_{22} \left(\hat{E}_2 \right)^2}{2\, \Gamma_s} \qquad (D;9;7)$$

The energy stored in a resonant cavity can be shown to be given by :

$$\text{Energy stored} = \frac{P_{in}\, Q}{\omega} \qquad (D;9;8)$$

where P_{in} is the power input to the cavity , Q the quality factor and ω the angular frequency .

Now solving for E_2 between equations (D;9;8 and 4) and inserting into (D;9;7) yields the expression:

$$P_{s(2)} = \frac{P_{in}\, Q\, K^2\, A\, C}{V} \qquad (D;9;9)$$

where V is the volume of the cavity gap, A the cross sectional area of the gap region and C the velocity of propagation.

The above expression was originally given by Bommel and Dransfield, (36) , and gives the acoustic energy conversion in terms of the electromagnetic power input to the cavity.

The one way electromechanical conversion efficiency may be obtained from equation (D;9;9), and so:

$$\eta = \frac{P_{s(2)}}{P_{in}} = \frac{Q\, K^2 \lambda_s}{2\pi d} \qquad (D;9;10)$$

where η is the one way conversion efficiency, λ_s the sonic wavelength and d the cavity gap width.

Obviously the process is reciprocal and hence the overall conversion efficiency η_o is equal to the square of equation (D;9;10)

$$\eta_o = \left(\frac{Q\, K^2 \lambda_s}{2\pi d}\right)^2 \qquad (D;9;11)$$

Inspection of equation (D;9;11) reveals that the conversion efficiency is inversely proportional to the square of the operating frequency . Also it is noted that η_o varies as the square of the cavity Q and from this point of view , a very high Q cavity is desirable. As is explained in section (. F; 1;2) however, bandwidth considerations limit the maximum usable Q to a relatively low value. It follows therefore that the only other variable in equation (D;9;11) is the crystal thickness d , and this dimension is in fact found to be restricted in minimum value as a consequence of the shortest acoustic travel time that can be accommodated.

In practice it is found that not all the electrical energy is stored in the cavity gap, as was assumed in the foregoing analysis. This means that the, cavity gap electrical energy storage efficiency, must be determined before the overall electromechanical conversion efficiency may be obtained.

It can easily be shown that if the cavity electrical energy storage efficiency is $\eta_{e\,(gap)}$, the overall electromechanical conversion efficiency is given by the expression:

$$\eta_o = \left(\frac{K^2 Q \lambda_s \eta_{e(gap)}}{2\pi d} \right)^2 \qquad \text{(D;9;12)}$$

where $$\eta_{e(gap)} = \frac{W_{e(gap)}}{W_{e(total)}} \qquad \text{(D;9;13)}$$

APPENDIX E

RESONANCE ISOLATOR THEORY

E: 1 (MAGNETODYNAMIC EQUATIONS)

It is beyond the scope of this work to develop the quantum mechanical theory regarding the electronic structure of ferrites which give rise to their unique magnetic properties at high frequencies. It will suffice to state the well known theory of Uhlenbeck and Goudsmit, (41), which proposes that an electron spins on its axis with an angular momentum $\underline{Ps}$, where:

$$\underline{Ps} = \pm \underline{ms}\, \hbar \qquad (E;1;1)$$

and here $\underline{ms}$ is the spin quantum number and can only assume values of $\pm \frac{1}{2}$, while $\hbar$, is Planck's constant.

The values of $\pm \frac{1}{2}$ indicate that the electron spin can be either positive or negative. An electron spinning on its axis creates a magnetic dipole which gives rise to a magnetic moment $\underline{us}$, which is expressed as:

$$\underline{us} = -2\left(\frac{\mu_o\, e}{2\, m}\right) \underline{ms}\ \hbar = -2\left(\frac{\mu_o\, e}{2\, m}\right) \underline{Ps} \qquad (E;1;2)$$

Here:

μ_o = free space permittivity , in henries/ meter
m = electron mass , in kilograms
e = electron charge , in coulombs

There is no significant contribution to the magnetic moment of an electron due to its orbital motion since in general the plane of the electron orbit moves in such a manner that the time average value of the component of angular momentum in a fixed direction is zero. This is a result of the nonuniform fields present in compounds.(43).

The torque acting on the electron due to its spin is given by the expression :

$$\underline{\tau} = d\, \underline{Ps} \,/\, dt \qquad (E;1;3)$$

The magnetic moment us and the angular momentum Ps are vector quantities and their ratio is termed the Gyromagnetic ratio,(e)(44).

Thus:

$$\Gamma_e = - \frac{u_o e}{m} \cong 2.8 \text{ Mc/sec./ oersted} \qquad (E;1;4)$$

E;2 (PRECESSIONAL MOTION)

Magnetism in materials results from the alignment of the the electron magnetic dipoles due to coupling of uncompensated electron spins. This coupling of the spins gives rise to magnetic regions or domains in which all the spins are aligned even in the absence of an external magnetic field. The material in aggregate does not appear to be magnetised due to the random orientation of these domains, however application of an external magnetic field swings the domains into alignment and hence the material exhibits magnetic properties. Saturation implies complete domain alignment throughout the material . It is of interest to note however that within the individual domains the material is always magnetised to saturation.

If a D.C. magnetic field H is applied , as indicated in FIG.(E:-2;1) , a torque will be exerted,on the magnetic moment us , of magnitude:

$$\tau = us_x H \qquad (E;2;1)$$

The direction of this torque is such that it is mutually perpendicular to both H and us and hence produces a change in spin angular momentum in that direction. Since the magnetic moment and spin angular momentum vectors are parallel the torque causes the electron spin axis to precess about the applied field H . The frequency of this precession,known as the Larmor precessional frequency is given by the relation:

$$\omega_o = - \Gamma_e H \qquad (E;2;2)$$

Damping forces , which are always present in ferrites, quickly bring the magnetic moment into alignment with the applied field $\underline{H}$, the time required for such a process to occur being of the order of nanoseconds.

If a linearly polarised alternating magnetic field of frequency ω is applied a right angles to $\underline{H}$, the electron spins are again made to precess at the same frequency as the applied alternating field. Since damping forces come into play the precessing spins extract energy from the alternating magnetic field. When the alternating field has the same frequency as the natural precessional frequency ω_o , of the magnetic moment, energy absorption reaches its maximum value. This condition is termed ferromagnetic resonance.

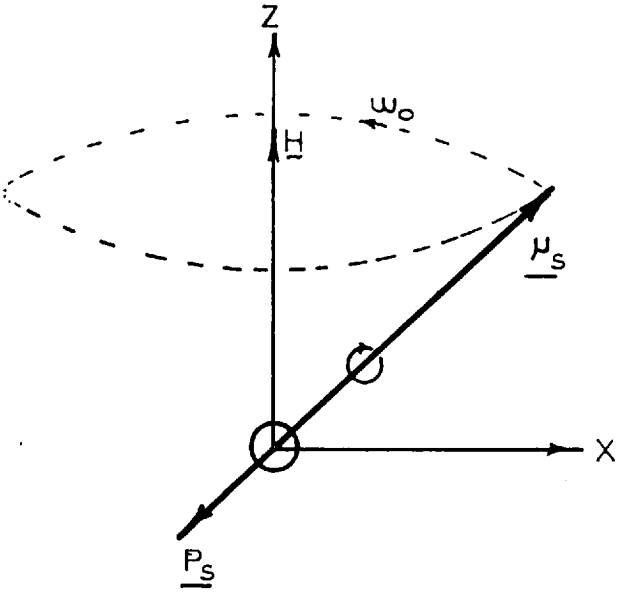

F I G. (E;2;1) **Spin axis precession**

The above description was applied to a linearly polarised wave, however linear polarisation may be considered as a combination of both positive and negative circular polarisation. Thus one can appreciate that if the sense of rotation of the circularly polarised field component is the same as that of the spin precession , considerable coupling is possible and so high energy absorption will occur. However for the

other sense of polarisation ,little coupling takes place. The above indicates the basic concept upon which the resonance isolators built for this system operate, since it signifies the operation of a nonreciprocal device.

E;3 (FERRITE EQUATIONS OF MOTION)

Considering FIG.(E;3;1) , the electron magnetic moment per unit volume is given as:

$$\underline{M} = \underline{us}\ N \qquad (E;3;1)$$

where N is equal to the number of uncompensated electron spins per unit volume.

Through suitable manipulation of equations (E;1;3,E;1;4,and E;2-;1) and substitution of (E;3;1) , it may be shown that:

$$\frac{d\,\underline{M}}{dt} = \Gamma_e\,(\,\underline{M} \times \underline{H}\,) \qquad (E;3;2)$$

which is the well known Bloch equation.

Since there is a damping effect present in all materials such a phenomenon may be represented by a torque $\underline{\tau}_d$ of the form proposed by Landau and Lifshitz, (45).

$$\underline{\tau}_d = \frac{\alpha}{\{\underline{M}\}}\,(\,\underline{M} \times (\,\underline{M} \times \underline{H}\,)\,) \qquad (E;3;3)$$

where α is an amplitude coefficient and $\{\underline{M}\{$ is meant to signify that $\underline{M}$ is taken as a constant.

Inserting the above equation in (E;3;2) and neglecting higher order terms , one arrives at the expression:

$$\frac{d\,\underline{M}}{dt} = \Gamma_e(\,\underline{M} \times \underline{H}\,) + \frac{\alpha}{\{\underline{M}\{}\,(\,\underline{M} \times \frac{d\,\underline{M}}{dt}\,) \qquad (E;3;4)$$

Equation (E;e;4) is known as the modified Bloch equation and may be considered to be the equation of motion for the material.

E:4 (PERMEABILITY TENSOR)

The nonreciprocal behaviour of ferrites can best be visualised if one develops an expression for the permeability of the medium, with respect to R.F. magnetic fields, which are very small in magnitude in comparison to the static D.C. magnetisation.

If a small R.F. alternating component of magnetic field is assumed, one may write:

$$\underline{H} = \underline{k}\, H(i) + \underline{h}\, e^{j\omega t} \qquad (E;4;1)$$

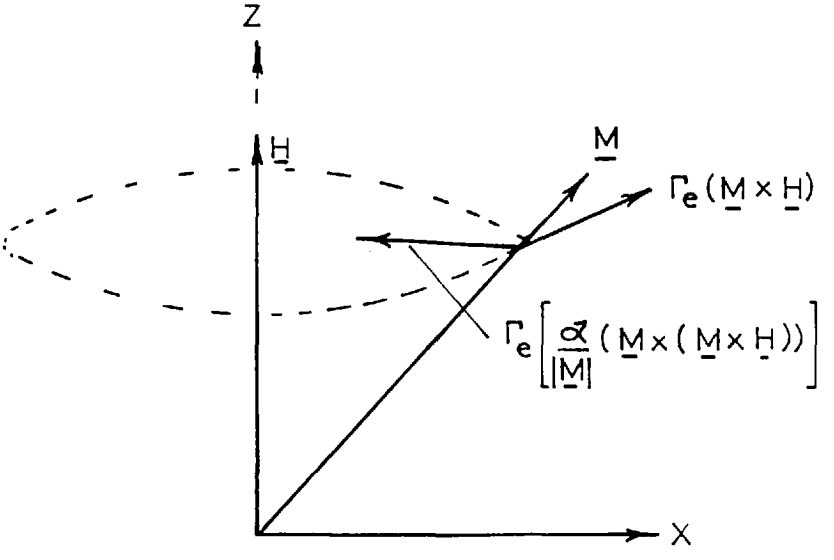

FIG. (E;3;1) **Ferrite vectors**

and $$\underline{M} = \underline{k}\, M_o + \underline{m}\, e^{j\omega t} \qquad (E;4;2)$$

where H(i) is the total internal D.C. field in the medium and M_o is the saturation magnetisation. ($\underline{h}$ and $\underline{m}$ correspond to the R.F. field and magnetisation components, while $\underline{k}$ is the unit vector for the Z coordinate.

Substituting equation (E;4;2) into (E;3;7) and separating out the R.F. components of magnetisation, remembering that :

$$\underline{m} = \underline{i}\, m_x + \underline{j}\, m_y + \underline{k}\, m_z \qquad (E;4;3)$$

and

$$\underline{h} = \underline{i}\, h_x + \underline{j}\, h_y + \underline{k}\, h_z \qquad (E;4;4)$$

one arrives at the result:

$$m_x = \chi h_x - j\kappa h_y \qquad (E;4;5)$$

$$m_y = j\kappa h_x + \chi h_y \qquad (E;4;6)$$

where

$$\chi = \left(\frac{\Gamma_e M_o (\omega_o + j\omega\alpha)}{(\omega_o + j\omega\alpha)^2 - \omega^2} \right) \qquad (E;4;7)$$

and

$$\kappa = -\left(\frac{\Gamma_e M_o \omega}{(\omega_o + j\omega\alpha)^2 - \omega^2} \right) \qquad (E;4;8)$$

also

$$m_z = 0 \qquad (E;4;9)$$

In matrix form the above equations become;

$$\begin{vmatrix} m_x \\ m_y \\ m_z \end{vmatrix} = \begin{vmatrix} \chi & -j\kappa & 0 \\ j\kappa & \chi & 0 \\ 0 & 0 & 0 \end{vmatrix} \begin{vmatrix} h_x \\ h_y \\ h_z \end{vmatrix} \qquad (E;4;10)$$

where the term

$$\begin{vmatrix} \chi & -j\kappa & 0 \\ j\kappa & \chi & 0 \\ 0 & 0 & 0 \end{vmatrix} = \bar{\bar{S}} = \frac{\underline{m}}{\underline{h}} \qquad (E;4;11)$$

is defined as the susceptibility tensor.

The permeability tensor $\underline{\mu}$ is given by the expression:

$$\underline{\mu} = \mu_o (1 + \bar{\bar{S}}) \qquad (E;4;12)$$

E;5 (DEMAGNETISATION FACTORS AND RESONANCE FIELD)

The field components expressed in the previous analysis are those which exsist within the ferrite medium, and thus in order to obtain expressions for the field components within the wave guide, it is necessary to introduce demagnetisation factors. One may write:

$$h_x = h_{x(e)} - N_x m_x \qquad (E;5;1)$$

$$h_y = h_{y(e)} - N_y m_y \qquad (E;5;2)$$

$$H_z = H_{z(e)} - N_z M_z \qquad (E;5;3)$$

where h_x , h_y, and H_z are the internal field components and $h_{x(e)}$, $h_{y(e)}$ and $H_{z(e)}$ are the internal or waveguide components. The terms N_x , N_y, and N_z , are meant to represent the demagnetisation factors for the x,y, and z, directions respectively.

It is possible to obtain expressions for m_x and m_y in terms of the external magnetic field components by suitable manipulation of the above equations, remembering that:

$$\underline{b} = \mu_o \underline{h} + \underline{m} \qquad (E;5;4)$$

and so one arrives at the result:

$$m_x = h_{x(e)} \frac{(\omega_M (\omega_o + \omega_M N_y))}{D'} - h_{y(e)} \frac{(j\omega \omega_M)}{D'} \qquad (E;5;5)$$

and

$$m_y = h_{x(e)} \frac{(j\omega \omega_M)}{D'} + h_{y(e)} \frac{(\omega_M(\omega_o + \omega_M N_x))}{D'} \qquad (E;5;6)$$

where:

$$\omega_M = -\Gamma_e M_o \qquad (E;5;7)$$

and

$$D' = (\omega_o + N_x \omega_M)(\omega_o + N_y \omega_M) - \omega^2 \qquad (E;5;8)$$

To find the resonance field condition one may set D' equal to zero so that both m_x and m_y approach infinity. Thus from (E;5;8):

$$\omega^2 = (\omega_o + N_x\omega_M)(\omega_o + N_y\omega_M) \qquad (E;5;9)$$

which when combined with equations (E;2;2 and (E;5;7) leads to:

$$\omega/\gamma_e = \left((H_{z(e)}+(N_x-N_z)M_o)(H_{z(e)}+(N_y-N_x)M_o) \right)^{\frac{1}{2}} \qquad (E;5;10)$$

where: $$\omega/\gamma_e = H_{eff} \qquad (E;5;11)$$

H_{eff}, being the internal magnetic field required for resonance.

Equation (E;5;10) is usually known as Kittel's resonance equation and is based on the M.K.S. system of units where:

$\mu_o = 4\pi \times 10^{-7}$ farads / meter

$\varepsilon_o = 1/36\pi \times 10^{-9}$ henries / meter

B(gauss) $\times 10^{-4}$ = B webers / meter

M_o(gauss) x 79.5 = M_o ampere turns/ meter

H (oersteds)x 79.5 = H ampere turns/ meter

The saturation magnetisation is defined as $4\pi M_o$ in the cgs system of units.

Equation (E;5;10) may be used in the cgs. system of units by proper choice of field units.

E;6 (WAVEGUIDE CIRCULAR POLARISATION)

The magnetic field components in a rectangular waveguide, shown in FIG.(E;6;1), supporting the dominant ,($T.E._{10}$) mode , are given in section (D;4) as :

$$H_x = j\frac{2a}{\lambda_g}\sin(\pi x/a) \quad , H_z = \cos(\pi x/a) \quad , H_y = 0$$

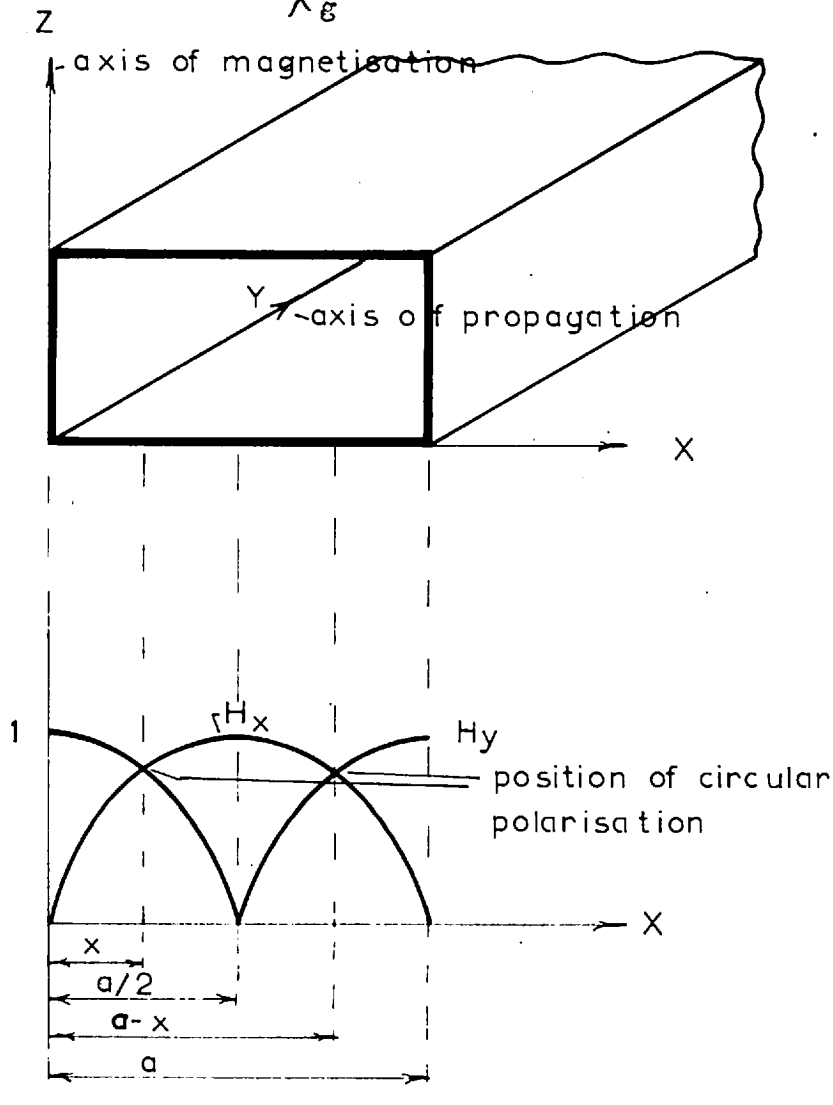

FIG.(E;6;1) **Waveguide circular polarisation**

If one now changes the axis of propagation from the Z axis to the Y axis, in the above field expressions, to be consistant with the notation adopted for the transversely magnetised ferrite, one has:

$$H_y = \cos(\pi x/a) \qquad \text{and } H_z = 0 \qquad (E;6;1)$$

and as before:

$$H_x = j\frac{2a}{\lambda_g} \sin(\pi x/a)$$

Now:

$$\lambda_g = \lambda \; / \; (1 - \lambda/(2a)^2)^{\frac{1}{2}} \qquad (E;6;2)$$

and so:

$$H_x = j \; (\; (2a/\lambda)^2 - 1 \;)^{\frac{1}{2}} \sin(\pi x/a)) \qquad (E;6;3)$$

The position of circular polarisation are found by setting H_x equal to H_y. Thus with reference to FIG.(E:6;1) :

$$x = \frac{a}{\pi} \tan^{-1}(1/ ((2a/\lambda)^2 - 1)^{\frac{1}{2}}) \qquad (E;6;4)$$

From symmetry considerations it can be shown that the magnetic field is again circularly polarised at the point (a-x).

If a thin slab of ferrite is positioned at (x) one finds that for one direction of propagation the sense of electron spin precession is the same as the sense of rotation of the circularly polarised wave and so there is strong interaction, which results in energy transfer from the electromagnetic wave to the ferrite, when the ferrite is biased to resonance, corresponding to the frequency of the electromagnetic wave. For the other direction of propagation the senses of rotation are opposite and therefore little coupling exsists, which naturally yields little attenuation.

It can easily be shown that the sense of circular polarisation is opposite on either side of the waveguide and consequently if strips of ferrite are placed at each of these positions , it is necessary to have the external magnetisation of opposite polarity to obtain non-reciprocal performance.

E:7 (PRACTICAL CONSIDERATIONS)

The optimum position of the ferrite slab, determined experimentally, is closer to the waveguide wall than simple empty guide theory predicts due to the fact that the normal waveguide fields are perturbed by the presence of the ferrite. It is possible to calculate the effect of a full guide height slab of width d on the distribution of field components within the guide, (47) however since in this particular case the ferrite slabs were very small , it was not possible nor practical to analyse the field perturbations. In addition the waveguide was dielectrically loaded in order to obtain an improved forward to reverse ratio. The function of the dilectric is to make the position of circular polarisation extend over a larger region , which results in greater isolator bandwidth. The dielectric also concentrates more energy in the region of the ferrite slab and it follows therefore that greater spinprecession-wave coupling is achieved , resulting in higher reverse loss for a given quantity of ferrite.

APPENDIX F

MICROWAVE RESONANT CAVITY THEORY

The theory of operation of the various types of resonant microwave cavities, used in this system , will now be considered and expressions developed from which the pertinent cavity characteristics may be calculated.

F;1 (COAXIAL CAVITY)

The first cavity considered in the developement of this system was of the re-entrant coaxial type shown in FIG:(F:1;1) . This cavity may be considered to be a resonant tank circuit in which the capacity

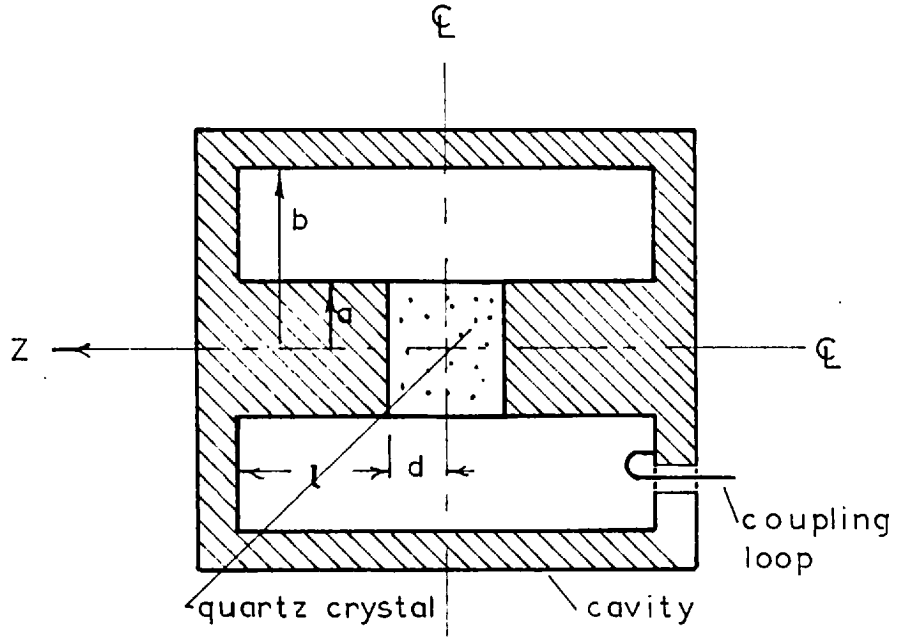

FIG. (F;1;1) **Coaxial cavity**

formed primarily by the gap between the re-entrant posts, in which the piezoelectric quartz crystal is placed, is resonated by the inductance of a short circuited length of coaxial transmission line. It follows therefore that the cavity will support a modified T.E.M. mode.

F;1;1 (CAVITY DIMENSIONS AND FREQUENCY)

As a first approximation one can equate the capacitive reactance presented by the parallel plate capacitor, formed by the gap region, to the inductive reactance supplied by the short circuited transmission lines and hence obtain an expression for the resonant frequency of the system. The problem can be simplified somewhat, due to the symmetry involved, by placing an electric wall along the center line and considering only one half of the cavity.

The equivalent circuit is therefore as shown in FIG.(F;1;1;1), and so one has:

$$Y_{in} = Y_{gap} + Y_{line} \qquad (F;1;1;1)$$

where Y_{in} is the input susceptance seen at the center line of the cavity, Y_{gap} the gap susceptance, and Y_{line} the coaxial line susceptance.

Now inserting the appropriate expressions into equation (F;1;1;1) gives:

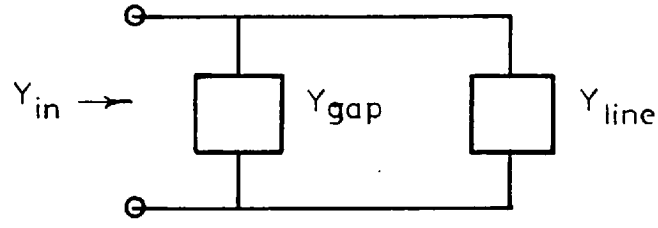

FIG (F;1;1;1) Cavity equivalent circuit

$$Y_{in} = j\omega C - j\,(1/ Z_o \tan(2\pi l/\lambda)) \qquad (F;1;1;2)$$

where
$$C = \varepsilon_r \varepsilon_o \pi a^2 / d \qquad (F;1;1;3)$$

and
$$Z_o = (1/ 2\pi)(\mu_o/\varepsilon_o)^{\frac{1}{2}} \ln(b/a) \qquad (F;1;1;4)$$

Applying now the condition that at resonance Y_{in} must vanish and solving for the cavity length L gives:

$$L = 1/\beta_o \tan^{-1}(2d / a^2 \varepsilon_r \beta_o \ln(b/a)) \qquad (F;1;1;5)$$

where: $\beta_o = 2\pi/\lambda_o$, free space propagation constant

ln = Naperian logarithm

ε_r = relative permittivity of material in gap.

and a, b, and d, are cavity dimensions as indicated in FIG:(F;1;1).

Equation (F;1;1;5) is found to be accurate to approximately 5 % in the design of a symmetrical cavity, where the fringing fields are small and where the gap cross sectional diameter is small in comparison with the wavelength. For larger post diameters the parallel plate capacitor assumption is no longer justified and so equation (F;1;1;5) can not be used.

F;1;2 (CAVITY Q)

The quality factor or Q of a cavity is defined as: (51)

$$Q = \frac{(2\pi)\ \text{Energy stored}}{\text{energy dissapated per cycle}} = \frac{\omega W_s}{P_{in}} \qquad (F;1;2;1)$$

where W_s represents the energy stored and P_{in} is the power input to the cavity.

If only losses within the cavity itself are included in the denominator of equation (F;1;2;1) , the so called " unloaded Q " is obtained, however if coupling losses are considered the " loaded Q " is given.

The energy stored in a cavity can be found by integration over cavity volume with respect to the magnetic field. (52).

Thus: $$W_s = \tfrac{1}{2}\mu \int_v \left\{ \hat{\underline{H}}_v^{\,2} \right\} dv \qquad (F;1;2;4)$$

where $\left\{ \hat{\underline{H}}_v \right\}$ is meant to represent the mean value throughout the volume.

Now the power dissipated is obtained by integrating the wall losses over the inside surface of the cavity , and so one has:

$$P_{dis.} = (1/\sigma\delta) \tfrac{1}{2} \int_s \left\{ \hat{\underline{H}}_s^2 \right\} ds \qquad (F;1;2;5)$$

where here $\left\{ \hat{\underline{H}}_s \right\}$ signifies the magnetic field at the cavity wall and σ is the conductivity , while δ is the skin depth.

It is found that the value of the magnetic field at the cavity wall is approximately equal to twice the mean value of the field in the cavity volume and so one has from equations (F;1;2;3),(F;1;2;4) and (F;1;2;5). (53).

$$Q_{unloaded} \cong \tfrac{1}{2}\omega\mu\sigma\delta \left(\frac{\int_v \left\{ \hat{\underline{H}}_v^2 \right\} dv}{\int_s \left\{ \hat{\underline{H}}_s^2 \right\} ds} \right) \qquad (F;1;2;6)$$

which gives

$$Q_{unloaded} \cong 1/\delta \ (V / S) \qquad (F;1;2;7)$$

where , the skin depth is given by the relation: (54).

$$\delta = (2/\omega\sigma\mu)^{\frac{1}{2}} = 2.5 \times 10^{-4} \text{ cm. for brass at } \lambda_o = 10 \text{ cm.} \qquad (F;1;2;8)$$

and also where the term (V/S) is the volume to surface ratio of the cavity.

The loaded cavity Q is defined as: (55).

$$Q_{loaded} = \frac{Q_{unloaded}}{(1 + \chi\beta)} \qquad (F;1;2;9)$$

where $\chi\beta$ is the coupling parameter and is equal to :

$$\beta = Z_o / Z_{shunt} \qquad (F;1;2;10)$$

where Z_o is the characteristic impedance of the transmission line, to which the cavity is coupled, and Z_{shunt} is the effective shunt impedance presented by the cavity to the transmission line. At resonance Z_{shunt} is purely real and becomes equal to Z_o for critical coupling. It follows that for conditions of critical coupling:

$$\beta_{crit} = 1 \quad \text{and} \quad Q_{loaded} = \frac{Q_{unloaded}}{2} \qquad (F;1;2;11)$$

Inspection of equation (F;1;2;8) indicates that one expects to obtain very large values of Q in microwave cavities , of the order of 1×10^5 , and this in fact is normally found to be the case. However due to the particular type of construction imposed on the design of the cavities used in this system, very high Q's were not obtained, typical values of approximately 500 being obtained for the unloaded Q.

As a result of the very fast rise times associated with the R.F. pulse used in the system, higher values of cavity Q could not be used

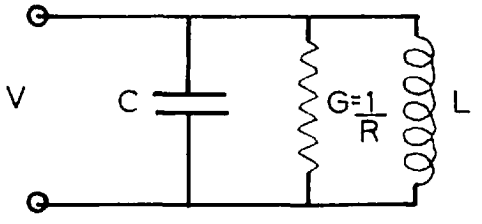

FIG.(F;1;2;1) **Cavity equivalent circuit**

even if they had been obtained. This can easily be appreciated if one considers the time constant associated with a cavity of a given Q. The energy $W_{s(t)}$ stored in a cavity at any time t can be found from the familiar expression common to all freely oscillating circuits, namely:

$$W_{s(t)} = W_{s(o)} e^{-t/RC} \qquad (F;1;2;12)$$

where $W_{s(o)}$ is the initial energy stored in the cavity at time t equal to zero, R is the equivalent lumped cavity shunt resistance and C is the equivalent cavity shunt capacity.

The values of RC may be obtained from a simple cavity equivalent circuit, shown in FIG.(F;1;2;1), along with equation (F;1;2;1). Thus:

$$Q = \omega W_s / P_{in} \qquad (F;1;2;1)$$

but $$W_s = \tfrac{1}{2} C V^2 \quad \text{and} \quad P_{in} = \tfrac{1}{2} V^2 / R \qquad (F;1;2;13)$$

and so $$Q = \omega CR \quad \text{or} \quad RC = Q / \omega \qquad (F;1;2;14)$$

Taking now the half power points of cavity response, it is a simple matter to show,with equations (F;1;2;12 and 14), that:

$$Q = t f / 0.11 \qquad (F;1;2;15)$$

where t is now the three db. response time of the cavity and f is the operating frequency.

It follows,from the above equation , that for 3 Gcs. operation and an R.F. rise time of ten nanoseconds, the maximum value of cavity Q permissible is:

$$Q_{\text{loaded (max)}} = \frac{0.01 \times 10^{-6} \times 3 \times 10^{9}}{0.11} = 273$$

It has been found in practice that a loaded Q of 100 to 150 is the highest that can be used if good pulse cancellation and low cavity frequency drift areto be achieved. This forced restriction to a low cavity Q is very regrettable since,as was indicated in section (D;9) , the electromechanical conversion efficiency is proportional to the square of the cavity Q.

F;1;3 (CAVITY POWER LEVEL)

The equivalent circuit of FIG.(F:1;2;1) may be used to evaluate the maximum power level which can be pumped into the cavity without electrical breakdown of the cavity environment occurring. It can be shown with the aid of equations (F;1;2;14 , and 13) that:

$$P_{in} = \left(\frac{E^2 \varepsilon_r \varepsilon_o a^2 \pi^2 f\, d}{Q_{unloaded}} \right) \qquad (F;1;3;1)$$

where E is the maximum electric field intensity in the cavity gap, ε_r the relative permittivity of the gap material , f the operating frequency , P_{in} the power input to the cavity , while a and d are cavity dimensions as indicated in FIG.(F:1;1).

Unfortunately it is essential , for measurements purposes,that there be an air gap between the quartz crystal and the cavity posts. Consequently the maximum electrical field intensity is limited to the breakdown strength of this air space,and is found to be approximately 30 K.V./ cm. for dry nitrogen. Upon inserting this value into equation (F;1;3;1), along with the typical cavity dimensions and loaded Q, one finds that the maximum power level that can be used is approximately 2 kilowatts. By using a controlled atmosphere of Sulphurhexafluoride, (SF_6) within the cavity it has been possible to increase the maximum usable power level by a factor of approximately 10.

Since in general not all the electrical energy is stored in the cavity gap ,equation (F;1;3;1) should be written as:

$$P_{in} = \left(\frac{E^2 \varepsilon_r \varepsilon_o a^2 \pi^2 f\, d}{\eta_{e(gap)} Q_{unloaded}} \right) \qquad (F;1;3;2)$$

where η_e is the cavity electrical energy storage efficiency of section (D;9;13).

F;1;4 (CAVITY FIELDS)

It is desirable to define a cavity efficiency, with respect to the maximum electrical field E_z developed in the gap, in relation to the maximum value of the excited circumferential magnetic field H_θ , and hence compare various cavity configurations. To do this however one must obtain an expression for the gap fields and this can best be accomplished in the following manner.

The gap admittance may be obtained from field theory using the technique developed by Collins ,(56).

If the gap region is considered to be a cylindrical resonator supporting an E_{01} mode, which is symmetrical with respect to θ and possessing no axial dependence, one finds that an expression for the gap fields can be obtained from the solution to the wave equation for propagation in circular waveguide, given in section (B;4;3). This assumption neglects fringing fields but even so it is found to lead to higher accuracy than the parallel plate capacitor assumption adopted previously, especially when the re-entrant post diameter becomes an appreciable fraction of a wavelength.

Gap fields

The general field solutions to the case of propagation in circular waveguide are given in section (B;4;3) for T.M. modes as:

$$E_z = e^{j\chi\theta} J_\chi(k_c r) \qquad (B;4;3;4)$$

$$H_r = \frac{\chi \omega \varepsilon}{r k_c^2} J_\chi(k_c r) e^{j\chi\theta} \qquad (B;4;3;8)$$

$$H_\theta = -\frac{j\omega\varepsilon}{k_c} J'_\chi(k_c r) e^{j\chi\theta} \qquad (B;4;3;9)$$

$$E_r = Z_e H_\theta \qquad (B;4;3;10)$$

$$E_\theta = -Z_e H_r \qquad (B;4;3;11)$$

where $Z_e = \Gamma / j\omega\varepsilon$ (B;4;3;12)

and $k_c = t\chi n / a$ (B;4;3;6)

The term $e^{j\chi\theta}$ is meant to signify that two solutions are possible, namely $\cos(\chi\theta)$ and $\sin(\chi\theta)$, (58). By suitable choice of the zero of the θ coordinate it is possible to simplify the solutions to $\cos(\chi\theta)$, (57), only.

If now a field dependence of the form $e^{-\Gamma z}$ is assumed and a chamber formed from the circular waveguide such that standing waves are set up, one obtains, from the addition of incident and reflected wave components:

$$E_z = J_\chi(k_c r)\cos(\chi\theta)\cos(\Gamma z) \qquad (F;1;4;1)$$

which upon insertion of an amplitude coefficient and the expression for Γ from equation (B;4;1;9 amd C;1;6) becomes:

$$E_z = E_o J_\chi(k_c r) \cos(\chi\theta) \cos(2\pi z/\lambda_g) \qquad (F;1;4;2)$$

where E_o is the maximum value of the electric field in the cavity.

Now specifying a resonant condition such that the chamber or cavity length L is given by the expression:

$$L = (\lambda_g/2)\, p, \text{where } p \text{ is an integer} \qquad (F;1;4;3)$$

and so $\Gamma = \pi p / L$ (F;1;4;4)

thus the field expressions become:

$$E_z = E_o J_\chi(k_c r) \cos(\chi\theta) \cos(\pi pz/L) \qquad (F;1;4;5)$$

$$H_\theta = -jE_o \frac{\omega\varepsilon}{k_c} J'_\chi(k_c r)\cos(\chi\theta)\cos(\pi pz/L) \qquad (F;1;4;6)$$

and $$H_r = -j \frac{E_o \omega \varepsilon \chi J_\chi (k_c r) \sin(\chi \theta) \cos(\pi pz/l)}{r k_c^2} \quad (F;1;4;7)$$

$$E_r = -\frac{E_o \pi p J'_\chi (k_c r) \cos(\chi \theta) \sin(\pi pz/l)}{k_c l} \quad (F;1;4;8)$$

$$E_\theta = \frac{E_o \pi p \chi J_\chi (k_c r) \sin(\chi \theta) \sin(\pi pz/l)}{r l k_c^2} \quad (F;1;4;9)$$

Applying now the original assumption of no axial dependence, it is evident that:

$$\nabla = 0 \text{ and so } p = 0 \quad (F;1;4;10)$$

But from equation (B;4;2;2):

$$k_c^2 = \nabla^2 + \omega^2 \mu \varepsilon \quad (B;4;2;2)$$

and so $$k_{c(1)} = \beta_o (\varepsilon_{r(1)})^{\frac{1}{2}} \quad (F;1;4;11)$$

here the subscript (1) refers to the gap region.

Considering now the lowest E mode, namely the E_{01}, one has that $\chi = 0$, and consequently the gap field expressions reduce to:

$$E_z = E_o J_o(k_{c(1)} r) \quad (F;1;4;12)$$

and $$H_{\theta(r)} = j E_o (\varepsilon_o \varepsilon_{r(1)} / \mu_o)^{\frac{1}{2}} J_1(k_{c(1)} r) \quad (F;1;4;13)$$

while all the other field components are zero.

Gap admittance

The gap voltage may be expressed as the integral of the electric field as follows:

$$V = \int_o^d \underline{E} \cdot ds \quad (F;1;4;14)$$

Now the gap admittance can be defined as:

$$Y_{gap} = \underline{I} \ / \ \underline{V} \qquad (F;1;4;15)$$

and upon multiplying both numerator and denominator by $\underline{V}^*$ it follows that:

$$Y_{gap} = \frac{\underline{I}\,\underline{V}^*}{\underline{V}\,\underline{V}^*} = \frac{2\,\underline{S}^*}{V^2} \qquad (F;1;4;16)$$

where $\underline{S}^*$ is the complex conjugate of the power flow.

From electromagnetics, the complex power flow is given by Poynting's Vector as:

$$\underline{S} = \tfrac{1}{2}\int_S (\ \underline{E} \times \underline{H}^*\ ) \cdot ds \qquad (F;1;4;17)$$

where the integration is carried over the surface. Hence the gap admittance may be written as:

$$Y_{gap} = \frac{\int_S (\ \underline{E}^*_x \underline{H}\ ) \cdot ds}{\left\{\int_o^d \underline{E} \cdot ds\right\}^2} = \frac{\int_o^d (\underline{E}^*_x\ \underline{H}\ )\ 2\pi a\ dz}{\left\{\int_o^d E_z \cdot dz\ \right\}^2} \qquad (F;1;4;18)$$

where the path of interration is the same in both cases.

Performing the integration and substituting in the value of $(\ \underline{E} \times \underline{H}\ )$ from equations (F;1;4;12 and 13) , gives.

$$Y_{gap} = j\,(\varepsilon_o \varepsilon_{r(1)} / \mu_o)^{\frac{1}{2}} \frac{2\pi a}{d} \frac{(\ J_1(k_{c(1)}a)\ )}{(\ J_o(k_{c(1)}a)\ )} \qquad (F;1;4;19)$$

Resonance

At cavity resonance the total admittance must vanish and so:

$$Y_{line} + Y_{gap} = 0 \qquad (F;1;4;19_a)$$

where Y_{line} is as given previously in equation (F;1;1;2).

Using the expressions for Y_{gap} and Y_{line} in equation $(F;1;4;19_a)$ results in the expression:

$$\left(\frac{J_1(k_{c(1)}a)}{J_o(k_{c(1)}a)} \right) \tan\left(\frac{2\pi l}{\lambda_o}\right) \ln(b/a) \frac{a}{d} (\mathcal{E}_{r(1)})^{\frac{1}{2}} = 1 \qquad (F;1;4;19_b)$$

which may be considered to be the resonance equation.

Cavity fields in terms of the excited magnetic fields

Having derived expressions for the gap fields,it is now possible to determine their magnitude in terms of the excited cavity magnetic field H_o, at the cavity top.

The magnetic field in the coaxial region of the cavity is,from section (B;4;1) , using E_z as reference vector:

$$H_{\theta(z)}{}_{(coax)} = \frac{j H_o}{r} \cos(\beta_o z) \qquad (B;4;1:12)$$

At the gap position , ie, z= l and r= a , the magnitude of the magnetic field in the coaxial region is :

$$H_{\theta\left(\substack{z=l \\ r=a}\right)}{}_{(coax)} = \frac{j H_o}{a} \cos(\beta_o l) \qquad (F;1;4;20)$$

while the magnitude of H_θ in the gap region at the same position is given by equation (F;1;4;13) as;

$$H_{\theta(r=a)}\underset{gap}{=} j\,E_o(\varepsilon_o\varepsilon_{r(1)}/\mu_o)^{\frac{1}{2}}\,J_1(k_{c(1)}a) \qquad (F;1;4;20)$$

Clearly for H_θ to be continuous the above two expressions must be equal and so upon equating and solving for E_o one has:

$$E_o = \frac{H_o\cos(\beta_o l)}{a\;J_1(k_{c(1)}a)}\;(\mu_o/\varepsilon_o\varepsilon_{r(1)})^{\frac{1}{2}} \qquad (F;1;4;21)$$

Thus the maximum electric field E_o in the cavity gap is obatined in terms of the maximum value of the excited magnetic field H_o .

The gap fields may now be written as:

$$H_{\theta(r)}\underset{gap}{=}\frac{jH_o}{a}\cos(\beta_o l)\left\{\frac{J_1(k_{c(1)}r)}{J_1(k_{c(1)}a)}\right\} \qquad (F;1;4;22)$$

$$E_{z(r)}\underset{gap}{=}\frac{H_o}{a}\;(\mu_o/\varepsilon_o\varepsilon_{r(1)})^{\frac{1}{2}}\cos(\beta_o l)\left\{\frac{J_o(k_{c(1)}r)}{J_1(k_{c(1)}a)}\right\} \qquad (F;1;4;23)$$

The value of the electric field E_z , at the gap edge,ie, r=a , therefore becomes:

$$E_{z(r=a)}\underset{gap}{=}\frac{H_o}{a}\;(\mu_o/\varepsilon_o\varepsilon_{r(1)})^{\frac{1}{2}}\cos(\beta_o l)\left\{\frac{J_o(k_{c(1)}a)}{J_1(k_{c(1)}a)}\right\} \qquad (F;1;4;24)$$

In the above equations $k_{c(1)}$ is given by the equation:

$$k_{c(1)} = \beta_o(\varepsilon_{r(1)})^{\frac{1}{2}} \qquad (F;1;4;11)$$

Cavity Q

A more accurate expression for the cavity Q may now be obtained since the gap field expressions are now available. From equations (F;1;2;3 to 8) it follows that:

$$\frac{Q_{un}\delta}{2} = \sum \left| \frac{\left(\int_v |\hat{\underline{H}}|^2 \, dv\right)}{\left(\int_s |\hat{\underline{H}}|^2 \, ds\right)} \right| \qquad (F;1;4;25)$$

for a complex shaped cavity. Here Q_{un} is meant to represent the unloaded cavity Q.

For the re-entrant coaxial cavity, considered here, the above equation may be expressed as;

$$\frac{Q_{un}\delta}{2} = \frac{\int_{v\ \text{coaxial region}} |\hat{\underline{H}}|^2 dv + \int_{v\ \text{gap region}} |\hat{\underline{H}}|^2 dv}{\int_{s\ \text{coaxial region}} |\hat{\underline{H}}|^2 ds + \int_{s\ \text{gap region}} |\hat{\underline{H}}|^2 ds} \qquad (F;1;4;26)$$

Considering now the coaxial part of the cavity, and performing the integration indicated in the above equation, with respect to the dimensions given in FIG.(F;1;1) , one has that:

$$\int_{v\ \text{coaxial region}} |\hat{\underline{H}}|^2 dv = H_o^2 \, 2\pi \int_d^b \frac{dr}{r} \int_o^L \cos^2(\beta_o z) dz$$

$$" \quad = H_o^2 \ln(b/a) \left(L + \frac{\sin(2\beta_o L)}{2\beta_o}\right) \qquad (F;1;4;27)$$

and also

$$\int_{s\ \text{coaxial region}} |\hat{\underline{H}}|^2 ds = \int_{\text{outside wall}} + \int_{\text{post surfaces}} + \int_{\text{top end}}$$

$$" \quad = H_o^2 \left(\int_o^L \frac{2\pi}{b} \cos^2(\beta_o z) dz + \int_o^L \frac{2\pi}{a} \cos^2(\beta_o z) dz + \right.$$

$$\left. + \int_a^b \frac{2\pi}{r} \cos^2(\beta_o z) dz \right.$$

so that finally

$$\int_{\substack{S\\ \text{coaxial}\\ \text{region}}} \{\hat{\underline{H}}\}^2 ds = H_o^2 \pi \left\{ \frac{(L + \sin(2\beta_o L))}{2\beta_o} (1/b+1/a) + 2(\ln(b/a)) \right\} \qquad (F;1;4;28)$$

Now considering the gap region:

$$\int_{\substack{V\\ \text{gap}\\ \text{region}}} \{\hat{\underline{H}}\}^2 dv = \frac{H_o^2 \cos^2(\beta_o L)}{a^2 J_1^2(k_{c(1)}a)} 2\pi d \int_o^a \frac{r J_1^2(k_{c(1)}r)}{} dr$$

and upon changing the limits of integration from ,a to $k_{c(1)}a$, one has:

$$\int_{\substack{V\\ \text{gap}\\ \text{region}}} \{\hat{\underline{H}}\}^2 dv = \frac{H_o^2 \cos^2(\beta_o L)}{a^2 J_1^2(k_{c(1)}a)} 2\pi d \int_o^{k_{c(1)}a} \frac{r J_1^2(r) dr}{k_{c(1)}^2} \qquad (F;1;4;29)$$

The last term in the above equation may be evaluated by Lommel's integrals, (60), since,(61) :

$$\int_o^a x J_1^2(x) dx = \frac{a^2}{2}\left\{ J_1^2(a) - J_o(a) J_2(a) \right\} \qquad (F;1;4;30)$$

and so the last term of equation (F;1;4;29) becomes:

$$\int_o^{k_{c(1)}a} \frac{r J_1^2(r) dr}{k_{c(1)}^2} = \frac{a^2}{2}\left\{ 1 - \frac{2 J_o(k_{c(1)}a)}{k_{c(1)}a J_1(k_{c(1)}a)} + \frac{J_o^2(k_{c(1)}a)}{J_1^2(k_{c(1)}a)} \right\}$$

$$(F;1;4;31)$$

Now combining the above equation with (F;1;4;29), gives:

$$\int_{\substack{V\\ \text{gap region}}} \{\hat{\underline{H}}\}^2 dv = H_o^2 \cos^2(\beta_o L) \pi d \left\{ 1 - \frac{2 J_o(k_{c(1)}a)}{k_{c(1)}a J_1(k_{c(1)}a)} + \frac{J_o^2(k_{c(1)}a)}{J_1^2(k_{c(1)}a)} \right\}$$

$$(F;1;4;32)$$

Now the expression for the gap dissipation term is:

$$\int_{\substack{s\\ \text{gap}\\ \text{region}}} \{\hat{\underline{H}}\}^2 ds = \frac{H_o^2}{a^2} \frac{\cos^2(\beta_o L)}{J_1(k_{c(1)}a)} \int_o^a 2\pi r\, J_1^2(k_{c(1)}r)\, dr \qquad (F;1;4;33)$$

which is obviously the same expression as equation (F;1;4;29) except that the integration is not carried over z. The result therefore may be written by inspection of equation (F;1;4;32), and so:

$$\int_{\substack{s\\ \text{gap}\\ \text{region}}} \{\hat{\underline{H}}\}^2 ds = H_o^2 \cos^2(\beta_o L) \left\{ 1 - \frac{2\, J_o(k_{c(1)}a)}{k_{c(1)}a\, J_1(k_{c(1)}a)} + \frac{J_o^2(k_{c(1)}a)}{J_1^2(k_{c(1)}a)} \right\}$$

(F;1;4;34)

Finally if all the previously derived expressions are inserted into the Q expression of equation (F;1;4;26) , the result is:

$$Q_{un} = \frac{2}{\delta} \left\{ \frac{\ln(b/a)\left[L + \frac{\sin(2\beta_o L)}{2\beta_o}\right] + d\cos^2(\beta_o L)\left\{1 - \frac{2J_o(k_{c(1)}a)}{k_{c(1)}a\, J_1(k_{c(1)}a)} + \frac{J_o^2(k_{c(1)}a)}{J_1^2(k_{c(1)}a)}\right\}}{\left(L + \frac{\sin(2\beta_o L)}{2\beta_o}\right)\left(\frac{1}{b} + \frac{1}{a}\right) + 2\ln\left(\frac{b}{a}\right) + \cos^2(\beta_o L)\left\{1 - \frac{2J_o(k_{c(1)}a)}{k_{c(1)}a\, J_1(k_{c(1)}a)} + \frac{J_o^2(k_{c(1)}a)}{J_1^2(k_{c(1)}a)}\right\}} \right\}$$

(F;1;4;35)

The above expression is thus a general equation for the unloaded Q of a symmetrical coaxial cavity having large radius b, inner radius a, with post length equal to 2L and gap height 2d, as shown in FIG.(F;1;1) .

F;1;5 (CAVITY EFFICIENCY)

It is of interest at this point to investigate the efficiency of a particular cavity design with respect to its usefulness in exciting the piezoelectric crystal, which it contains. Obviously since the quartz crystal is contained within the re-entrant gap, some qualitative indication of the effectiveness of the cavity design can be obtained by determining the percentage energy storage in the gap region with respect to the total energy storage in the cavity.

From equation (F;1;2;4) one has the expression for the cavity magnetic energy storage as:

$$W_{s\ magnetic} = \tfrac{1}{2}\mu \int_v \{\hat{\underline{H}}\}^2 dv \qquad (F;1;2;4)$$

and so the energy storage in the gap region may be obtained simply by multiplying equation (F;1;4;32) by $\mu/2$ . .Similarly the energy storage in the coaxial region is given by the product of $\mu/2$ and equation (F;1;4;27). It follows therefore that the gap magnetic energy storage efficiency $\eta_{s(m)\ gap}$ is given by the relation:

$$\eta_{s(m)gap} = \frac{W_{s(m)gap}}{W_{s(m)gap} + W_{s(m)coaxial}} \qquad (F;1;5;1)$$

Upon insertion of the appropriate expressions into the above equation, gives:

$$\eta_{s(m)gap} = \frac{d\cos^2(\beta_o l)\left\{ \text{III} \right\}}{\ln\left(\frac{b}{a}\right)\left\{1+\frac{\sin(2\beta_o l)}{2\beta_o}\right\}+d\cos^2(\beta_o l)\left\{ \text{III} \right\}} \qquad (F;1;5;2)$$

where

$$\text{III} = 1 - \frac{2\,J_o(k_{c(1)}a)}{k_{c(1)}a\,J_1(k_{c(1)}a)} + \frac{J_o^2(k_{c(1)}a)}{J_1^2(k_{c(1)}a)} \qquad (F;1;5;3)$$

The electrical energy stored in the gap region , $W_{s(e)gap}$ can be found through use of equations(F;1;4;23 and D;9;4). So:

$$W_{s(e)gap} = \tfrac{1}{2}\varepsilon_o \varepsilon_{r(1)} \int_v |\tilde{E}_z|^2 dv$$

$$" \quad = \frac{\mu_o \pi d H_o^2}{2} \cos^2(\beta_o L) \left\{ 1 + \frac{J_o^2(k_{c(1)}a)}{J_1^2(k_{c(1)}a)} \right\} \qquad (F;1;5;4)$$

Similarly the electrical energy stored in the coaxial section of the cavity is obtained by integrating E_r over the volume. Now:

$$E_r = Z_w H_\theta = (\mu_o/\varepsilon_o \varepsilon_r)^{\frac{1}{2}} H_\theta \quad \text{from} \qquad (B;4;1;10)$$

and so

$$E_{r(z)} = j \frac{H_o}{r} (\mu_o/\varepsilon_o \varepsilon_{r(2)})^{\frac{1}{2}} \sin(\beta_o z) \qquad (F;1;5;5)$$

Thus:

$$W_{s(e)\ \text{coaxial}} = \tfrac{1}{2}\varepsilon_o \varepsilon_{r(2)} \int_v |\tilde{E}_r|^2 dv$$

$$" \quad = \frac{\mu_o H_o^2}{2} \ln(b/a) \left\{ L - \frac{\sin(2\beta_o L)}{2\beta_o} \right\} \qquad (F;1;5;6)$$

The gap electrical energy storage efficiency $\eta_{s(e)gap}$ is therefore given by the expression.

$$\eta_{s(e)gap} = \frac{W_{s(e)gap}}{W_{s(e)gap} + W_{s(e)\ \text{coaxial}}}$$

$$" \quad = \frac{d \cos^2(\beta_o L) \left\{ \text{Π} \right\}}{d \cos^2(\beta_o L) \left\{ \text{Π} \right\} + \ln(\frac{b}{a}) \left\{ L + \frac{\sin(2\beta_o L)}{2\beta_o} \right\}} \qquad (F;1;5;7)$$

where $$\mathcal{I} = 1 + \frac{J_o^2(k_{c(1)}a)}{J_1^2(k_{c(1)}a)} \qquad (F;1;5;8)$$

From equation (D;9;3) the average sonic energy density in the crystal is found to be given by the relation:

$$W_{k(\text{ sonic})} = \tfrac{1}{2} \frac{e^2_{ijm}}{C_{ijkl}} (\hat{E}_m)^2 \qquad (D;9;3)$$

where e_{ijm} is the piezoelectric constant tensor, C_{ijkl} is the elastic constant tensor and $\hat{E}_m$ is the maximum value with respect to time, of the average value of electric field over the crystal surface.

It follows , from consideration of the above equation, that the acoustic power generated in the crystal is proportional to $E_m{}^2 A$, where A is the cross sectional area of the excited surface. It is desirable , if possible, to arrange the cavity design such that the above term is maximised with respect to the value of the exciting magnetic field H_o. Clearly E_m is a function of the gap width (d), but since this dimension is fixed by the minimum crystal thickness which can be accommodated,from acoustic travel time considerations, the only other variable is the cross sectional area A. It is found on the other hand however, that the cross sectional area , although variable , is constrained within certain limits imposed by the size of cavity required for resonance at the fixed system frequency of 3 Gcs. It would appear therefore that from sonic energy generation considerations alone, it is desirable to arrange the cavity design such that the coaxial portion of the cavity is as small as resonance and coupling conditions will permit, while the crystal diameter should be as large as possible. Large crystal diameters, on the other hand impose exacting requirements on surface flatness and parallelism if acoustic interference problems are to be avoided, and consequently a compromise must usually be reached.

F;2 (RADIAL CAVITY)

F:2;1 (CAVITY DIMENSIONS AND FREQUENCY)

The second cavity type investigated in this work operated in a radial mode, in which propagation was in the r, direction, there being no field variation along the Z axis. The particular mode used was the lowest E mode , in which only E_z and H_θ exsist, and so may be considered to be a T.E.M. mode.

The cavity configuration adopted is shown in FIG.(F;2;1). Due to the symmetry about the center line, it is necessary to consider only one half of the cavity in the analysis.

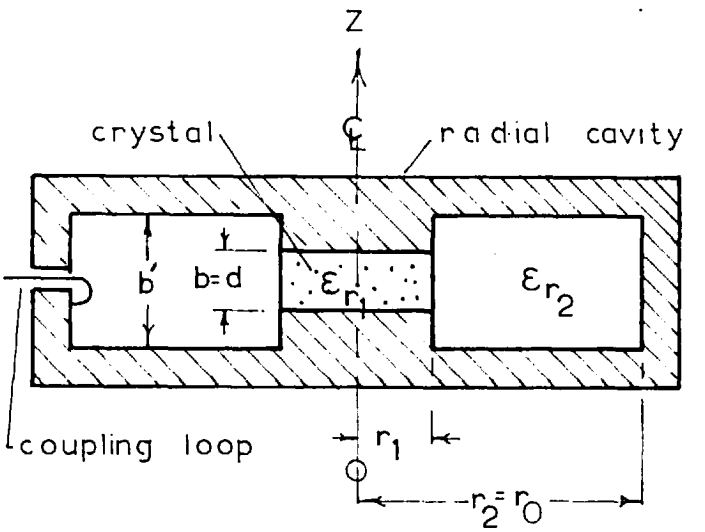

FIG.(F;2;1) Radial cavity

The device may be considered to be constituted of two radial transmission lines of unequal characteristic admittances , $Y_{o(r)(1)}$ and $Y_{o(r)(2)}$ respectively, coupled at the point $r=r_1$ by a junction admittance of (jB) ,(64) .

The equivalent circuit of the cavity may be drawn as shown in FIG.(F:2;1;2). The first radial line ,corresponding to the gap region, is open circuited while the second line is short circuited. The propagation constant of both of these lines is different due to the relative dielectric constant of the crystal in the gap region.

Considering first the case where the size of the quartz crystal is such as to just completely fill the gap space, as shown in FIG.(F;-2;1;1) , one has from equation (B;4;4;11) in appendix B:

$$Y_{o(r)(1)} = \frac{2\pi r}{b} \left(\varepsilon_o \varepsilon_{r_{(1)}} / \mu_o \right)^{\frac{1}{2}}$$

and

$$Y_{o(r)(2)} = \frac{2\pi r}{b'} \left(\varepsilon_o \varepsilon_{r_{(2)}} / \mu_o \right)^{\frac{1}{2}} \qquad \text{(B;4;4;11)}$$

where $\varepsilon_{r_{(1)}}$ and $\varepsilon_{r_{(2)}}$ represent the relative permittivity of the material in the gap and outer radial section respectively.

It follows that:

$$Y_{o(r)(1)} / Y_{o(r)(2)} = (b'/b)\left(\varepsilon_{r_{(1)}} / \varepsilon_{r_{(2)}} \right)^{\frac{1}{2}} \qquad \text{(F;2;1;1)}$$

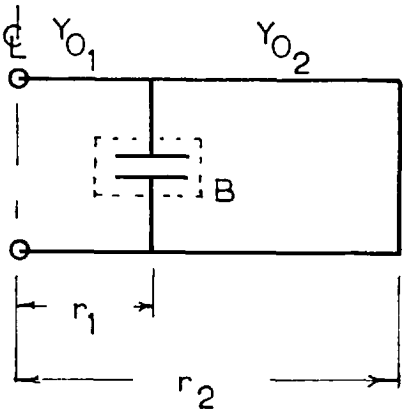

FIG. (F;2;1;2)

Radial cavity equivalent circuit.

Marcuvitz has given , that the junction admittance,normalised with respect to the characteristic admittance of the second radial line, as: (65)

$$\frac{\overleftarrow{B}}{Y_{o(r_1)(2)}} = \frac{k_{(1)}b'}{\pi} \ln\left\{\left(\frac{1-\alpha^2}{4\alpha}\right)\left(\frac{1+\alpha}{1-\alpha}\right)^{\frac{1}{2}(\alpha+1/\alpha)}\right\} \qquad (F;2;1;2)$$

where $\alpha = b/b'$ and $k_{(1)} = (\mathcal{E}_{r_{(1)}})^{\frac{1}{2}} k_o$ (F;2;1;3)

k_o being the unbounded wave number of equation (B;4;2;2), for free space propagation, and so:

$$k_{(1)} = (\mathcal{E}_{r_{(1)}})^{\frac{1}{2}} \beta_o \qquad (F;2;1;4)$$

Using the plane $r=r_1$ as reference, one finds that the total relative admittance seen at thispoint, normalised with respect to $Y_{o(r_1)(2)}$,the characteristic admittance of the second radial line at $r=r_1$, is:

$$\frac{Y'_{total}}{Y_{o(r_1)(2)}} = \frac{1}{Y_{o(r_1)(2)}} \left(\overleftarrow{Y}_{(r_1)(1)} + \overleftarrow{B} + \overrightarrow{Y}_{(r_1)(2)} \right) \qquad (F;2;1;5)$$

where $\overleftarrow{Y}_{(r_1)(1)}$ is the absolute admittance of the open circuited radial line looking in the direction of decreasing radius. From equations (B;4;4; 11 , 30, 32 and 35) one finds that:

$$\overleftarrow{Y}_{(r_1)(1)} = \left\{\frac{2\pi r_1}{b} (\mathcal{E}_o \mathcal{E}_{r_{(1)}}/\mu_o)^{\frac{1}{2}}\right\}\left\{\frac{j J_1(k_1 r_1)}{J_o(k_1 r_1)}\right\} \qquad (F;2;1;6)$$

where k_1 is as given by equation (F;2;1;4).

Similarly $Y_{(r_1)(2)}$ represents the absolute admittance of the short circuited radial line, looking in the direction of increasing radius, and is given by equations (B;4;4;11, 30, and 34) as:

$$\vec{Y}_{(r_1)(2)} = Y_{o(r_1)(2)} \left(-j\, ct(x,y) \right) \qquad (F;2;1;7)$$

where ct(x,y) is as given by equation (B;4;4;31) , and:

$$x = k_2 r_1 \quad , \quad y = k_2 r_o \qquad (F;2;1;8)$$

while: $$k_2 = (\mathcal{E}_{r_{(2)}})^{\frac{1}{2}} k = (\mathcal{E}_{r_{(2)}})^{\frac{1}{2}} \beta_o \qquad (F;2;1;9)$$

Now upon substituting the above expressions into equation (F;2;1;5) and imposing the resonance condition that $\frac{Y'_{total}}{Y_{o(r_1)(2)}}$ must vanish, one arrives finally to the expression:

$$ct(k_2 r_1, k_2 r_o) = (\mathcal{E}_{r_{(1)}}/\mathcal{E}_{r_{(2)}})^{\frac{1}{2}} \frac{b'}{b} \frac{J_1(k_1 r_1)}{J_o(k_1 r_1)} + \frac{k_1}{\pi} b' \ln\left\{ \left(\frac{1-\alpha^2}{4\alpha}\right) \left(\frac{1+\alpha}{1-\alpha}\right)^{\frac{1}{2}(\alpha + 1/\alpha)} \right\} \qquad (F:2;1;10)$$

The above expression is a transcendental equation which is best solved with the aid of the graphs of the function ct(x,y) versus (y/x) and (y-x), given in FIG.(F:2;1;3) . (66).

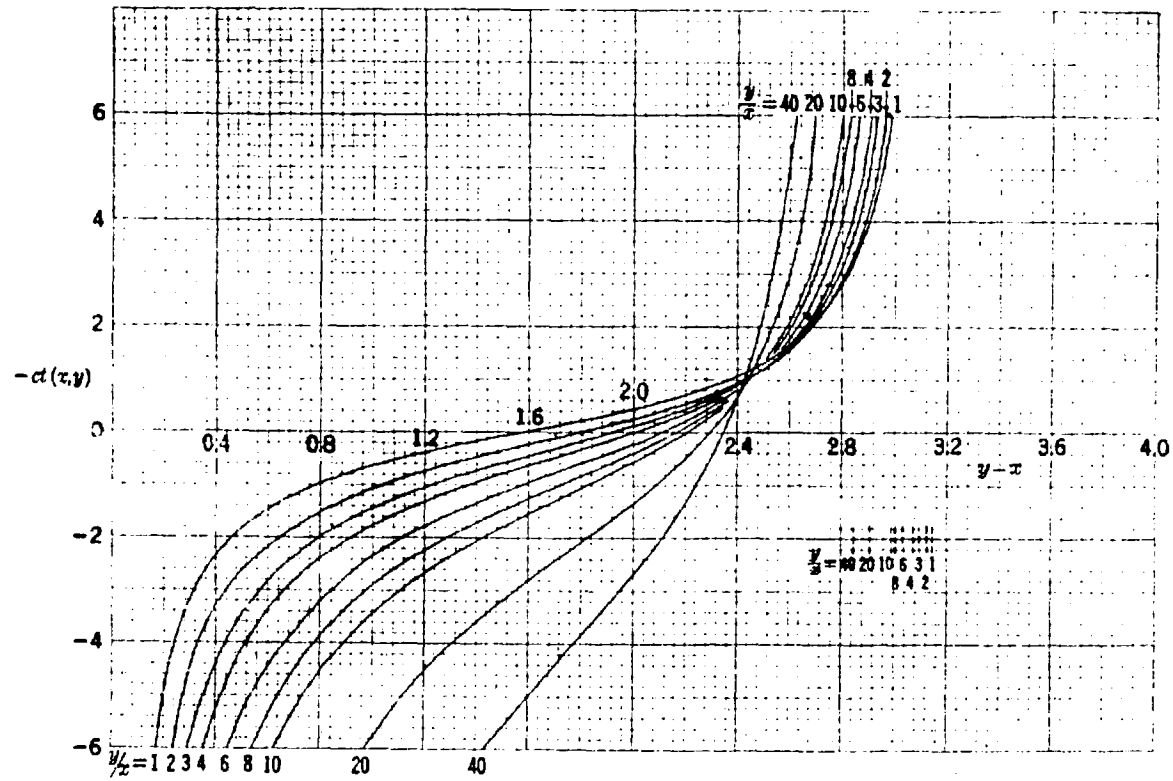

– Relative inc ur $\frac{\text{admittance}}{\text{impedance}}$ of an $\frac{E}{H}$-type radial line with zero $\frac{\text{admittance}}{\text{impedance}}$ termination ($y > x$).

FIG(F; 2;1;3)

Unfortunately , in the actual cavities used in this system, the configuration and dimensions are not nearly so simple as those assumed in the foregoing analysis, but rather are of the form shown in FIG.(F:2;1;4) .

From FIG.(F:2;1;4) it can be seen that the crystal is held by a special P.T.F.E. holder and that the crystal and holder dimensions are such that they extend into the second radial line for an appreciable distance. Since there are three different materials of non-uniform dimensions and different relative permittivity in each of the cavity radial sections, it follows that a number of approximations must be made if the resonant equation is to be obtained, with reasonable accuracy.

A logical approximation is to assume that the medium in each radial line is homogeneous and characterised by an effective relative permittivity $\mathcal{E}_{r_{(eff)}}$. The requirement therefore is to determine the value of $\mathcal{E}_{r(eff)}$ for each of the radial sections.

Open circuited radial section , ie: gap region.

The case of the gap region is quite straight forward since the boundaries between the various media are continuous throughout the section. It is possible therefore to use the equivalent series capacitance of the region to determine the effective relative permittivity.

Thus with reference to FIG.(F:2;1;4) it is easily shown that:

$$\mathcal{E}_{r_{(1)(eff)}} = d_{t(1)} \left\{ \frac{1}{\frac{d_1}{\mathcal{E}_{r_{(1)}}} + \frac{d_2}{\mathcal{E}_{r_{(2)}}} + \frac{d_3}{\mathcal{E}_{r_{(3)}}}} \right\} \qquad (F;2;1;11)$$

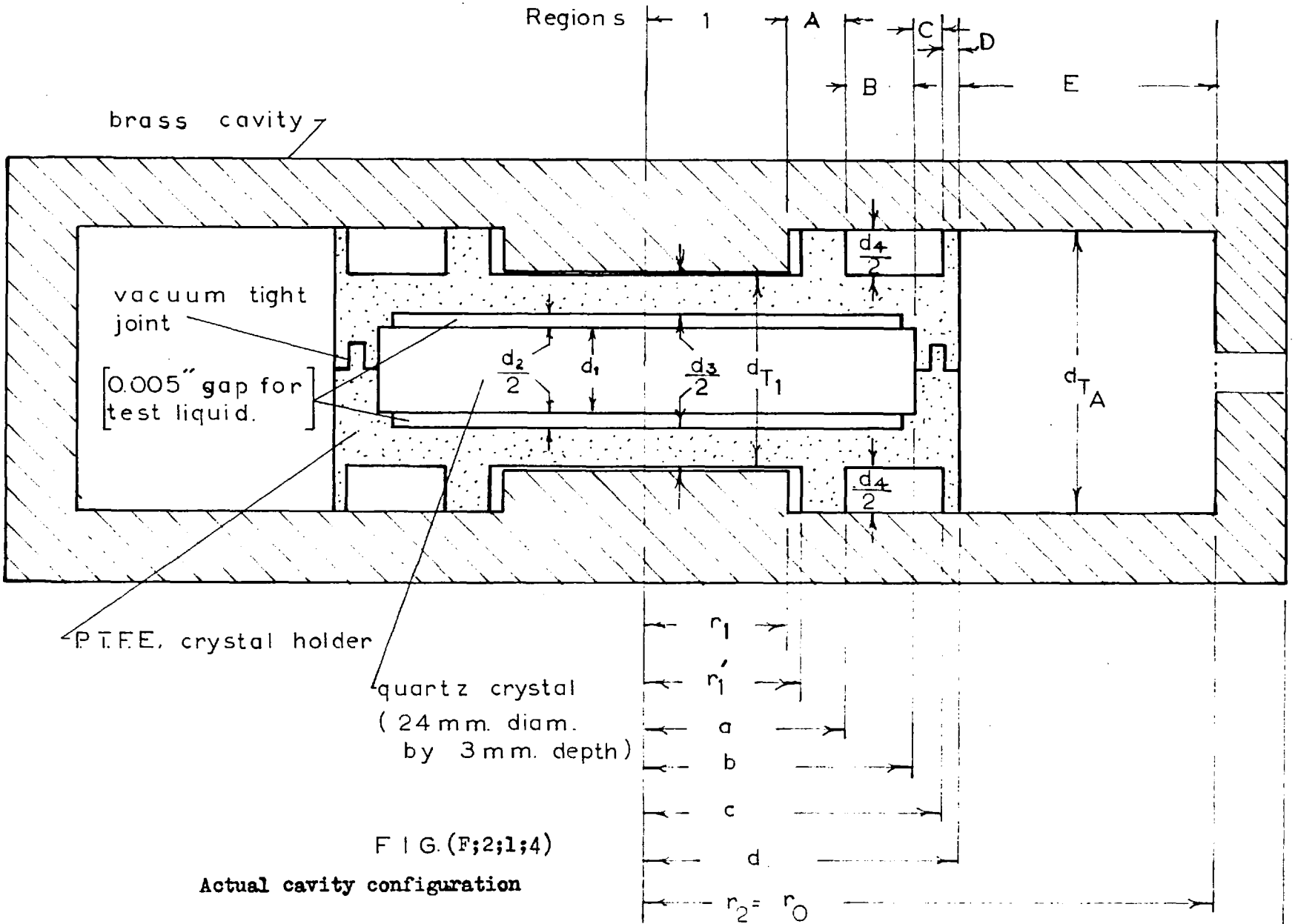

F I G. (F;2;1;4)

Actual cavity configuration

where of course:

$$d_{t(1)} = d_1 + d_2 + d_3 \qquad (F;2;1;12)$$

Short circuited radial section

The second radial section is somewhat more difficult to deal with , in that the dielectric boundaries are not continuous. A reasonable approximation to the effective dielectric constant can be obtained however by subdividing the line into five regions and evaluating the regional $\mathcal{E}_{r(eff)}$ and then finally combining the regional contributions into an overall effective permittivity.

Again with reference to FIG.(F:2;1;4), it can be shown that:

$$\mathcal{E}_{r_{(A)(eff)}} = d_{t(A)} \left\{ \frac{1}{\frac{d_1}{\mathcal{E}_{r_{(1)}}} + \frac{d_2}{\mathcal{E}_{r_{(2)}}} + \frac{(d_{t(A)} - (d_1 + d_2))}{\mathcal{E}_{r_{(3)}}}} \right\} \qquad (F;2;1;13)$$

where

$$d_{t(A)} = d_1 + d_2 + d_3 + d_4 \qquad (F;2;1;14)$$

Similarly for region B , one finds that:

$$\mathcal{E}_{r_{(B)(eff)}} = d_{t(A)} \left\{ \frac{1}{\frac{d_1}{\mathcal{E}_{r_{(1)}}} + \frac{d_2}{\mathcal{E}_{r_{(2)}}} + \frac{d_3}{\mathcal{E}_{r_{(3)}}} + \frac{d_4}{\mathcal{E}_{r_{(1)}}}} \right\} \qquad (F;2;1;15)$$

and for region C:

$$\mathcal{E}_{r_{(C)(eff)}} = d_{t(A)} \left\{ \frac{1}{\frac{d_{t(A)} - d_4}{\mathcal{E}_{r_{(3)}}} + \frac{d_4}{\mathcal{E}_{r_{(2)}}}} \right\} \qquad (F;2;1;16)$$

while regions D and E yield respectively:

$$\mathcal{E}_{r_{(D)(eff)}} = d_{t(A)} \left\{ \frac{1}{\frac{d_{t(A)}}{\mathcal{E}_{r_{(3)}}}} \right\} \qquad (F;2;1;17)$$

and $$\mathcal{E}_{r_{(E)(eff)}} = 1 \qquad (F;2;1;18)$$

Since in the cavity design the dimensions of regions A,B,C, and D are fixed by crystal size and coupling considerations, it is possible to assign an effective relative permittivity $\mathcal{E}'_{r(eff)}$ to the combined regions, by considering these sections to be in parallel.

Thus:

$$\mathcal{E}'_{r(eff)} = \frac{(\mathcal{E}_{r(A)}(a^2-r_1'^2)+\mathcal{E}_{r(B)}(b^2-a^2)+\mathcal{E}_{r(C)}(c^2-b^2)+\mathcal{E}_{r(D)}(d^2-c^2))}{(d^2-r_1^2)} \qquad (F;2;1;19)$$

Finally the effective relative dielectric constant of the complete short circuited radial line may be expressed as:

$$\mathcal{E}_{r_{(2)(eff)}} = \frac{(\mathcal{E}'_{r_{(eff)}}(d^2-r_1^2) + (r_2^2-d^2))}{(r_2^2-r_1^2)} \qquad (F;2;1;20)$$

Thus the effective electrical length of the short circuited radial line is given by equation (B;4;4;23) as:

$$(y-x) = (\mathcal{E}_{r_{(2)(eff)}})^{\frac{1}{2}} k_o (r_2-r_1) \qquad (F;2;1;21)$$

where as before:

$$k_o = \beta_o = 2\pi/\lambda_o$$

As previously stated, the dimensions of the regions A to D are fixed both by the size of the crystal available and the minimum amounts of P.T.F.E. allowable , from machining considerations. The minimum internal cavity height is also fixed by the smallest coupling loop which can be fitted into the cavity and still not break down electrically, under high pulsed power conditions. On the other hand, the maximum allowable cavity height is governed by fringing field considerations. This can be seen , since the gap height is fixed and hence any increase in the cavity height requires that the re-entrant posts be longer. Clearly the longer the electrodes , in relation to the cavity size, especially the inner electrode diameter, the greater will be the component of fringing field present. These fringing fields are undesirable in the gap region since they give rise to a radial electric field component which can excite unwanted modes in the quartz crystal. It follows therefore that the cavity height should be made as small as possible.

Furthermore from energy storage considerations it is desirable to restrict the volume of the short circuited radial line to the absolute minimum. That this is so can be appreciated by reference to the equations of energy storage developed for the coaxial type cavity. Since the energy storage in any part of the cavity is a function of its volume and since only the energy stored in the gap region can be utilised in electromechanical conversion, it is desirable to keep the remainder of the cavity as small as possible.

Having the condition that most of the cavity dimensions are fixed by external factors, the only other variable is r_2, the outer diameter, and consequently the resonance equation may be used to determine its value.

The resonance equation for the modified cavity configuration is again given by (F;2;1;10) except that terms $\mathcal{E}_{r(1)(eff)}$ and $\mathcal{E}_{r(2)(eff)}$ are used.

F;2;2 (CAVITY FIELDS)

As in the case of the coaxial cavities it is desirable to develop an expression for the gap fields E_z and E_o in terms of the excited magnetic field H_o . It is found however that this can not be accomplished,using the assumption that the gap region is an open circuited radial waveguide, since there is a singularity at the point r=0. Thus in order to be able to compare this radial cavity performance to the coaxial design it is necessary to once again regard the gap region as supporting an E_{o1} mode, as was done in the coaxial cavity analysis.

The gap fields are therefore given from section (F;1;4;) as:

$$E_z = E_o \, J_o(k_{c(1)}r) \qquad (F;1;4;12)$$

$$H_{\phi(r)} = j \, E_o \, (\varepsilon_o \varepsilon_{r(1)} / \mu_o)^{\frac{1}{2}} \, J_1(k_{c(1)}r) \qquad (F;1;4;13)$$

where

$$k^2_{c(1)} = 0 + \omega^2 \mu \varepsilon = k^2 = \beta_o (\varepsilon_{r(1)})^{\frac{1}{2}} \qquad (F;1;4;11)$$

Resonance conditions

The gap admittance expression is the same as derived earlier and so :

$$\overleftarrow{Y}_{gap} = \frac{j \, 2\pi r_1}{b'} (\varepsilon_o \varepsilon_{r(1)(eff)} / \mu_o)^{\frac{1}{2}} \frac{(J_1(k_1 r_1))}{(J_o(k_1 r_1))} \qquad (F;2;2;1)$$

The admittance of the second radial line is , from equation (F;2;1;7)

$$\overleftarrow{Y}_{(r_1)(2)} = \frac{-j \, 2\pi r_1}{b'} (\varepsilon_o \varepsilon_{r(2)(eff)} / \mu_o)^{\frac{1}{2}} \, ct(x,y) \qquad (F;2;2;2)$$

Now the junction admittance is from (F;2;1;2)

$$\overleftarrow{B} = \frac{2\pi r_1}{b'} \left\{ \frac{\varepsilon_o \varepsilon_{r(2)(eff)}}{\mu_o} \right\}^{\frac{1}{2}} k_{(1)} b' \ln \left\{ \frac{(1-\alpha^2)}{4\alpha} \left\{ \frac{1+\alpha}{1-\alpha} \right\}^{\frac{1}{2}(\alpha+1/\alpha)} \right\} \qquad (F;2;2;3)$$

Now applying the resonance condition that Y'_{total} must vanish, where:

$$Y'_{total} = Y_{gap} + Y_{\substack{second\ radial \\ line}} + B \qquad (F;2;2;4)$$

gives the following equation:

$$ct(x_2,y_2) = \frac{b'}{b}\left(\varepsilon_{r(1)(eff)}/\varepsilon_{r(2)(eff)}\right)^{\frac{1}{2}} \left\{ \frac{J_1(x_1)}{J_o(x_1)} \right\} +$$

$$+ \frac{k_1}{\pi} b' \ln\left\{ \left(1-\alpha^2\right)\left(\frac{1+\alpha}{1-\alpha}\right)^{\frac{1}{2}(\alpha+1/\alpha)} \right\} \qquad (F;2;2;5)$$

where:

$$x_1 = k_1 r_1$$

$$x_2 = k_2 r_1$$

$$y_2 = k_2 r_2 = k_2 r_o$$

and

$$k_1 = \beta_o \left(\varepsilon_{r(1)(eff)}\right)^{\frac{1}{2}}$$

$$k_2 = \beta_o \left(\varepsilon_{r(2)(eff)}\right)^{\frac{1}{2}} \qquad (F;2;2;6)$$

It is of interest to compare equation (F;2;2;5) with equation (F;2;1;10) since these two resonance equations are found to be identical, although they were derived separately and under different assumptions. It would appear therefore that the assumption that the cavity gap region is a cutoff E_{o1} mode is justified since it leads to the same admittance expression as is obtained from an open circuited radial waveguide mode.

Gap fields in terms of the excited magnetic field

From equation (B;4;4;26) one has the magnetic field in the radial line as:

$$H_{\phi(r)} = \frac{j\, I_{(r)}}{2\pi r} \qquad (B;4;4;26)$$

using E_z as reference, and where:

$$I_{(r)} = \frac{\left(Z_{o(r_o)} I_{(r_o)}\, cs(x,y) - j\, V_{(r_o)}\, Sn(x,y) \right)}{Z_{o(r)}} \qquad (B;4;4;15)$$

Upon inserting the boundary conditions that at the cavity wall, ie: $r = r_2 = r_o$:

$V_{(r_o)} = 0$, one has from the above equation:

$$I_{(r)} = \left(Z_{o(r_o)}\, I_{(r_o)}\, cs(x_2,y_2)\right) / Z_{o(r)} \qquad (F;2;2;7)$$

where from equation (B;4;4;20 and 22) :

$$Z_{o(r)} = b/2\pi r \left(\mu_o/\varepsilon_o \varepsilon_{r_{(2)(eff)}}\right)^{\frac{1}{2}} \qquad (F;2;2;8)$$

Now then,

$$H_{\phi(r_1)} = \frac{j\, Z_{o(r_o)}\, I_{(r_o)}\, cs(x_2,y_2)}{2\pi r_1\, Z_{o(r_1)}} \qquad (F;2;2;9)$$

and so

$$H_{\phi(r_1)} = \frac{j\, H_o}{r_o}\, cs(x_2,y_2) \qquad (F;2;2;10)$$

radial line

where from equation (B;4;4;17) :

$$cs(x_2,y_2) = \left(N_o(y_2)\, J_1(x_2) - J_o(y_2)\, N_1(x_2)\right)(\pi y_2/2) \qquad (F;2;2;11)$$

and where H_o is the maximum value of the excited magnetic field at the cavity wall.

Equating now the value of the magnetic field in the gap region at $r=r_1$, to the value of the magnetic field in the radial region at the same radius gives:

$$E_o = \frac{H_o}{r_o} \left(\mu_o / \mathcal{E}_o \mathcal{E}_{r_{(1)(eff)}} \right)^{\frac{1}{2}} \frac{cs(x_2, y_2)}{J_1(x_1)} \qquad (F;2;2;12)$$

where now E_o represents the maximum value of the electric field in the cavity gap region.

Upon substitution of the above expression back into equations (F;1;4;12 and 13) one arrives at the following:

$$E_{z(r)}_{gap} = \frac{H_o}{r_o} \left\{ \frac{\mu_o}{\mathcal{E}_o \mathcal{E}_{r_{(1)(eff)}}} \right\}^{\frac{1}{2}} cs(x_2, y_2) \frac{J_o(k_1 r)}{J_1(x_1)} \qquad (F;2;2;13)$$

$$H_{\theta(r)}_{gap} = \frac{j H_o}{r_o} cs(x_2, y_2) \frac{J_1(k_1 r)}{J_1(x_1)} \qquad (F;2;2;14)$$

The value of E_z at $r = r_1$ is simply:

$$E_{z(r_1)}_{gap} = \frac{H_o}{r_o} \left\{ \frac{\mu_o}{\mathcal{E}_o \mathcal{E}_{r_{(1)(eff)}}} \right\}^{\frac{1}{2}} cs(x_2, y_2) \frac{J_o(x_1)}{J_1(x_1)} \qquad (F;2;2;15)$$

F;2;3 (CAVITY Q)

The magnetic energy stored in the gap region is found in the same manner as was done in the case of the coaxial design, and so:

$$\int_v \{\underline{\hat{H}}\}^2 dv = \frac{H_o^2}{r_o^2} \frac{cs^2(x_2,y_2)}{J_1^2(x_1)} 2\pi d \int_o^{r_1} r\, J_1^2(k_1 r) dr$$

and upon evaluation of the integral from equation (F;1;4;30) gives:

$$\int_{v_{gap}} \{\underline{\bar{H}}\}^2 dv = H_o^2 \left\{\frac{r_1}{r_o}\right\}^2 cs^2(x_2,y_2) \pi d \; (\text{IIII}) \qquad (F;2;3;1)$$

where $$\text{IIII} = \left(1 - \frac{2\, J_o(x_1)}{(x_1)\, J_1(x_1)} + \frac{J_o^2(x_1)}{J_1^2(x_1)} \right) \qquad (F;2;3;2)$$

and as before: $x_1 = k_1 r_1$, $x_2 = k_2 r_1$, $y_2 = k_2 r_2$

The gap region energy dissipation term is again given by equation (F;1;4;33) , suitably modified for the different expression of E_o . Thus allowing for the fact that two faces must be considered one has:

$$\int_{s_{gap}} \{\underline{\bar{H}}\}^2 ds = 2\left(H_o \frac{r_1}{r_o} cs(x_2,y_2) \right)^2 \pi \; (\text{IIII}) \qquad (F;2;3;3)$$

The energy stored in the second radial line is found by integration of the magnetic field over the volume , and so:

$$\int_{v_{\substack{\text{second}\\ \text{line}}}} \{\underline{\bar{H}}\}^2 dv = \text{radial} \int_{r_1}^{r_2} \int_o^{b'} H_{\bullet(r)}^2 \, 2\pi r \, dr \, dz \qquad (F;2;3;4)$$

Now from equations (F;2;2;6, 10 and 11) one finds that:

$$H_{\theta(r)}=\frac{jH_o}{2r_o}\ k_2\ (N_o(y_2)\ J_1(x_2)-\ J_o(y_2)\ N_1(x_2)\ ) \qquad (F;2;3;5)$$

Thus:

$$\int_v|\underline{\tilde{H}}|^2dv=\frac{(H_o k_2)^2\pi^3\ b'}{2}\left(\int_{r_1}^{r_2=r_o} r\left\{A^2J_1^2(k_2r)+B^2N_1^2(k_2r)-2ABJ_1(k_2r)N_1(k_2r)\right\}dr\right.$$

(F;2;3;6)

where $A = N_o(y_2)$ and $B= J_o(y_2)$

The first two terms in the above expression are similar to those previously encountered and hence their solution is given by equation (F;1;4;30). Thus:

$$A^2\int_{r_1}^{r_o} r\,J_1^2(k_2r)dr = \frac{A^2}{2}\left\{ r_o^2\left\{J_1^2(y_2)-2\frac{J_1(y_2)J_o(y_2)}{y_2}+J_o^2(y_2)\right\} - \right.$$
$$\left. r_1^2\left\{J_1^2(x_2)-2\frac{J_1(x_2)J_o(x_2)}{x_2}+J_o^2(x_2)\right\}\right\}$$

$$= A^2/2\ (\text{IV}) \qquad (F;2;3;7)$$

Similarly the second term becomes:

$$B^2\int_{r_1}^{r_o} r\,N_1^2(k_2r)dr = \frac{B^2}{2}\left\{ r_o^2\left\{N_1^2(y_2)-2\frac{N_1(y_2)N_o(y_2)}{y_2}+N_o^2(y_2)\right\} - \right.$$
$$\left. r_1^2\left\{N_1^2(x_2)-2\frac{N_1(x_2)N_o(x_2)}{x_2}+N_o^2(x_2)\right\}\right\}$$

$$= B^2/2\ (\text{V}) \qquad (F;2;3;8)$$

The last term of equation (F;2;3;6) may be evaluated by Lommel's integrals , using the standard form given below: (67)

$$\int^{z} zN_x(kz)J_x(kz)dz = \frac{z^2}{4}\left\{ \begin{array}{l} 2N_x(kz)J_x(kz) - N_{x-1}(kz)J_{x+1}(kz) - \\ \quad N_{x+1}(kz)\ J_{x-1}(kz) \end{array} \right\}$$

(F;2;3;9)

Consequently:

$$2AB\int_{r_1}^{r_o} r(J_1(k_2r)N_1(k_2r))dr =$$

$$= \frac{AB}{2}\left\{ \begin{array}{l} r_o^2\left\{2N_1(y_2)J_1(y_2)+2N_o(y_2)J_o(y_2)-\frac{2}{y_2}\left\{(N_o(y_2)J_1(y_2)+\right.\right. \\ \qquad \left.\left.+(N_1(y_2J_o(y_2)\right\}\right. \\ -r_1^2\left\{2N_1(x_2)J_1(x_2)+2N_o(x_2)J_o(x_2)-\frac{2}{x_2}\left\{(N_o(x_2)J_1(x_2)+\right.\right. \\ \qquad \left.\left.+(N_1(x_2)J_o(x_2)\right\}\right. \end{array} \right\}$$

$$= \frac{AB}{2}\ (\text{VI})$$

(F;2;3;10)

Finally therefore:

$$\int_v \{\tilde{\underline{H}}\}^2 dv = \frac{(H_o k_2)^2 \pi^3 b'}{4}\left\{ \begin{array}{l} A^2(\text{IV}) \\ + B^2(\text{V}) \\ - AB\ (\text{VI}) \end{array} \right\}$$

(F;2;3;11)

where IV, V, VI, are as indicated in equations (F;2;3;7, 8 and 10), respectively, and A , B , are as given by equation (F;2;3;6).

The dissipation term in the second radial portion of the cavity is given by the equation:

$$\int_{s}\{\underline{\tilde{H}}\}^2 ds = 2\int_{r_1}^{r_2=r_o} \{\hat{H}_{\theta(r)}\}^2 \, 2\pi r dr + \int_{o}^{b'} \{\tilde{H}_{\theta(r_o)}\}^2 \, 2\pi r_o dz$$

second radial line. (F;2;3;12)

From inspection of the previous calculations and the above expression one may write the result as:

$$\int_{s}\{\underline{\hat{H}}\}^2 ds = \frac{(H_o k_2)^2 \pi^3}{2}\left(A^2(\text{IV})+B^2(\text{V})-AB(\text{VI})\right)+2\pi b' H_o^2 \frac{}{r_o}$$

second radial line (F;2;3;13)

Finally the cavity Q may be formulated with reference to equation (F;1;4;26), and so:

$$Q_{un} = \frac{2}{\delta}\left\{\frac{\left\{\left(\frac{r_1}{r_o}\right) cs(x_2,y_2)\right\}^2 d(\text{III}) + \pi^2 k_2^2 b' \left(A^2(\text{IV})+B^2(\text{V})-AB(\text{VI})\right)}{2\left\{\left(\frac{r_1}{r_o}\right) cs(x_2,y_2)\right\}^2 (\text{III}) + \pi^2 k_2^2 \left(A^2(\text{IV})+B^2(\text{V})-2AB(\text{VI})+\frac{2b'}{r_o}\right)}\right\}$$

where as in equation (F;2;3;2):

$$\text{III} = 1 - \frac{2 J_o(x_1)}{(x_1) J_1(x_1)} + \frac{J_o^2(x_1)}{J_1^2(x_1)} \qquad (F;2;3;14)$$

and as previously:

$$x_1 = k_1 r_1 \quad , \quad x_2 = k_2 r_1 \quad , \quad y_2 = k_2 r_2 = k_2 r_o$$

and $$k_1 = \beta_o \left(\varepsilon_{r_{(1)(eff)}}\right)^{\frac{1}{2}} \quad , \quad k_2 = \beta_o \left(\varepsilon_{r_{(2)(eff)}}\right)^{\frac{1}{2}}$$

F;2;4 (CAVITY EFFICIENCY)

As in the coaxial cavity case, the magnetic energy storage efficiency of the radial cavity is defined as:

$$\eta_{s(m)gap} = \frac{W_{s(m)\ gap}}{W_{s(m)gap} + W_{s(m)\text{ second radial line}}} \qquad (F;2;4;1)$$

Here also the terms $W_{s(m)\ gap}$ and $W_{s(m)\text{ radial line}}$ are found simply by multiplying equations (F;2;3;2 andll) by $\mu/2$, and so the expression for the gap magnetic energy storage efficiency becomes:

$$\eta_{s(m)gap} = \frac{(r_1/r_o)^2\ cs^2(x_2,y_2)\ d\ (\text{III})}{(r_1/r_o)^2\ cs^2(x_2,y_2)\ d\ (\text{III}) + \frac{k_2^2\ {}^2b'(\text{VII})}{4}} \qquad (F;2;4;2)$$

where $\text{VII} = A^2(\text{IV}) + B^2(\text{V}) - AB(\text{VI})$ (F;2;4;3)

and III, IV, V, VI, are as previously specified.

Energy storage in electric field

The electrical energy stored in the gap region electric field is given by the expression:

$$W_{s(e)gap} = \tfrac{1}{2}\,\varepsilon_{r(1)(eff)}\,\varepsilon_o \int_v |\bar{E}|^2\ dv$$

$$" = \frac{H_o^2}{2}\left(\frac{r_1}{r_o}\right)^2 \mu_o\ cs^2(x_2,y_2)\,\pi\,d\left\{1 + \frac{J_o^2(x_1)}{J_1^2(x_1)}\right\} \qquad (F;2;4;4)$$

The electrical energy storage of the second radial line is found by integrating E_z , in the radial line, over the volume.

Now from section (B;4;4) one has that :

$$E_{z(r)} = - \frac{V_{(r)}}{b} \qquad (B;4;4;24)$$

where $$V_{(r)} = V_{(r_o)} \, Cs(x,y) - j \, Z_{o(r_o)} \, I_{(r_o)} \, sn(x,y) \qquad (B;4;4;15)$$

Applying the boundary conditions that at the outer cavity wall, $(r=r_2=r_o)$, the mode potential $V_{(r_o)}$ must vanish, it follows that:

$$V_{(r)} = Z_{o(r_o)} \, I_{(r_o)} \, sn(x,y) \qquad (F;2;4;5)$$

taking E_z as the reference vector.

Upon substitution of the expressions for $Z_{o(r_o)}$ and $I_{(r_o)}$ into equation (F;2;4;5) and then substituting this expression into (B;4;4;24) one finds that:

$$E_{z(r)} = \frac{H_o}{r_o} \left(\mu_o / \varepsilon_o \varepsilon_{r_{(2)(eff)}} \right)^{\frac{1}{2}} sn(x,y). \qquad (F;2;4;6)$$

which leads to:

$$E_{z(r)} = \frac{H_o k_2 \pi}{2} \left\{ \frac{\mu_o}{\varepsilon_o \varepsilon_{r_{(2)(eff)}}} \right\}^{\frac{1}{2}} \left\{ J_o(y_2) N_o(k_2 r) - N_o(y_2) J_o(k_2 r) \right\} \qquad (F;2;4;7)$$

Thus the expression for the electric energy stored in the second radial line may be written as:

$$W_{s(e)\ \text{second radial line}} = \frac{\mu_o k_2^2 H_o^2 \pi^3 b'}{4} \left\{ \int_{r_1}^{r_2=r_o} r \left[A^2 J_o^2(k_2 r) + B^2 N_o^2(k_2 r) - 2AB N_o(k_2 r) J_o(k_2 r) \right] dr \right\} \qquad (F;2;4;8)$$

The first two terms of equation (F;2;4;8) are easily evaluated with the aid of Lommel's integrals, using the relation: (63)

$$\int_0^z zJ_x^2(kz)dz = \frac{z^2}{2}\left[J_x'^2(kz) + \frac{(1-x^2)}{k^2z^2} J_x^2(kz) \right] \qquad (F;2;4;9)$$

Thus:

$$A^2\int_{r_1}^{r_2} r^2 J_o^2(k_2r)dr = \frac{A^2}{2}\left\{ \begin{array}{l} r_o^2 \left[J_1^2(y_2) + J_o^2(y_2)\right] - \\ r_1^2 \left[J_1^2(x_2) + J_o^2(x_2)\right] \end{array} \right\}$$

$$= A^2/2 \quad (\text{VIII}) \qquad (F;2;4;10)$$

and similarly:

$$B^2\int_{r_1}^{r_2=r_o} r\, N_o^2(k_2r)dr = \frac{B^2}{2}\left\{ \begin{array}{l} r_o^2 \left[N_1^2(y_2) + N_o^2(y_2)\right] - \\ r_1^2 \left[N_1^2(x_2) + N_o^2(x_2)\right] \end{array} \right\}$$

$$= B^2/2 \ (\text{IX}) \qquad (F;2;4;11)$$

The third term in equation (F;2;4;8) is again found using Lommel's integrals, and so:

$$2AB\int_{r_1}^{r_2=r_o} r(N_o(k_2r)J_o(k_2r))dr =$$

$$= \frac{AB}{2}\left\{ \begin{array}{l} r_o^2\left(2 N_o(y_2)J_o(y_2) + 2 N_1(y_2)J_1(y_2)\right) - \\ r_1^2\left(2 N_o(x_2)J_o(x_2) + 2 N_1(x_2)J_1(x_2)\right) \end{array} \right\}$$

$$= AB / 2 \ (\text{X}) \qquad (F;2;4;12)$$

Finally the expression for the electrically energy stored in the second radial line may be written as:

$$W_{s(e)} = \frac{\mu_o k_2^2 H_o^2 \pi^3 b'}{8} \left(A^2(\text{VIII}) + B^2(\text{IX}) - AB(\text{X}) \right) \qquad \text{(F;2;4;13)}$$

where A and B have the values as given in equation (F;2;3;6).

The gap electrical energy storage efficiency is again defined as:

$$\eta_{\substack{s(e)\\gap}} = \frac{W_{s(e)\ gap}}{W_{s(e)\ gap} + W_{s(e)\ \text{second radial line}}} \qquad \text{(F;2;4;14)}$$

and so:

$$\eta_{\substack{s(e)\\gap}} = \frac{(r_1/r_o)^2 cs^2(x_2,y_2)\ d\ (\text{XI})}{\left(\frac{r_1}{r_o}\right)^2 cs^2(x_2,y_2)\ d(\text{XI}) + \frac{k_2^2\ \ 3\ b'(\text{XII})}{4}} \qquad \text{(F;2;4;15)}$$

where $$\text{XI} = 1 + J_o^2(x_1)/\ J_1^2(x_1) \qquad \text{(F;2;4;16)}$$

and $$\text{XII} = A^2(\text{VIII}) + B^2(\text{IX}) - AB(\text{X}) \qquad \text{(F;2;4;17)}$$

VIII, IX , and X have the values given by equations (F;2;4;10, 11, and 12) respectively.

APPENDIX G

PARAMETRIC AMPLIFIER THEORY

G;1 (GENERAL CONSIDERATIONS)

The parametric amplifier used in this system utilised a "varactor" as its nonlinear element. This varactor is in reality a PN junction semiconductor diode whose capacitance depends upon the voltage across the junction. It is this property in addition to its low loss that enables the varactor to be used in the construction of a low noise microwave amplifier.

The particular varactor used in this amplifier was of the diffused silicon mesa type shown in FIG. (G;1;1)

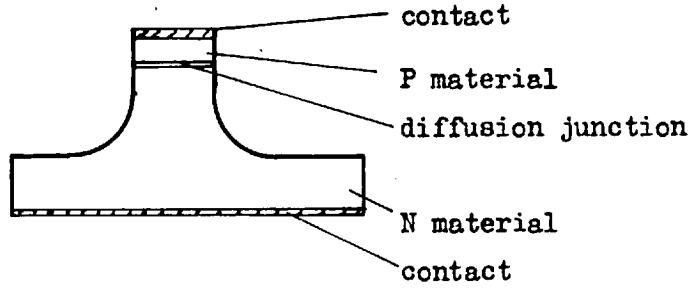

FIG. (G;1;1)

The P section has a large density of holes while the N side has a large density of electrons. A very narrow region between these two section,known as the "depletion layer" , is virtually free of both holes and electrons and so forms a parallel plate capacitor whose capacitance is a function of the width of the depletion layer. The thickness of the depletion layer is in turn dependent upon the voltage across the junction and hence one has a voltage variable capacitor, having a typical voltage-capacitance characteristic as shown in FIG. (G;1;2).

The equivalent circuit for an actual varactor diode is given in FIG:(G;1;3). The symobls C_c and L are meant to represent the capacitance and lead inductance of the varactor case, while R_s signifies the diode series resistance.

It is found that under operational conditions, the equivalent circuit may be simplified to that shown in FIG.(G;1;4) , since the diode holder reactance is tuned out and only effects bandwidth considerations.

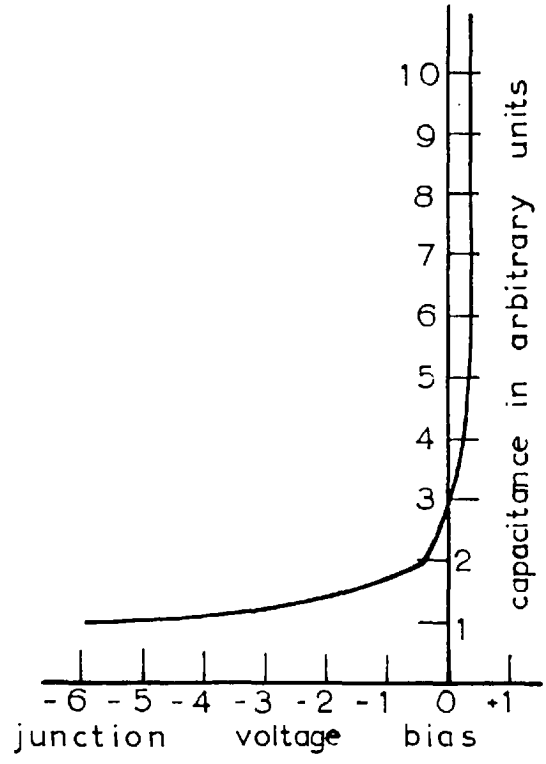

FIG. (G;1;2)

Voltage-capacitance characteristic of a typical varactor.

For good low noise performance the diode series resistance must be very small and in addition the minimum capacitance of the diode must also be low. It is obvious from FIG.(G;1;2) that the minimum capacitance is determined by the bias voltage, however there is a limit imposed on the maximum value of the bias voltage that can be used, this limit being the reverse breakdown voltage.

The instantaneous capacitance of a linearly graded junction , subjected to an alternating voltage, is given by the relation.(68).

$$C_{(t)} = C_o / (1-V_{ac} / V_o)^{\frac{1}{2}} \qquad (G;1;1)$$

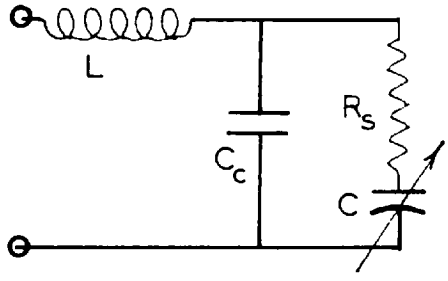

F I G. (G;1;3)

Varactor equivalent circuit

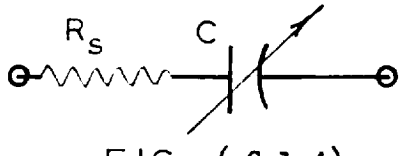

F I G. (G;1;4)

Simplified varactor equivalent circuit

where C_o is the static diode capacitance at zero bias, V_o is the D.C. bias voltage and V_{ac} is the amplitude of the applied alternating signal, or pump source.

Now the pump voltage may be given as:

$$V_{ac} = V \cos(\omega t) \qquad (G;1;2)$$

and so equation (G;1;1) becomes:

$$C_{(t)} = C_o / \left(1 + a \cos(\omega t) \right)^{\frac{1}{2}} \qquad (G;1;3)$$

where of course, $a = V / V_o$

Expanding the above equation in terms of Fourier series leads to:

$$C_{(t)} = C_o(1 + \Gamma'_1 \cos(\omega t) + \Gamma'_2 \cos(2\omega t) + \Gamma'_3 \cos(3\omega t) + \ldots) \qquad (G;1;4)$$

where $$\Gamma'_n = 2C_n / C_o = \Gamma_n 2 \qquad (G;1;5)$$

It may be shown that: (69) .

$$C_n = C_o \left\{ \frac{2}{\pi} - \int_0^{\pi} \frac{\cos(nx)}{(1+a\cos(x))^{\frac{1}{2}}} \, dx \right\} \qquad G;1;6)$$

here x represents the depletion layer thickness.

The Q_d or quality factor of a varactor is usually defined as:

$$Q_d = 1 / \omega R_s C_{min} \qquad (G;1;7)$$

and the often quoted diode figure of merit is expressed as:

$$F_d = \Gamma Q_d \qquad (G;1;8)$$

while the diode cutoff frequency is defined as:

$$f_c = 1 / 2\pi R_s C_{min}.$$

where R_s is the series diode resistance given earlier and C_{min} is the minimum diode capacitance obtained under 6 volts reverse bias, commonly accepted as the reference bias voltage.

G;2 (POWER RELATIONS)

Manley and Rowe,(7o) have analysed the general properties of non-linear elements and have shown that it is possible, under suitable conditions , to obtain gain from a circuit comprised of such elements. The particular problem which has been investigated is indicated in FIG.(G;2;1) . Here two voltage generators of frequencies f_1 and f_2, along with their internal impedances and bandpass filters, are connected to a nonlinear element. In addition an infinite series of selective loads , tuned to the sum and difference frequencies and higher harmonics are also coupled to the varactor. Only those frequencies lying within the pass band of any of the filters are allowed to exsist.

Manley and Rowe,(70) have shown that under the above conditions the following equations apply.

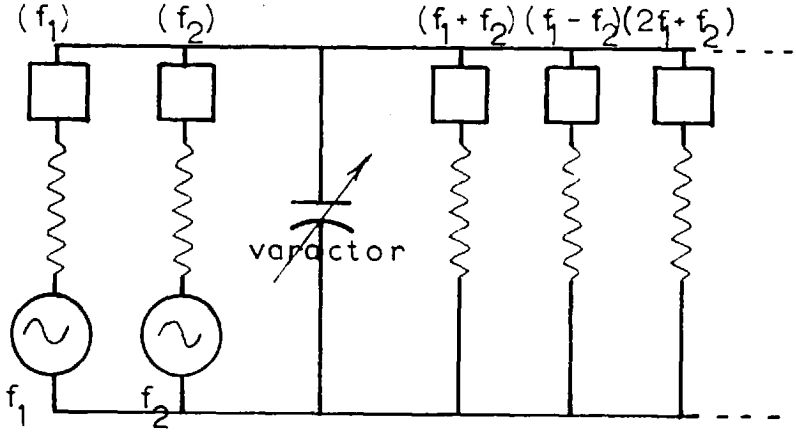

F I G. (G;2;1)

Manley and Rowe Power relations circuit.

$$\sum_{m=0}^{\infty} \sum_{n=-\infty}^{\infty} \frac{m P_{mn}}{m f_1 + n f_2} = 0 \qquad (G;2;1)$$

$$\sum_{n=0}^{\infty} \sum_{m=-\infty}^{\infty} \frac{n P_{mn}}{m f_1 + n f_2} = 0 \qquad (G;2;2)$$

where P_{mn} is the power flowing into the nonlinear reactance at frequencies mf_1 and nf_2, adopting the convention that power flowing into the reactance is positive while power flowing from the reactance , into the load resistances is negative. Equations (G;2;1 and 2) are rather remarkable in that they have no dependence on the nature of the nonlinear element.

Applying now the above equations to the case in question where only three frequencies are allowed to exsist, these being , the signal frequency f_1 , the idler frequency f_2 and the pump frequency f_3, the pump frequency is here taken to be the sum of the signal and idler frequencies, one finds that they become:

$$\frac{P_1}{f_1} + \frac{P_3}{f_3} = 0 \qquad (G;2;3)$$

$$\frac{P_2}{f_2} + \frac{P_3}{f_3} = 0 \qquad (G;2;3)$$

From the two above equations it can be seen that if power is supplied at frequency f_3 and power allowed to flow at frequencies f_1 and f_2 , the signal and idler frequencies respectively, both P_1 and P_2 are negative. This means that power is being delivered to the loads at f_1 and f_2 . Now since f_1 is the signal it follws that amplification is obtained.

If the gain is now defined as the ratio of the power supplied to the f_1 generator resistance by the nonlinear element, at frequency f_1, to the power supplied by the generator itself, it is evident that theoretically infinite gain is possible since power can be delivered at f_1 and f_2 regardless of whether or not a signal is supplied. The device therefore can become unstable and oscillate. A device possessing the above characteristics is termed a negative resistance parametric amplifier and is the type used in this system.

It is possible to construct two different types of negative resistance parametric amplifiers. The first " degenerate" type has the idler frequency within the pass band of the amplifier and often the same frequency as the signal frequency. The second " nondegenerate" kind has the idler frequency considerably larger than the signal frequency and so it is confined within the amplifier. The latter of these two types is the one used here and hence discussion will be restricted to that case.

G;3 (GAIN CONSIDERATIONS)

To analyse the operation of the parametric amplifier the so called "small signal " method will be adopted in which the signal frequency power is considered to be very small in comparison to the pump power. This assumption is completely justified in this case since the signal input is the order of micro-micro watts where as the pump level is tens of milliwatts.

Neglecting higher order terms in equation (G;1;4) gives the capacitance variation as:

$$C_{(t)} = C_o(1+\Gamma_1 (e^{j\omega_3 t} + e^{-j\omega_3 t}) \qquad (G;3;1)$$

where $$\Gamma_1 = C_1 / C_o \qquad (G;3;2)$$

Here the ratio C_1/C_o is merely the ratio of the minimum diode capacitance to the static diode capacitance. The value of C_1 may be determined from equation (G;1;6) using the relation that:

$$a = V_3 / V_o \qquad (G;3;3)$$

where V_3 represents the maximum value of the pump voltage.

The current through the capacitor is given by the time derivative of the charge and so:

$$i_{(t)} = \frac{dq}{dt} = \frac{d}{dt} \left(C_{(t)} V_{(t)} \right) \qquad (G;3;4)$$

Upon inserting the expressions for $C_{(t)}$ and $V_{(t)}$ from equations (G;3;1) and (G;1;2) into the above equation and assuming sinusoidal time dependence, gives:

$$i_{(t)} = \left(j\omega C_o + j\omega C_o \Gamma_1 \cos(\omega_3 t) \right) V_{(t)} \qquad (G;3;5)$$

Now specifying the condition that only signal and idler currents are allowed to exsist, one may write the instantaneous voltage across the varactor as:

$$V_{(t)} = V_1 \cos(\omega_1 t + \bullet) + V_2 \cos(\omega_2 t + \phi) \qquad (G;3;6)$$

where $\bullet$ and ϕ are phase angles and V_1, V_2 are purely real amplitude coefficients.

Equation (G;3;6) may be written as:

$$V_{(t)} = \underline{V}_1 e^{j\omega_1 t} + \underline{V}_1^* e^{-j\omega_1 t} + \underline{V}_2 e^{j\omega_2 t} + \underline{V}_2^* e^{-j\omega_2 t} \qquad (G;3;7)$$

where now $\underline{V}_1$ and $\underline{V}_2$ are complex quantities and the symbol * denotes the complex conjugate.

Similarly the instantaneous current flowing through the varactor may be expressed as:

$$i_{(t)} = \underline{I}_1 e^{j\omega_1 t} + \underline{I}_1^* e^{-j\omega_1 t} + \underline{I}_2 e^{j\omega_2 t} + \underline{I}_2^* e^{-j\omega_2 t} \qquad (G;3;8)$$

Now inserting the above expressions for $i_{(t)}$ and $V_{(t)}$ into the equation (G;3;5) and expanding, one obtains two equations which may be expressed in matrix form as:

$$\begin{vmatrix} \underline{I}_1 \\ \underline{I}_2^* \end{vmatrix} = \begin{vmatrix} j\omega_1 C_o & j\omega_1 \Gamma_1 C_o \\ -j\omega_2 \Gamma_1 C_o & -j\omega_2 C_o \end{vmatrix} \begin{vmatrix} \underline{V}_1 \\ \underline{V}_2^* \end{vmatrix} \qquad (G;3;9)$$

Thus the admittance matrix of the varactor diode is:

$$Y_d = \begin{vmatrix} j\omega_1 C_o & j\omega_1 \Gamma_1 C_o \\ -j\omega_2 \Gamma_1 C_o & -j\omega_2 C_o \end{vmatrix} \qquad (G;3;10)$$

The equivalent diode impedance matrix may now be obtained by inversion of the admittance matrix above. Upon such inversion the impedance matrix is found to be:

$$Z_d = \begin{vmatrix} 1/j\omega_1 C & \Gamma/j\omega_2 C \\ -\Gamma/j\omega_1 C & -1/j\omega_2 C \end{vmatrix} \qquad (G;3;11)$$

where now:

$$\Gamma = \Gamma_1$$

and

$$C = C_o(1-\Gamma_1^2) \qquad (G;3;12)$$

The impedance matrix may also be written as: (71)

$$Z_d = \begin{vmatrix} Z_{11} & Z_{12} \\ Z_{21} & Z_{22} \end{vmatrix} \qquad (G;3;13)$$

The approximate equivalent circuit for a negative resistance parametric amplifier has been given by Blackwell and Kotzebue as shown in FIG.(G;3;1) . (72).

where:

R_L = load resistance
R_1 = resistance of input signal circuit
R_2 = resistance of idler circuit
X_1 = reactance of signal circuit
X_2 = reactance of idler circuit
R_s = diode series resistance.

When power is allowed to flow only at the signal and idler frequencies, ω_1 and ω_2 respectively , the device is found to possess a bilateral negative resistance characteristic and hence

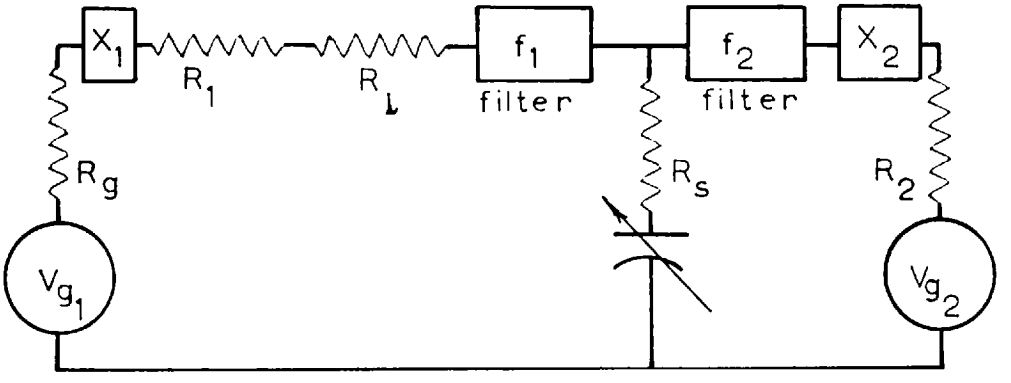

FIG. (G;3;1)

Approximate equivalent circuit for negative resistance parametric amplifier.

gain is possible if operation is restricted to the stable region just below the oscillation condition.

In the above equivalent circuit, the diode may be replaced by its equivalent impedance matrix of equation (G;3;13), and so the approximate equivalent circuit becomes as shown in FIG.(G;3;2).

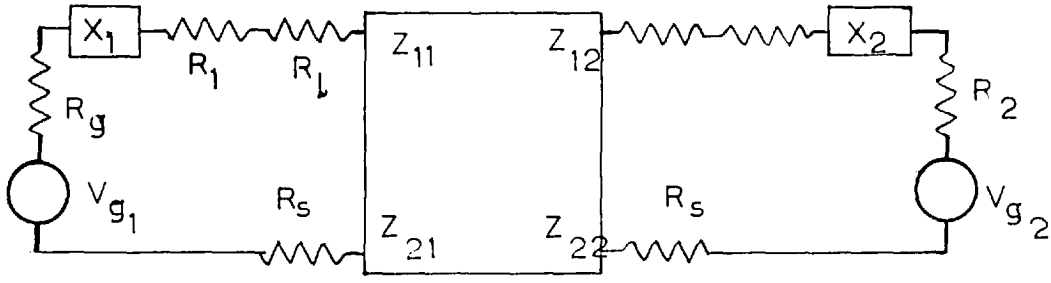

FIG.(G;3;2)

Impedance matrix form of approximate equivalent circuit for negative resistance parametric amplifier.

It should be noted at this point that the series resistance and shunt capacitance of the diode holder are not included in the approximate equivalent circuit since they are tuned to resonance at midband and hence do not effect gain considerations. They do however restrict amplifier band width by increasing the circuit Q .

Now considering FIG.(G;3;2) , one may write:

$$\begin{vmatrix} V_{g_1} \\ V_{g_2}^* \end{vmatrix} = \begin{vmatrix} Z_{11} + Z_{T_1} & Z_{12} \\ Z_{21} & Z_{22} + Z_{T_2}^* \end{vmatrix} \begin{vmatrix} I_1 \\ I_2^* \end{vmatrix} \qquad (G;3;14)$$

where:

$$Z_{T_1} = X_1 + R_g + R_L + R_s + R_1 \qquad (G;3;15)$$

and

$$Z_{T_2} = X_2 + R_s + R_2 \qquad (G;3;16)$$

In the above expressions the external circuit impedances have been added to the impedance of the nonlinear element.

The available gain at the signal frequency is defined as the ratio of the power dissipated in the load resistance R_1 to the available input power at the same frequency.

Now for maximum power transfer conditions the load resistance must be equal to the generator resistance R_g and therefore only $V_{g_1}/2$ appears across the amplifier terminals. It follows therefore that the available power input is:

$$\text{Available power input} = V_{g_1}^2 / 4 R_g \qquad (G;3;17)$$

The power output is:

$$\text{Power output} = I_1^2 R_L \qquad (G;3;18)$$

The value of I_1 may be found in terms of V_{g_1} by setting $V_{g_2}^* = 0$ in equation (G;3;14), and so:

$$I_1 = V_{g_1} (Z_{22} + Z_{T_2}^*) / ((Z_{11}+Z_{T_1})(Z_{22}+Z_{T_2}^*) - Z_{12}Z_{21}) \qquad (G;3;19)$$

Thus the gain expression becomes:

$$G = 4 R_g R_L I_1^2 / V_{g_1}^2$$

$$= \frac{4 R_g R_1 (Z_{22} + Z_{T_2}^*)^2}{((Z_{11}+Z_{T_1})(Z_{22}+Z_{T_2}^*) - Z_{12} Z_{21})^2} \qquad (G;3;20)$$

At the center frequency of operation both signal and idler circuits are resonant and so:

$$-X_1 = Z_{11} \quad , \quad -X_2 = Z_{22} \qquad (G;3;21)$$

which upon substitution into equation (G;3;20) gives:

$$G = 4 R_g R_L / (R_{T_1} - \Gamma_1^2 / \omega_1 \omega_2 C^2 R_{T_2})^2 \qquad (G;3;22)$$

Equation (G;3;22) may be written in the form:

$$G = 4 R_g R_L / (R_{T_1} - R_{neg})^2 \qquad (G;3;23)$$

where R_{T_1} is the total series resistance a frequency ω_1 , R_{T_2} represents the total series resistance at frequency ω_2, and R_{neg} is the effective negative resistance of the diode. It follows that:

$$R_{T_1} = R_g + R_L + R_s + R_1 \qquad (G;3;24)$$

$$R_{T_2} = R_s + R_2 \qquad (G;3;25)$$

$$R_{neg} = \Gamma_1^2 / \omega_1 \omega_2 (C_o(1-\Gamma_1^2))^2 R_{T_2} \qquad (G;3;26)$$

Inspection of equation (G;3;22) reveals that the gain of a negative resistance nondegenerate parametric amplifier is a very rapid function of the generator input impedance. Consequently any slight variations in the input impedance will result in very large variations in gain. The foregoing is especially true in this system application, where a T.R. cell is inserted before the amplifier, since the output impedance of such a cell varies from a short circuit, when the cell is fired, to a matched section of transmission line,upon recovery. It follows therefore that direct connection of the parametric amplifier to the T.R. cell would result in very unstable operation.

Fortunately the above mentioned undesirable characteristics of the parametric amplifier may be completely overcome by the insertion of a circulator at its input terminals, as this effectively presents a constant matched input impedance to the amplifier regardless of any line impedance variations. Another reason for the inclusion of a circulator at the amplifier input is to electrically seperate the input and output circuits, as they are comprised of the same elements and are consequently indistinguishable. It can also be shown that use of a circulator doubles the amplifier gain-bandwidth product and improves noise figure.(73)

The approximate equivalent circuit of the nondegenerate negative resistance parametric amplifier, with attached circulator, is shown in FIG.(G;3;3).

If the circulator is assumed matched , the power gain of the amplifier , at the signal frequency ω_1 , may be obtained merely by the square of the voltage reflection coefficient seen at the number 2 circulator port. Thus:

$$G = (\rho)^2 = \left(\frac{Z_1 - Z_o}{Z_1 + Z_o} \right)^2 \qquad (G;3;27)$$

where : $$Z_o = R_g = R_1 \qquad (G;3;28)$$

and $$Z_1 = R_1 + R_s - R_{neg} \qquad (G;3;29)$$

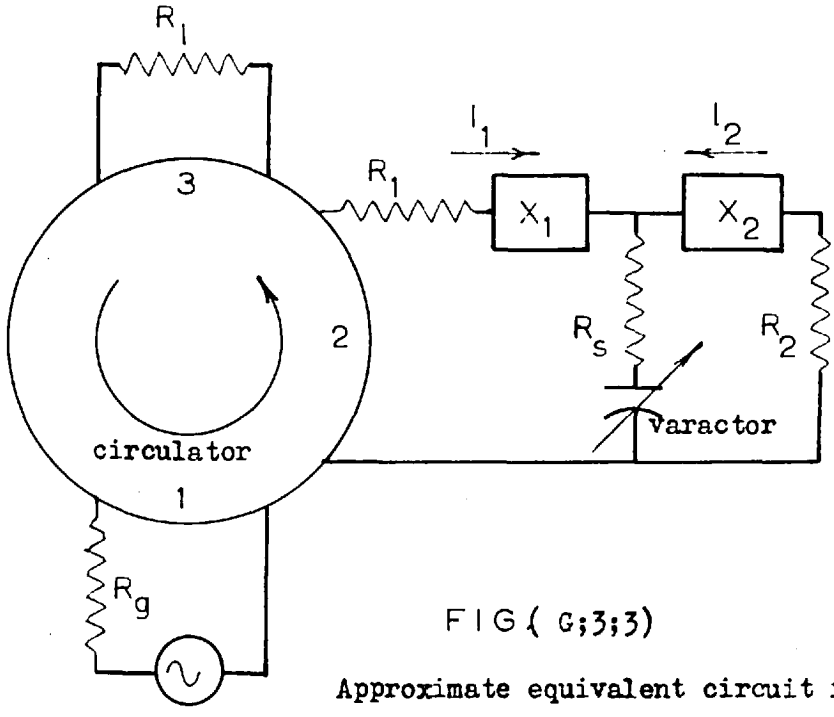

FIG(G;3;3)

Approximate equivalent circuit for a nondegenerate negative resistance parametric amplifier with circulator.

Substitution yields:

$$G = (R_{T_1} - R_{neg} - 2 R_g)^2 / (R_{T_1} - R_{neg})^2 \qquad (G;3;30)$$

where now: $$R_{T_1} = R_g + R_s + R_1 \qquad (G;3;31)$$

and as before $$R_{neg} = \Gamma_1^2 / \omega_1 \omega_2 (C_o(1-\Gamma_1^2)^2) R_{T_2} \qquad (G;3;32)$$

also $$R_{T_2} = R_s + R_2 \qquad (G;3;33)$$

For the high Q and high gain case one has that:

$$R_{T_1} \cong R_{neg} \qquad (G;3;34)$$

and $$R_{T_1} \cong R_g + R_s \qquad (G;3;35)$$

while $$R_{T_2} \cong R_s \qquad (G;3;36)$$

and so the gain expression becomes:

$$G = 4R_g^2 / (R_g + R_s - \Gamma_1^2 /(\omega_1 \omega_2 R_s (C_o(1-\Gamma_1^2)^2)) \qquad (G;3;37)$$

The specifications of the actual varactor diode used in this system, are as follows:

Type = M.A. 4252

f_c = 140 K.M.C.

C_o = 1.09 $\mu\mu$f

R_s = 3 ohms

Γ_1 = 0.33

$\Gamma_1 Q \cong 5$

Upon substitution of the varactor values into the gain expression of equation (G;3;37), for the system operation conditions of:

$$\omega_1 = 18.85 \times 10^9 \quad \text{and} \quad \omega_2 = 41.5 \times 10^9 \text{ rad./sec.}$$

one finds that:

$$G = 31 \text{ db.}$$

Thus from the above calculation it would appear that some 30 db. of gain is possible with the varactor used and this in fact has been obtained experimentally. It has been found however that at this level the amplifier is somewhat unstable and tends to break into oscillation, thus the pump drive was adjusted to give a slightly lower value of which resulted in 20 db.gain. Under these reduced gain conditions the device was found to be very stable.

G;4 (AMPLIFIER BANDWIDTH)

As is to be expected, the bandwidth of an negative resistance amplifier is determined largely by the effective loaded Q of the tuned signal and idler circuits. For single tuned circuits , at both signal and idler frequencies, it has been shown that the gain bandwidth product of a two port amplifier ,under assumed high gain conditions , is given approximately by the expression: (74).

$$G\,B^2 = \frac{4\,R_g R_L}{R_{T_1}^2} \left(1/\left(Q_1 + Q_2(\omega_1/\omega_2) \right)^2 \right) \qquad (G;4;1)$$

where

B = amplifier fractional bandwidth

R_g = input generator impedance

R_L = load impedance

R_{T_1} = total series resistive loading at signal frequency

R_{T_2} = total series resistive loading at idler frequency

$Q_1 = 1/\omega_1 C R_{T_1}$, loaded Q of signal circuit

$Q_2 = 1/\omega_2 C R_{T_2}$, loaded Q of idler circuit

Now for the case in point, $R_g = R_1$, (well matched amplifier), and $R_{T_1} = 2 R_g$, equation (G;4;1) may be written as:

$$G B^2 \cong \frac{Q_1^2}{(1 +(\omega_1/\omega_2)^2)^2} \qquad (G;4;2)$$

Also for high gain conditions one has:

$$R_{neg}/ R_{T_1} \cong 1 \qquad \text{from} \qquad (G;3;34)$$

and so

$$\Gamma_1^2 /\omega_1\omega_2 C^2 R_{T_2} R_{T_1} = 1 \qquad (G;4;3)$$

Upon substituting the expressions for Q_1 and Q_2 into the above equation one finds that:

$$Q_2 = 1/\Gamma_1^2 Q_1 \qquad (G;4;4)$$

which when inserted into equation (G;4;2) gives:

$$G B^2 = 1/ (Q_1 +(\omega_1/\omega_2)(1/\Gamma_1^2 Q_1))^2 \qquad (G;4;5)$$

The maximum possible bandwidth is obtained when $Q_1+\frac{\omega_1}{\omega_2\Gamma_1^2 Q_1}$ is minimum and this occurs when $\Gamma_1^2 Q_1 = \omega_1/\omega_2$.

It follows therefore that:

$$G B^2_{max} = 1/(\omega_1 /\omega_2\Gamma_1)^2 \qquad (G;4;6)$$

or

$$B_{max} = (\Gamma_1/ (G)^{\frac{1}{2}}) (\omega_2/\omega_1)^{\frac{1}{2}} \qquad (G;4;7)$$

Upon inserting the actual values of Γ_1 and ω_2/ω_1 , used in the practical amplifier, one finds that for 20 db. gain conditions:

$$B_{max} \cong 4.9\ \%$$

Using a circulator it should be possible to double the gain bandwidth product and so the maximum theoretical bandwidth is approximately 10% for a single tuned parametric amplifier. In actual fact only about 2% bandwidth was achieved, however since this was adequate for the pulse shape resolution required, no attempt was made at improvement.

G;5 (NOISE FIGURE OF PARAMETRIC AMPLIFIER)

There are two sources of noise in a negative resistance amplifier namely noise generated in the signal circuit and noise originating in the idler circuit. If only thermal noise is considered, which is quite realistic for amplifiers operating near room temperature, it is possible to compute the amplifier noise figure from the expression for the available noise power present at the amplifier output. This output noise power may be evaluated using the same technique utilised to determine the amplifier gain, except in this instance the voltage generators in the equivalent circuit of FIG.(G;3;2) present thermal noise voltages at both signal and idler frequencies.

The noise figure of the amplifier is specified in terms of the definition of noise figure given in section (H:1).

$$F = N_o / G\,K\,T_o\,B = (N_1 + N_2) / GKT_oB \qquad (G;5;1)$$

where N_o is the total noise output of the amplifier, G is the amplifier gain, B represents the operating bandwidth, T_o is the standard temperature of 290 degrees Kelvin, while N_1 and N_2 represent the noise power generated in the signal and idler circuits , respectively.

By using equation (G;3;14) and alternately setting e_{g_1} and e_{g_2} equal to zero, where here e_{g_1} and e_{g_2} are now the magnitudes of the noise voltages arising from the thermal noise generators at frequencies

ω_1 and ω_2 respectively, it is possible to determine the noise contributions of the signal and idler circuits. Thus:

$$N_1 = I_1^2 R_g = \frac{e_{g_1}^2 R_g (Z_{22} + Z_{T_2}^*)^2}{((Z_{11}+Z_{T_1})(Z_{22}+Z_{T_2}^*) - Z_{12} Z_{21})^2} \qquad (G;5;2)$$

$$N_2 = I_2^2 R_g = \frac{e_{g_2}^2 R_g (Z_{12})^2}{((Z_{11}+Z_{T_1})(Z_{22}+ Z_{T_2}^*) - Z_{12} Z_{21})^2} \qquad (G;5;3)$$

Now using the gain expression of equation (G;3;20), one may write the noise figure equation as:

$$F = (e_{g_1}^2 + e_{g_2}^2 (Z_{12}) / (Z_{22}+Z_{T_2}^*)^2) / 4KT_o B R_g \qquad (G;5;4)$$

The thermal noise power is given from equation (H;1;1) as:

$$N_1 = K T_1 B \qquad (G;5;5)$$

and $$N_2 = K T_2 B$$

where T_1 and T_2 represent the temperature of the signal and idler circuits respectively.

Using equation (G;3;17) with the above expressions leads to :

$$e_{g_1}^2 = 4 K T_1 B R_{T_1}$$

$$e_{g_2}^2 = 4 K T_2 B R_{T_2} \qquad (G;5;6)$$

Now remembering that at resonance $Z_{22} + Z_{T_2} = R_{T_2}$ and also that $R_g = R_L$, while $Z_{12} = -1/ j\omega_2 C$ and substituting these expressions along with the above equations into (G;5;4) , one obtains :

$$F = 1 + \frac{T}{R_g T_o}\left(R_s + R_1 + R_{neg}\,(\omega_1/\omega_2)\frac{(R_s+R_2)}{R_{T_2}} \right) \qquad (G;5;7)$$

where T is here the temperature of both the signal and idler circuits

If now high gain conditions are assumed, one has that:

$$R_{neg} \cong R_{T_1}$$

and so

$$F = 1 + T/T_o\left(\frac{R_{T_1}\,\omega_3}{R_g\,\omega_2} - 1 \right) \qquad (G;5;8)$$

and when $T = T_o$, which is very nearly the case in this system,

$$F \cong \frac{(R_g + R_s)}{R_g}\,(\omega_3/\omega_2) \qquad (G;5;9)$$

where in the above expressions ω_3 represents the pump frequency.

Upon inserting the values of the actual varactor parameters into the above equation, under the system operating conditions , one finds that:

$$F = 1.54 = 1.88 \text{ db.}$$

The above value is very low and in practice is not achieved since the resonant circuits do have an appreciable loss . In addition the analysis assumed R_{neg} equal to R_{T_1} which is true only for very high gain conditions , bordering instability and is thus not a practical situation.

The actual amplifier was found to have a 3 db. noise figure at 20 db. gain. This value includes the circulator loss of approximately 0.3 db..

The noise figure expression of equation (G;5;9) is very useful in that it provides an indication of the range of values to be expected from a specific amplifier using a practical varactor. In addition equation (G;5;7) may be manipulated to indicate the conditions desirable to achieve minimum noise figure. Blackwell has shown that the optimum pump frequency conducive to minimum noise figure is given by the relation. (75)

$$\omega_3/\omega_1 = (1+ (\Gamma_1 Q)^2)^{\frac{1}{2}} \qquad (G;5;10)$$

or $$\omega_3/\omega_1 \cong \Gamma_1 Q \quad \text{for good diodes} \qquad (G;5;11)$$

where $\Gamma_1 Q$ is the diode figure of merit.

Similarly it can be shown that the proper generator loading necessary to achieve minimum noise figure is determined by:

$$R_g/ R_s = (1 + (\Gamma_1 Q)^2)^{\frac{1}{2}} \qquad (G;5;12)$$

and so as an approximation:

$$R_g/ R_s \cong \Gamma_1 Q \qquad (G;5;13)$$

which means that the amplifier must have greater than critical coupling.

When the above conditions are fulfilled the minimum noise figure obtained is:

$$F_{min} = 1 + \frac{2 T_o}{T_d} (1/\Gamma_1 Q + 1/ (\Gamma_1 Q)^2) \qquad (G;5;14)$$

where T_d is the varactor diode temperature.

When the diode temperature is equal to T_o , equation (G;5;14) is found to be:

$$F = \Gamma_1 Q^2 / (1-(\omega_1/\omega_3)) (\Gamma_1 Q^2-(\omega_3/\omega_1)+1) \qquad (G;5;15)$$

Blackwell has shown that the above equation may be expressed in nomograph form as given in FIG.(G;5;1)

From the nomograph it can be seen that provided the diode figure of merit is sufficiently large, the ratio of pump to signal frequency isnot especially critical,provided it is greater than approximately 3. Since considerable pump power of some 40 milliwatts is required, it is desirable to have the pump frequency as lew as possible , consistant with acceptable noise figure. This in fact was one of the reasons why the pump frequency of the amplifier used in this system was set in the "X" band range,where c.w. power levels of this magnitude are quite easily obtainable with conventional low voltage klystrons.

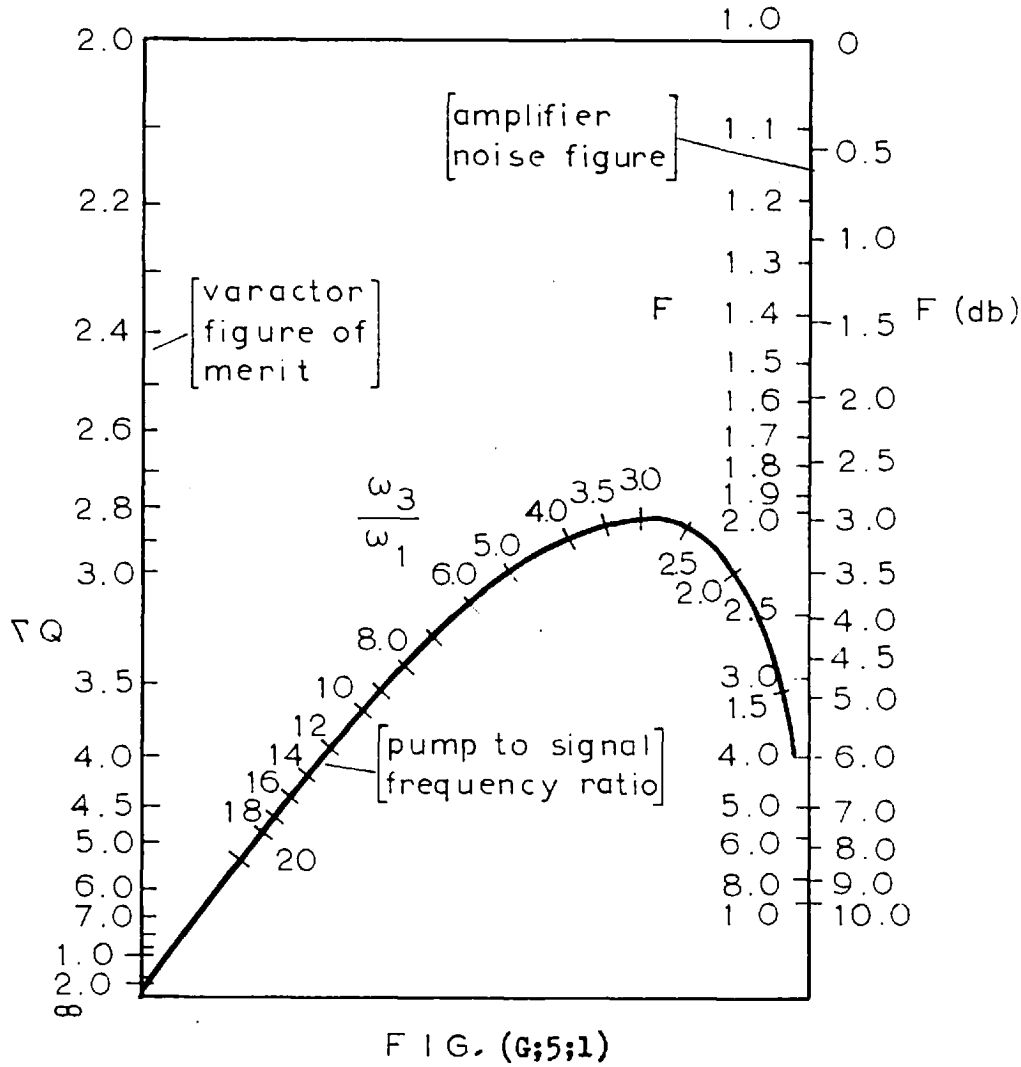

FIG. (G;5;1)

Noise figure nomograph for nondegenerate , negative resistance parametric amplifier. After Blackwell.

G;6 (PARAMETRIC AMPLIFIER ALIGNMENT PROCEDURE)

In the event of varactor burn out or failure, replacement should be made with pill varactor type M.A. 4252 , having static capacitance C_o lying between limits of 1.0 to 1.2 uu f. Subsequent alignment procedure to be followed is here given for completeness.

(A) Determination and adjustment of signal circuit resonance.

1. Insert a D.C. millivoltmeter in the D.C. diode return link of the varactor . Set millivoltmeter to maximum sensitivity ,(0 to 0.1 millivolts). Inject low level c.w. signal frequency of -20 dbm. , into amplifier with pump supply off. Manually sweep injected signal frequency until an indication is obtained on millivoltmeter. Adjust inductance of coaxial line until resonace occurs at the desired signal frequency of 3020 Mcs.

2. With the same apparatus and set up as above, increase frequency of the injected signal until another resonance is observed. This is the idler circuit resonance. The pump frequency required is therefore given by the relation:

$$f_3 = f_1 + f_2 .$$

(B) Adjustment of Pump circuit

1. Apply c.w. pump at frequency f_3 and adjust shorting plungers and tuning stubs in pump circuit, until a large indication is obtained on the millivoltmeter. Maximise.

2. Complete varactor D.C. return to the operational self bias condition, and apply pump power at 50 milliwatts level, and frequency f_3 . Electronically sweep pump source while injecting modulated c.w. signal at f_1 , into amplifier at - 25 dbm. Observe amplifier output on oscilloscope,having the same time base sweep as the pump source. The amplifier output is obtained from special monitoring device permanently built into the system.

3. Adjust short circuiting plunger and tuning stubs in pump circuit until a display , as shown in FIG.(G;6;1), occurs. Vary attenuator and shorting plunger in pump circuit until display is stable. Manuallly alter center frequency of swept pump source until trace is centered on oscilloscope.

4. If procedure 3 gives no results, display on oscilloscope, the reflected power from the amplifier in the pump circuit, while having the pump source electronically swept. Manually alter center frequency of pump until the opposite of FIG.(G:6;1) is observed. Repeat procedure 3.

5. Adjust pump power level until amplitude of FIG.(G:6;1) is approximately 20 db. Turn pump source off while applying constant,square wave modulated, signal to amplifier at frequency f_1 , to determine the 20 db gain condition. Adjust center of pump source sweep during power level adjustment,to keep trace centered. This is necessary since variations in the pump level also effect the operating frequency by altering the effective diode capacitance through changing the biasing point.

6. Now turn pump source to c.w. operation and signal source to square wave modulated, sweep. Vary power level, and frequency of pump source to center response about the desired center signal frequency. This is easily accomplished by connecting a high Q wave meter in shunt with the swept signal source. The display obtained is shown in FIG.(G;6;2) .

7. Turn signal input to square wave modulation only and slowly manually sweep signal about center frequency, observing the response on an Ave, coupled to the selective amplifier output. Center response and fix to 20 db. gain,by very slight pump frequency and power adjustments.

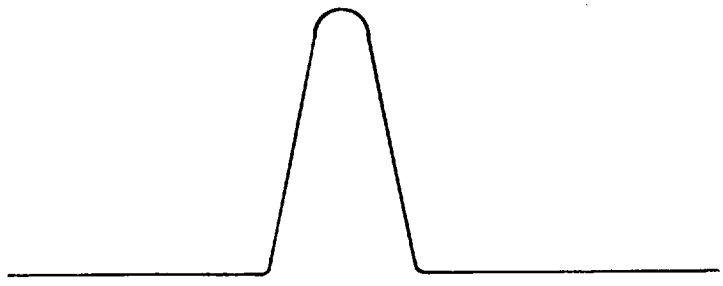

FIG. (G;6;1)

Oscilloscope display obtained during parametric alignment procedure.

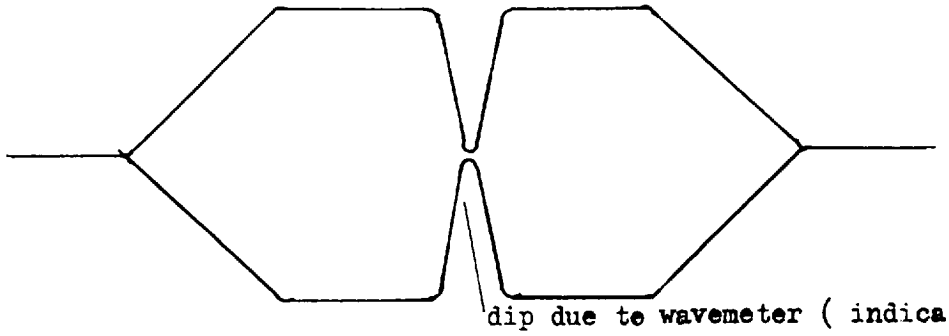

FIG. (G;6;2)

Parametric amplifier response as seen through special monitoring system, during alignment procedure.

APPENDIX H

NOISE FIGURE CONSIDERATIONS

A short section on noise considerations will here be given, where various definitions will be presented so that they may be refered to in subsequent sections.

H;1 (GENERAL NOISE FORMULAE)

The noise figure of a two port network is defined as the ratio of the total noise power per unit bandwidth available at the output to that portion of this power derived from the input termination, at a standard temperature of 290 degrees K.

As is well known the available noise power of a resistance is given by Nyquist as:

$$N = K\ T\ B \qquad (H;1;1)$$

where K is Boltzmans constant = 1.38×10^{-16} ergs/ degree Kelvin, T is the absolute temperature of the resistor and B is the operating bandwidth.

The noise output $N_{o(i)}$ of an ideal amplifier which introduces no noise is given simply by the product of the amplifier gain and the input power, thus:

$$N_{o(i)} = G\ K\ T\ B \qquad (H;1;2)$$

However a proctical amplifier introduces extra noise and hence its output N_o is not equal to $N_{o(i)}$. The noise figure of a practical amplifier is therefore given by the expression.

$$F = N_o / N_{o(i)} = N_o / G\ K\ T_o B \qquad (H;1;3)$$

The noise fiure of a network may also be expressed in terms of the degradation of the signal to noise ratio. So:

$$F = \frac{S_i / N_i}{S_o / N_o} = \frac{S_i / K T_o B}{S_o / N_o} \qquad (G;1;4)$$

where S_i = input signal power
N_i = input noise power
S_o = output signal power
N_o = output noise power

It should be noted that the noise figure is given by the ratio of the signal to noise ratio at the amplifier input , to the signal to noise ratio at the amplifier output, only when the input temperature is 290 ^{o}K.

Occasionally the noisiness of an amplifier is given in terms of an effective input noise temperature T_e . This is defined as the temperature of the input termination which gives rise to an output noise power per unit bandwidth, double that which would occur if the input terminals were at absolute zero. The relationship between noise figure and effective noise temperature is as follows:

$$T_e = T_o (F-1) \qquad (H;15)$$

Noise Figure of a resistor

The noise figure of a resistor R is easily determined from equation (H;1;3) since the available gain from a source impedance R_g shunted by a resistance R is simply:

$$G = R / R_g + R \qquad (H;1;6)$$

and so the noise figure is

$$F = 1 + R_g / R \qquad (H;1;7)$$

Noise figure of an attenuator can be shown to be given by :(76)

$$F = 1 + (L - 1) T / T_o \qquad (H;1;8)$$

where L is the network loss $= 1 / G$, and T is the temperature of the attenuator.

Cascaded networks

The overall noise figure of n networks connected in cascade is:

$$F_{1 \text{ to } n} = F_1 + \frac{F_2 - 1}{G_1} + \frac{F_3 - 1}{G_2 G_1} + ; ; ; + \frac{F_n - 1}{G_{n-1}!} \qquad (H;1;9)$$

where F_1 is the noise figure of network one, F_2 the noise figure of the second network and so on.

Similarly the overall effective input noise temperature of n cascaded networks is:

$$T_{e_{1 \text{ to } n}} = T_{e_1} + \frac{T_{e_2}}{G_1} + \frac{T_{e_3}}{G_1 G_2} + ; ; ; + \frac{T_{e_n}}{G_{n-1}!} \qquad (H;1;10)$$

Operating noise temperature.

The effective operating noise temperature , T_{op} of a receiver is as follows:

$$T_{op} = N_o / G K B \qquad (H;1;11)$$

where N_o is the available noise power at the receiver output and G is again the receiver gain.

Considering now the situation depicted in FIG.(H;1;1), where an attenuator having a loss L, at a temperature T_n , is inserted between the receiver,having noise figure F_r , and a resistance at temperature T_b . The effective operating noise temperature for this condition, refered back to the point of R, is from equations (H;1;5 and 10):

$$T_{op} = T_b + \frac{T_e}{G_r} = T_b + T_o(F - 1)$$

$$" \quad = L (T_a + T_e) \qquad (H;1;12)$$

where $$T_a = (T_b + (L - 1) T_n) / L \qquad (H;1;13)$$

and $$T_e = T_o (F_r - 1) \qquad \text{from} \qquad (H;1;5)$$

Thus T_a is the actual temperature that the receiver sees due to the insertion of the attenuator.

H;2 (MEASUREMENT OF NOISE FIGURE)

The accurate measurement of the low noise figures commonly associated with parametric amplifiers is rather difficult since any small errors introduced in the measurement can have significant

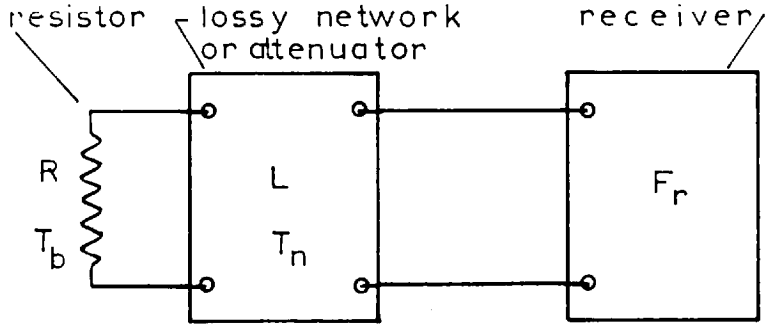

FIG (H;1;1)

effects on the result. Because of the above, both of the two standard techniques usually adopted for noise figure determination, were employed, these being the " signal generator method " and the "noise source method " .

Signal generator method

The technique which was adopted in the signal generator method is as follows:

A well matched signal generator, having an accurately calibrated attenuator and power output moniter, was connected to one of the microwave bridge arms, while the other arm was terminated in a matched lead. A push button attenuator was also inserted between the second and third intermediate amplifiers. With the signal generator off, the gain of the third I.F. strip was adjusted to give mid-scale indication on a detector. Three db. of I.F. attenuation was then inserted by means of the push button attenuator. The signal generator was then turned on and its output increased until the same mid-scale indication was again observed on the detector. The overall noise figure of the complete receiver system was then calculated from equation (H;1;4).

$$F = Si \,/\, K\,T_o\,B \qquad (H;2;1)$$

since $S_o / N_o = 1$

now $K\,T_o = 4 \times 10^{-15}$ watts per megacycle of bandwidth.

The signal generator method has the disadvantage that a seperate accurate measurement of bandwidth is necessary.

Noise source method

The other method used to determine noise figure involved the design and construction of a special waveguide noise source. This item is discussed in section (8;2 P.197) . The measurement procedure this time involved connecting the noise source to one of the bridge arms in place of the signal generator, while the push button attenuator was still left in the I.F. circuit. With the noise source off , an indication of noise power was again obtained as in the former case. Similarly three db of I.F. attenuation was then inserted in the receiver system and the noise source turned on. Next a precision,

variable , waveguide attenuator, which was already inserted in the bridge arm, was adjusted to achieve the same detector reading. This procedure of resetting the detector indication to its original value eliminates the detector characteristic as a possible source of error. The noise power obtained due to the noise source is found from equations (H;1;11 and 13).

$$N_o = G K B T_{op} \qquad (H;1;11)$$

and so the excess noise power is:

$$N_{o\ excess} = G K B (T_a - T_o) \qquad (H;2;2)$$

Upon substitution for T_a one has:

$$N_{o\ excess} = GKB(T_b + \frac{(L- 1) T_n}{L} - T_o) \qquad (H;2;3)$$

Now using the original definition of noise figure from equation (H;1;3), and letting $T_n = T_o$, ie,(room temperature measurement), one finds that:

$$F = \frac{T_b - T_o}{L T_o} = (T_b / T_o - 1) L \qquad (H;2;4)$$

For the commercial lamp used, (CV 1881), T_b = 11,000 ^{o}K. and so :

$$F = 15.7 \text{ db} - L \qquad (H;2;5)$$

where F is now the noise figure in db.,and L is the attenuator insertion in db.

REFERENCES

Number	Author	Publication	Year	Page
1	Hague,B.	An introduction to vector analysis	1950	
2	Montgomery,C.G.	M.I.T.8 (radiation lab. series)	1948	250
3	"	" "	"	254
4	Marcuvitz,N.	M.I.T.10(radiation lab. series)	1951	31
5	Montgomery,C.G.	M.I.T.8	1948	246
6	Mason,W.P.	Piezoelectric crystals and their application to ultrasonics	1950	22
7	"	"	1950	25
8	Mason,W.P.	Physical acoustics	1958	380
9	Ritcher,J.	Lecture series	1962	2
10	Mason,W.P.	Piezoelectric crystals and their application to ultrasonics	1950	27
11	Kolsky, H.	Stress waves in solids	1953	8
12	Love,A.E.H.	The mathematical theory of elasticity	1927	
13	Mason,W.P.	Piezoelectric crystals and their application to ultrasonics	1950	28
14	Love,A.E.H.	The mathematical theory of elasticity	1927	99
15	"	"	"	149
16	Kolsky, H.	Stress waves in solids	1953	39
17	Redwood,M.	Mechanical waveguides	1960	369
18	Love,A.E.H.	The mathematical theory of elasticity	1927	
19	Mason,W.P.	Piezoelectric crystals and their application to ultrasonics	1950	369
20	Kolsky, H.	Stress waves in solids	1953	39
21	Kelvin,	Baltimore lectures , London	1904	
22	Aitken,A.A.	Determinants and Matrices	1959	59
23	Musgrave,M.J.	Rep.Prog.Phy. Vol.22	1959	80

Number	Author	Publication	Year	Page
24	Love,A.E.H.	The methematical theory of elasticity	1927	373
25	Mason,W.P.	Physical acoustics and the properties of solids	1958	373
26	Musgrave,M.J.	Rep.Prog.Phy. Vol.22	1959	85
27	Kyame,J.J.	Wave propagation in Piezoelectric crystals. J.A.S.A.	1959	159
28	Mason,W.P.	Piezoelectric crystals and their application to ultrasonics.	1950	39
29	Kyame,J.J.	J.A.S.A. Vol.21	1949	160
30	White,D.L.	J.Applied Physics.Vol.33	1962	47
31	Mason,W.P.	Physical acoustics and the properties of solids	1959	364
32	Ritcher,J.	Lecture series	1963	48
33	Knott, C.G.	Phil.Mag. No.48	1899	64
	Zoeppritz, K.	Nach d Konigl, Math-phys.Berlin	1919	66
	Sohon ,F.W.	Introduction to Theoretical	1936	
	Macelwane,J.B.	Seismology	1936	
	Kolsky, H.	Stress waves in solids	1953	40
34	"	"	"	45
35	Jacobson,E.H.	Sources of sound in piezoelectric crystals. J.A.S.A. Vol.32	1960	949
36	Bommel,H.E. Dransfield,K	Physical review letters.	1958	234
37	Glasoe Lebacqz	M.I.T.5(radiation lab series)	1951	
38	Reuben,	I.R.E. transactions on component parts. July	1962	58
39	Glasoe Lebacqz	M.I.T.5	1951	600
40	"	"	"	350
41	Uhlenbeck, Goudsmit		1925	

Number	Author	Publication	Year	Page
42	Soohoo,R.F.	Theory and application of ferrites	1960	17
43	"	"	"	61
44	Clarricoats,P.J.	Microwave ferrites.	1961	37
45	Landau,L Lifshitz,L	On the theory of the dispersion of magnetic permeability in ferromagnetic bodies. Physik Zeitschrift Sowjetunion	1935	153
47	Clarricoats,P.	Microwave ferrites.	1961	193
48	Kittel,C.	On the theory of ferromagnetic absorption.	1948	155
49	McLean,R Aitken,F.M.	Electronic technology.Vol.39,Jan.	1962	3
50	"	"	"	4
51	Montgomery,C.G.	M.I.T.11 (radiation lab series)	1947	288
52	Moreno,T.	Microwave transmission design data	1948	214
53	"	"	"	215
54	Montgomery,C.G.	M.I.T.8 (radiation lab. series.)	1948	47
55	Montgomery,C.G.	M.I.T.11	1947	289
56	Collins,	M.I.T.6 (radiation lab.series)	1948	51
57	Lemont,H.R.	Waveguides	1942	24
58	Montgomery,C.G.	M.I.T.8	1948	39
59	Collins,	M.I.T.6 (radiation lab.series)	1948	50
60	McLachlan,N.W.	Bessel functions for engineers	1934	160
61	"	"	"	94
62	Peirce-Foster	Short table of integrals	1956	92
63	McLachlan,N.W.	Bessel functions for engineers	1934	160
64	Montgomery,C.G.	M.I.T.8(radiation lab. series)	1948	273
65	Marcuvitz,N.	M.I.T.10 "	1951	307
66	Montgomery,C.G.	M.I.T.8 "	1948	260
67	McLachlan,N.W.	Bessel functions for engineers.	1934	96
68	Blackwell,L.A. Kotzebue,K.L.	Semiconductor diode parametric amplifiers.	1961	120

Number	Author	Publication	Year	Page
69	Blackwell,L.A Kotzebue,K.L.	Semiconductor diode parametric amplidiers.	1961	127
70	Manley,J.M. Rowe,H.E.	Proc.I.R.E. July. Vol. 44	1956	904
71	Blackwell,L.A. Kotzebue,K.L.	Semiconductor diode parametric amplifiers.	1961	10
72	"	"	"	50
73	"	"	"	59
74	"	"	"	56
75	"	"	"	64
76	"	"	"	20
77	Ragan,G.L.	M.I.T. 9 (radiation lab. series)	1948	476
78	Bosma,H.	On the principle of stripline circulation . I.E.E. Jan.	1962	137
79	Bommel,H.E. Dransfield,K.	Physical review. March	1960	1245
	Jacobson,E.H.	Physics review letters. March	1959	249
80	Montgomery,C.G.	M.I.T. 11(radiation lab. series)	1947	304
81	Bommel,H.E. Dransfield,K	Physcis review letters. April Vol.2 No.6	1959	249
82	"	"	"	250
83	Jacobson,E.H.	Physics review letters. March Vol.2. No. 6	1959	
84	Lamb,J. Redwood,M. Shteinshleifer.	Physics review letters. July,	1959	28
85	Jacobson,E.H.	Physics review letters. March	1959	247
88	Frenkel, J.	Kinetic theory of liquids.	1946	190
89	Maxwell,J.C.	Phil,Trans.Roy.Soc.London.Vol.157	1867	49
90	Voigt,W.	Acm.D'Phys. Vol.47	1892	671
91	Barlow,J.	Ph.D. thesis,University of London	1959	24

Number	Author	Publication	Year	Page
92	Tobolsky,A.V. Andrews,R.D.	J. Chemical Phys. Vol.11	1943	125
93	Litovitz,A Herzfeld,F	Absorption and dispersion of ultrasonic waves.	1959	470
94	Gross, B.	Theories of Viscoelasticity	1953	
95	Litovitz,A Herzfeld,F	Absorption and dispersion of ultrasonic waves	1959	454
96	Eyring,H	J.Chem.Phys. Vol.3	1935	107
97	Glasstone,S Eyring,H	Theory of rate processes	1941	
98	Barlow,J.	Ph.D. thesis ,London	1959	19
99	"	"	"	21
100	Alfrey,T	The mechanical behaviour of high polymers. Interscience Pub.N.Y.	1948	
102	T.R.E. Memorandum	Discharge tube noise sources	1953	3
103	Harwick, Johnson	Proc. I.R.E. Vol. 39	1951	908
104	Munford,W	Bell system tech. J.	1949	608
105	Barlow,J Harrison,G Ritcher,J	Electrical methods for the visco-elastic behaviour of liquids under cyclic shearing stress. Laboratory Practice. Vol.10 No.11 . Nov.	1961	786
106	Spencer,E.G.	Physical review, Vol.125, March	1962	
107	Montgomery,C.G.	M.I.T.11(radiation lab. series)	1947	517
108	"	"	"	877
109	Ritcher,J	Lecture series	1963	
110	Mason,W.P.	Physical acoustic and the properties of solids.	1958	185
111	Barlow,J.	Ph.D. thesis, London	1959	

Number	Author	Publication	Year	Page
112	Ritcher,J.	not published	1963	
113	"	Lecture series (not published)	1963	
115	Harrison,G	Ph.D. thesis,London , to be presented		
114	Barlow,J.	Ph.D. thesis, London	1959	63
116	Ritcher,J.	not published	1963	